Striatal Function Explored Through a Biophysical Model of a Medium Spiny Neuron

Martin Guthrie

PhD
The University of Edinburgh
2006

Abstract

The basal ganglia are a dynamic neural network of telencephalic subcortical nuclei, involved in adaptive control of behaviour.

There has been much experimental evidence on the anatomy and physiology of the basal ganglia published over the last 25 years showing that the basal ganglia are involved in the learning of many adaptive behaviours, including motor planning, working memory and cognitive functions. Current qualitative basal ganglia models of the box and arrow type, whilst explaining much of the anatomical data, do not give enough insight into the mechanisms involved in basal ganglia function either in health or in disease states.

The striatum is the main input nucleus of the basal ganglia, integrating widespread cortical and thalamic inputs to perform behaviour selection. Convergent data from control theory learning models and experimental data have shown that the phasic dopamine signal in the striatum could be performing a similar function to a scalar teaching signal in reinforcement learning models, both signals indicating the occurrence of reward. Similarly, both models and electrophysiological data have shown how the timing of this reward signal can be changed during learning so as to occur at the point in time of the earliest predictor of forthcoming reward. These models do not, however, show how this teaching signal is used in the striatum to learn to select the action most likely to lead to reward.

Computational models have been produced to investigate the circuitry involved in striatal action selection. These models have tended to be of winner-takes-all networks, using a mechanism of recurrent lateral inhibition between the medium spiny cells of the striatum to select the winner and thus releasing the behavioural action judged to be correct in the current environmental context. However, the necessary biological circuitry to implement a winner-takes-all network is absent in the striatum. This leads to a requirement for new models of striatal function incorporating current biological data to provide a more realistic mechanism for behavioural selection.

This thesis develops a biophysically inspired, minimal current model of a striatal

medium spiny neuron which utilises transitions between two membrane potential states, both below firing threshold, to filter excitatory input. The behaviour of the model is first validated against experimental electrophysiological data and then used to demonstrate how the striatum could perform two of the tasks required for behaviour selection; accurately timed release of behaviours and learning a sequence of action selections to obtain reward. In the first series of simulations timed release of behaviours is demonstrated to be linearly related to the timing of firing of feedforward inhibitory interneurons. In a second set of simulations learned sequences of action selection, using a simulated dopamine reward signal, are shown in a reward location task performed by a small network of model medium spiny striatal neurons.

Taken together these studies show that this simple model of a striatal medium spiny neuron is capable of simulating the basic functionality required for behaviour selection in a manner which has greater biological plausibility than previously published models.

Declaration

I declare that this thesis was composed by myself, that the work contained herein is my own except where explicitly stated otherwise in the text, and that this work has not been submitted for any other degree or professional qualification except as specified.

(Martin J Guthrie)

Acknowledgments

I would like to thank David Wilshaw and Gordon Arbuthnott, my supervisors for their time, patience and especially for their willingness to listen to my ideas.

Also to my wife Nathalie, much appreciation is due for her support over the long haul of this project.

Contents

Abbreviations

ACh	Acetylcholine
AChE	Acetylcholine esterase
Ca^{2+}	Calcium ion
C_d	Amount of depression from one pairing
CR	Calretinin
DA	Dopamine
DYN	Dynorphin
E_i	Reversal potential for ion type i
ENK	Enkephalin
ENT	Entopeduncular nucleus
EPSP	Excitatory post-synaptic potential
F	Faraday's constant
FS	Fast spiking (interneuron)
GABA	Gamma aminobutyric acid
GPe	Globus pallidus externa
GPi	Globus pallidus interna
Hz	Hertz
$I_{Ca\text{-}L}$	L-type calcium current
I_{Kir}	Inwardly rectifying potassium current
I_{Krp}	Persistent potassium current
I_{Ksi}	Slowly inactivating A-type potassium current
I_L	Leakage current
ICSS	Intra-cranial self stimulation
IPSC	Inhibitory post-synaptic current
IPSP	Inhibitory post-synaptic potential
I_S	Current due to excitatory synaptic input
K^+	Potassium ion
kHz	Kilohertz
LTD	Long term depression
LTP	Long term potentiation
ms	Millisecond
MS	Medium spiny (neuron)
mV	Millivolt
Na^+	Sodium ion
NAcc	Nucleus accumbens
NOS	Nitric oxide synthase
nS	NanoSiemen
$P_{L\text{-}Ca}$	Membrane permeability to calcium
PPTN	Pedunculopontine tegmental nucleus
PV	Parvalbumin
SC	Superior colliculus
SNc	Substantia nigra pars compacta

SNr	Substantia nigra pars reticulata
SOM	Somatostatin
SP	Substance P
STDP	Spike timing dependant plasticity
STN	Subthalamic nucleus
STR	Striatum
T	Temperature
TAN	Tonically active neuron
T_{STDP}	Time constant for synaptic trace
TTX	Tetrodotoxin
VA	Ventroanterior
V_c	Slope of activation curve in Boltzmann function
V_h	Half activation parameter for Boltzmann function
VL	Ventrolateral
V_m	Membrane potential
VTA	Ventral tegmental area
W	Synaptic weight
δt_{fire}	Time since neuron fired
δt_{Input}	Time since synaptic input occurred
ΔD	Proportional change in dopamine level
μm	Micrometer

1 Introduction

1.1 Background

The basal ganglia are a set of interconnected subcortical nuclei which form a complex network of loops integrating cortical, thalamic and brainstem information[1]. Although they do not have a direct access to the spinal cord, much clinical and experimental data associates the function of these nuclei with the control of movement and posture[2 3 4]. More recently experimentation shows that they have, in addition, a role in the more general control of behaviours[1 5 6].

They were originally described in the 17th century by Willis, but came more to prominence at the start of the twentieth century when S.A. Kinnier Wilson in 1912[7] described a disease he called hepatolenticular degeneration. This disease is characterised by pathological changes to the liver and basal ganglia. Symptoms of this disease include, amongst others, muscular rigidity, tremor and weakness. This differs from symptoms of diseases associated with the pyramidal tract and led Wilson to postulate that the basal ganglia were a major part of a so-called extrapyramidal motor system, which operated independently of, and in parallel to, the pyramidal system. Since then it has first been shown that the output of the basal ganglia mainly returns to the cortex in a loop via the thalamus[8], producing an emphasis that the system is more prepyramidal than extrapyramidal. Later work shows that the basal ganglia output is sent to both the thalamus and the brainstem[9], indicating that the system could be considered as both extrapyramidal and prepyramidal.

Study of the basal ganglia has been driven by investigation of movement disorders, most notably Parkinson's disease and Huntington's chorea (for review of anatomy in these disorders see Crossman (2000)[10]). However there is no single agreed theory of what the basal ganglia contribute to normal movement or the exact mechanisms of basal ganglia function which lead to normal movement[11]. Indeed, neuroanatomical studies over the last two decades have produced much detail on the internal interconnections of the basal ganglia nuclei[12] and their external connections to a wide variety of other brain

structures, allowing for a proliferation of qualitative theories of function based on anatomical considerations. Also, electrophysiological studies, in vitro and in vivo, have provided much data related to the function of various classes of neurons in all nuclei of the basal ganglia and the effects of pharmacological manipulation on behaviour of these neurons without giving a clear idea of how these functions conspire to produce normal movement[13].

This would seem to indicate that there is a place for modelling studies to integrate aspects of known anatomical and electrophysiological data and suggest theories of function, from behavioural to sub-cellular levels that could provide direction for future experimental investigation.

To start to get a clearer view of what the fundamental functions of the basal ganglia may be, it may be useful to take a step back. The evolutionary antiquity and high degree of structural conservation of the basal ganglia[14] [15] augment clinical findings in suggesting that their role in the control of movement is very basic.

This does not mean that current function can be assumed to be the same as the original function, especially in light of at least two major stages in evolution where alterations to the circuitry of the basal ganglia have occurred[15]. At both the anamniote/amniote and non-mammalian/mammalian divides there has been a dramatic increase in the number and complexity of the cortico/pallio striatal projections. Nevertheless, many aspects of basal ganglia anatomy have been remarkably well conserved over the course of tetrapod evolution. Amongst these are

- The existence of distinct dorsal and ventral striatopallidal systems[16].
- The presence of two distinct populations of striatal projection neurons, one expressing SP and the other ENK[17],
- Dopaminergic innervation of both dorsal and ventral components of the striatum is highly conserved across tetrapods[18].
- Cholinergic interneurons are present in amniotes and at least some amphibians[19], although the quantity, location and physiological characteristics of these cells exhibits some variation[20].

GABAergic interneurons may also be present in amphibians, birds and reptiles[21] as well as being found in mammals[22].

This would imply that a model containing some of these conserved aspects of basal ganglia anatomy, even where simplifying assumptions have been made, could still capture some fundamental aspects of basal ganglia functionality in a useful manner. It is on this basis that the current studies were undertaken.

The next sub-section will look at the main current qualitative model of the basal ganglia and how this explains information flow among the nuclei of the basal ganglia, the thalamus and the cortex. It also points out how the proliferation of data has thrown some aspects of this model into doubt and why more quantitative models may be required to advance understanding of functionality.

1.1.1 Standard qualitative model

Models of the basal ganglia have been produced at various levels over the last 30 years or so and these models have been used to drive theories of basal ganglia function. The most influential of these has been the Albin-De Long box and arrow model[23] [24] developed in the early 1980s and shown in Figure 1-1.

In this model the main input nucleus of the basal ganglia, the striatum (STR), receives widespread input from the cortex and passes on processed signals via two pathways to the output nuclei of the basal ganglia, the globus pallidus interna (GPi) and substantia nigra pars reticulata (SNr) (in primates, known as the globus pallidus (GP) and entopeduncular nucleus (ENT) in rodents). The output nuclei project via the thalamus back to the cortex.

The two striatal signalling pathways through the basal ganglia proposed in this model are known as the direct and indirect pathways. The direct pathway arises from medium spiny projection neurons of the matrix of the striatum which are GABAergic and therefore inhibitory. They also co-express substance P (SP) [25] and/or dynorphin (DYN)[26]. They have a predominance of D1 dopamine receptors over D2 receptors[27]. The direct pathway projects directly to the output nuclei of the basal ganglia, GPi[28] [29] and SNr[30].

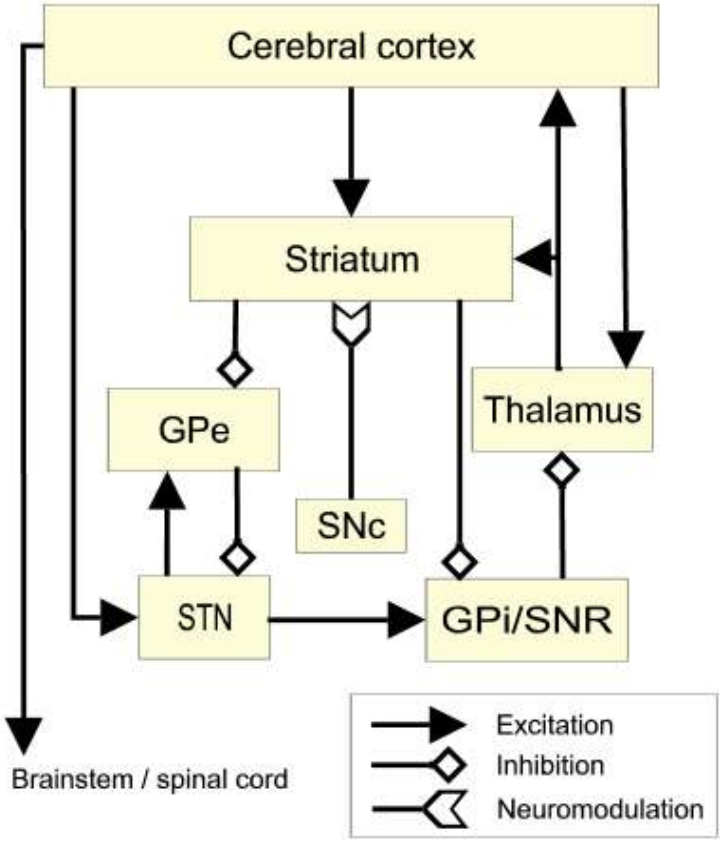

Figure 1-1 Box and arrow model of basal ganglia information flow (derived from a diagram in Smith et al (1998)[31]). Squares represent inhibitory projections and arrowheads excitatory projections. The inverted arrowhead represents the dopaminergic neuromodulatory input. The striatum receives input from virtually all regions of cerebral cortex. There are two pathways from the striatum to the output nuclei of the basal ganglia (GPi/SNr). The first is a direct inhibitory connection and the second is an indirect pathway via the Globus pallidus externa (GPe) and subthalamic nucleus (STN). These output nuclei project back to the same areas of the cortex that gave input to the striatum via the thalamus, thus forming closed loops.

The striatum also passes signals via a second pathway, the indirect pathway. This pathway arises from medium spiny projection neurons also located in the matrix of the striatum. These are also GABAergic but co-express enkephalin (ENK)[32] and have a predominance of D2 dopamine receptors over D1 receptors[27]. The indirect pathway projects firstly to the globus pallidus externa (GPe) [33] which passes the signal via the subthalamic nucleus (STN) [34] to the output nuclei[35].

The MS neurons of the direct and indirect pathways are indistinguishable

morphologically and are not topographically separated within the striatum[36] [37]. This suggests that they receive similar inputs and convey similar information to their respective output structures.

The outputs of the basal ganglia nuclei are mainly inhibitory, using GABA as their transmitter[38]. The GPi and SNr output nuclei fire tonically, maintaining inhibition on specific thalamic relay nuclei, mainly the ventrolateral (VL)[39] and ventroanterior (VA)[40] nuclei which project back to the cortex, as well as to the habenula, pedunculopontine tegmental nucleus (PPTN) and superior colliculus (SC)[41] [42] [43].

Thus the model is postulated to function as follows. When there is cortical input causing striatal projection neurons to fire, the GPi/SNR projection neurons are inhibited via the direct pathway, decreasing their tonic firing rate. This in turn decreases the inhibitory effect on the thalamus which therefore excites the same cortical neurons which stimulated the striatum in the first place. Similarly, a different population of striatal MS neurons inhibits the GPe via the indirect pathway, thereby decreasing the tonic inhibitory control which the GPe exerts over the STN. As a consequence, the excitatory drive of the subthalamic input to the GPi and SNr would be enhanced, leading to heightened inhibition of the thalamic target neurons to which GPi and SNr project, and thereby enhanced suppression of behaviour.

This means that the direct pathway is part of a positive feedback loop and the indirect pathway is part of a negative feedback loop connecting the cortex-striatum-GPi back to the cortex.

The presence of these two antagonistic pathways has led to two differing functional interpretations based on differing anatomical assumptions. In the first interpretation the direct and indirect pathways are assumed to converge on the same neurons in the GPi. This is proposed to lead to scaling of the pallidal output[44]. The opposing assumption that the direct and indirect pathways act on different neurons in the GPi leads to the idea that the divergent STN input suppresses competing behavioural programs[45].

This qualitative model has been very influential in directing research into many areas of basal ganglia function. It has also led to a resurgence of interest in the surgical treatment of Parkinson's disease based on the proposed altered functioning of the direct and

indirect pathways in this disease[46 47 48 49]. The model has also been used to improve understanding of other disease processes related to the basal ganglia such as Huntingdon's Chorea and schizophrenia. It has been a very effective model and could be said to be a very model of a modern major model (with apologies to W.S. Gilbert).

However it has not been able to explain much of normal functioning of the basal ganglia. Indeed, Albin et al[50] in a follow up article in 1995 called for the development of new models to explain both normal function and pathophysiological findings that their original model was not able to satisfactorily cover. Subsequent modifications of this model have increased the complexity of the interconnections. In particular the role of the indirect pathway has been called into question[51 52 53]. Tract tracing experiments find that the GPe is not simply connected to the STN, but also:

- Directly connects to the output nuclei of the basal ganglia, with a particularly prominent projection to GPi[54 55].
- Up to a quarter of all GPe neurons feed back to interneurons of the striatum[56 57].
- Projects to the reticular thalamic nucleus where it is in a position to influence other thalamocortical neurons via a relay[58].

Most of the original neuroanatomical work which led to the production of the Albin-De Long model was performed in rats. More recent work has shown that the output of the striatum in primates is not so clearly divided. Levesque et al (2003)[59] summarize several tract tracing experiments which show that "the majority of striatofugal axons arborize within most striatal target structures ".

One of the basic factors in interpretation of the direct and indirect pathways has been the differential effect of dopamine on the striatal MS neurons in each pathway. MS neurons forming the direct pathway have been said to express D1-class receptors. MS neurons in the indirect pathway have, by contrast, been said to express D2-class receptors. An increase in dopamine levels has opposing effects on these two sub-types of dopamine receptor, leading to an increase in the excitability of neurons with D1 receptors and a decrease in the excitability of neurons with D2 receptors. However,

recent confocal microscopy findings show that virtually all striatal neurons, both *in vitro* and *in vivo*, contained both D1 and D2 dopamine receptors[60].

It may be that MS neurons located in the matrix do project predominantly via one pathway or the other and do possess predominantly one class of dopamine receptors or the other, but these findings muddy the waters, especially with respect to the indirect pathway.

There is also a third pathway arising from the striatum. The division of the striatum into two compartments, the matrix and the striosomes was first proposed by Graybiel and Ragsdale in 1978 [61]. They noted that acetylcholine esterase (AChE) poor regions, comprising 10-20% of the striatum, which they called striosomes, were embedded in an AChE rich matrix. The striosomal MS neurons are innervated by corticostriatal neurons arising from deep layer V and layer VI of the cortex, whilst those of the matrix are innervated by superficial layer V and the supragranular layers[62]. The output targets of the two compartments also differ. As detailed above, the MS neurons of the matrix form the direct and indirect pathways. The striosomal MS neurons project to the substantia nigra pars compacta (SNc)[63] which reciprocates a dopaminergic neuromodulatory input to the striatum[64 65]. Since the actions of dopamine as a reward signal in learning[66] are relevant mainly to the chapter on learning spatial navigation, this pathway will not be considered further here.

More recently oscillations within the GPe-STN complex have been an increasing focus of attention, with speculation on their role in producing symptoms in Parkinson's disease[67 68]. This has taken emphasis further away from simple flow of information along the indirect pathway.

Although this box and arrow model, and subsequent modifications with increasingly complex interactions and loops, show to some extent the flow of information through the basal ganglia, they do not tell us much about the nature of the computations performed by the constituent nuclei.

This leads to the possibility that constructing lower level models of the constituents of the basal ganglia, which quantitatively capture the dynamics of the computations of the component nuclei, would be a useful step in forming a more accurate picture of

information processing throughout the whole basal ganglia system.

The next sub-section explains the reason for choosing a particular part of the basal ganglia to model and the step-by-step approach taken in producing and verifying the model before any conclusions regarding function are drawn.

1.1.2 What to model

The main input nucleus of the basal ganglia is the striatum, shown in a diagram of the rat and primate basal ganglia and associated structures in Figure 1-2[69]and a box and arrow diagram in Figure 1-3. The striatum receives excitatory inputs from many areas including the entire cerebral cortex (except for the primary visual and auditory cortices)[70 71 72 73] and the centromedian and parafascicular nuclei of the thalamus[74 75] as well as dopaminergic neuromodulatory inputs from the substantia nigra pars compacta (SNc) and ventral tegmental area (VTA)[76 77].

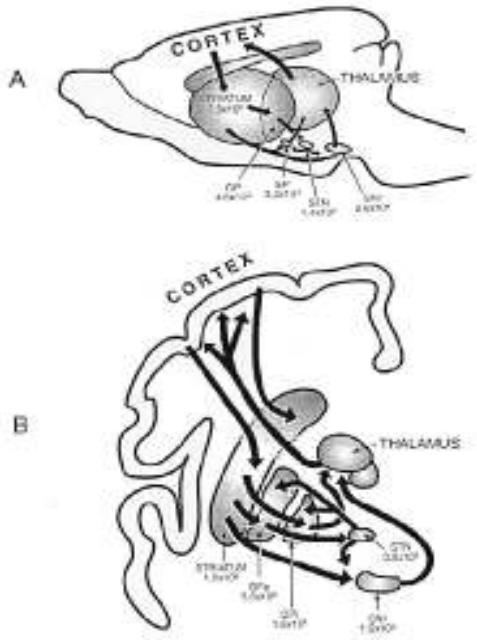

Figure 1-2 Major structures of the basal ganglia in (A) rat and (B) human brain (acknowledged to Wickens [69]). This shows that the striatum is the largest structure in the basal ganglia and the main recipient of cortical input.

This input stage would seem a good choice to begin investigation of the computational functions of the basal ganglia and has therefore been chosen for the modelling studies in this thesis.

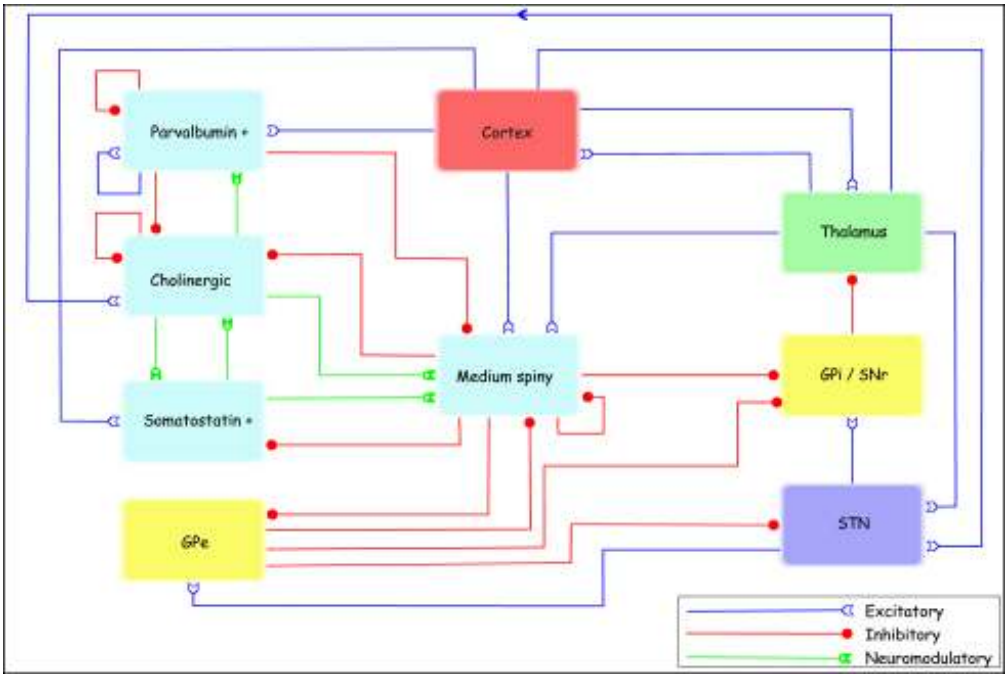

Figure 1-3 Box and arrow diagram of connections between main basal ganglia neuronal types. Striatal neurons are shown in light blue, globus pallidus in yellow. The SNc is not shown on this diagram. This illustrates some of the classes of striatal interneuron and the complexity of interconnections between them.

The striatum contains several cell types. The principal cell is the medium spiny (MS) neuron, which accounts for approximately 90% of neurons within the rat striatum[78] and approximately 75% within the primate striatum[79]. These MS neurons are the main recipients of the cortical and thalamic excitatory inputs and also the projection neurons, thus effectively forming a single layer, processing the corticothalamic input and producing the striatal output.

These are therefore the neurons which will be modelled in these studies. The other striatal cell types, which comprise at least four classes of interneurons fall into two broad classes; cholinergic interneurons and inhibitory interneurons[22 80], some of which, along with their interconnections are shown in Figure 1-3.

Cholinergic interneurons, also known as tonically active neurons (TANs) have complex reciprocal connections with medium spiny neurons, as shown in Figure 1-4. The interactive effects of these connections are beyond the scope of the current simulations and will not be considered further. The TANs also have an effect on the release of dopamine within the striatum[81], which will be discussed further in chapter 6 where

learning in a striatal network is considered.

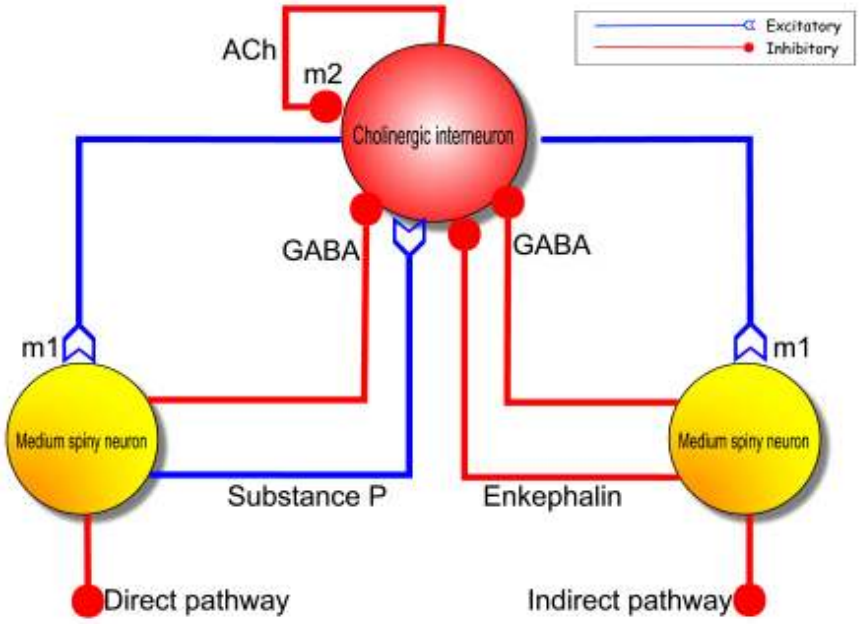

Figure 1-4 Reciprocal connections of medium spiny neurons and cholinergic neurons in the striatum. The interaction of inhibitory inputs from MS neurons, neuroactive compound influences, also from MS neurons, and feedback influence from TANs on themselves makes determining function complicated especially when, as here, the effects of dopamine are not taken into account.

There are three recognised classes of inhibitory interneuron, all using GABA at their primary neurotransmitter, but in conjunction with other neuroactive compounds[82 83 84]. One class has GABA co-localized with parvalbumin (PV)[85 86], another with calretinin (CR) [87] and a third with somatostatin, NADPH-diaphorase, neuropeptide Y and nitric oxide synthase (NOS) [88 22]. The most common of these interneurons, those co-localizing PV are also known as fast spiking (FS) interneurons[89] due to their high frequency of firing in response to cortical stimulation[83]. These FS interneurons are thought to play a part in controlling the firing of the medium spiny neurons and they will be discussed further in chapter 5 where this is investigated computationally. The role of the other GABAergic interneurons is not yet clear, especially the role of their other possible neurotransmitters and neuromodulators.

The following sub-section considers some of the current quantitative modelling efforts,

with particular reference to striatal models to justify the development of a new computational model of striatal MS neurons.

1.1.3 Computational models

Whatever functionality has been proposed for the basal ganglia, the striatum, as the main input nucleus, has been considered to perform an important stage of the computational process. There have therefore been many computational models produced over the last fifteen years with the striatum being modelled at some level as part or all of the modelling process.

Models of the basal ganglia have been classified by Gillies and Arbuthnott (2000)[90] into three categories; models of reinforcement learning[91 92 93], models of action selection[94] and models of serial processing[95]. These categories are not exclusive and have some aspects in common. The main areas of commonality are the use of the striatum to detect cortical contexts and the use of dopamine as a learning signal. The use of dopamine in reward based learning will be discussed in chapter 6.

All three types of model include, of necessity, some modelling of striatal function, but in none of the models referenced is the striatum modelled with any degree of biophysical reality, rather having individual neurons modelled as a simple differential equation or a logic function. This means that the striatal models used in these networks do not capture the essence of the computations performed by the striatum. As Schultz et al stated in a recent Trends in Neuroscience review "Despite 30 years of intense research and numerous suggestions, still no unifying concept of striatal function has been accepted"[96].

Notwithstanding this lack of understanding of striatal computational mechanisms, the predominant view is that the striatum functions to select between competing behaviours which have been formulated in the cortex[44]. These may be cognitive or motor behaviours, depending on the area of cortex producing the proposed program but, since the anatomy of the striatum is fairly homogeneous, the nature of the computations selecting for any type of behaviour is likely to be very similar. As it is simpler to conceptualize examples of motor control and consider the striatum as selecting between competing motor programs, examples used will therefore be couched in motor terms.

To account for this selection between motor programs, computational models of the striatum from the 1980s onwards have tended to use lateral inhibition to produce a 'winner takes all' competitive network[97 98 99 100 101 102]. This was not an unrealistic assumption given the known anatomy of the medium spiny neuron. The dendritic field of the medium spiny neuron extends in an ovoid disc with a diameter of 250-500μm [103] overlapping extensively with its own local axonal arborisation[104 105]. There are on average approximately 2840 other MS neurons located within the dendritic volume of one MS neuron[106] and symmetrical synapses, presumed to be inhibitory, had been seen on the proximal dendritic tree of MS neurons[107 108 109]. However, the methods used to detect these synapses were indirect so it could not be certain they arose from other MS neurons. Several lines of thought in the late 1990s have led to discarding the concept of the striatum as a winner takes all network. Firstly, the expected electrophysiological evidence for lateral inhibition did not materialise[110] and GABA-A receptors were found in lower concentrations than expected[111]. Secondly, there were findings of strong feedforward inhibition within the striatum from various classes of GABAergic interneuron[112 113]. Finally, it is clear that neurons firing at such a low rate, typically 0.1 to 1Hz[114 115], can be individually exerting little inhibitory effect on neighbouring neurons. An interesting review of the chronological development of these lines of thought by some of those who developed them has recently been published by Tepper et al in Basal Ganglia VIII[116].

This has led to a necessary rethink of striatal function. There remains the requirement for something similar to a winner takes all network as, if selection between competing motor programs is considered to be the aim of the computations performed in the striatum, false positives in releasing behaviours would be problematic. One candidate mechanism for controlling the network firing in the striatum would be a combination of the up and down states of the MS neurons with the effect of feedforward inhibition. These are mechanisms that will be investigated in the simulations in this thesis.

It should be mentioned, however, that over the last 4 years lateral inhibition in the striatum has been reported by several authors[117 118]. With improving techniques these connections have been shown to be relatively common, occurring unidirectionally in up

to a third of MS neurons examined[119] [120]. The effect of the inhibition from a single event, seen at the soma, is however much weaker for the feedback lateral inhibition than for the feedforward inhibition[121]. The latest figures suggest that the feedforward inhibition is slightly quicker, twice as large and less likely to fail[122]. Conversely, because there are far more MS neurons than feedforward inhibitory neurons, the total amount of inhibition due to the lateral feedback connections may be larger than due to the feedforward connections. Indeed, Guzman et al [118] estimated that two thirds of all GABAergic synapses seen on MS neurons are from other MS neurons, one third being divided between two classes of feedforward interneuron. The explanation for the greater strength of the feedforward inhibition proposed was that the lateral inhibition acts electronically distantly, on the terminal dendrites and is therefore greatly attenuated when viewed from the soma.

Although this lateral inhibition has now been shown to be present, it does not seem to have the characteristics necessary to create a winner takes all network. One problem that illustrates this is that there have been only occasional reciprocal connections found. This is a requirement for a competitive network. Also synchronous activation of groups of MS neurons, necessary to produce effective suppression of action potentials at the soma, has not been seen. Therefore, other functions have been suggested for this lateral inhibitory network, such as cooperative depolarization when the MS neurons are in their hyperpolarized state[123]. The effects of lateral inhibition have not been considered in these simulation studies.

1.2 Hypotheses

1. A simple, biophysically inspired model of a striatal medium spiny neuron can reproduce behaviours that are consistent with those observed in electrophysiological experiments.
2. One putative function of medium spiny neurons, timed release of behaviours, can be controlled by the action of feedforward inhibition on the model MS neuron.
3. A small network of model MS neurons can use a scalar reward signal to learn the location of a reward within a grid.

1.3 Layout of thesis

Chapter 2 develops a minimal current model of the MS neuron that replicates certain aspects of electrophysiological properties. The reasons for including some currents in the model and excluding others are considered in this section, along with details of the calculations necessary to track the temporal changes of membrane potential under changing excitatory and inhibitory input.

This model is then be evaluated against criteria from electrophysiological data in chapter 3 in order to assess whether its characteristics make it suitable for use in the subsequent modelling studies.

Chapter 4 examines the parameter space of the model to elucidate whether the aspects of MS neuron function considered important in the simulation studies are highly dependent on precise values of any of the model parameters.

A mechanism is then demonstrated in chapter 5 to show how the timing of the firing of the model MS neuron could be accurately controlled. These simulations use feedforward inhibition to demonstrate how accurately timed release of behaviours could be actioned using the timing of the first spike after the MS neuron has transited to the up state.

The final experimental section, chapter 6, shows how a small network of model MS neurons learns to navigate using a simple reward signal. This section develops LTP and

LTD rules based on spike timing dependent plasticity (STDP) and a dopamine pulse and shows how these learning rules could interact to provide learning of a spatial navigation task.

Discussions at the end of each section consider the implications of the results from the simulations, but a brief general conclusion is drawn in chapter 7 to bring together some of the findings across chapter boundaries.

The final section, chapter 8, considers some directions in which the model could be extended to provide further insight into basal ganglia function.

2 Construction of Model Neuron

2.1 Level of Model

To more fully understand the computations performed by the striatum it is necessary to model the medium spiny neuron on some level. To decide on the level of detail to be included in the model it is first necessary to consider the uses to which the model will be put.

As stated in chapter 1, these simulations will be investigating the computational use of the state transitions in MS neurons. The MS neurons will therefore need to be modelled at a greater level of detail than simple integrate and fire neurons. This lower level of modelling will have to be traded against computational tractability.

The most computationally demanding part of the studies to be undertaken here is the demonstration of learning in a small network of MS neurons. This demonstration will require simulating the membrane potential of several MS neurons over durations of up to a few minutes and repeating the simulation hundreds of times to demonstrate learning. Simulation of the varying membrane potential will require the assimilation of the effects of a large number of excitatory inputs on a millisecond time scale. This implies a large number of calculations over the course of a simulation.

To produce a computationally tractable model therefore requires simplifications to be made.

The first simplification to be made in these studies is to treat the MS neuron as a single compartment point neuron. The MS neuron has a complex dendritic tree, with several primary dendrites which branch extensively over a volume with a diameter of approximately 500μm[124]. Each MS neuron has, on average, 10,000 excitatory synapses, spread mainly over the distal dendritic tree[125], of which probably half are corticostriatal and half thalamostriatal[126]. There is a high probability that each corticostriatal input arises from a different cortical neuron[127]. Therefore each cortical neuron has little influence on the overall excitation of the MS neuron. This, and the large amount of excitation required to move the MS neuron from the hyperpolarised down state to the sub-threshold up state, has led to the idea that it is necessary to have excitatory activity

coordinated over much of the medium spiny dendritic tree to cause the neuron to transfer from the down to the up state and then to fire. Indeed, in work in the late 1990s, Wilson produced a simulation in which hundreds (but not thousands) of inputs were required to effect the state shift[128]. In his simulations the number of inputs required was totally dependent on the value assigned to the peak synaptic conductance.

Electrophysiological data on membrane conductance changes due to individual synaptic events is only available at the soma. It therefore seems a reasonable simplification to view all events from the perspective of the soma and not attempt multi-compartmental modelling of the dendritic tree. As we are not at this stage interested in propagation of the action potential to recipient nuclei, it also seems reasonable to ignore the axonal compartment in this model.

The next step is to consider which currents are required to produce the typical behaviour of an MS neuron.

One of the most striking features of the MS neurons is how quiet they are. The majority of striatal neurons have low baseline discharge rates of 0.1 to 1 spike/second[129]. This has been found to be due to the intrinsic membrane properties of the medium spiny projection neuron. A large proportion of the time, the neuron sits in a resting state with a hyperpolarized membrane potential of approximately -85mV[130] (shown in Figure 2-1 [131])[132]. Under conditions of coordinated excitatory synaptic input from many corticostriatal and thalamostriatal neurons, the MS neuron transits to an up state, only a few millivolts below the firing threshold[128]. In this up state the neuron may fire, although it does not always do so, as shown in several of the up states in Figure 2-1. This figure also shows that the first action potential often does not occur immediately the neuron reaches the up state, but may be delayed for periods up to hundreds of milliseconds into the up state.

A small set of potassium currents have been shown to be responsible for this two state behaviour of MS neurons[133]. This model will therefore be based on this set of currents which will allow investigation of the behaviour of the MS neuron as it transits between these two states.

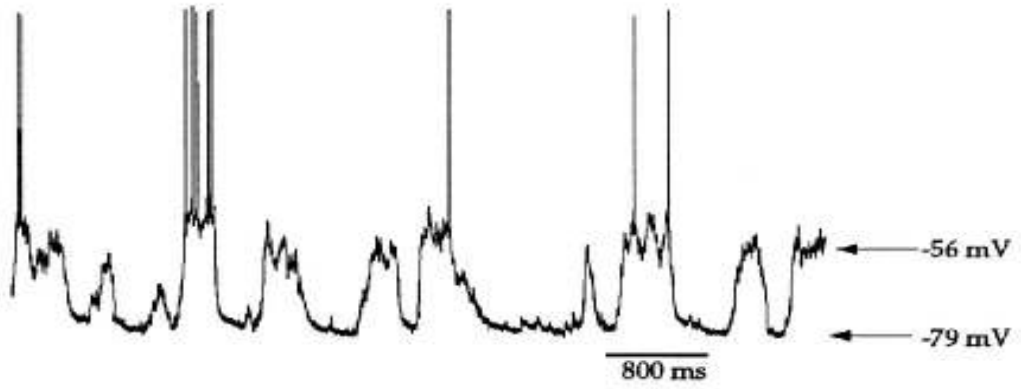

Figure 2-1 Spontaneous membrane potential fluctuations in a MS neuron in vivo (acknowledged to Stern et al. 1997 [131]). This electrophysiological trace shows the fluctuations between a hyperpolarized down state and a sub threshold up state in which firing can, but does not always, occur. It also shows that the first action potential after the up state has been reached may not occur until some considerable time into the up state.

2.2 Previous models

One previous model has been based on this set of currents, that of Gruber et al(2003)[134]. This showed that modelling at this level can reproduce some aspects of the behaviour of the MS neuron. They chose this minimal current model for essentially the same reasons as those expressed here, interest in the computational properties of the state transition in the MS neurons and computational tractability. The main difference in construction between the two models is that the Gruber model did not contain an inactivating element in the inwardly rectifying potassium currents. They used their model to investigate the effects of varying the dopamine level on state transitions in the simulated MS neuron. In the simulations here more attention will be paid to the effects of phasic dopamine changes on learning, although the effects of different levels of tonic dopamine on various aspects of the model are examined in chapters 4, 5 and 6.

Mahon et al (2000) have also produced a current level model of the MS neuron which was used to investigate state transitions[135]. Although this was also a single compartment model, it attempted to incorporate all the known MS neuron currents and used more complex representations of the current equations to take greater account of activation and inactivation particles of the currents. Although this approach is likely to produce a more realistic model, the computational overhead is far higher. One of the aims of the

model produced here is to show that the subset of currents chosen are adequate for investigation of the chosen functionality and that this level of abstraction from the full current model of Mahon et al can therefore be justified.

In the following sub-section the set of currents used in the model are introduced and their roles in the control of the model function considered. The basic equations used in the model are then explained

2.3 Model Currents

Before the model equations are introduced, the functions of the currents used in the model are considered individually.

2.3.1 Inwardly rectifying potassium current

The hyperpolarized down state is principally determined by an inwardly rectifying potassium current[136 137 138 139], here designated I_{Kir}. At hyperpolarized membrane potentials I_{Kir} provides a current that resists depolarization and therefore stabilises the down state, accounting for approximately 50% of resting conductance[140]. I_{Kir} activates rapidly and does not inactivate[141].

2.3.2 Outwardly rectifying potassium currents

In the absence of Na^+ and Ca^{2+} currents outwardly rectifying potassium currents are revealed experimentally by saturation in the amplitude of depolarizing voltage responses as a result of increasing current intensity[142]. There have been three main outward rectifying potassium currents demonstrated in MS neurons[138], two transient A-type currents and a non-inactivating current[143 144 145].

One of the A-type currents is fast inactivating and only available above spike threshold[146]. This current can therefore be excluded from this model as it does not contribute to the transitional behaviour of the neuron.

The second A-type current is the slowly inactivating potassium current, I_{Ksi}. This current is available at subthreshold membrane potentials and inactivates over a time course of hundreds of milliseconds to seconds [143 146]. This slow inactivation reduces the effect of I_{Ksi} gradually whilst the cell is in the up state, leading to a gradual ramp

increase in the plateau membrane potential in the up state.

The non-inactivating potassium current, I_{Krp}, is also available at subthreshold membrane potentials. These two outwardly rectifying currents contribute to the plateau membrane potential of the up state by opposing the depolarizing influence of excitatory synaptic input and inward ionic currents.

The transition from the hyperpolarized down state to the relatively depolarized up state is produced by a barrage of excitatory input from glutamatergic corticostriatal and thalamostriatal neurons [131 136 147]. Interruption of either pathway leads to the abolition of transitions to the up state[148 149 150].

As the cell is depolarized by excitatory inputs, the inwardly rectifying potassium current becomes less and less available and the outwardly rectifying potassium currents come to dominate[151]. These maintain the MS neuron at a membrane potential which is subthreshold, but only by a few millivolts. This state is generally known as the up state and is maintained from a few hundred milliseconds to a second or so until the level of excitatory input drops and the cell returns to the hyperpolarized down state. During the up state relatively small increases in excitation can cause the cell to fire [147].

2.3.3 L-type calcium current

Another current that activates at subthreshold membrane potentials in MS neurons and will therefore be considered in this model is an L-type calcium current, $I_{L\text{-}Ca}$ [152 153]. This is a high threshold calcium current which supplies an inward, depolarizing drive. Such slowly inactivating Ca^{2+} currents have been shown to be of importance in the maintenance of depolarized plateau potentials in many neurons[154 155 156.].

2.3.4 Leakage current

The model will also implement a leakage current, I_L. This current is an inevitable consequence in all electrical circuits in which capacitance is present.

2.3.5 Excitation

As stated earlier, many excitatory events occurring on distal dendrites are required to cause the transition to the up state and therefore to firing in the MS neuron. Since this is a point model, viewing the effects of conductance changes at the soma, it is necessary to

estimate the conductance change at the soma due to a synaptic event at a distal dendrite.

This can be estimated from data in a model of the medium spiny neuron dendrite and spines produced by Wilson in 1984[157]. This model investigates a cable model of the linear properties of dendritic spines. The main finding, from the point of view of consideration of quantities of cortical input required to drive MS neurons into the up state, was the voltage deflection produced at the soma by a synaptic input to a spine. Above a distance of 100μm, the distance of the spine from the soma had little influence on the somatic voltage. As the primary dendrite does not tend to branch for some 200μm from the cell body and spines do not generally occur on the primary dendrite, this is likely to be the case for cortical inputs. A single synaptic incident producing a conductance change of 0.5nS, sufficient to produce a maximal synaptic current in the dendritic spine, produced a voltage of approximately 0.2mV at the soma. This figure of 0.5nS will therefore be used as the default parameter for the maximum conductance change produced by a single synaptic event. The input rise time can be measured from figures in the study. The exponential decay is calculated by taking the time for the peak voltage to decay almost back to the baseline in the figures and considering this to be a multiple of five times the time constant.

2.3.6 Effect of dopamine on modelled currents

Two of the currents to be used in this model are known to be affected by dopamine levels. Since changing levels of dopamine will be used in the models to demonstrate learning, the effect of dopamine on these currents will have to be considered. The inwardly rectifying potassium current I_{Kir} has been shown to be enhanced by D1 dopamine agonists[158 159]. This would mean that increasing dopamine levels would make the transition from the down state to the up state more difficult.

The L-type calcium current is also enhanced by D1 agonists[160 161 162]. In this case increasing dopamine levels would lead to increased excitability in the up state, so less excitatory input would be required to maintain the cell in the up state. The maximum increase in the L-type calcium current seen during the application of D1 dopamine agonists is 40%[160]. This sets an upper limit on dopamine pulses to be used in these simulations of 1.4 times the tonic level.

As the concern within these simulations is to model the neurons which are most likely to be selecting actions, the MS neurons of the direct pathway, only the effects of dopamine on D1 receptors need to be considered at this stage.

2.3.7 Model Equations

Standard Hodgkin-Huxley techniques are used to simulate an isopotential model of a medium spiny neuron.

The change in membrane potential is modelled as a differential equation relating the rate of change of the membrane potential to the ionic currents as shown in equation (2.1). The moment-to-moment membrane potential is calculated from this using numerical integration. In these simulations a fifth order Runge-Kutta algorithm is used for the numerical integration with a maximum step size of 1ms[163]. This algorithm has the advantage that it allows the error to be estimated and the calculation to be redone if the estimated error exceeds a preset value, in this case 0.1mV/ms. This means that at times of rapid change of membrane potential, the time step used for the numerical integration is reduced below 1ms. When the rate of change of the membrane potential decreases, the time step for integration increased until it reaches a maximum of 1ms.

$$-C\frac{dV_m}{dt} = \mu\left(I_{Kir2} + I_{L-Ca}\right) + I_{Ksi} + I_{Krp} + I_L + I_S \qquad (2.1)$$

where C is the membrane capacitance, V_m is the membrane potential, I_s is the current due to the synaptic input, I_L is the leakage current, I_{xxx} are the model currents and μ is the neuromodulatory factor, representing the dopamine level, which acts as a multiplier on the inwardly rectifying potassium current and the L-type calcium current.

Each current, except for the L-type calcium current, is modelled as the product of a conductance and a linear driving force

$$I_i = g(V_m - E_i) \qquad (2.2)$$

where I_i is the ionic current, g_i is the conductance, V_m is the membrane potential and E_i is the reversal potential for that ion. For the potassium currents the conductance is voltage dependent, and is fitted to a Boltzmann function of the form:

$$g_i = \frac{\bar{g}}{1 + e^{\left(\frac{-(V_m - V_h)}{V_c}\right)}} \qquad (2.3)$$

where $\bar{g}$ is the maximum conductance, V_h is the half-activation parameter, the voltage at which 50% of the current is available, and V_c controls the slope of the activation curve. Values of V_h and V_c for the inwardly rectifying potassium current[138 139], the non-inactivating potassium current[164] and the slowly inactivating potassium current[165] have been obtained from electrophysiological recordings.

2.3.8 Inactivating potassium current

The model of Gruber et al [134] did not contain an inactivating potassium current. This has been shown to be necessary for the slow ramp depolarisation that is seen in MS neurons in the up state (shown in Figure 1 of Nisenbaum et al.[1994] [142]). The model of Mahon et al[135] did use a slowly inactivating A-type potassium current. To implement this current they used activation and inactivation particles requiring the calculation of exponentials at each time step. This adds a significant amount of computational overhead. To maintain the computational tractability of the model, a linear approach to the inactivation has been used. This eliminates the exponential factor from the inactivation equations.

Since the activation kinetics of the two outwardly rectifying potassium currents are similar, they are modelled as one and using one set of activation variables, V_h and V_c, for the resultant current. The inactivation is represented by a linear decrease in a proportion of the peak conductance at each time step when the membrane potential is above -60mV, and, for reactivation, an increase when V_m is below -60mV. An inactivation and activation time constant are set to control the time to complete inactivation/reactivation of the inactivating portion of the current. The default value used for both is 1000ms.

2.3.9 L-type calcium current

The L-type calcium currents are not well modelled by a linear driving force as the low level of intracellular calcium leads to a large concentration gradient across the membrane. This leads to a non-linearity in the voltage/current relationship of the open

channel. Following Hille[166], this current has therefore, been modelled using the Goldman-Hodgkin-Katz equation. This is a variant of the Nernst equation

$$\gamma = \frac{z^2 F^2 V_m}{RT} \cdot \left([Ca]_i - [Ca]_o \cdot \left(\frac{-zFV_m / RT}{1 - e^{-zFV_m / RT}} \right) \right) \tag{2.4}$$

where z = 2, F = 9.648 x l0^4 C mol^{-1}, R = 8.315 V C K^{-1} mol^{-1} and T = 273.16 + 37K.

$[Ca]_o$ is the extracellular calcium concentration and $[Ca]_i$ is the intracellular calcium concentration. From this the current is obtained by:

$$I_{L-Ca} = \gamma P_{L-Ca} \tag{2.5}$$

where $P_{L\text{-}Ca}$ is the membrane permeability to calcium. Bargas et al[152] showed that the membrane permeability can be represented as a Boltzmann function of the form seen in (2.6)

$$P_{L-Ca} = \overline{P}_{L-Ca} \left(1 + e^{\left(\frac{-(V_m - V_h)}{V_c} \right)} \right)^{-1} \tag{2.6}$$

where $\overline{P}_{L-Ca}$ is the maximum permeability to calcium. The values used by Gruber et al [134] for V_h and V_c for this current differ from those found experimentally. In their paper they explain that they have modified the values to account for the use of Ba^{2+} instead of Ca^{2+} in the experiments. I have adopted their values of V_h and V_c for this current

2.3.10 Synaptic input

Excitation is modelled as discrete conductance changes, each synaptic event having a linear rise to a maximum level and an exponential decay. The influence of each synaptic event at a given time on the synaptic current is the conductance at that time multiplied by the membrane potential. The nature of the synaptic train causing the excitation varies depending on the nature of the simulation.

For some simulations the excitation is non-random. This produces a steady train of input pulses which resulted in a smooth temporal distribution of excitation and thus a steady plateau membrane potential. This allows the study of how parameters affect

spike timing and plateau membrane potential without having to take into account effects due to input noise.

To demonstrate the robustness of the mechanisms used, some of the large amount of noise in the up state membrane potential seen experimentally[167] must also be modelled. To this end variables are introduced to the timing of the excitatory inputs to produce a more random input. In each simulation multiple excitatory inputs are used, the number dependent on the type of simulation. Each variable controlling the timing of firing of each input is capable of being varied randomly. There are three main randomness inducing variables.

Firstly, the time that the excitatory train from a given input starts is varied. This is referred to as the input start stagger. This causes the input to fire its first action potential at a time after the specified onset of excitation. The amount of time after the onset of excitation that an individual input starts firing is a random number between 0 and the firing period of that input.

Secondly, the frequency of the input is also varied randomly. Besides specifying an input frequency, the user can also specify a standard deviation of that frequency. The firing frequencies of all inputs are then a Gaussian distribution about the firing frequency mean. A standard deviation of 2Hz is used in these simulations.

Finally, a firing jitter can be assigned. This variable changes the firing of each input spike by a random amount with a maximum specified by the firing jitter set by the user. In these simulations a firing jitter maximum of 2ms is generally used.

2.3.11 Firing

In these simulations, the main focus of attention is on the timing of the first spike produced after transition to the up state. This can simply be modelled as occurring at the first time step that the membrane potential exceeds a firing threshold.

Since the occurrence of subsequent spikes is not relevant to the simulations, it is not necessary to model the sodium currents producing the spikes or the afterhyperpolarization. In some of the simulations multiple action potentials are visible in the simulator output. These are implemented as having a membrane potential

dependent probability of occurring at every time step where the membrane potential is above the firing threshold, once a time for the absolute refractive period has passed. They provide a useful visual indicator of potential firing trains, but are not sufficiently realistic to be used for any form of quantitative spike train analysis.

2.3.12 Basic parameters

Parameter	Value
Membrane capacitance ($\mu F/cm^2$)	1
Temperature (°C)	37
Excitatory reversal potential (mV)	0
Firing threshold (mV)	-45
Input amplitude ($\mu S/cm^2$)	0.5
Input rise time (ms)	7
Input decay time constant (ms)	8
Leakage conductance (mS/cm^2)	0.008
Leakage reversal potential (mV)	-75
Potassium reversal potential (mV)	-85
I_{Kir} maximum conductance (mS/cm^2)	1.2
I_{Kir} V_h (mV)	-110
I_{Kir} V_c (mV)	-11
I_{Ksi} maximum conductance (mS/cm^2)	0.5
I_{Ksi} maximum variable conductance (mS/cm^2)	0.1
I_{Ksi} variable conductance activation time (ms)	1000
I_{Ksi} variable conductance inactivation time (ms)	1000
I_{Ksi} V_h (mV)	-13.5
I_{Ksi} V_c (mV)	11.8
Calcium concentration outside ($mmol/cm^3$)	0.002
Calcium concentration inside ($mmol/cm^3$)	0.00001
Calcium maximum permeability (nm/s)	4.2
Calcium V_h (mV)	-34
Calcium V_c (mV)	6.1
Tonic dopamine level	1

Table 2-1 Default simulator parameter values

2.3.13 Programming considerations

All programming has been done using Borland Delphi, an object oriented, Pascal derived language with a visual programming environment for rapid production of user interfaces. The simulations were carried out under Window XP on a personal computer equipped with a Pentium 4 microprocessor (minimum required level 1GHz) and 1GB of RAM (minimum required 256MB).

2.3.14 Runge-Kutta algorithm

The Runge-Kutta algorithm used in these simulations is adapted from that available in NetLib (http://www.netlib.org/fmm/rkf45.f). In these simulations there is no requirement for the parallel processing of multiple first-order derivative equations. Therefore, to increase computational efficiency, the code has been adapted to only accept a single equation at each time step.

The Runge-Kutta algorithm is able to vary the time step dependant on the rate of change, using smaller time steps with higher gradients, but an upper limit can be set on the step size used. In all the simulations here, the upper limit on the step size for integration was 1ms.

2.3.15 Model design

As an object oriented language has been used, the model has been designed as a hierarchy of objects. The lowest level object is the synapse. Synapses can be either excitatory or inhibitory and (speaking anthropomorphically for simplicity) keep track of the time that each input to them occurs. At each time step the total synaptic conductance is calculated. For this each synapse calculates its own total conductance at that time point. Each synaptic event that has occurred before that time point has a conductance based on a linear rise time and an exponential decay, enabling calculation of their influence at that time point. Each synaptic event is removed from the array of synaptic events when the current simulation time is greater than five times the exponential decay time constant plus the rise time after the event occurred.

Synapse objects are owned by dendrite objects. Dendrite objects do not have much functionality in these simulations, but have been included for forward compatibility.

Dendrite objects are owned by neuron objects. The neuron object calculates the total current by summing the ionic currents from the earlier equations based on the current membrane potential and adding the synaptic currents from all synapse objects. This total current is then used to calculate the new membrane potential using the Runge-Kutta algorithm.

This hierarchy of objects allows for a simple interface to the simulator to plot the evolution of the membrane potential.

2.3.16 Results

All results for the simulations are automatically exported to Excel spreadsheets, along with the parameter settings used in the simulation. This gives a simple method of reproducing results.

3 Validation of Model Neuron

3.1 Introduction

In this chapter the performance of the model MS neuron developed in chapter 2 is compared with electrophysiological data. Three main criteria have been used for the comparison as these criteria capture the unusual dynamics of the MS neuron membrane potential. The aim of this validation is to provide a level of confidence that the behaviour of the model in the following simulation studies does indeed give a good picture of how the MS neuron behaves in vivo.

The criteria chosen to assess the model are that, compared to electrophysiological studies, the model had to:

- Demonstrate a similar current-voltage (IV) relationship
- Perform similarly under current injection conditions
- Show similar state transitions

These criteria are considered at an intermediate time range of 50ms to a few seconds using the principle of separation of time scales[168]. This is similar to the approach taken by Gruber et al[134] and allows rapidly inactivating effects to be ignored. Since most of the figures for V_h, V_c and maximum conductances are taken from work originating from Wilson's group in the 1990s, the behaviour of the model neuron is compared with synaptic tracings and current-voltage curves published by this group. As the behaviour that will be considered in the remainder of this thesis is based on modifying the characteristics of the transition from the down to the up state, all the criteria chosen reflect aspects of this transition.

3.2 IV Relationship

The medium spiny neuron has an IV relationship that displays both inward and outward rectification, as would be expected from the discussion of the potassium currents in chapter 2 (sections 2.3.1 and 2.3.2, page 20). This model does not use any sodium currents, so a valid comparison is with the IV relationship of a TTX treated neuron. Figure 3-1 shows the IV relationship of a TTX treated MS neuron in a slice preparation,

taken from Nisenbaum and Wilson (1995)[138] along with the IV relationship produced by the model neuron.

Note that with sodium currents present, the IV characteristics remain the same at hyperpolarized levels but the plateau does not start to appear at ~-55mV. Instead the characteristic curve continues to accelerate as the sodium currents come into play.

The following correspondences can be seen between the electrophysiological data and the model neuron:

A.

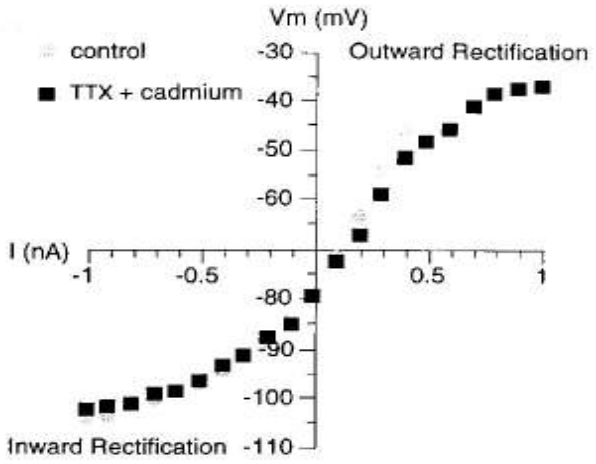

B.

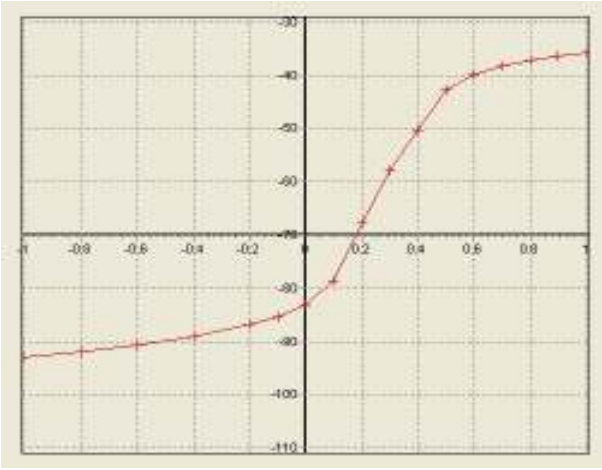

Figure 3-1: Comparison of electrophysiological (a) (acknowledged to Nisenbaum and Wilson[138]) and model (b) IV characteristics. The model neuron has the same zero current point, similar plateau potential and gradient over the range between the down state and firing potential as that found in a MS neuron in vivo.

- The transition from outward to inward rectification occurs at approximately -80mV
- The current is approximately 0.3nA at the chloride reversal potential of -60mV.
- The membrane potential plateaus at approximately -35mV.

The only discrepancy is that the plateau membrane potential in the hyperpolarisation direction is some 10mV higher in the model than in the electrophysiological data. As the model will not be used at membrane potentials lower than -90mV this discrepancy should not affect the validity of the model in the simulations proposed.

3.3 Current Injection

As with the IV relationship, the experimental current injection shown in Figure 3-2 is taken from Nisenbaum and Wilson (1995)[138]. This shows both depolarizing and hyperpolarizing responses of the MS neuron. The behaviour of the neuron under current injection conditions is a re-representation of the IV relationship shown in the previous section. It does show more clearly the difference in gradient of the down-up state transition under conditions of different constant current. It also shows the slowly developing ramp in the up state plateau potential which is a result of the inactivation of I_{Ksi}.

The model displays the following similarities to the experimental results:

- A resting potential just below -80mV.
- Rectification of the membrane potential in response to hyperpolarizing current pulses.
- A rise to the up state in approximately 60-70ms (note the time scales are different on the two components of the figure).
- A slowly developing ramp depolarization in response to slightly sub-threshold current pulse

In the experimental data the largest injected current is sufficient to produce a spike. As

this model does not feature sodium currents there is no spiking, but this does give an indication of where the threshold for presumed spikes could be set in the model.

The main discrepancy is that the return from the up state to the down state when the current injection is stopped is much slower in the model neuron than in the electrophysiological data. This is due to the lack of sodium currents in the model. Since this does not affect the area of interest in the modelled neuron, which is the transition from the down to the up state and the time to firing of the first spike, this can be ignored in the simulations.

A.

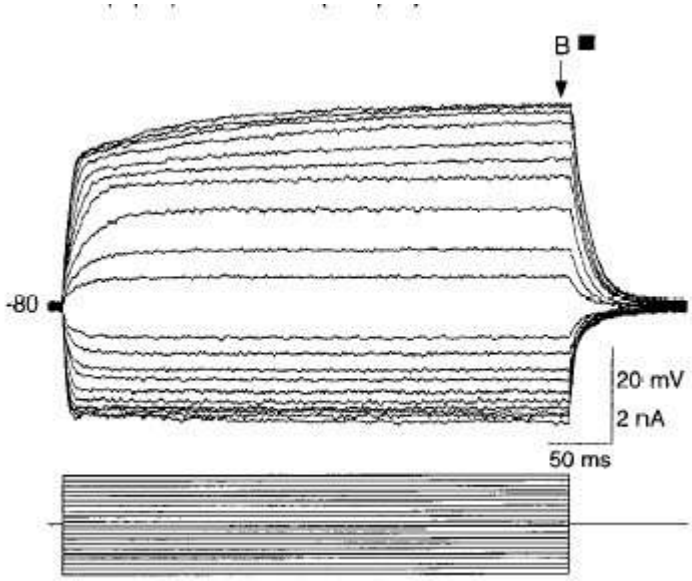

B.

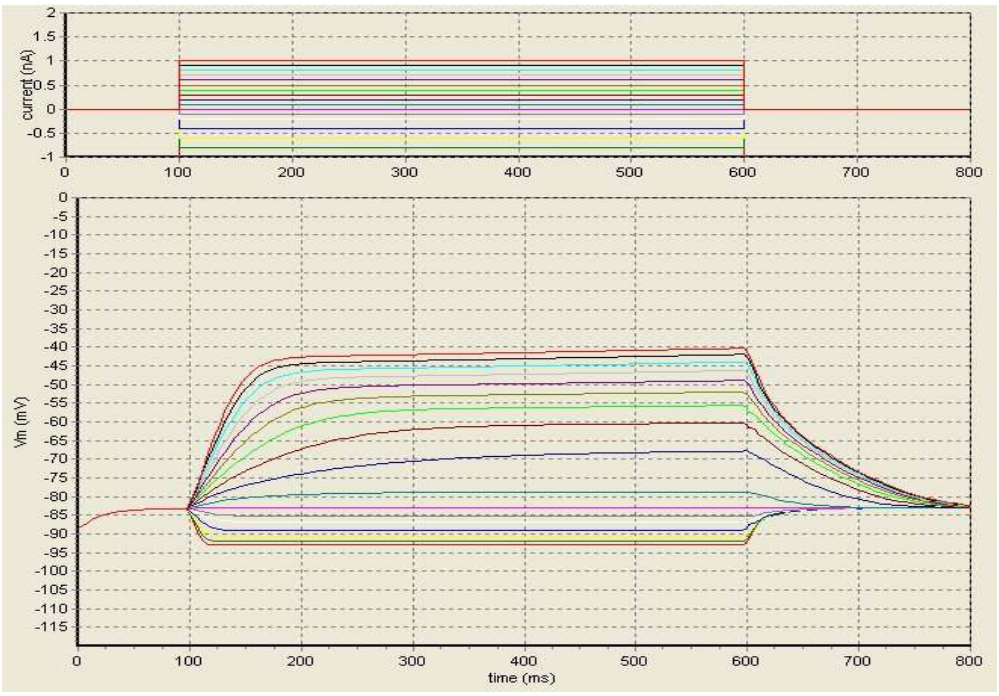

Figure 3-2: Comparison of electrophysiological (a) (acknowledged to Nisenbaum and Wilson[138]) and model (b) response to current injection. The model neuron has a similar resting potential (~-80mV), rectification in response to hyperpolarizing current pulses, a rapid rise from the down state to the up state in response to depolarizing pulses and a gradually rising plateau potential during the period of excitation . The return to the resting potential after excitation ceases is slower in the model neuron.

3.4 State Transitions

Comparison of state transitions is more subjective than the two previous methods of comparison. Neurons in slice preparations display variation in such characteristics as resting potential, plateau potential and amount of noise in the up state. This could be due to factors such as the methods used to produce the preparations.

The model neuron could be configured to produce quite widely variable values for the resting state and plateau membrane potentials by changing the parameters for the calcium and potassium currents. It has not been considered necessary to show this here as variations in the resting and plateau membrane potentials amongst neurons does not affect the general arguments proposed in the following sections.

The state transitions in the current injection state in the model are similar to the experimental data. A comparison of the state transitions with those produced by Wilson and Kawaguchi[133] using in vivo intracellular recordings of spontaneous activity is shown in Figure 3-3. As well as the rapid rise to the up state and the more gradual decay back to the down state, this also shows the delay to the first action potential in the up state commonly seen in vivo recordings and reproduced here in the model. The amount of noise seen in the up state is less in the model neuron than in the experimental preparation. This is probably not an artefact as the noise in the down state is much less than the noise in the up state. It may well be due to other factors, such as effects of inhibition, variations in the conduction of excitation to different parts of the dendritic tree or fluctuations in neuromodulators.

The figures for the membrane potential in the up and down state are here taken from Wilson and Kawaguchi (1996)[133]. These values were measured in slice preparations and may not agree with other figures produced by different groups in different preparations. Nevertheless, as most of the data for the individual currents that are used in constructing the model were also produced by the same group, these are the figures that will be used for reference in these studies.

A.

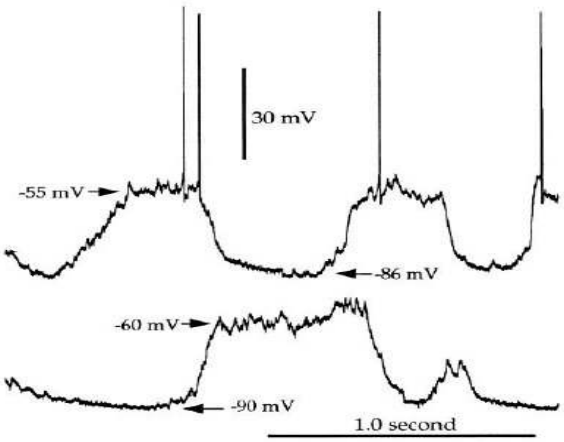

B.

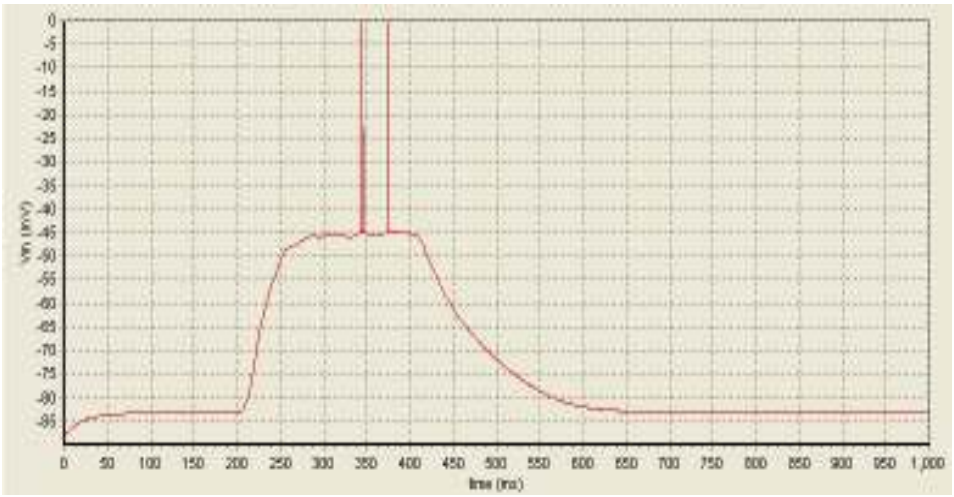

Figure 3-3: Comparison of electrophysiological (a) (acknowledged to Wilson and Kawaguchi[133]) and model (b) state transitions. The in vivo neurons display a degree of variation in characteristics. The model neuron replicates some of those characteristics; the rapid rise seen in the second down-up transition in vivo, the delay to firing in the up state seen in the first down-up transition, and a low spike count in the up state seen in all the in vivo up states where the neuron fired. The firing threshold is higher in the model neuron although this value could be set to the same value as in the in vivo neuron with some adjustment of the potassium and calcium current parameters.

3.5 Conclusions

The model medium spiny neuron replicates the relevant characteristics of known medium spiny neuron electrophysiological data sufficiently well to make it suitable for use in simulations investigating the filtering properties of the state transitions and the time to firing of the first spike.

4 Effect of Parameter Variation on MS Model Properties

The previous two chapters detailed the development of the MS model and showed that it replicated experimental data. The following chapters use the computational model in a series of simulations.

This chapter first details some aspects of the user interface of the simulator used in order to aid in interpretation of the figures used in the simulation results, and then considers how the timing of the first action potential and the plateau membrane potential vary with some of the parameters used to characterize the model behaviour.

4.1 Interpretation of Spiny Neuron Simulator Results

The simulator is supplied on the accompanying CD. Whilst screen captures of the simulator are shown for some simulations in this document, many of the simulations are best viewed as an animation using the simulator itself The simulator can be installed on any personal computer running the Windows™ operating system (Windows 95 and above) by running SimulatorSetup.exe. The program will, by default, be installed in the location C:\Program Files\Martin Guthrie\. The program can be started by clicking Start -> Programs -> Martin Guthrie -> Spiny Neuron Simulator. The ini files for setting up the parameters for replicating simulations are also installed in the same directory using the setup program and can be loaded from the load button on the toolbar. All buttons for controlling the program have hints which should enable easy discovery of the operation of this simulator.

The effect of varying parameters on ionic currents and voltage dependencies can be seen by clicking View -> Ionic currents. Similarly, to test varying parameters on current injection and view the IV relationship produced click View -> Current injection. All parameters are available for inspection and modification on the various undocked toolbars.

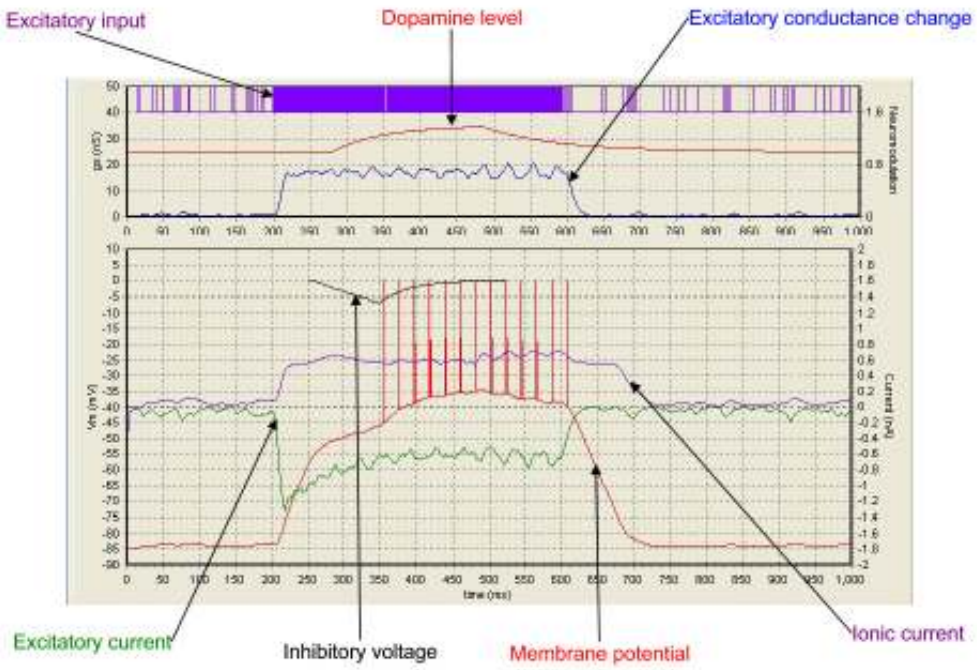

Figure 4-1 Screen capture of simulator output. The excitatory input spikes are shown in purple at the top. During the period of high excitation (200-600m) the density of spikes is too high to distinguish individual inputs. The dopamine level is shown in red in the upper graph. This shows an exponential rise from a base level of 1 to a peak level of 1.4 (right hand scale) occurring over a period of 300ms and then an exponential decay back to the baseline value over a period of ~200ms. The excitatory conductance due to the synaptic input is shown in blue in the upper graph, rising from a level close to zero with the low frequency input to approximately18nS under conditions of high excitation, although with much noise reflection the randomness of the input train. The excitatory current due to this excitatory conductance change is shown in green in the lower graph (right hand scale). The negative peak in excitatory current shortly after the start of the high excitation period is due to the hyperpolarized membrane potential at this point in time and decreases as the membrane potential rises. The ionic current is shown in purple on the lower graph (right hand scale). This is the current due to the sum of all the potassium, calcium and leakage currents. The membrane potential is shown in red on the bottom graph (left hand scale). The change to membrane potential caused by inhibition is shown in black on the lower graph (left hand scale).

Figure 4-1 shows an annotated screen capture of a typical run from the simulator. The following lines are shown on the two charts:

4.1.1 Excitatory input.

This is in purple at the top of the upper graph and shows a spike for each simulated afferent excitatory input pulse. The excitation is here modelled as 100 separate inputs, each firing at 25Hz. The start time and duration of excitatory input are user defined,

here shown starting at 200ms into the simulation and lasting for 400ms.

The inputs can be set to occur randomly or non-randomly. When they are set to be non-random, each input fires in turn at a time defined by their input frequency divided by the number of inputs. So in the example of 100 inputs firing at 25Hz, an input would occur every 0.4ms. When the inputs are random, they have three random factors defining their firing, as detailed sub-section 2.3.10, page 25. Each input is firing at a random frequency with a mean of 25Hz and a standard deviation of 2Hz. The time of the first spike when the excitation period starts is staggered by a random number between zero and the period of firing of the individual neuron (the mean of which is 40ms). After the first spike, there is a user defined jitter for the firing of each input. A random amount between ± the input jitter is added to the time of each input spike subsequent to the first.

An expanded view of the input train under the random conditions detailed is shown in Figure 4-2. This section of 50ms shows approximately 125 excitatory inputs occurring and gives an indication of how the programmed randomness affects the afferent spike train. No analysis has been done of the randomness of this train.

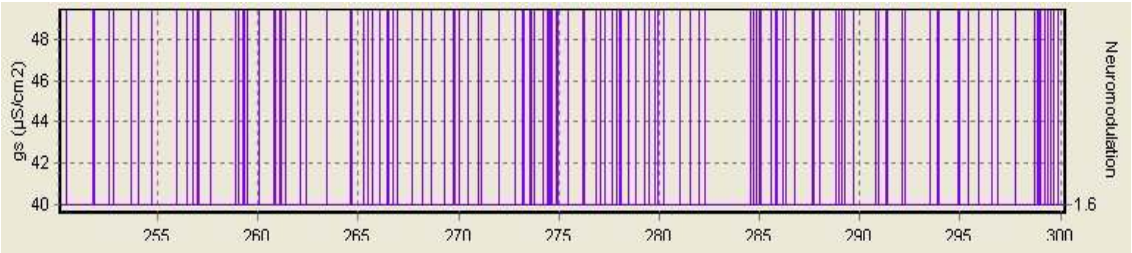

Figure 4-2 Expanded view of modelled random excitatory train. This is an expansion of fifty milliseconds of the high excitation shown in Figure 4-1, resolving the solid mass of spikes seen in that figure into single action potentials. This illustrates the random nature of the excitatory input.

4.1.2 Excitatory conductance change

Also shown in the top chart, as the blue line, is the excitatory conductance change due to the excitatory inputs. In these simulations the timing of each excitatory input is first calculated over the duration of the simulation. Each occurrence of an input then has four user defined characteristics; the maximum amplitude, the rise time, the decay time and the number of multiples of the decay time that the input is used for. The excitatory conductances of each input at each time step are then added to give the overall excitatory conductance change seen in the simulator. The scale is shown on the left of

the upper graph.

4.1.3 Dopamine level

As discussed previously (sub-section 2.3.6, page 22), the dopamine level affects two of the currents used in these simulations, the inwardly rectifying potassium current I_{Kir} and the L-type calcium current $I_{L\text{-}Ca}$. The change in dopamine level is modelled as an exponential rise and an exponential decay. The time constants for the exponential rise and decay are taken from amperometric in-vivo measurements of dopamine release[169]. The dopamine level is shown in red on the upper graph and the scale is on the right-hand vertical axis.

An upper bound for the dopamine effect on these currents of 1.4 is taken from physiological data of the maximal effect of D1 receptor stimulation on the L-type calcium current[160].

4.1.4 Excitatory current

In the lower chart the excitatory current is the current due to the excitatory conductance changes and is shown in green. This is plotted against the right-hand vertical axis.

4.1.5 Ionic current

The ionic current is the total current due to the opening of ion channels. This is the sum of the currents due to the potassium, calcium and leakage currents and is determined by the equations from the previous chapter. This is plotted in purple on the lower graph and also uses the right-hand vertical axis.

4.1.6 Membrane potential

This is the end result of all the conductance changes and ionic currents and the main point of interest in these simulations. All the other lines plotted are mainly to give confidence in the trajectory of the membrane potential and can be turned off in the simulator if desired. This is plotted in red on the lower graph and uses the left-hand vertical axis.

4.1.7 Inhibitory voltage

This is the effect that the inhibitory burst has on the membrane potential. The derivation

of the constants for this calculation is explained in chapter 5. The timing of the inhibitory burst is known at the start of the simulation so can be pre-calculated before the dynamic effects of the excitatory conductance changes are considered. The inhibitory voltage is subtracted from the membrane potential due to the excitation at each time step. This is shown in black on the lower graph and uses the left-hand vertical axis.

4.2 Simulations

In this section, for each variable parameter, the name of the ini file used to replicate the simulation is given to enable simulations to be easily replicated. For each simulation using that ini file, key user settings are laid out in a table at the start of the description of the simulation. Variables that are changed between simulations whilst still using the same ini file are shown in bold type.

Each simulation is run with non-random excitatory input to isolate the effects of the parameter variation. Excitatory events therefore occur at regular intervals, determined by the number of synapses and the frequency that they fire at. To avoid coincident synaptic events from separate synapses, the start time for the first synaptic event at each synapse is staggered by the period between synaptic events for one synapse divided by the number of synapses. For instance, with 100 inputs firing at 25Hz gives a regular spike train input at 2.5kHz.

It is only necessary to run each step of the simulation once with non-random excitation as the time to the first spike is identical on every repeat.

Where plateau potentials are shown, they are measured 200ms after the start of excitation, with firing turned off in the model.

The parameters considered in these simulations are:

- Membrane capacitance.
- Environmental temperature.
- Leakage conductance.
- Excitation frequency with and without a dopamine pulse.

- Varying tonic dopamine levels.
- Half activation, slope and maximum conductance variables for each of the ionic currents.

4.2.1 Varying Membrane Capacitance

Ini File: Cm.ini

Setting	State
Variable parameter	Membrane capacitance
Start value	0.5μF/cm^2
End value	3μF/cm^2
Step size	0.1μF/cm^2
Dopamine pulse	No
Inhibition	Off

Table 4-1 Settings for variable membrane capacitance

From (4.1) it can be seen that the membrane capacitance acts as a multiplier for the 1st derivative of the membrane potential. So changing the membrane capacitance should change the rate of change of membrane potential in the simulation, and this is the case found here.

$$-C\frac{dV_m}{dt} = \mu\left(I_{Kir2} + I_{L-Ca}\right) + I_{Ksi} + I_{Krp} + I_L + I_S \tag{4.1}$$

This has the effect, shown in Figure 4-3, of linearly increasing the time to the first action potential as the capacitance increases. Increasing the membrane capacitance delays the firing by slowing the state transitions, as shown in the extreme case with a membrane capacitance of 3μF in Figure 4-4.

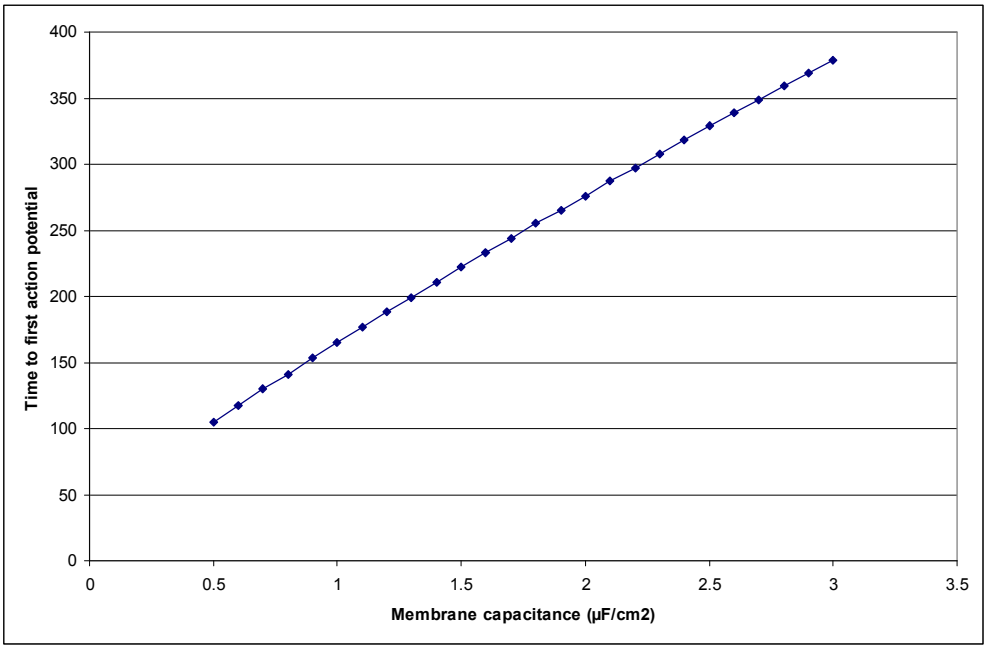

Figure 4-3 Variation of earliest action potential with membrane capacitance. The linear relationship between the membrane capacitance and time to first action potential is expected as increasing the membrane capacitance slows the rate of change of membrane potential linearly.

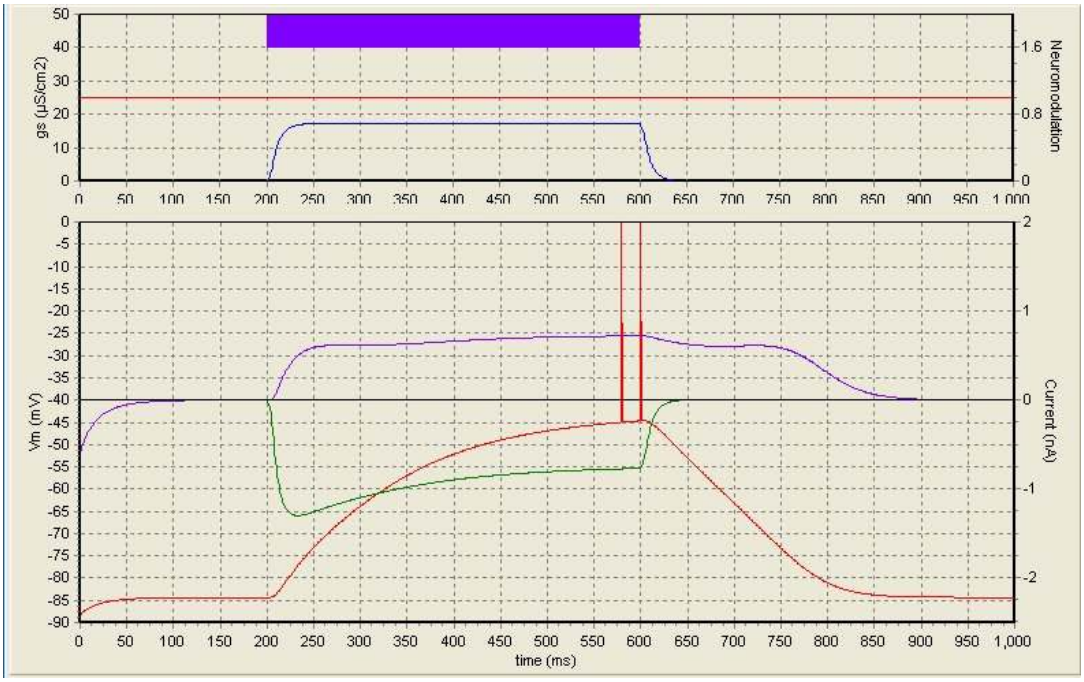

Figure 4-4 State transition with 3µF membrane capacitance. With a high membrane capacitance the transition from down to up state is no longer rapid and only just reaches the firing threshold before the end of the excitatory period. The high membrane capacitance also slows the transition from the up to down state after the excitation has finished, causing the ionic current to remain active for a prolonged period.

4.2.2 Varying Environmental Temperature

Ini File: Temperature.ini

Setting	State
Variable parameter	Temperature
Start value	20°C
End value	40°C
Step size	1°C
Dopamine pulse	No
Inhibition	Off

Table 4-2 Settings for varying environmental temperature

Changing the temperature affects the L-type calcium current as it is used as a factor in the Goldman-Hodgkin-Katz equation.

$$\gamma = \frac{z^2 F^2 V_m}{RT} \cdot \left([Ca]_i - [Ca]_o \cdot \left(\frac{-zFV_m / RT}{1 - e^{-zFV_m / RT}} \right) \right) \tag{4.2}$$

In the range 20 to 50°C this effect is very small when the ionic currents are plotted (Figure 4-5 - left line is at 20°C, right line is at 50°C), but it does have an effect on the plateau membrane potential produced, as shown in Figure 4-6.

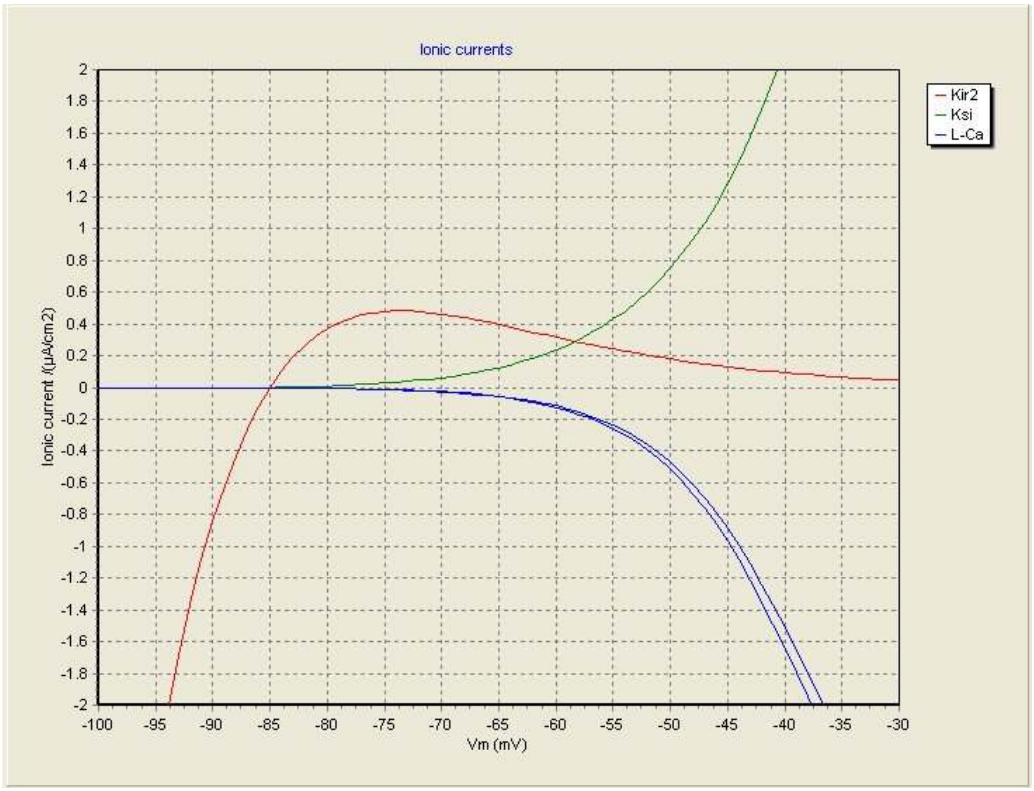

Figure 4-5 Variation of calcium current with temperature. The blue lines show the L-type calcium current at 20°C on the left and at 50°C on the right. There is an increase of 1mV in membrane potential at an ionic current of 1µA/cm^2 as the temperature is increased.

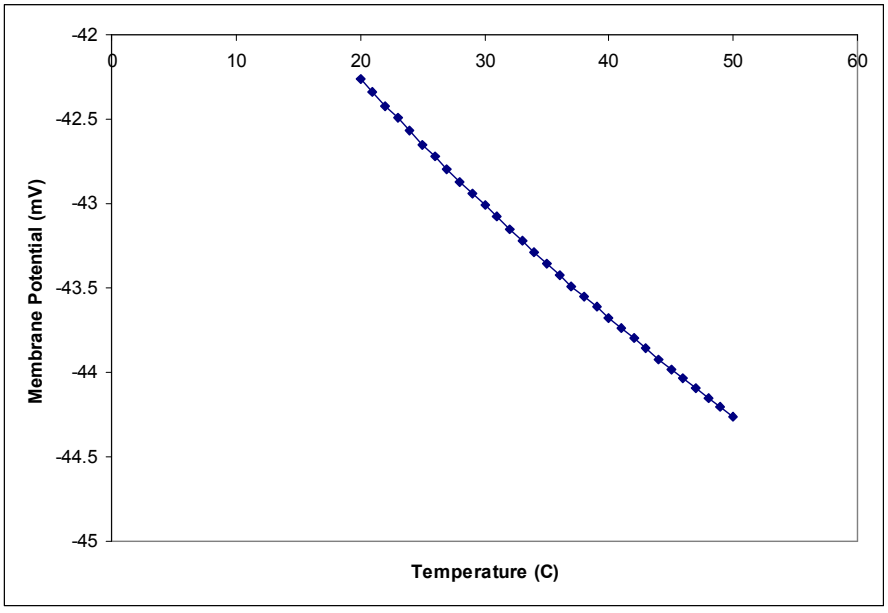

Figure 4-6 Variation of plateau membrane potential with temperature. Despite the relatively small changes in membrane potential induced by changing temperature seen in Figure 4-5, varying the temperature from 20 to 50°C changes the plateau membrane potential by -2mV.

4.2.3 Varying Leakage Conductance

Ini File: Leakage.ini

Setting	State
Variable parameter	Leakage conductance
Start value	0.016 mS/cm^2
End value	0.002 mS/cm^2
Step size	-0.001 mS/cm^2
Excitation Random	No
Dopamine pulse	No
Inhibition	Off

Table 4-3 Settings for varying leakage conductance

In the simulations where ionic conductance parameters are varied, the effect is of changing one of the factors in the Boltzmann function:

$$g_i = \frac{\bar{g}}{1 + e^{\left(\frac{-(V_m - V_h)}{V_c}\right)}} \tag{4.3}$$

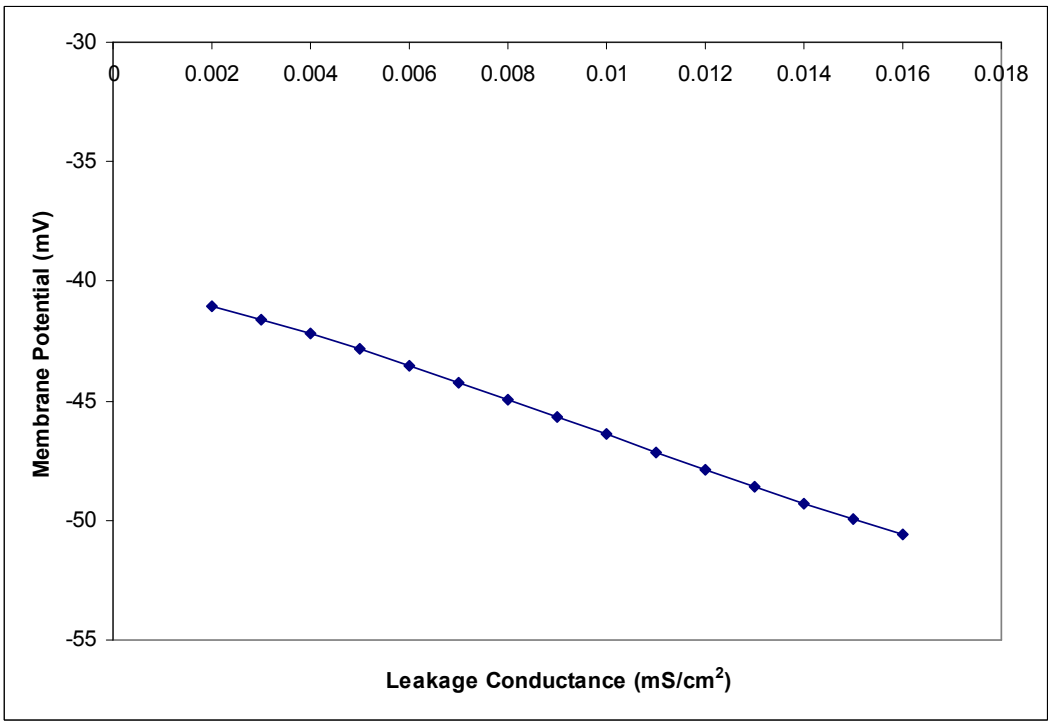

Figure 4-7 Variation of plateau membrane potential with leakage conductance. Changing the leakage current linearly changes the plateau membrane potential.

Unlike the potassium conductances, the leakage conductance is not voltage dependent.

At hyperpolarized potentials, it produces a small outward current and at more depolarized potentials an inward current. The relationship shown in Figure 4-7 demonstrates a linear change in plateau membrane potential.

4.2.4 Varying Excitation Frequency

Ini File: ExcitationFrequency.ini

In this section the simulations show how changing the excitation frequency that leads to the up state affects the timing of the first action potential and how adding a dopamine pulse and inhibition change that timing. Changing the excitation frequency changes the synaptic current in (5.1)

4.2.4.1 Varying excitation frequency with no dopamine pulse or inhibition

Setting	State
Variable parameter	Up state excitation frequency
Start value	25Hz
End value	35Hz
Step size	0.1Hz
Excitation Random	No
Dopamine pulse	No
Inhibition	Off

Table 4-4 Settings for varying excitation frequency with no dopamine pulse or inhibition

Figure 4-8 shows the simulator as it reaches the point where excitation becomes sufficient for action potentials start to occur. Note that in this simulation that there is no dopamine pulse (red line in the top graph) and that, because the excitation is non-random, the excitatory conductance reaches a plateau and then is unvarying until the excitation reverts to the lower level (blue line on upper graph).

Of interest in this simulation is the time delay to the first action potential. This is due to the kinetics of the slowly inactivating potassium current (I_{Ksi}). As Figure 4-9 shows, the action potential first appears at the end of the excitation period and gradually becomes earlier as the frequency of excitation is increased. Over the range 25.5-28Hz this variation in timing of the first action potential is roughly linear. Above this frequency the first action potential starts to occur on the non-linear shoulder of the transition from down to up state.

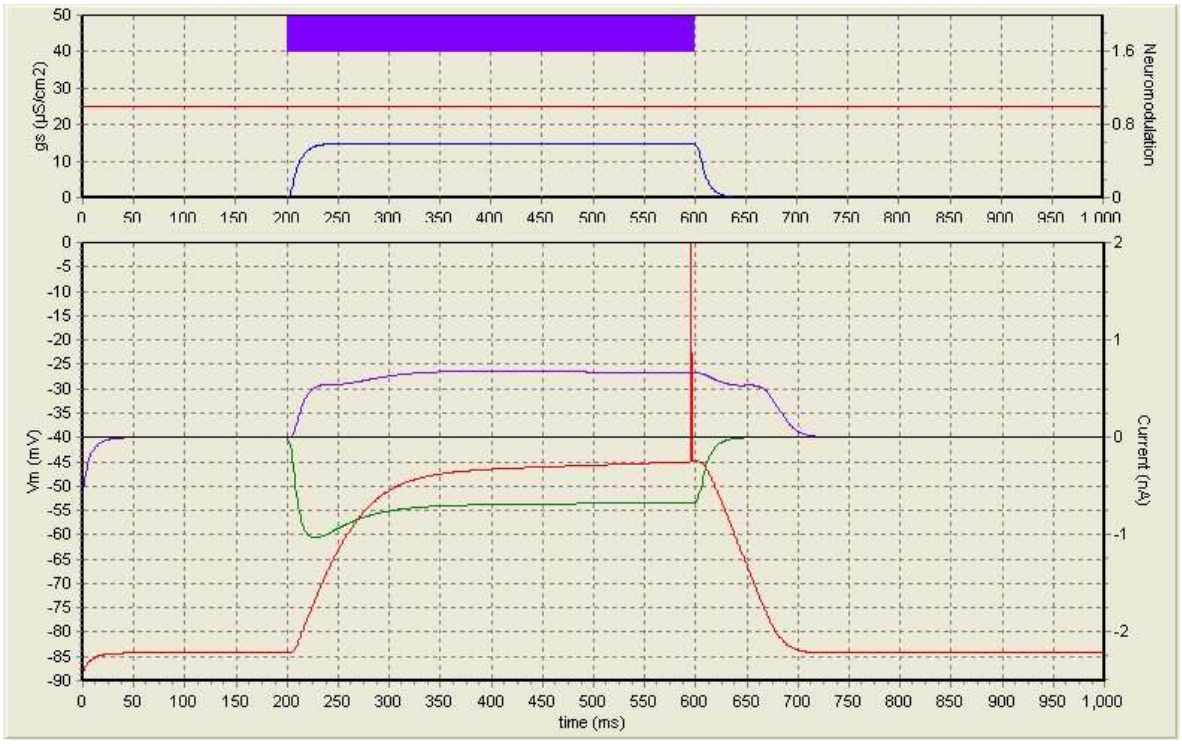

Figure 4-8 As the excitation frequency is increased step by step, the first action potential occurs at 25.5Hz excitation frequency with 100 inputs. The action potential occurs at the end of the up state as the ramp in plateau potential just brings the membrane potential to the firing threshold before the high level of excitation finishes.

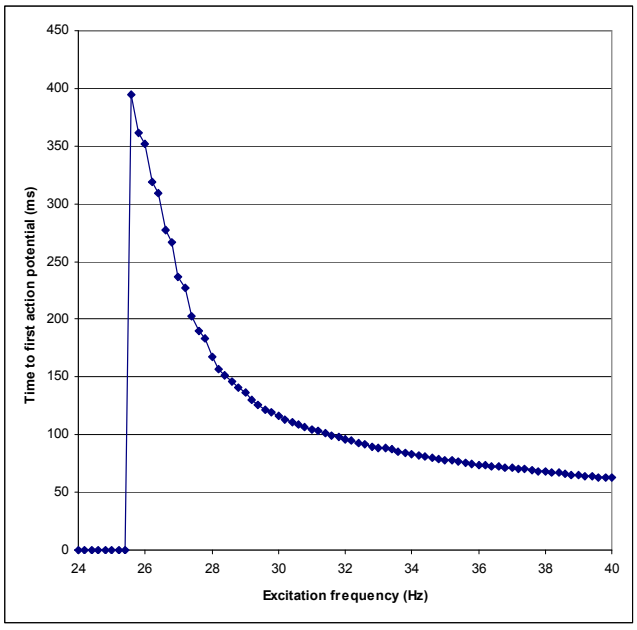

Figure 4-9 Variation of first action potential time with up state excitation frequency - no dopamine pulse. The first action potential occurs at 25.5Hz and then occurs earlier as the excitation frequency is increased, with a rapid decrease in time to first action potential with only small changes in firing frequency occurring at first.

4.2.4.2 Varying excitation frequency with a dopamine pulse during excitation

Setting	State
Variable parameter	Up state excitation frequency
Start value	15Hz
End value	30Hz
Step size	0.2Hz
Excitation Random	No
Dopamine pulse	**Yes - starting at 280ms**
Inhibition	Off

Table 4-5 Settings for varying excitation frequency with a dopamine pulse during excitation

In this simulation the dopamine pulse has been turned on. The dopamine pulse affects both the outwardly rectifying potassium current I_{Kir} and the L-type calcium current as shown in Figure 4-10. In this figure ionic currents are shown for two levels of dopamine, 1.0 and 1.4. These are simply the factor that the current is multiplied by, but due to the non-linear nature of the currents, the effect of the dopamine varies across the membrane potential range shown.

In Figure 4-10 the I_{Kir} current is shown in red. The upper line in the area of interest for these simulations (-90mV to -45mV) is due to the higher neuromodulation level (1.4 times baseline level). The neuromodulatory effect is strongest at membrane potentials during the state transition, which would tend to oppose the change from down to up state. Note that at the resting membrane potential, there is virtually no neuromodulatory effect.

In contrast, the L-type calcium current, shown in blue is made more strongly negative by the higher level of neuromodulation. However, for the calcium current, the neuromodulatory effect does not come into play until about -65mV and then increases as threshold is approached. This would tend to have the effect of maintaining the cell in the up state as well as increasing the plateau membrane potential.

Changing the parameters of these two currents does not change the point at which the calcium current becomes stronger than the inward rectifying potassium current. In both the lower and higher neuromodulatory states, the two currents balance at approximately -55mV.

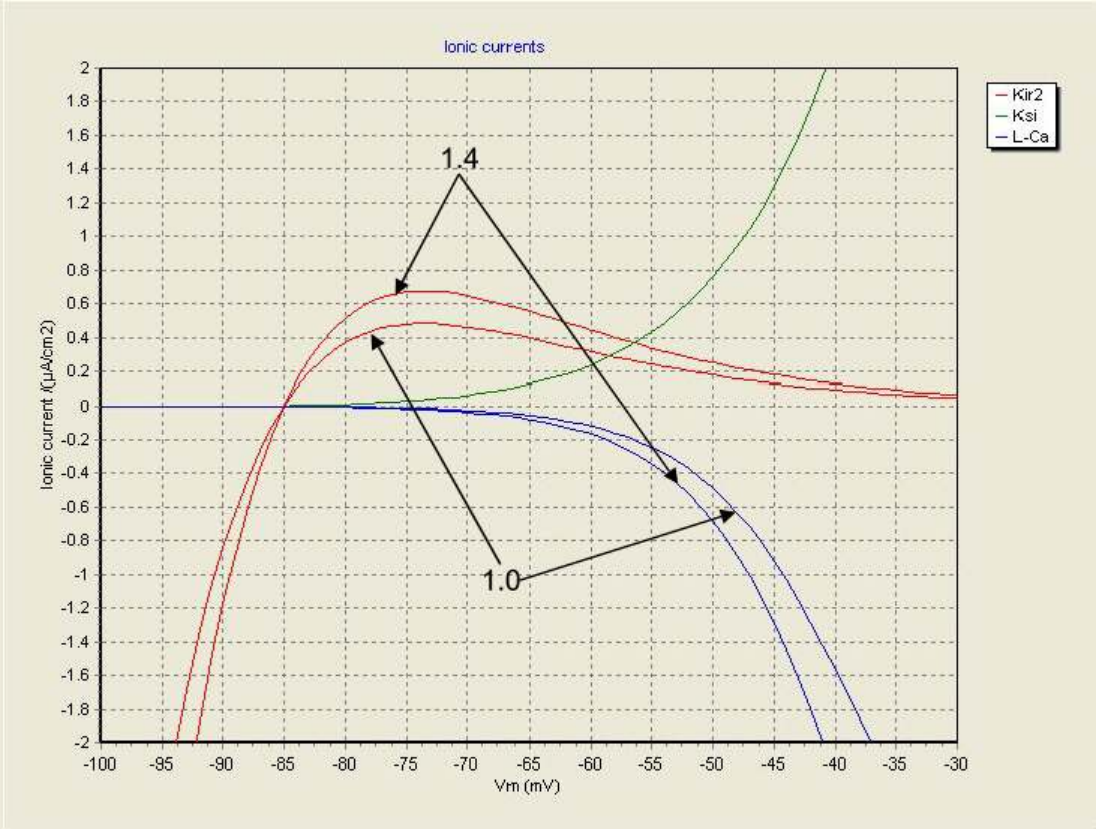

Figure 4-10 Ionic Currents - Effect of dopamine level on I_{Kir} and $I_{L\text{-}Ca}$ currents. Red: I_{Kir}, Blue: L-type calcium, Green: I_{Ksi}. Increasing the dopamine level raises the current produced by the inward rectifying potassium current at voltages close to the resting, down state but has little effect on this current near threshold. Conversely, increasing dopamine level modifies the L-type calcium current close to the threshold potential. The effect is to decrease the current due to this ion near threshold. The calcium current is negligible at membrane potentials around the resting state and the dopamine level therefore has little effect on the L-type calcium current in the down state.

In this simulation where the excitation is varied, the dopamine pulse occurs during the period of high excitation and is modelled as an exponential increase followed by an exponential decay. The simulation in Figure 4-11 shows an increase in membrane potential during the dopamine pulse. The excitation frequency in the simulation step shown was 20Hz, in Figure 4-11A. with no dopamine pulse and in Figure 4-11B. with a dopamine pulse. This shows that the dopamine first causes a small flattening of the down to up state trajectory, then as the membrane potential rises above -55mV, the dopamine pulse boosts the membrane potential above the firing threshold, which does not occur with this frequency of excitation without the dopamine pulse.

A.

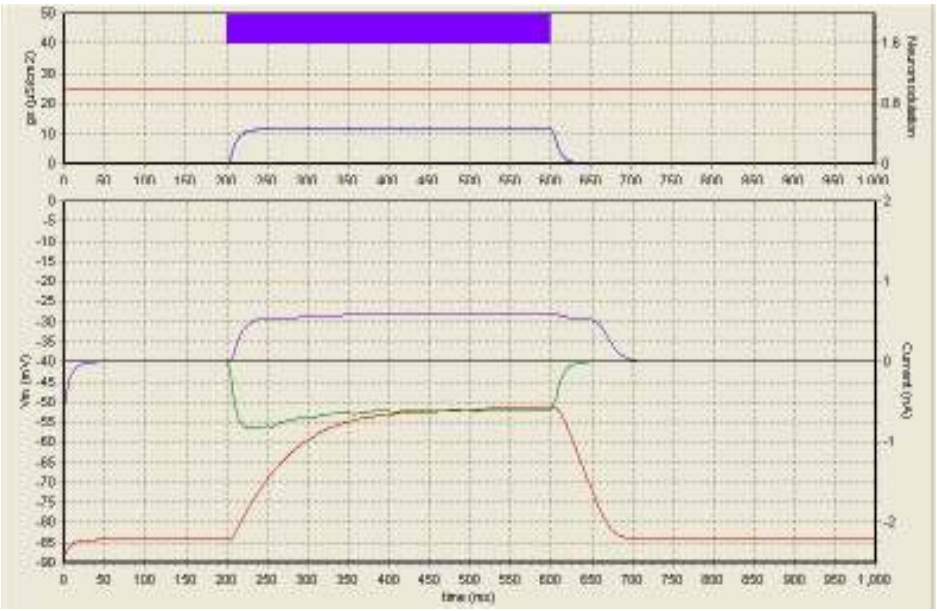

B.

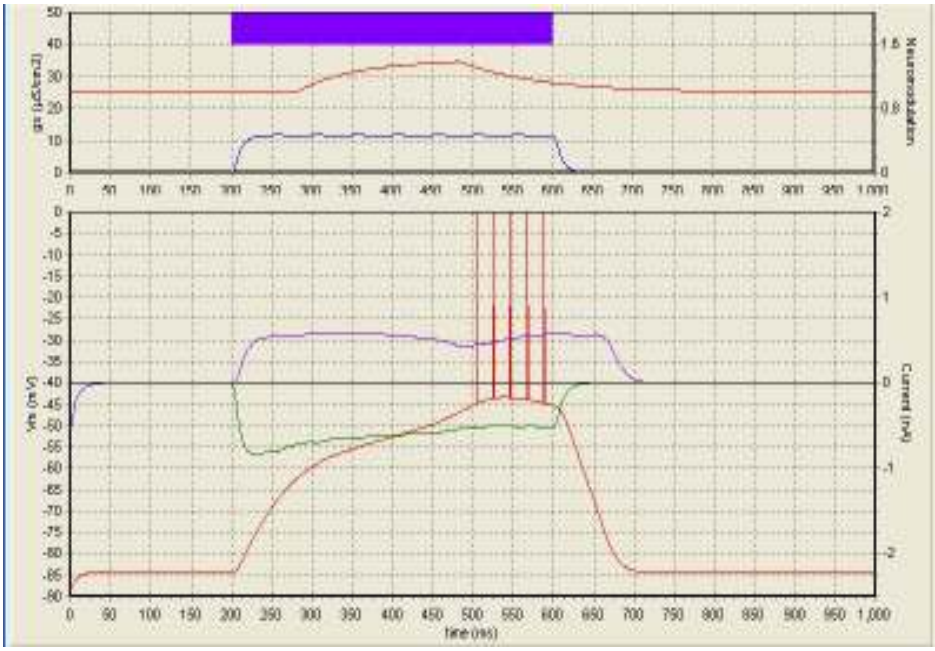

Figure 4-11: Effect of dopamine on up state membrane potential and firing - excitation frequency 20Hz. A. No dopamine pulse. B. Dopamine pulse present. With an excitation frequency of 20Hz there are no action potentials in the up state when the dopamine level remains at 1. However, when a pulse of dopamine occurs coincident with the MS neuron up state, the plateau membrane potential is increased and action potentials start just after the dopamine level has reached its maximum.

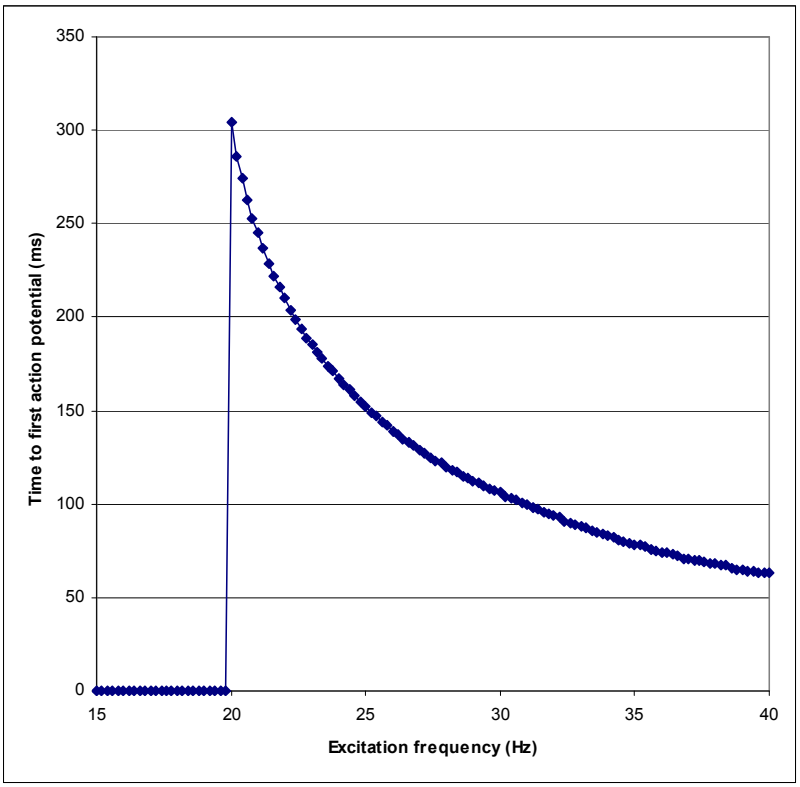

Figure 4-12 Variation of first action potential time with up state excitation frequency - dopamine pulse starting at 280ms. In comparison with Figure 4-9, where there is no dopamine pulse, action potentials start to occur at a lower excitation frequency. The decrease in time to first action potential as the excitation is increased is very similar to Figure 4-9.

Figure 4-12 shows how the timing of the first spike varies with excitation frequency when there is a dopamine pulse present during the excitation.

4.2.4.3 Varying excitation frequency with a dopamine pulse starting before excitation

Setting	**State**
Variable parameter	Up state excitation frequency
Start value	15Hz
End value	30Hz
Step size	0.2Hz
Excitation Random	No
Dopamine pulse	**Yes - starting at 50ms**
Inhibition	Off

Table 4-6 Settings for varying excitation frequency with a dopamine pulse starting before excitation

In this simulation the dopamine pulse was started before the period of high excitation. Of interest here is the evolution of the up state as the frequency is increased. Figure 4-13 and Figure 4-14 show the simulation with the excitation frequency at 20Hz and 24Hz. In the 20Hz step, where the dopamine is having little or no effect, at the end of the excitatory period, the excitation has been sufficient to change the state of the MS neuron under simulation from the down to the up state. However, where the dopamine is having the most effect, the MS neuron is kept in transition, well below firing threshold.

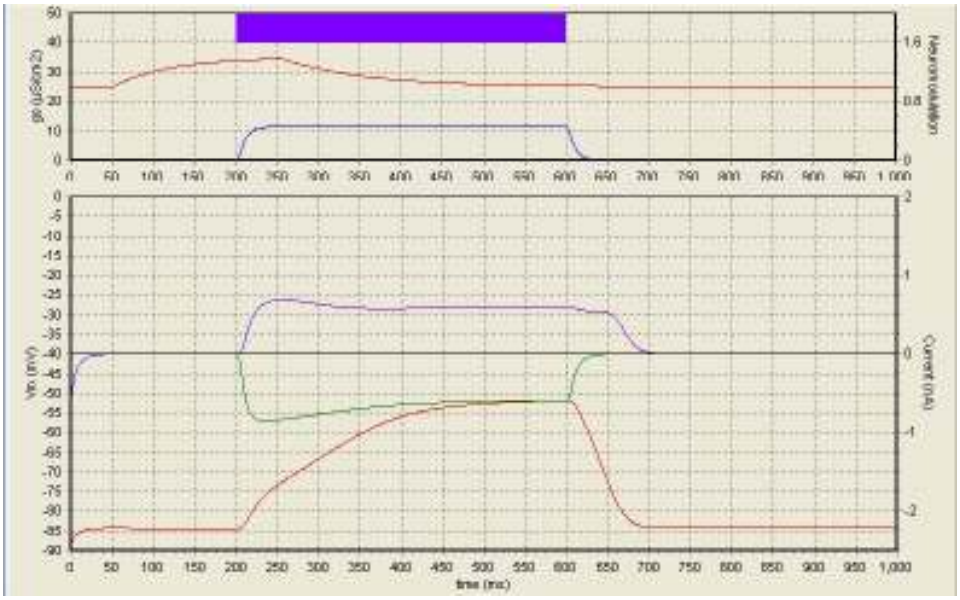

Figure 4-13 Effect of dopamine on stabilizing down state membrane potential - excitation frequency 20Hz. This should be compared to Figure 4-11 where the dopamine pulse occurs during the up state. In this case, rather than causing the first action potential to occur at a lower excitation frequency, the pulse of dopamine occurring before the up state is reached delays the transition to the up state.

In the 25.4Hz step, due to a slight overshoot effect in membrane potential negating the ramp effect of the inactivating potassium current as the dopamine level falls back to background level, the first action potential appears early in the up state, rather than at the end as in the case with no dopamine pulse.

Figure 4-15 shows how the timing of the first spike varies with excitation frequency when there is a dopamine pulse present starting before the excitation.

Figure 4-16 compares the time of the first action potential in the three previous simulations, with no dopamine pulse, with a dopamine pulse during the up state and

with a dopamine pulse starting during the down state.

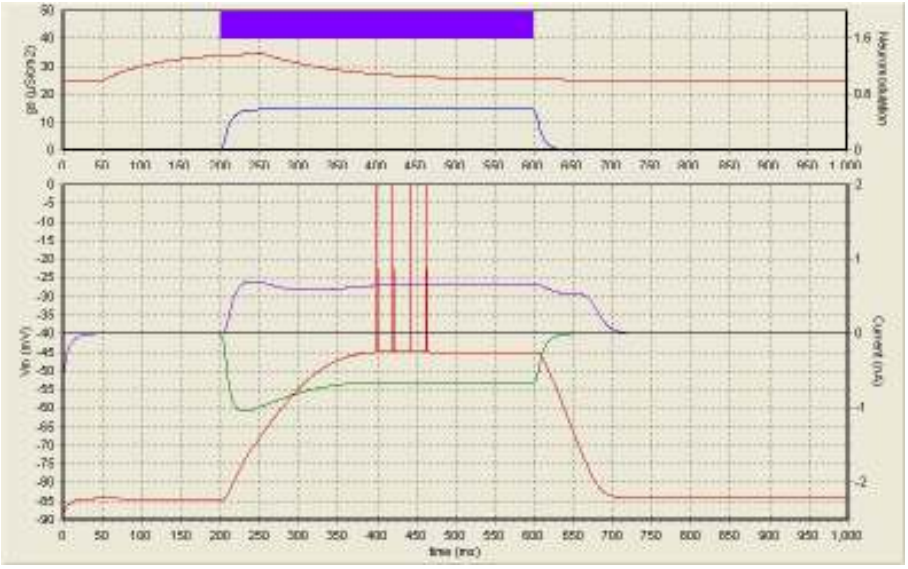

Figure 4-14 Effect of dopamine on stabilizing down state membrane potential - excitation frequency 25.4Hz. With the dopamine pulse occurring just before the high level of excitation starts, the frequency at which the first action potential occurs is slightly lower compared to the situation with no dopamine pulse. However the first action potential occurs much earlier in the up state than when no dopamine pulse is present.

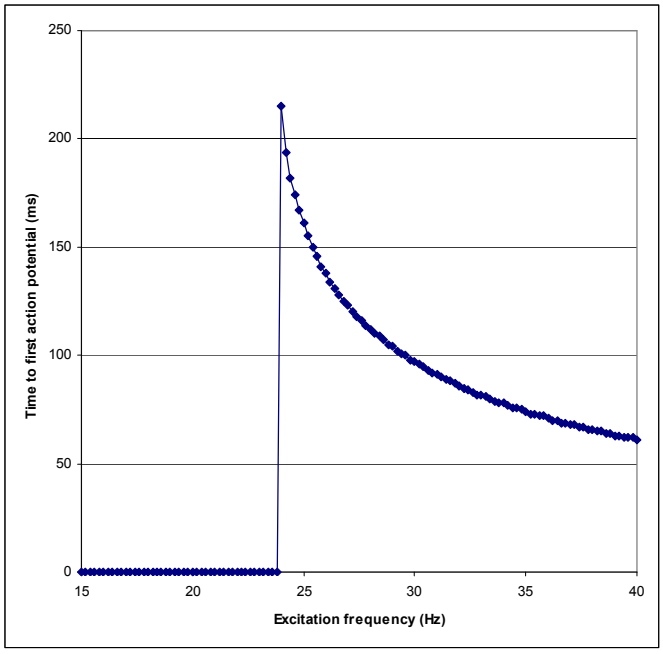

Figure 4-15 Variation of first action potential time with up state excitation frequency - dopamine pulse starting at 100ms. The excitation frequency at which the first action potential occurs is slightly lower than when there is no dopamine pulse, but the first action potential occurs 220ms after the start of excitation compared to the 390ms shown in Figure 4-9 when there was no dopamine pulse.

With the dopamine pulse occurring during the up state, the excitation frequency at which action potentials start to appear is lower than in the case with no dopamine pulse. But due to the effects of the dopamine pulse on the calcium current, the first action potential occurs earlier, as shown in Figure 4-11B.

With the dopamine pulse occurring in the down state, the excitation frequency at which the action potential first appears is only slightly changed, but the time after the start of excitation of the first action potential is much earlier, as shown above in Figure 4-14.

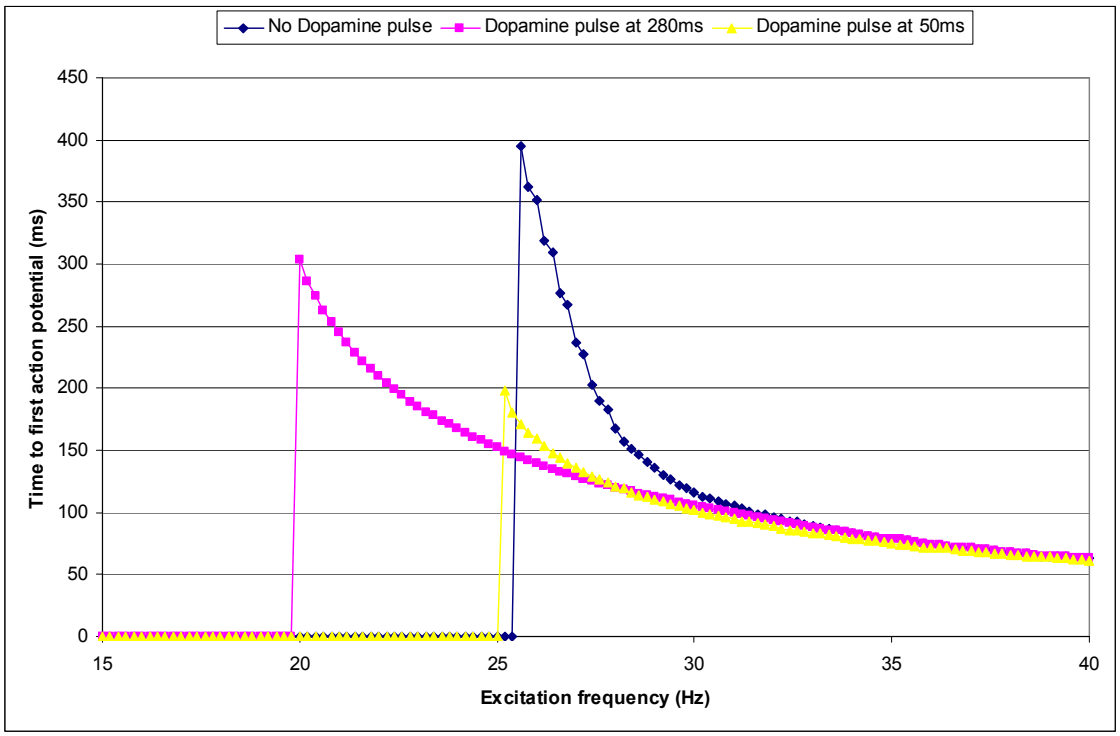

Figure 4-16 Comparison of timing of first action potential with differing timing of dopamine pulse. With no dopamine pulse present, the first action potential occurs at the highest frequency of excitation and latest after the start of excitation. A dopamine pulse occurring during the up state causes the first action potential to occur at a lower frequency and earlier in the excitatory period. A dopamine pulse before the start of the up state causes the excitatory frequency at which the first action potential is seen to be slightly lower than when there is no dopamine pulse, but nowhere near as low as with a dopamine pulse in the up state. However the dopamine pulse in the down state causes the first action potential to occur much earlier after the start of excitation compared to either of the other two conditions.

4.2.5 *Varying tonic dopamine level*

Ini file: DopamineLevel.ini

These simulations show how varying the tonic level of dopamine affects the timing of the first action potential.

Setting	State
Variable parameter	Tonic dopamine level
Start value	0.7
End value	1.4
Step size	0.05
Excitation Random	No
Dopamine pulse	No
Inhibition	Off

Table 4-7: Settings for varying tonic dopamine level

The tonic level of dopamine was varied alongside a range of excitation frequencies from 20 to 34Hz.

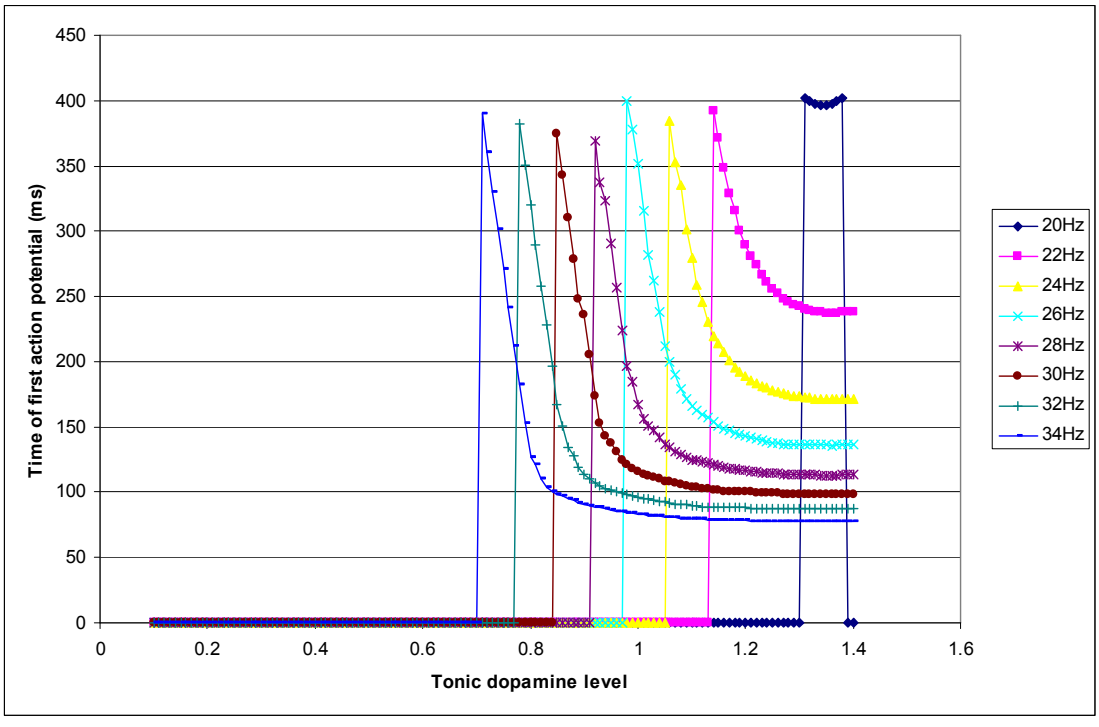

Figure 4-17 Variation of timing of first action potential with dopamine level at a range of excitation frequencies. As the dopamine level is decreased the excitation frequency required to produce an action potential before the end of the excitation period increases. The time after the start of excitation that the first action potential occurs remains relatively constant.

Figure 4-17 shows the results of several simulations run at a range of frequencies. Generally, higher tonic dopamine levels required less excitation to produce an action potential. The time of the first action potential was little changed, varying between 369 and 402ms after the start of excitation.

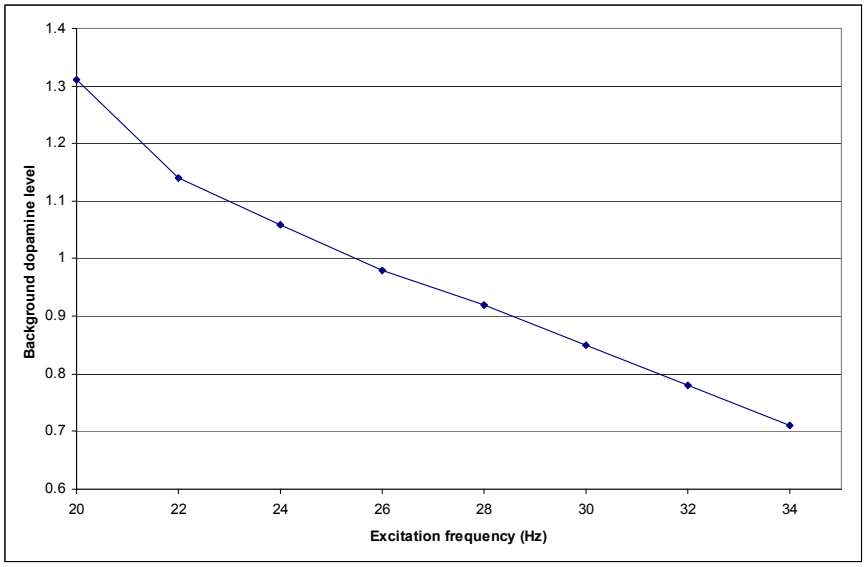

Figure 4-18 Variation of the excitation frequency at which the first action potential occurred with tonic dopamine level. This figure plots the dopamine level at which the first action potential occurred for each excitation frequency. These are the peaks seen in Figure 4-17 when the time of action potential rises abruptly from zero to approximately 400ms after the start of excitation.

From Figure 4-18 it can be seen that the excitation frequency at which the first action potential occurred was linearly related to the tonic dopamine level over much of the frequency range. This suggests that the product of the excitation frequency with the tonic dopamine level gives a constant. This constant has to be exceeded for firing to occur.

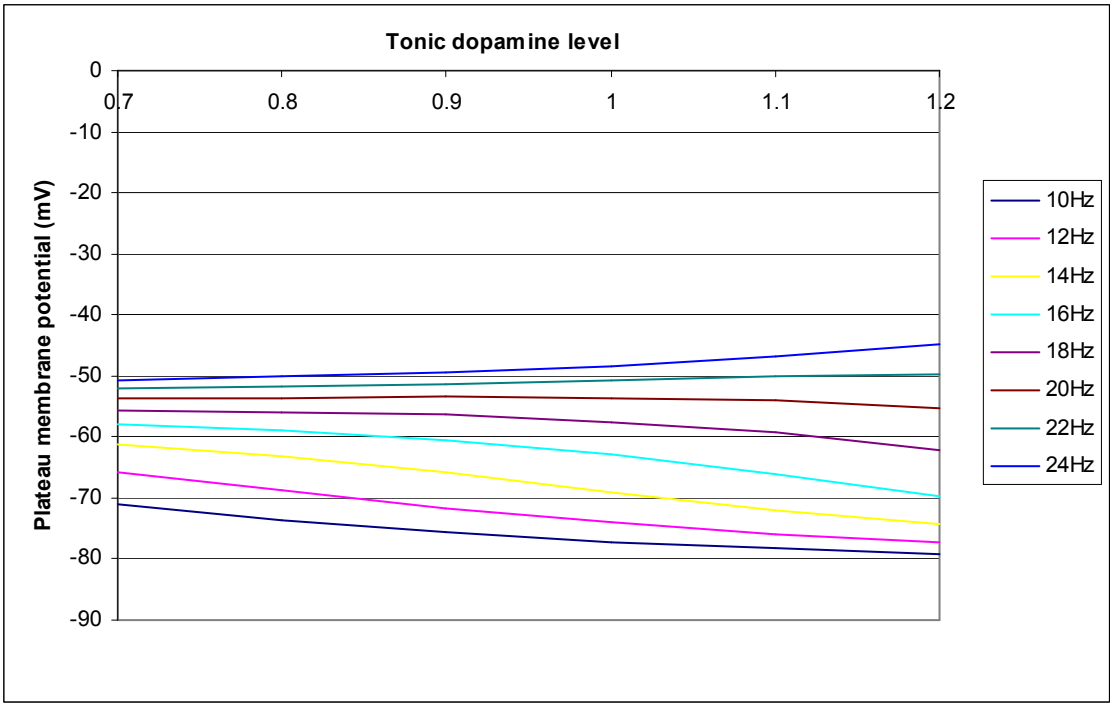

Figure 4-19 Variation of plateau membrane potential with tonic dopamine level at a range of excitatory input frequencies. For higher excitation frequencies the plateau membrane potential decreases across the range of tonic dopamine levels. For lower excitation frequencies the plateau membrane potential increases with increasing dopamine level. There is a switchover point at an excitation frequency just below 22Hz.

At higher frequencies, as shown in Figure 4-18, firing starts to occur above a threshold tonic dopamine level. The next simulation considers the effect of tonic dopamine on the plateau membrane potential with lower frequencies of excitatory input. Figure 4-19 shows that with excitatory input frequencies 20Hz and below (brown line), increasing the tonic dopamine level decreases the plateau membrane potential. Above 20Hz increasing tonic dopamine increases plateau membrane potential.

4.2.6 Varying potassium current parameters

In this section the simulations show how changing the values of the parameters governing the shape of the curve for the potassium currents affect the membrane potential in the up state. Again varying these parameters affects the Boltzmann function in (4.3).

4.2.6.1 Varying I_{Ksi} V_h

Ini File: Ksi Vh.ini

Setting	State
Variable parameter	I_{Ksi} V_h
Start value	-15mV
End value	-12mV
Step size	0.1mV
Excitation Random	No
Dopamine pulse	No
Inhibition	Off

Table 4-8 Settings for varying I_{Ksi} V_h

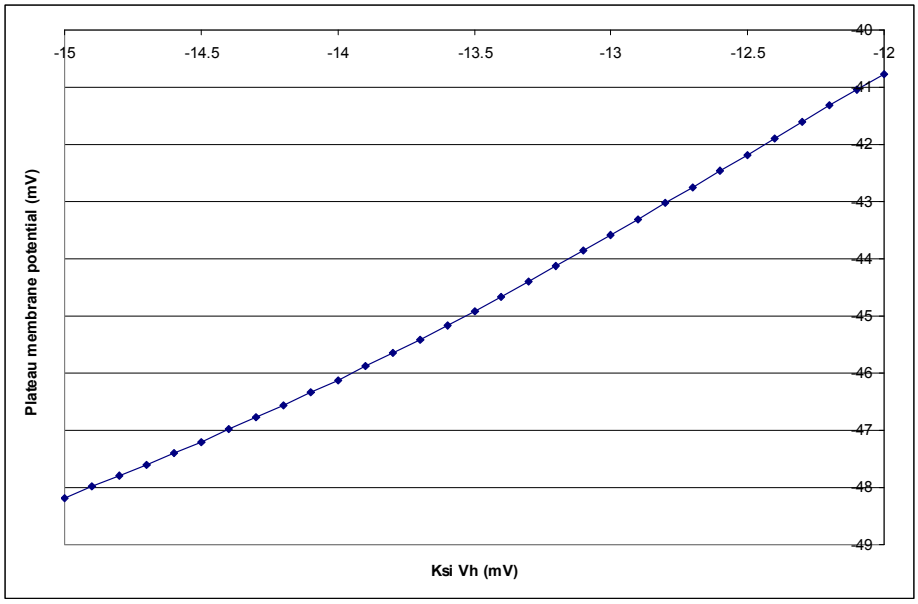

Figure 4-20 Variation of membrane potential with I_{Ksi} V_h. As the half activation point for the slowly inactivating potassium current is increased, the plateau membrane potential increases.

This simulation shows that as V_h becomes less negative, the plateau membrane potential in the up state also becomes less negative, in a fairly linear fashion.

4.2.6.2 Varying I_{Ksi} V_c

Ini File: Ksi Vc.ini

Setting	State
Variable parameter	I_{Ksi} V_c
Start value	13mV
End value	10mV
Step size	-0.1mV
Excitation Random	No
Dopamine pulse	No
Inhibition	Off

Table 4-9 Settings for varying I_{Ksi} Vc

This has a similar effect to varying I_{Ksi} V_h in changing the plateau membrane potential as shown in Figure 4-21.

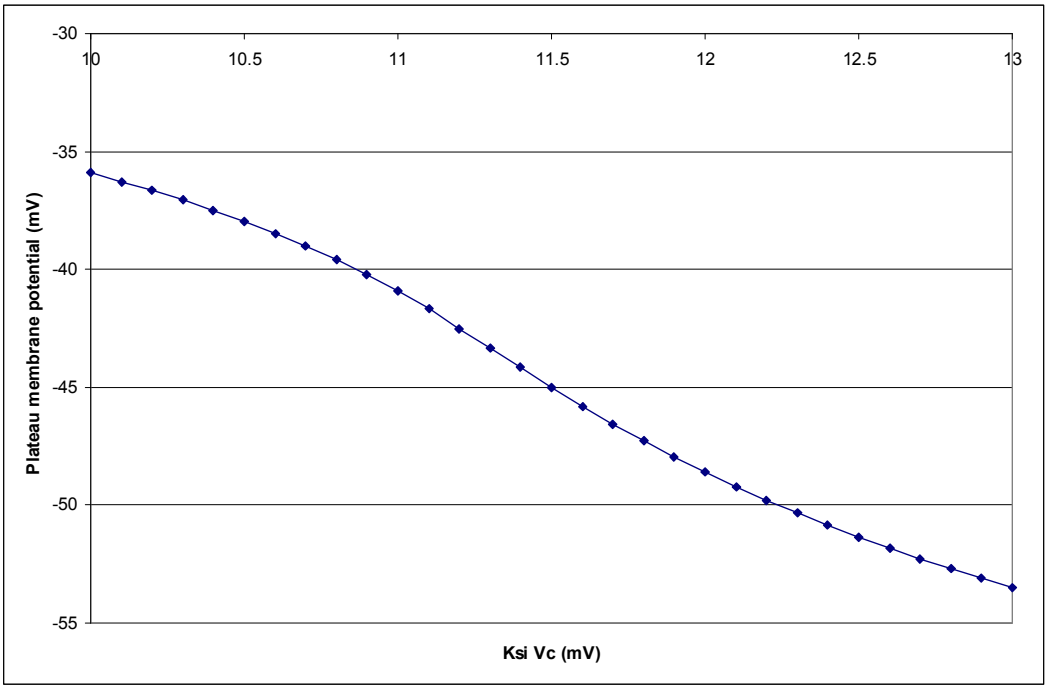

Figure 4-21 Variation of plateau membrane potential with I_{Ksi} V_c. Varying the slope of the slowly inactivating potassium current activation varies the plateau membrane potential. As the slope is increased, the plateau membrane potential decreases.

4.2.6.3 Varying I_{Ksi} Maximum conductance

Ini File: Ksi GMax.ini

Setting	State
Variable parameter	I_{Ksi} Max Conductance
Start value	0.7mS/cm^2
End value	0.4mS/cm^2
Step size	-0.02mS/cm^2
Excitation Random	No
Dopamine pulse	No
Inhibition	Off

Table 4-10 Settings for varying I_{Ksi} maximum conductance

Changing this parameter changes the maximum conductance attributable to the slowly inactivating potassium current. Figure 4-22 shows three maximum conductances; 0.6, 0.45 and 0.3 ms/cm^2, from left to right in green. Shifting this curve leftward by increasing the maximum conductance has the effect of bringing in the steeper part of the curve at a lower voltage. As can be seen, the current takes off in an exponential manner so the dynamics of the cell membrane potential will be very sensitive to bringing the steeper part of the curve below the firing threshold.

This effect can be seen from the plateau potential produced at each step of the maximum conductance shown in Figure 4-23. The value used in the simulations for the maximum I_{Ksi} conductance is 0.5mS/cm$^{2.}$. This gives a plateau potential at 200ms after the start of excitation of just below -46mV.This is just below the threshold used in the simulations. With the inactivation of the I_{Ksi} current, this rises to the firing threshold of -45mV at about 300ms after the start of excitation.

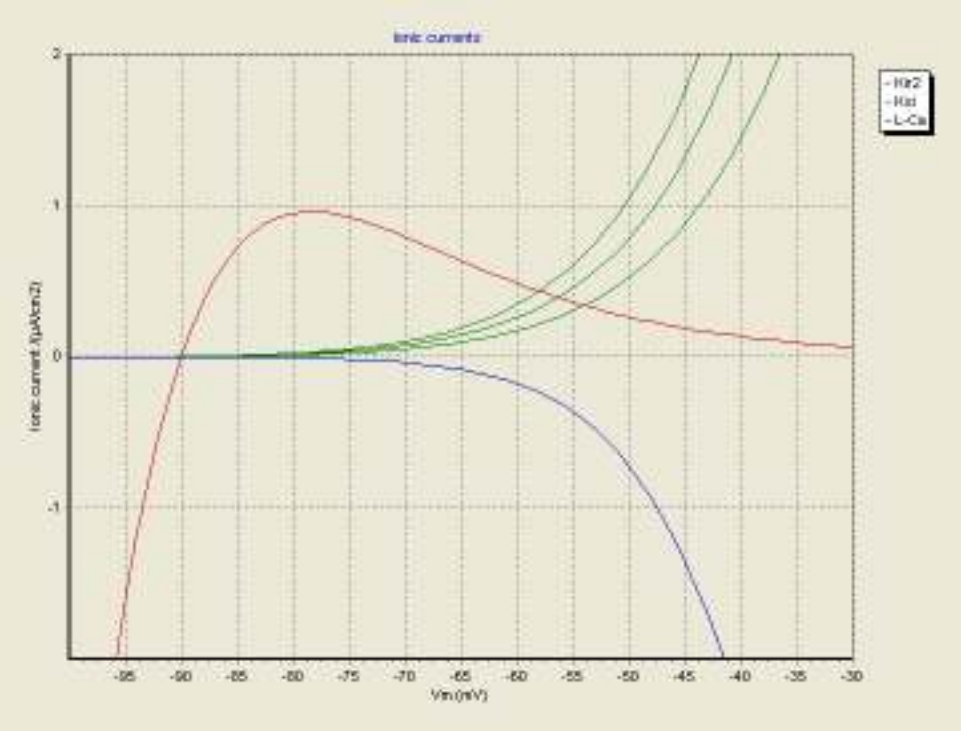

Figure 4-22 Ionic Currents - Effect of varying I_{Ksi} maximum conductance(green lines, using values of I_{Ksi} maximum conductances of 0.6, 0.45 and 0.3 ms/cm^2 from left to right). Increasing the maximum conductance causes this current to have a more significant activation at lower membrane potentials.

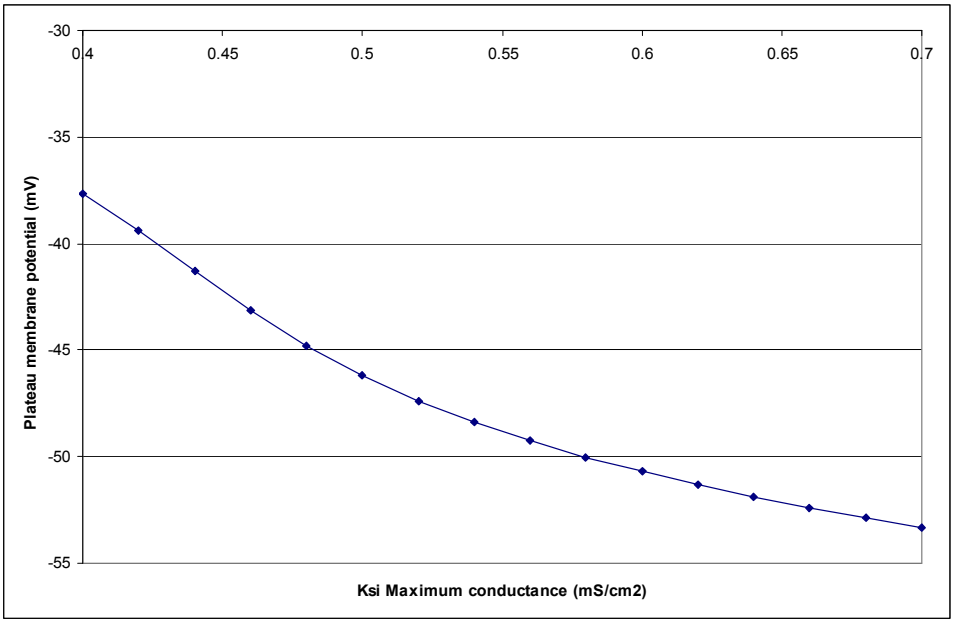

Figure 4-23 Variation of plateau membrane potential with I_{Ksi} maximum conductance. This is the plateau potential at 200ms after the start of excitation. As the current is inactivating, the plateau membrane potential will gradually rise. Increasing the maximum conductance of the slowly inactivating potassium current leads to a decreased plateau membrane potential, keeping the cell further away from the firing threshold.

4.2.6.4 Varying I_{Kir} V_h

Ini File: I_{Kir} Vh.ini

Setting	State
Variable parameter	I_{Kir} V_h
Start value	-100mV
End value	-120mV
Step size	-0.5mV
Excitation Random	No
Dopamine pulse	No
Inhibition	Off

Table 4-11 Settings for varying I_{Kir} V_h

Figure 4-24 shows how the voltage curve for the I_{Kir} current is shifted to the left as the value of V_h is decreased from -100mV to -120mV. The consequence of this is shown in Figure 4-25 where a more negative V_h leads to a lower ionic current.

This inwardly rectifying current keeps the membrane potential hyperpolarized, the peak rectifying current occurring at about -78mV. When the slowly inactivating current overcomes this, at about -55mV, the neuron is able to change from the down state to the up state. This is illustrated in Figure 4-26, which is a simulator snapshot at I_{Kir} V_h = -103mV. Here the I_{Kir} current dramatically slows the ramp potential.

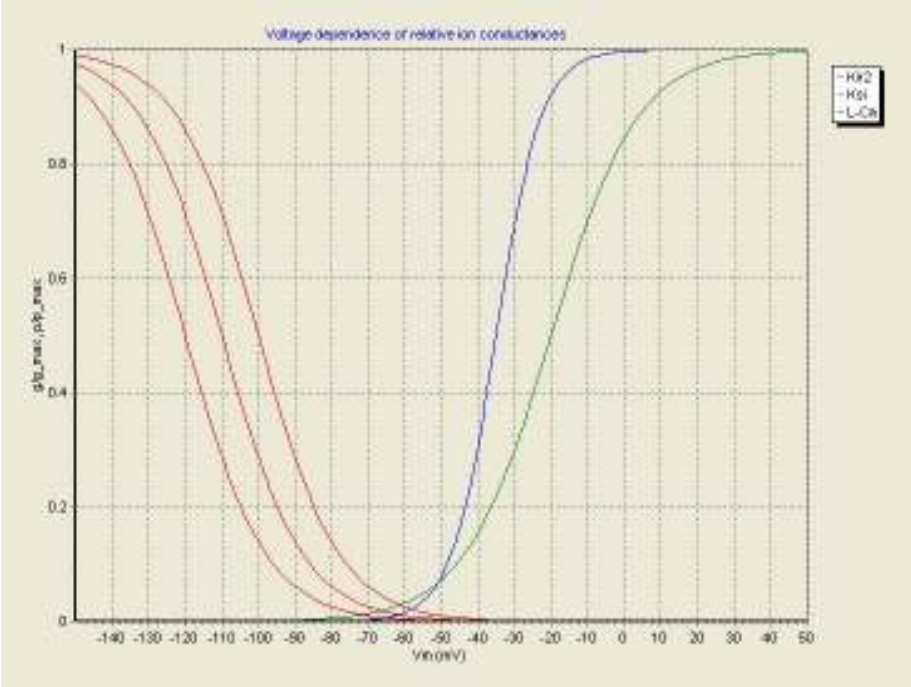

Figure 4-24 Voltage dependency of I_{Kir} conductance on V_h.Values used are -120, -110 and -100mV from left to right (red lines). Decreasing the half activation point of the inwardly rectifying potassium current moves the steepest part of the activation curve to higher membrane potentials and thus brings inward rectification into play at more positive membrane potentials.

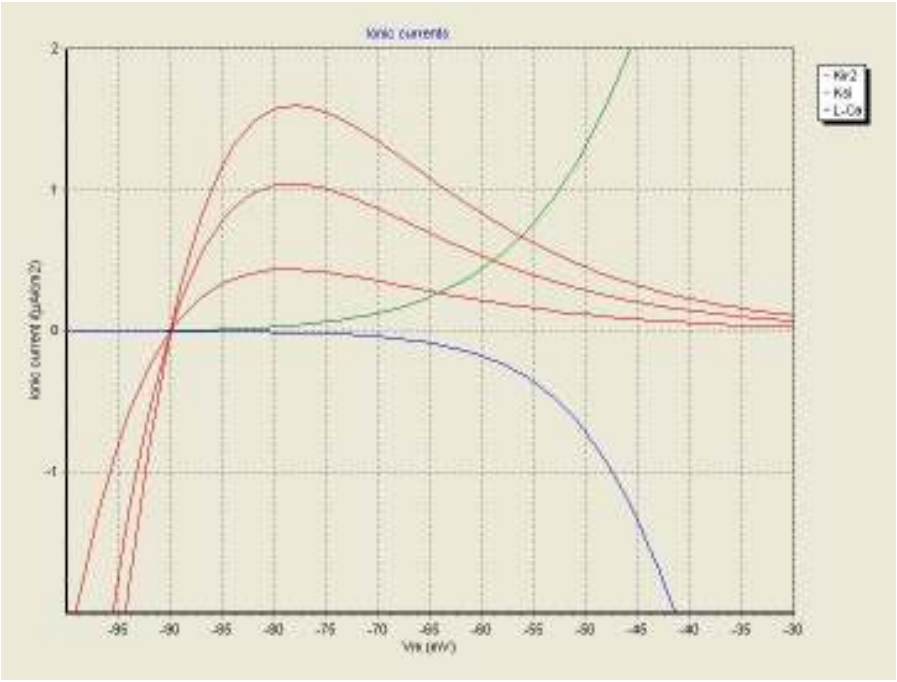

Figure 4-25 Ionic currents - dependency of I_{Kir} current on V_h (red lines). V_h values used are -100, -110 and -120mV from top to bottom at V_m = -80mV. A lower value of the half activation point for the inwardly rectifying potassium current produces a larger current at resting potentials, thus increasing the difficulty that excitation has in overcoming the inward rectification.

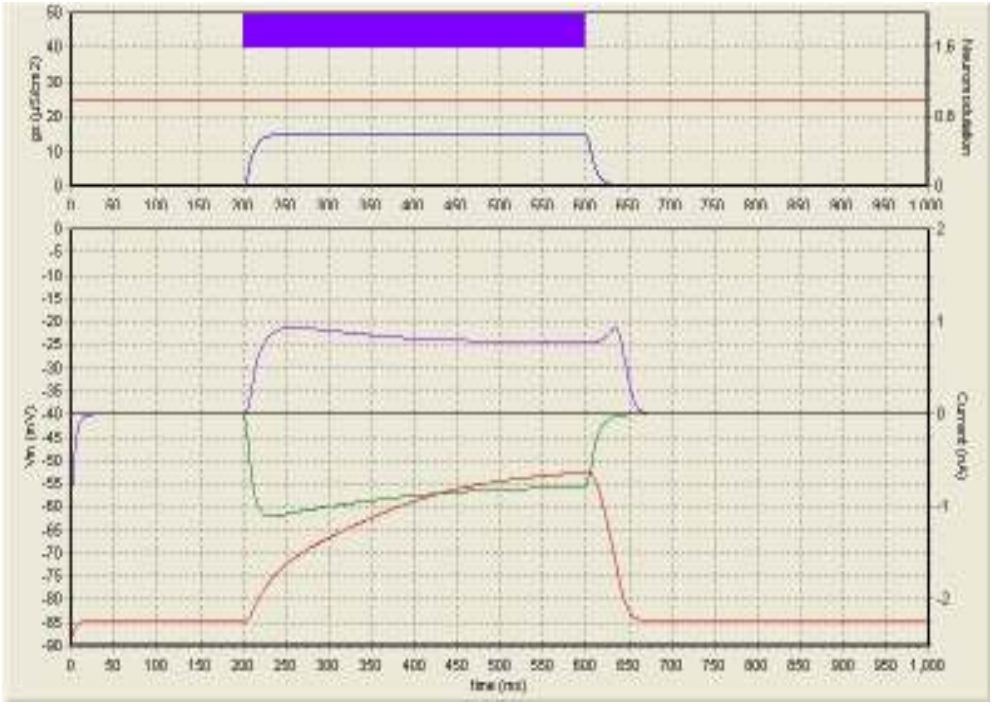

Figure 4-26 Membrane potential trajectory at I_{Kir} V_h = -103mV. The difficulty that excitation has in overcoming the inward rectification with lower values of half activation for the inwardly rectifying potassium current is illustrated here. The excitation cannot cause the usual rapid transit from the down to the up state due to the high level of inward rectification.

4.2.6.5 Varying I_{Kir} V_c

Ini File: Kir2 Vc.ini

Setting	State
Variable parameter	I_{Kir} V_c
Start value	-12mV
End value	-8mV
Step size	0.2mV
Excitation Random	No
Dopamine pulse	No
Inhibition	Off

Table 4-12 Settings for varying I_{Kir} Vc

Whereas decreasing I_{Kir} V_h shifts the voltage dependency curve to the left, decreasing I_{Kir} V_c decreases the gradient of the curve as shown in Figure 4-27 where I_{Kir} V_c is varied from -12mV to -8mV. This has the effect on the ionic current seen in Figure 4-28 where the zero crossover remains the same at -90mV, but higher inwardly rectifying currents are produced at more negative values of V_c, making it harder to depolarize the

neuron.

This leads to a similar effect to that seen with I_{Kir} V_h in Figure 4-26, except that the delay in the state transition is not so marked.

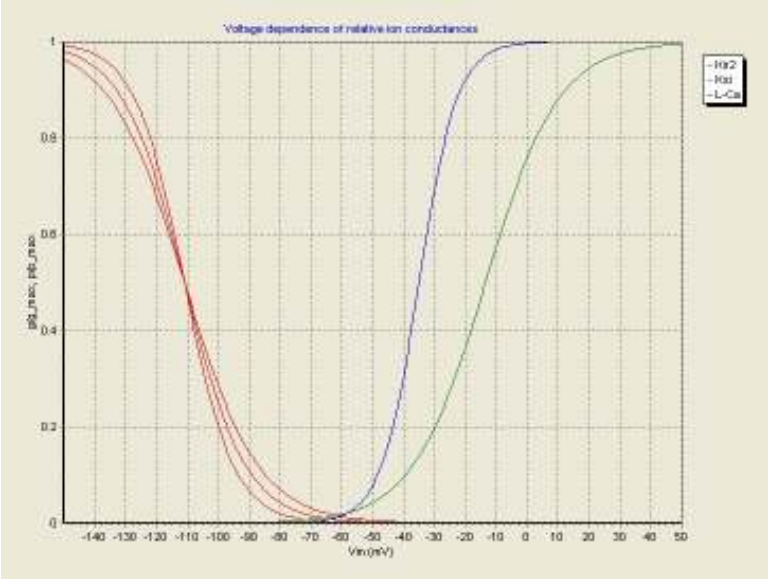

Figure 4-27 Voltage dependency of I_{Kir} conductance on V_c (red lines). Vc values shown here are -12, -10 and -8mV from left to right at g/gmax = 0.8. At resting membrane potentials decreasing the slope of the activation curve decreases the resistance to depolarization.

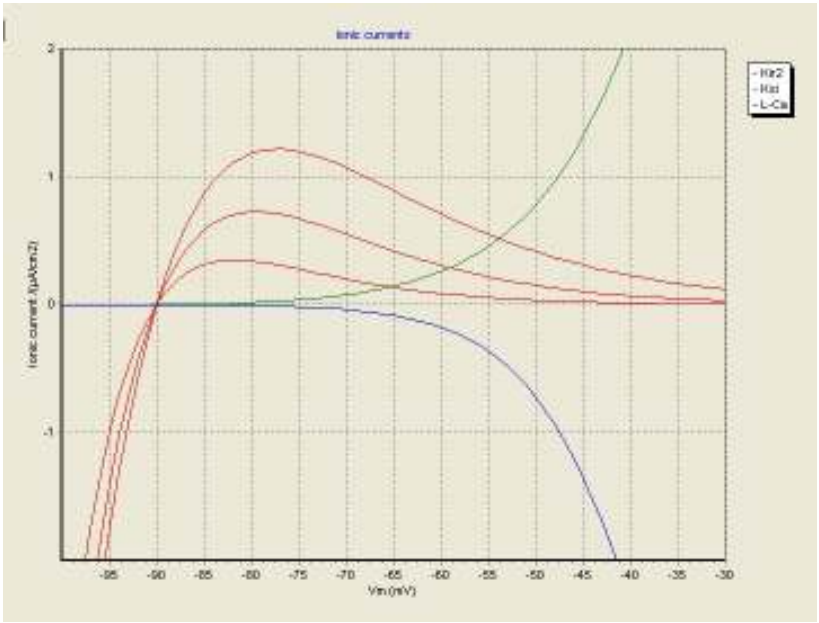

Figure 4-28 Ionic currents - dependency of I_{Kir} current on V_c. V_c values shown here are -12, -10 and -8mV from top to bottom at V_m = -80mV. The higher values for the slope of the activation curve for the inwardly rectifying potassium current lead to a greater current at resting membrane potentials, and therefore greater resistance to depolarization.

4.2.6.6 Varying I_{Kir} Maximum Conductance

Ini File: Kir2G Max.ini

Setting	State
Variable parameter	I_{Kir} Max Conductance
Start value	2.5mS/cm^2
End value	0.6mS/cm^2
Step size	-0.1mS/cm^2
Excitation Random	No
Dopamine pulse	No
Inhibition	Off

Table 4-13 Settings for varying I_{Kir} maximum conductance

The effect of varying the maximum conductance is very similar to varying I_{Kir} V_h, producing a very similar membrane trajectory effect to that seen in Figure 4-26.

4.2.7 Varying calcium current parameters

In contrast to the two potassium currents so far seen, the calcium current provides an inward, depolarizing drive.

4.2.7.1 Varying Calcium V_h

Ini File: CaVh.ini

Setting	State
Variable parameter	$I_{L\text{-}Ca}$ V_h
Start value	-20mV
End value	-50mV
Step size	-1mV
Excitation Random	No
Dopamine pulse	No
Inhibition	Off

Table 4-14 Settings for varying calcium V_h

The calcium V_h parameter affects the plateau membrane potential in a similar manner to the slowly inactivating potassium current variation. Varying this parameter shifts the voltage dependency curve of the calcium current as shown in Figure 4-29. In this figure calcium V_h increases from -50 to -20mV from left to right. This has a strong effect on the ionic current as shown in Figure 4-30. Here the -20mV curve is the flattest curve

and the -50mV curve becomes much steeper with a negative gradient at a more negative membrane potential.

This leads to a sigmoidal curve of the plateau membrane potential as calcium V_h is varied as shown in Figure 4-31. The steepest part of this curve is in the area around where the firing threshold for MS neurons is based. This would seem to suggest that firing of the neuron would be very sensitive to changes of this parameter, and indeed small changes of $I_{L\text{-}Ca}$ V_h cause the plateau membrane potential to vary from -50 to -40mV.

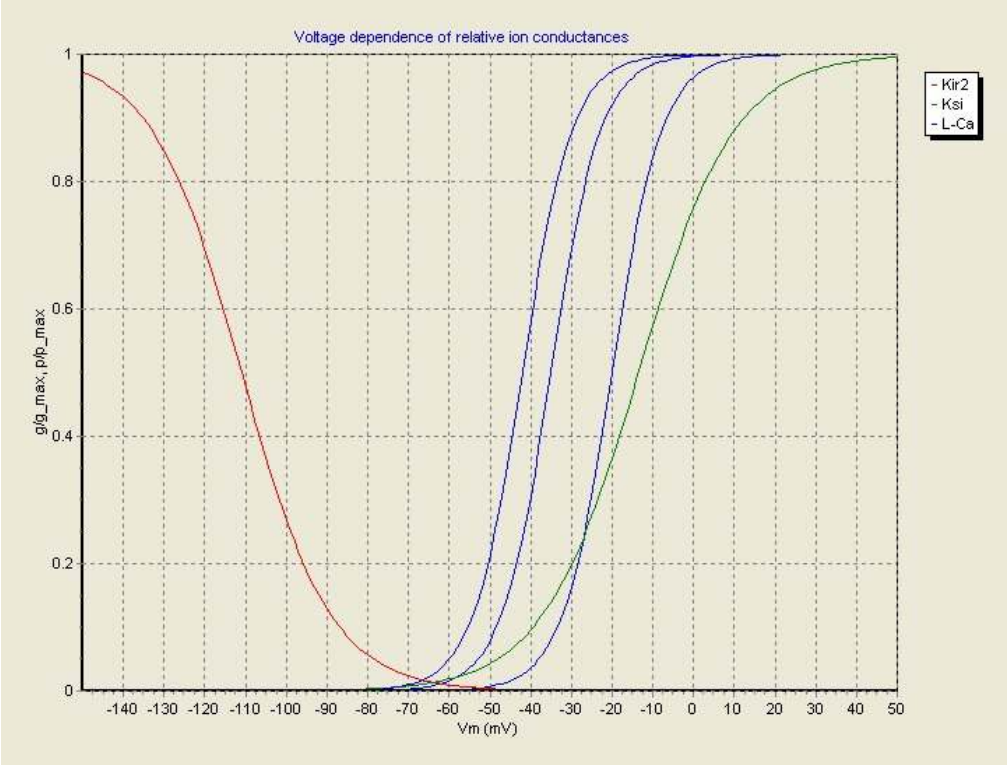

Figure 4-29 Voltage dependency of L-type calcium conductance on V_h. Increasing V_h from -50mV to -20mV (blue curves) shifts the activation curve to the right. This leads to the calcium current only becoming available at more depolarized membrane potentials.

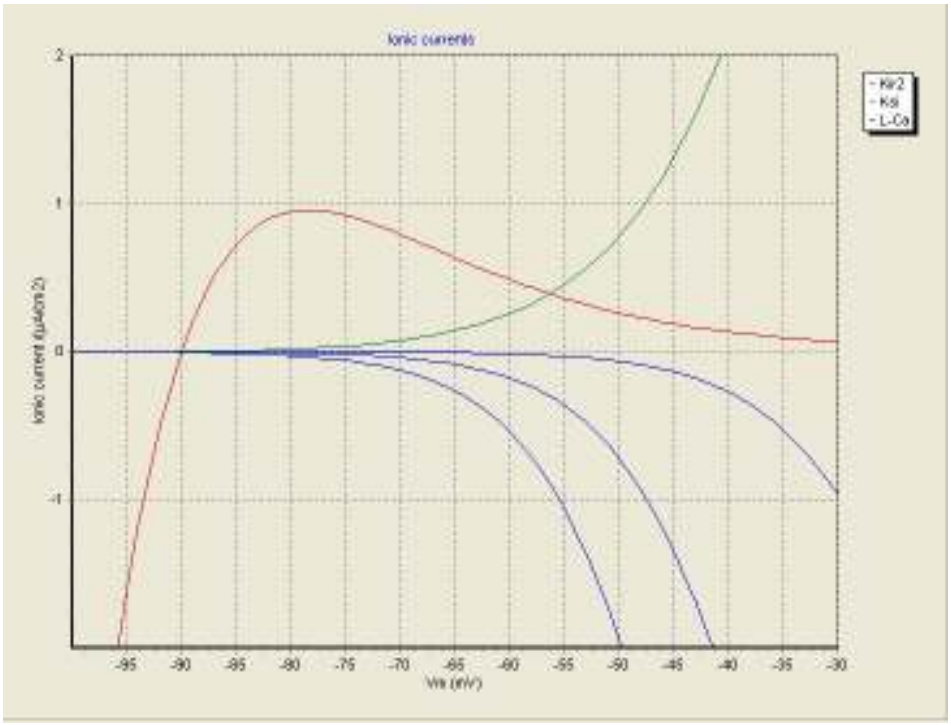

Figure 4-30 Ionic currents - dependency of L-type calcium current on V_h. Increasing V_h from -50mV to -20mV (blue curves) shifts the curve to the right. This illustrates how increasing the half activation parameter for the L-type calcium current makes this current less available during the transition from the down to the up state.

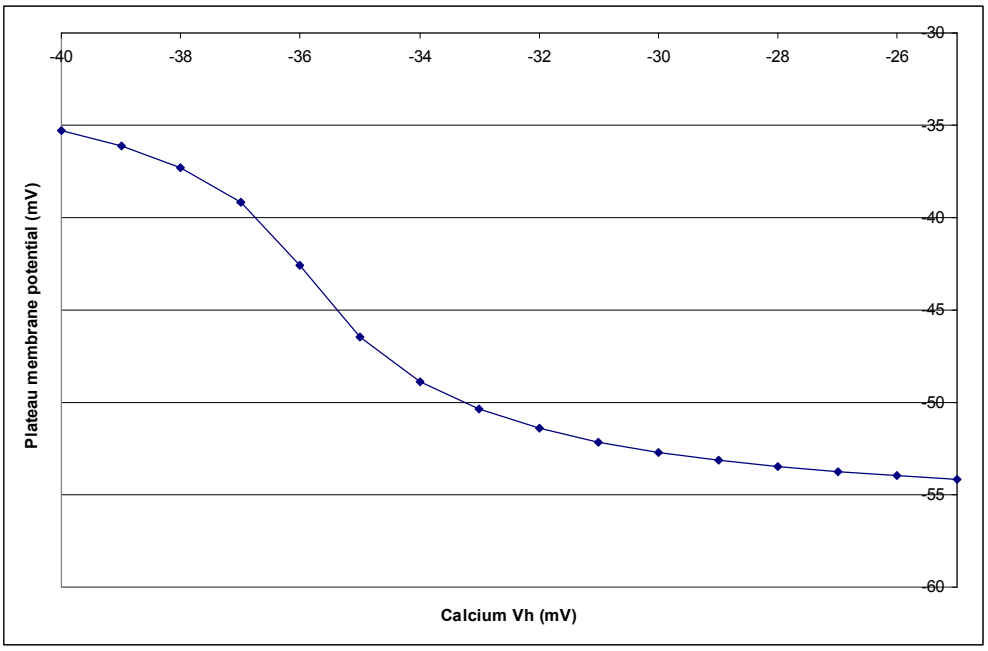

Figure 4-31 Variation of plateau membrane potential with calcium V_h. As the half activation parameter for the L-type calcium current is increased, the plateau membrane potential drastically decreases. The slope is steepest in the portion of the curve where the membrane potential is close to the firing threshold. Therefore the firing of the neuron will be sensitive to this parameter.

4.2.7.2 *Varying Calcium V_c*

Ini File: CaVc.ini

Setting	State
Variable parameter	$I_{L\text{-}Ca}$ V_c
Start value	4mV
End value	8mV
Step size	0.1mV
Excitation Random	No
Dopamine pulse	No
Inhibition	Off

Table 4-15 Settings for varying calcium V_c

The effect on the ionic currents of varying calcium V_c is very similar to that of varying calcium V_h. Varying this parameter also causes a variation in the plateau membrane potential with a sigmoidal curve as shown in Figure 4-32. This curve also has its maximum gradient between -50mV and -45mV.

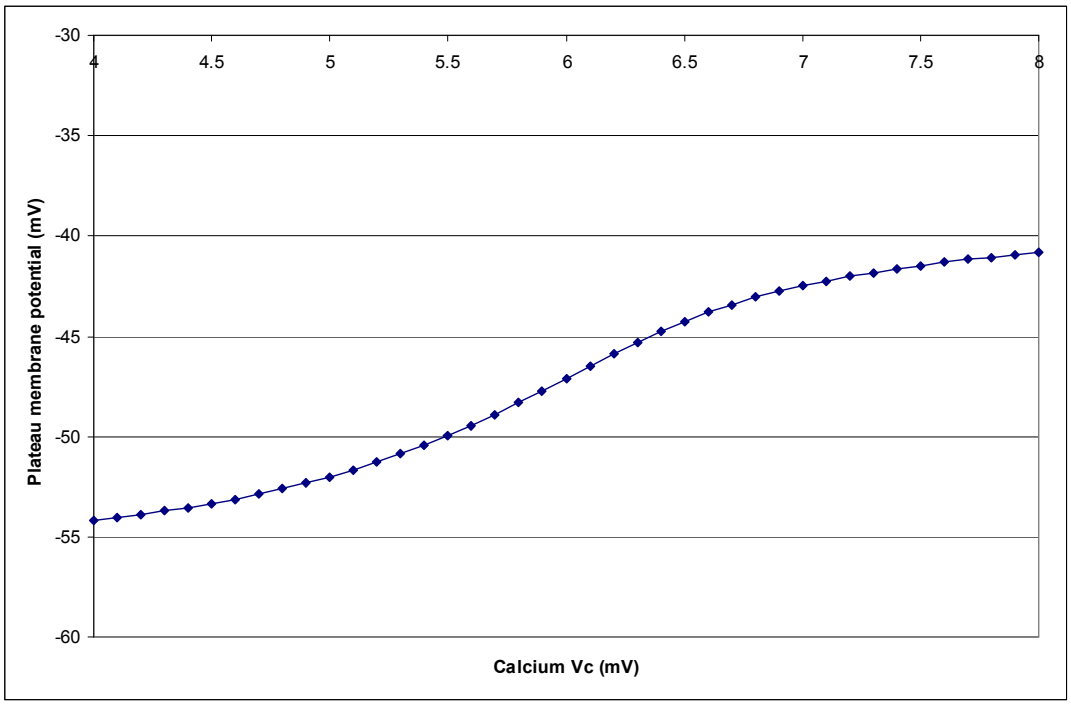

Figure 4-32 Variation of plateau membrane potential with calcium V_c. Increasing the slope of the activation curve for the L-type calcium current increases the plateau membrane potential over a range of more than 10mV. Again the slope is greatest at membrane potentials around the firing threshold so the firing of the neuron will be sensitive to the value of this parameter.

4.2.7.3 Varying Maximum Calcium Permeability

Ini File: CaPMax.ini

Setting	State
Variable parameter	Ca Max Permeability
Start value	2nm/s
End value	5nm/s
Step size	0.2nm/s
Excitation Random	No
Dopamine pulse	No
Inhibition	Off

Table 4-16 Settings for varying maximum calcium permeability

Varying the calcium permeability again varies the plateau membrane potential as shown in Figure 4-33, but the effect is not so marked over a physiological range.

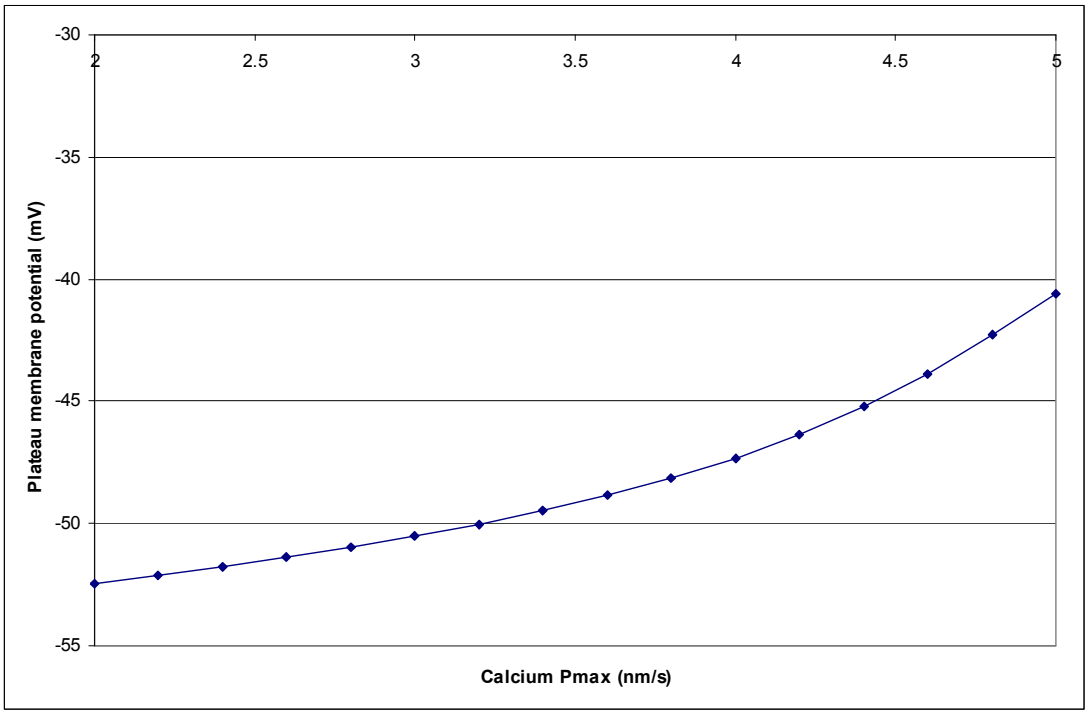

Figure 4-33 Variation of plateau membrane potential with maximum calcium permeability. Increasing the maximum permeability of the membrane to calcium ions leads to a more depolarized plateau membrane potential. The wide range of plateau membrane potentials again suggest that the firing of the neuron will be sensitive to the value of this parameter.

4.2.7.4 Varying Calcium Concentration

Ini File: CaO.ini

Setting	State
Variable parameter	Extracellular Ca
Start value	0.0016nmol/cm^3
End value	0.0026nmol/cm^3
Step size	0.0001nmol/cm^3
Excitation Random	No
Dopamine pulse	No
Inhibition	Off

Table 4-17 Settings for varying calcium concentration

Varying the extracellular calcium concentration varies the plateau membrane potential as shown in Figure 4-34. Varying the intracellular calcium concentration does not seem to have any effect on the membrane potential at biophysically realistic levels.

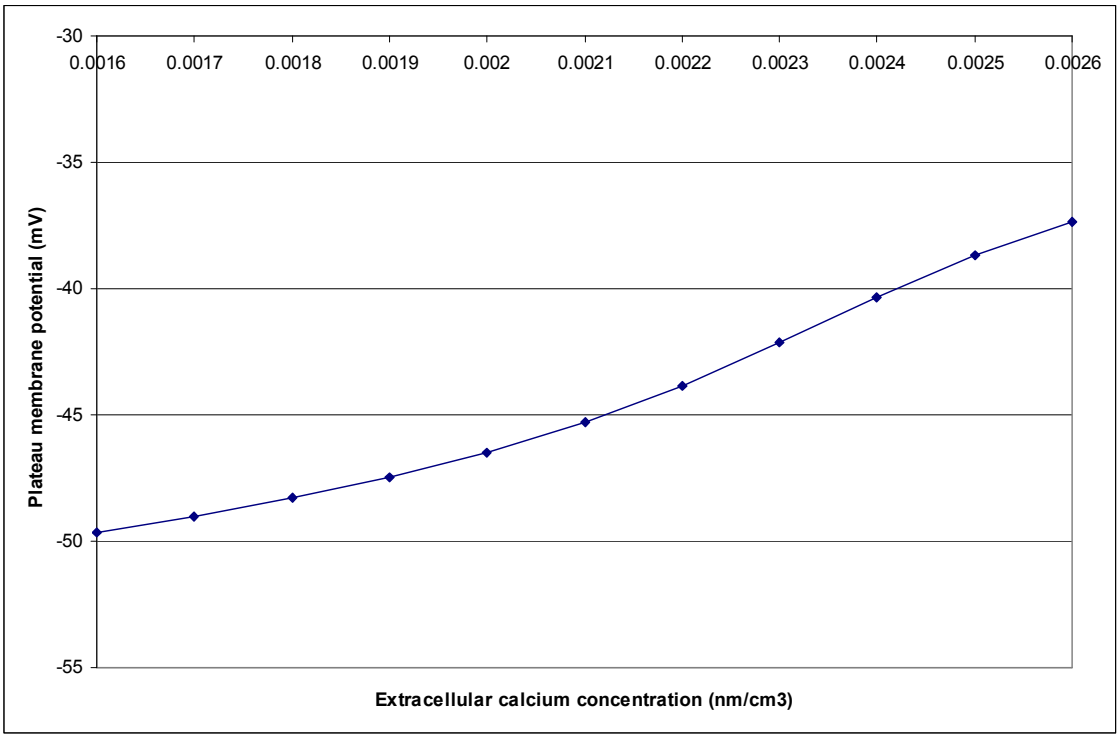

Figure 4-34 Variation of plateau membrane potential with extracellular calcium concentration. Small increases in the extracellular calcium concentration lead to relatively large changes in the plateau membrane potential.

4.3 Discussion

These simulations represent the effect of changing the values of all the major parameters used in this model of a medium spiny neuron. They show that varying some of the factors associated with the ionic currents had a large effect on the membrane potential achieved in the up state and, in some cases, on the firing of the neuron.

4.3.1 Currents

The potassium currents, the calcium current and the excitation frequency all had an effect on the plateau membrane potential reached during the excitatory phase of the simulation. Changing the parameters for the Boltzmann functions simulates changing physical parameters of the membrane proteins. Changing the V_h parameter shifts the voltage dependence curve left or right. This would be equivalent to changing the number of receptors in the membrane. Changing the V_c parameter changes the slope of the voltage dependence curve. This would be equivalent to changing the rate of activation of the receptors with respect to the membrane potential.

The inwardly rectifying potassium current has a large effect on the trajectory of the membrane potential. As the curve is left shifted, by making the value of V_h more negative or made shallower by making the value of V_c more negative, the ionic current hump at voltages between the down and up state becomes more pronounced and more difficult to overcome. The slow rise to the up state seen in these simulations at critical values is not seen in electrophysiological recordings. This suggests that the inwardly rectifying potassium current parameters are maintained within a tight band in medium spiny neurons.

The plateau membrane potentials for the calcium activation parameters and the extracellular calcium concentration were sigmoidal, with asymptotes above and below the usual up state membrane potential and the steepest part of their curves across the range of usual up state membrane potentials. This suggests that the plateau membrane potential achieved in the up state is highly sensitive to these parameters as, therefore, the firing rate would be.

4.3.2 Dopamine

It is stated in the literature that dopamine stabilises the MS neuron, either in the up state or the down state[170]. In that context two findings here are of interest.

Firstly, at levels of excitation that would normally take the MS neuron into the up state, decreasing the tonic level of dopamine increased the amount of excitation needed to cause firing. When the excitation was sufficient to cause firing, the delay to the first action potential was similar across the range of tonic dopamine levels investigated. As the tonic dopamine level was increased from that required to allow firing at a given excitation frequency, the time of the first action potential decreased rapidly. This would seem to indicate that as tonic dopamine levels drop there is little effect on the firing of the neuron until a critical point is reached where the action potential is increasingly delayed and then, suddenly, no action potential occurs at all.

Secondly the effect of tonic dopamine levels with lower levels of excitation was examined. This showed the expected effect of increasing the contrast between levels of excitation that would not normally be sufficient to cause the state to transfer from down to up and those that would.

This increased contrast has recently been cited as a method for facilitating selection between competing motor programs. In view of the results from these simulations this seems unlikely. The only motor programs which would be suppressed by this mechanism would be those which do not have sufficient excitatory drive to take the neuron into the up state in the first place.

In a recent review of the effects of dopamine, Nicola et al (2004) said[170] "…the exact effects of dopamine are likely to depend very particularly on the time course and magnitude of excitation occurring in a neuron." This phrase is illustrated by the findings from these simulations and may account for some of the varied interpretations applied to experimental results.

4.3.3 Firing threshold

As many of the parameters had an effect on the plateau membrane potential achieved by the MS neuron in the up state, it is interesting to speculate how changing these

parameters would affect the function of the neurons. This would seem to me to be entirely dependent on how the firing threshold is controlled. Wickens and Wilson (1998)[171] showed that the firing threshold decreased as the rate of rise of the membrane potential increased. It was suggested that this was due to the rapid inactivation kinetics of the sodium channels. This would mean that the availability of the sodium channels would decrease with a slow depolarisation. This effect would seem to magnify the effect of inhibition on the timing of the firing of the first action potential in the up state. It may therefore be a factor to consider incorporating into later models of the MS neuron.

5 Control of the Timing of the First Spike

5.1 Introduction

The simulations in chapter 4 showed how the dynamic characteristics of the model MS neuron are dependent on the parameters used in the modelling equations. These results have been used to set the parameter values for the following simulations.

In this chapter one necessary facet of control of any behaviour, not just motor actions, is examined; the timing of the behaviour release. It is proposed that accurate control of the timing of release could be obtained by some aspects of feedforward inhibition in the striatum. To investigate this hypothesis simulations were performed which considered how varying the timing, burst length and burst frequency of feedforward inhibition would affect the timing of the first action potential produced by the model MS neuron after transition from the down state to the up state.

Before the simulations reasons why the timing of the first spike from the MS neuron may be worth investigating are considered and what mechanisms may exist for controlling the timing. This is followed by a section deriving the parameters for the IPSPs from recent experimental work.

5.1.1 Importance of the first spike

Recent work has shown that the timing of the first spike in a single rat barrel cortex neuron contains virtually all of the information necessary to identify the whisker moved[172 173] (and for review[174]). Is there any evidence that the timing of the first spike from a medium spiny neuron after it has been put into the up state could identify the context in which it has been caused to fire?

Such a statistical analysis has not been attempted, probably mainly due to the technical reason that each medium spiny neuron has inputs from on average 5000 corticostriatal neurons[175].

There is, however, some indirect evidence that the timing of the first spike from the striatal projection neuron may be crucial, although exactly what information it contains and the relevance of the further spikes in the train is unclear.

Firstly, when a MS neuron transfers to the up state, it often does not fire immediately, and sometimes not at all. This would seem to imply the presence of mechanisms for controlling the timing of the firing of the first spike, even to the extent of suppressing it completely. This would not seem to be due to a change in rate of the excitatory afferent input. A large amount of excitation is needed to generate the up state due to the non-linearity of the MS currents. Simulations of these currents show that the amount of excitatory conductance change required to produce the rapid rise from the down state to the up state seen in MS neurons produces a plateau membrane potential very close to the firing threshold of the neuron[176]. This plateau is sufficiently close to the firing threshold that the increased noise seen in the up state in MS neurons should cause firing very soon after the up state is reached.

5.1.2 Timing Mechanisms

There are several mechanisms which could generate these timing delays in the firing of the MS neuron, and these may interact in cooperative and/or competitive manners.

The effect of dopamine on medium spiny neurons has been characterized to some extent. It is known that D1 receptors mediate increases of inward rectifying potassium and L-type calcium currents. Depending on the timing of the dopamine pulse, simulations in the previous chapter show that this can lead to a delay in the timing of the first spike from the MS neuron, although this may only be of relevance at the time of receiving reward.

MS neurons receive feedforward inhibition from three main classes of GABAergic interneuron[83]. The best characterised of these are the parvalbuminergic fast spiking (FS) interneurons. These are similar to other fast spiking interneurons found in cortex and hippocampus[177 178]. As implied by their name, they are capable of high frequency firing, of the order of 200Hz, with little or no adaptation[179]. Although they are the most common striatal GABAergic interneuron, they only constitute about 0.7% of striatal neurons in the rat[180]. The FS interneurons form multiple, symmetrical synapses on the somata (often with pericellular baskets) and the proximal dendrite of MS neurons[181 182], where they are in a position to exert strong inhibitory control of the MS neuron. In contrast to the MS neurons, which receive a major thalamic excitatory input, the FS

interneurons receive nearly all their excitatory input from the cortex[183]. The microcircuit formed by the two classes of neuron and their common excitatory and neuromodulatory inputs is shown in Figure 5-1.

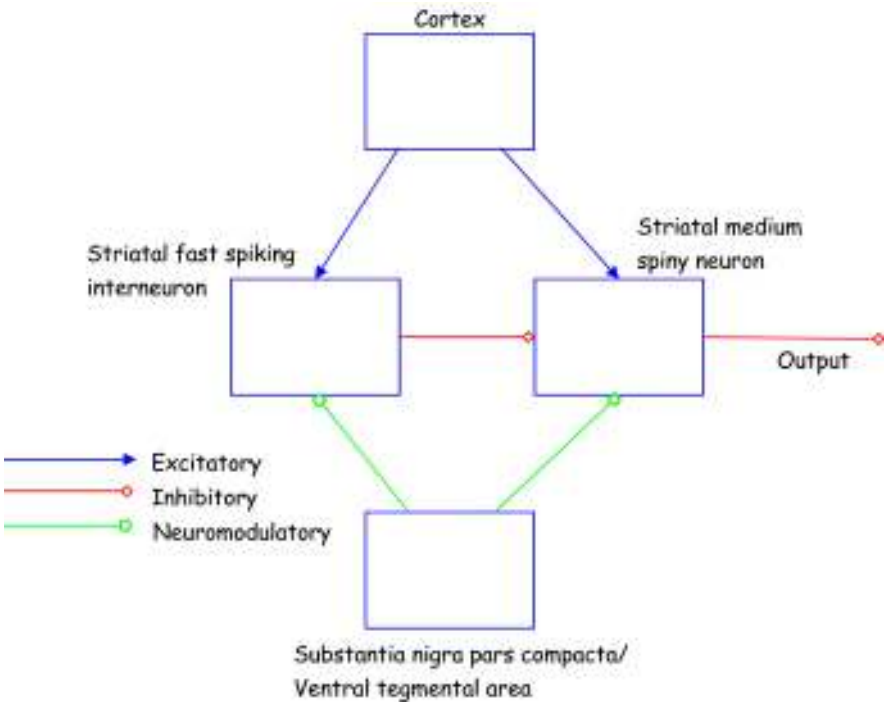

Figure 5-1 Striatal feedforward inhibition. This microcircuit shows the interaction of FS interneurons and MS projection neurons. The cortex has excitatory input to both the FS and MS neurons and dopamine also has a neuromodulatory effect on both classes of neuron. The FS interneuron provides feedforward inhibition to the MS projection neuron.

When the MS neuron is in the down state the GABAergic input is excitatory. Although a single pulse produces only approximately 0.5mV of depolarization[184], a burst of pulses could conceivably summate to make it quicker to boost the MS neuron into the up state when a high enough level of cortical excitation commences, possibly leading to a reduction in the time to the first spike from the MS neuron. Contrarily, when the MS neuron is in the up state, the GABAergic input produces inhibitory post-synaptic potentials (IPSPs). These are larger than the excitatory post-synaptic potentials (EPSPs) seen in the down state, producing a negative voltage deflection of approximately 1.5mV[184]. It has been shown that the up states of the MS and FS neurons are correlated[185], so it is probable that the main effect of the FS neuron occurs when the MS neuron is in the up state. However, Figure 11A3 from the study by Plenz and Kitai (1998)[185] shows that the firing of the first spike from the FS interneuron can occur

before the MS neuron reaches the up state and can therefore influence the timing of the firing of the first spike by the MS neuron.

A further mechanism whereby the timing of the first spike from a MS neuron could be influenced is cholinergic input, although this input has a more complicated effect (see Figure 1-3 and Figure 1-4 for details of the TAN connections) because the cholinergic neurons of the striatum, the tonically active neurons (TANs), are also influenced by the dopaminergic and GABAergic neurons.

These are mechanisms which could influence the timing of the first spike from the MS neuron, but why is the timing of the first spike worth investigating?

5.1.3 Significance of delaying the first spike

5.1.3.1 Reinforcement learning

One reason to consider first spike timing is experimental evidence of the timing of the first action potential on the level of calcium transients in the dendrites and soma[186]. The sooner an action potential occurs after the neuron goes into the up state, the larger the induced calcium transient. In itself this may not seem to be too significant, but when considered in the light of reinforcement learning in the striatum it could provide a solution to a problem with current models of striatal learning.

Although the transient dopamine signal has been identified as a biologically plausible mechanism for the scalar teaching signal of reinforcement learning, no equally credible mechanism for the credit assignment problem has been put forward. This is the problem of working out which neuron(s) are responsible for the behaviour which led up to a reward, even if the firing of the neurons that instigated the reward obtaining behaviour occurred at some temporal distance from the delivery of the reward.

In the most recent models, a mechanism of cascading activations of MS neurons has been suggested[187]. But this does not fit in with known striatal physiology. Firstly, the reduction in neuronal numbers between cortex and striatum already causes problems in explaining how information is not lost (see work on dimensionality reduction, such as Bar-Gad and Bergman (2001)[188]). Using many striatal neurons solely to produce a timing signal for the learning mechanism would exacerbate this problem. Secondly, it is

unlikely that any two striatal MS neurons receive identical cortical input[125]. However, if the number of corticostriatal neurons required to push the MS neuron into an up state is only a small proportion of the total number synapsing with that MS neuron, there could be matches in the corticostriatal patterns between MS neurons. This would still leave the problem of controlling the timing of the action potentials across the neurons to produce the credit assignment signal. In fact the problem reduces to controlling the timing of the first action potential in each spiny neuron. In that case a more effective solution would be to only use one neuron and keep a trace to indicate when it fired.

The dendritic calcium level could be the mechanism for instantiating that trace. The time course is of the right order, with a decay time constant of about ½ second. The calcium transients also occur in the higher order dendrites, which would be required in order to affect synaptic plasticity of the corticostriatal glutamatergic input. The magnitude and form of the calcium transients are repeated with repeated stimulation, suggesting that this would be a reliable signal[189]. Corticostriatal synaptic plasticity in spiny projection neurons is dependent on intracellular calcium concentration, $[Ca^{2+}]_i$, as it is blocked by intracellular calcium chelators[190].

This does not, however, necessarily mean that the calcium signal is encoding the timing of the first spike produced. It has to be considered that an earlier spike may lead to a higher peak, but the peak from a delayed spike will also be delayed. This may mean that the magnitude of the calcium signal at a point in time after an action potential would be related not to the timing of the action potential, but to the timing of the start of the up state. Modelling this would give an insight into the timing mechanisms of reward learning. This is considered further in chapter 6 which investigates learning of location of reward.

5.1.3.2 Gating of behaviour

Not only is which behaviour to perform important, but also the timing of the behaviour. A recent computational basal ganglia model from Brown et al (2004)[191] postulates that the function of the basal ganglia is in gating and releasing behaviours. Although this is not a new idea, it has been modelled in their work without the use of lateral inhibition in the striatum. One requirement of the timing of the gating would be controlling the

timing of firing of MS neurons. This does not necessarily mean controlling the timing of the first action potential, but could mean controlling the frequency of action potentials or the total number of action potentials during an up state. Demonstrating that the timing of the first action potential could be accurately controlled by aspects of the function of the feedforward inhibitory interneurons would, though, present this as a viable mechanism for controlling the timing of behaviours in such a network.

5.1.3.3 Efficiency

One reason to consider the use of the first action potential time as a signal is its efficiency. It provides the earliest possible signal and with the least energy consumption. Use of either the frequency of a spike train or the total count could only allow the recipient structure to assess the signal when the spike train had finished, or less accurately estimate it whilst occurring. This would lead to a delay in interpretation which could be vital where a rapid decision between competing movements must be made.

5.2 Modelling of inhibitory inputs

Recent investigations have produced evidence of the effect of unitary IPSPs on MS neurons both in slice preparations and in organotypic cultures. The results of these investigations are used here to provide a biophysically realistic simulation of the effects of inhibition on the MS neuron.

GABA has opposing effects on MS neurons when the neurons are in the up and down states. In the hyperpolarized down state, GABA is excitatory and in the less polarized up state, GABA is inhibitory. This is because the hyperpolarized membrane potential in the down state is more negative than the reversal potential for chloride ions, the conductors in GABAergic transmission.

Koos and Tepper (1999)[184] have measured the characteristics of IPSPs in the up and down states. They only published measurements at the two end points; in the down state at -94mV and in the up state, just sub-threshold, at -47mV. We can, however, put in a third point. At the reversal potential for chloride, the IPSP must be 0mV. In their paper, Koos and Tepper (1999) give a reversal potential of -78mV. More generally, the figure

given is closer to -60mV (as, for instance, in Figure 5-3, taken from Plenz and Kitai (1998)[185]). Using the higher figure would decrease the effect of IPSPs during the transition state and therefore minimise the effects of inhibition. It does not change the voltage change due to inhibition at subthreshold membrane potentials. In order to not overestimate the effect of inhibition during the state transitions, the figure of -60mV is therefore used in these studies.

This gives the graph in Figure 5-2 which shows that the relationship between the change in membrane potential induced by an IPSP and the membrane potential is not linear.

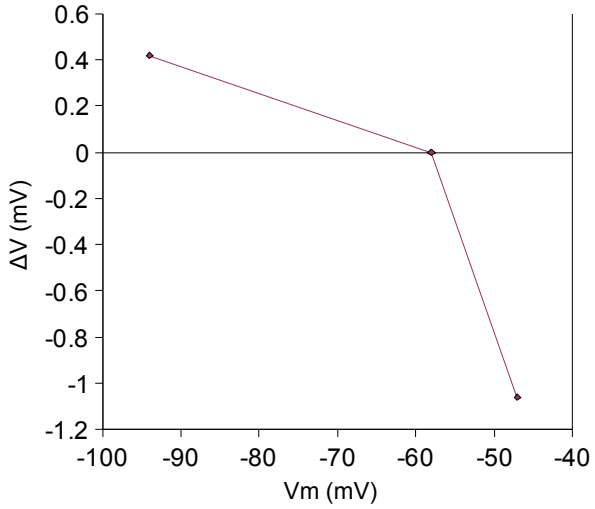

Figure 5-2 Dependence of voltage change produced by a single IPSP on membrane potential. The values at either end of the graph are taken from experimental measurements in striatal slices and extrapolated to form two lines intersecting with the zero point of effect on membrane potential at the reversal potential for chloride ions, taken as -60mV in these simulations..

A similar graph was produced from experimental results in organotypic culture by Plenz and Kitai (1998)[185] (Figure 5-3). Although this has a similar shape, the ΔV figures shown are larger. Comparison of resting membrane resistances in striatal slices[138] and in organotypic cultures[192] shows that organotypic cultures have a higher membrane resistance by a factor of six, which would account for the larger PSPs seen in response to similar sized IPSCs. To be conservative, the size of IPSPs measured by Koos and Tepper[184] will be used in these simulations.

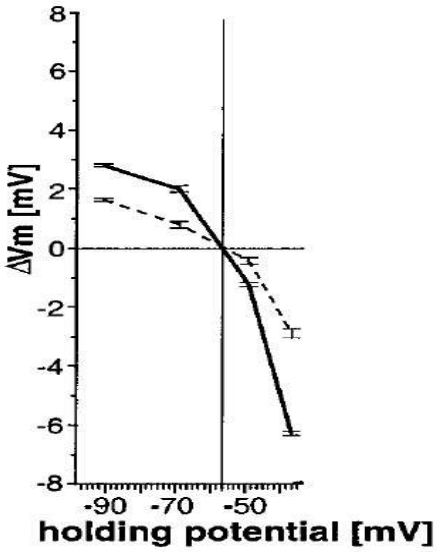

Figure 5-3 FS interneurons inhibit MS neurons via a fast monosynaptic connection (Acknowledged to Plenz and Kitai[185]). These results are obtained from measurements in organotypic cultures where the cells may have a markedly different membrane resistance from that seen in cells in vivo and in vitro.

This membrane potential dependent induced voltage change shows that the membrane resistance of the cell changes with membrane potential, and allows the use of these figures without having to take this effect into account further. The graph in Figure 5-2 allows the effect of the IPSP to be represented as one of two linear equations depending on whether or not the membrane potential is below -58mV.

$$\Delta V_D = -0.0117 V_m - 0.6767 \tag{5.1}$$

$$\Delta V_U = -0.0964 V_m - 5.5877 \tag{5.2}$$

Koos and Tepper[184] also showed the time course of the IPSPs evoked at both hyperpolarized and sub-threshold membrane potentials, as shown in Figure 5-4.

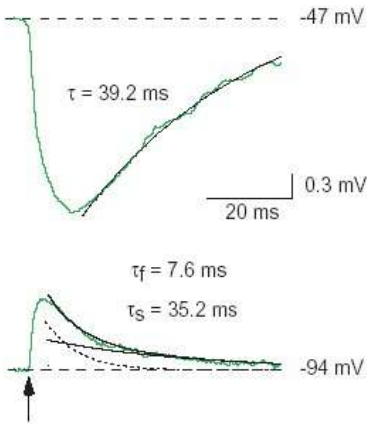

Figure 5-4 Properties of IPSPs elicited in spiny projection cells by FS interneurons (Acknowledged to Koos and Tepper[184]). This shows the time course of the excitation produced by a single IPSP in the down state and in the up state. The figures used for calculations in these simulations are based on the averages not these single examples.

In these simulations the inhibitory inputs are modelled as having a linear rise with a time to maximum effect and an exponential decay with a time constant. Both the rise time and the decay time constant are dependent on whether the membrane potential at the time of occurrence of the input is above or below the reversal potential. These are derived from the text of the Koos and Tepper paper[184] rather than the example shown in Figure 5-4 and the values for the characteristics used in these simulations are shown in Table 5-1.

Membrane potential	*Peak*	*Rise time*	*Decay time constant*
-47mV	-1.06±0.22mV	8ms	36.5ms
-94mV	0.42±0.13mV	4ms	15ms

Table 5-1 Inhibitory post-synaptic potential characteristics in up and down states

The peak voltage for the IPSP was modelled as dependent on the membrane potential and therefore changed from step to step during the simulation. This, to a large degree, eliminates the problem with using the wrong rise and decay times near the reversal potential as the low peak value makes these inputs less important.

FS interneurons are known to fire in high frequency bursts that cease abruptly[83]. They are modelled in these simulations as 100Hz trains with a burst count set by the user.

5.2.1 Shunting inhibition

As previously stated, GABA is excitatory to MS neurons in the down state and

inhibitory in the up state. The transition from inhibition to excitation occurs at the chloride reversal potential, which has been taken to be -60mV in this model (Figure 5-2). At this point, an IPSP still has an effect, even though it does not generate a change in the membrane potential. The IPSP lowers the membrane resistance. This has the effect of deflecting EPSPs, causing their current to flow across the membrane rather than on through the soma to the axon hillock. This deflection of the EPSP is termed shunting inhibition.

Synapses from FS interneurons are in an ideal position to cause shunting. Whereas the excitatory synapses are placed on the secondary and tertiary dendrites, the FS interneuron synapses are generally found on the proximal section of the primary dendrite or the soma of the cell. In this position all excitatory impulses have to pass the inhibitory synapse area to reach the axon hillock and contribute to depolarisation. Thus one inhibitory synapse can exert a large effect on the firing of the neuron due to many excitatory synapses.

In this model of the MS neuron, this effect is not generally significant. When the neuron is in transition from the down state to the up state there is a barrage of excitatory input. This large amount of excitation would be too large to be shunted to a significant degree.

5.3 Modelling of excitatory inputs

In chapter 4, where the effects of parameter variation on the behaviour of the model MS neuron were considered, all excitation was non-random. This produced a steady train of input pulses which resulted in a smooth plateau of excitation and produced a steady plateau membrane potential. This allowed the study of modelling how parameters affected spike timing and plateau membrane potential without having to take into account noise effects.

Some of the simulations in this chapter will continue on the same lines. However, one important aspect of the hypothesised action of feedforward inhibition is the control of the timing of the first action potential. For this to be a viable mechanism, it must be able to cope with the large amount of noise in the up state membrane potential seen experimentally[193]. To this end randomness is introduced to the firing of the inputs as detailed in the construction of the model neuron (section 2.3.10, page 25).

5.4 Simulations

In the following simulations one simulated spiny neuron and one inhibitory input are used.

5.4.1 Effect of IPSPs on membrane potential

First simulations were produced to examine the effect of single and multiple IPSPs on membrane potentials in the up and down states. In these simulations non-random excitation is used to produce a clear picture of the effect of the IPSP in membrane potential.

A single IPSP occurring in the up state at 200ms after excitation had started produced a voltage deflection of -1.39mV as shown in Figure 5-5. This produced the corresponding effect on membrane potential shown in Figure 5-6.

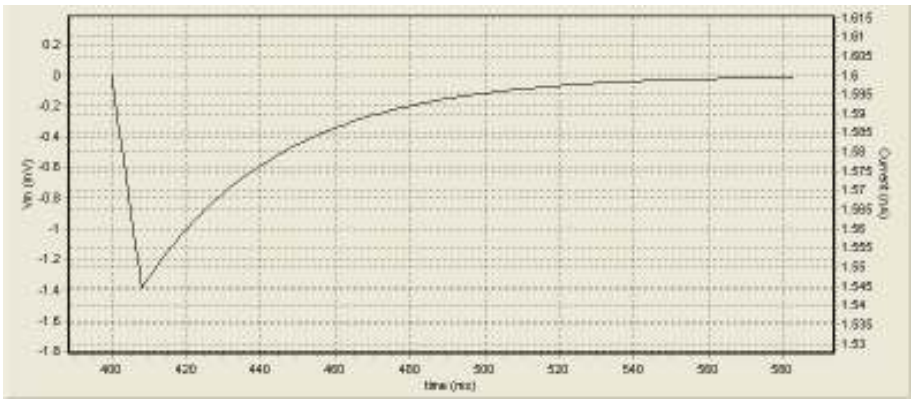

Figure 5-5 Simulated voltage deflection from single IPSP in the up state. Maximum voltage deflection is -1.39mV (left hand scale). This is the voltage deflection in isolation, not as it interacts with the membrane potential.

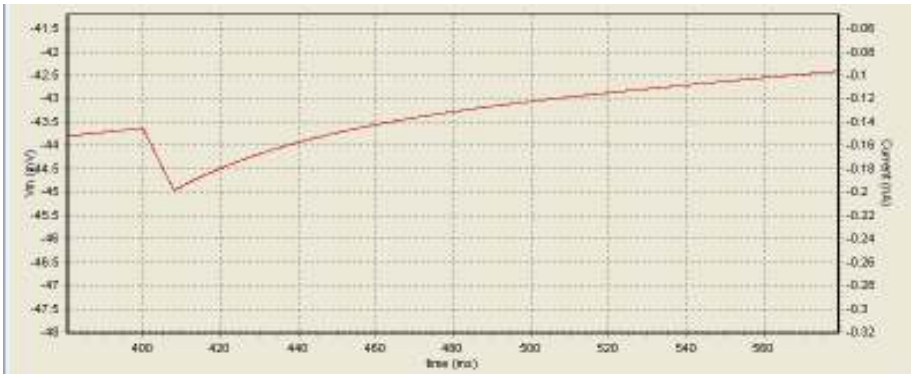

Figure 5-6 Effect of single IPSP on membrane potential in the up state. The ramp produced by the slowly inactivating potassium current in the up state is still present and offsets some of the effect of the IPSP.

A set of ten IPSPs summates to produce a voltage deflection -5.65mV as shown in Figure 5-7. This has a correspondingly larger and longer effect on the membrane potential, shown in Figure 5-8.

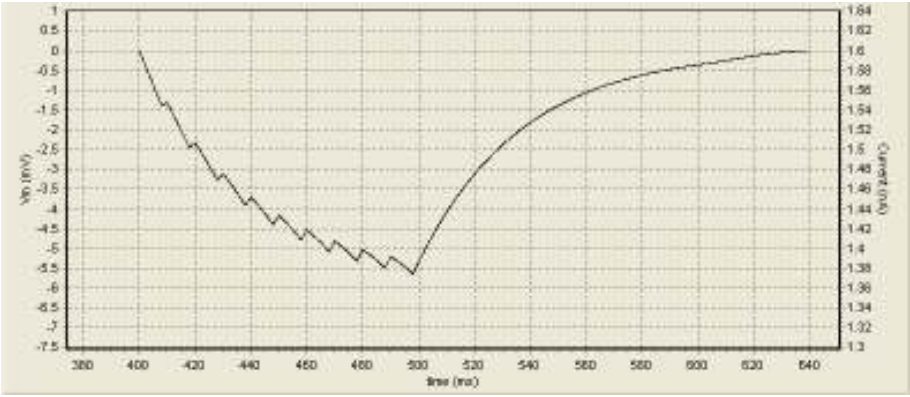

Figure 5-7 Simulated voltage deflection produced by a burst of ten IPSPs The IPSPs summate over a 100ms period and the summated voltage then decays exponentially over 140ms.

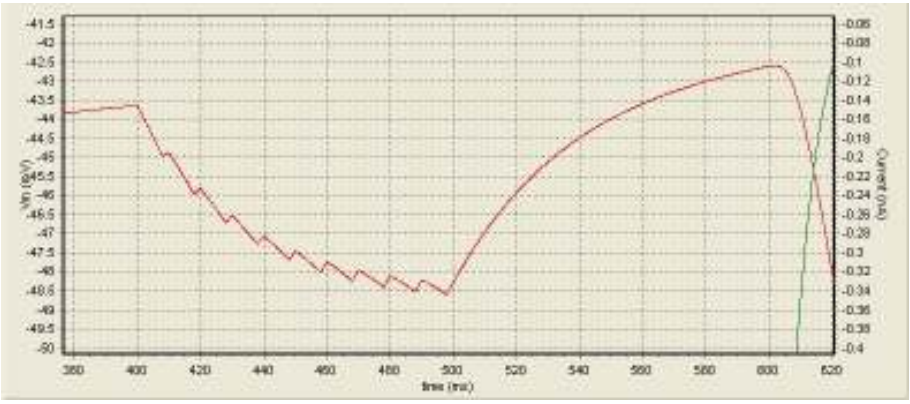

Figure 5-8 Effect of ten IPSPs on membrane potential in the up state. The train of IPSPs interrupts the ramp depolarization. At the end of the influence of the IPSPs the membrane potential is back at the value it would have reached had the IPSPs not occurred.

Similarly the effects of a single IPSP and a burst of ten IPSPs when the MS neuron is in the down state are shown in Figure 5-9 to Figure 5-12. A single IPSP produces a peak voltage deflection of 0.31mV and a burst of ten IPSPs summate to produce a maximal voltage deflection of 0.64mV, both at a membrane potential of -84.3mV.

In the up state, the IPSPs summate to produce a peak four times as great as a single IPSP. In the down state, the peak from the summation of the 10 IPSPs is only a little over twice that produced by a single IPSP. This is due to the shorter decay time constant in the down state.

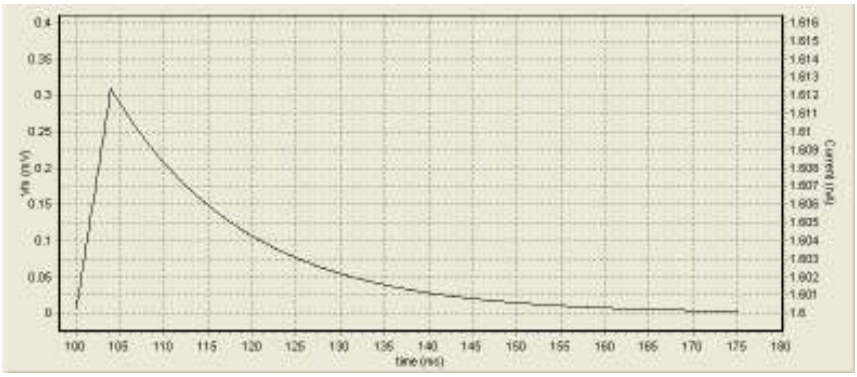

Figure 5-9 Voltage deflection from a single IPSP in the down state. As the resting membrane potential of the MS neuron is more hyperpolarized than the chloride reversal potential, the IPSP leads to a depolarizing deflection of 0.31mV in membrane potential.

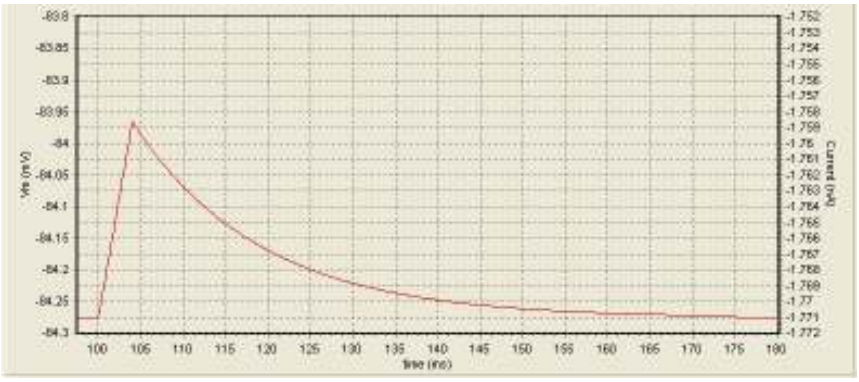

Figure 5-10 Effect of a single IPSP on membrane potential in the down state. As there is no excitatory influence, the IPSP voltage is exactly mirrored in the membrane potential of the MS neuron.

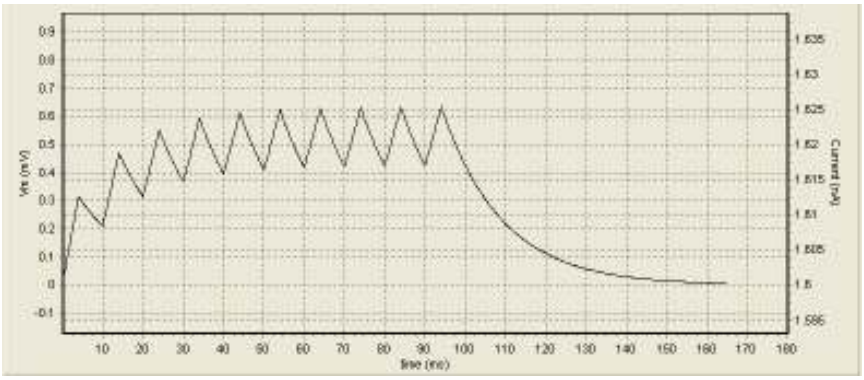

Figure 5-11 Voltage deflection from ten IPSPs in the down state. The ten IPSPs summate as in the up state. Because the decay time constant in the down state for each IPSP is less than in the up state, each IPSP has decayed further by the time of the next IPSP, so the summated influence is less and the duration of influence after the cessation of the train is shorter.

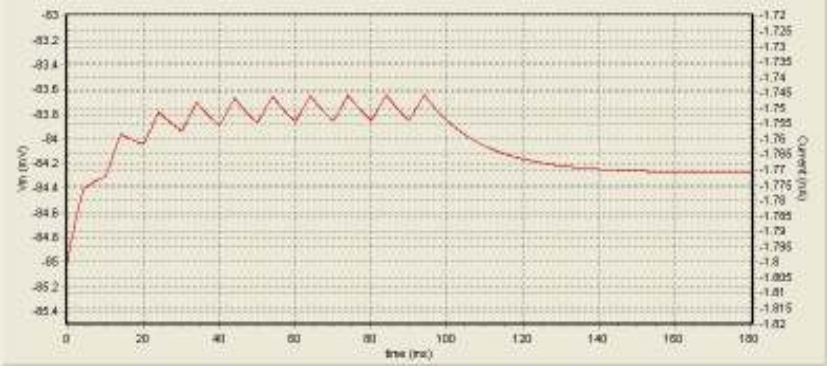

Figure 5-12 Effect of ten IPSPs on membrane potential in the down state. Due to the time constant of the membrane, the influence of the train of IPSPs on the membrane potential in the down state is more prolonged than the influence of the IPSPs themselves seen in Figure 5-11.

5.4.2 Variation of IPSP timing

In these simulations the effect of varying the timing of the inhibitory input is investigated. This is done using both single IPSPs and a burst of ten IPSPs

Parameter	*Value*
Excitation frequency (Hz)	30
Standard deviation of excitation frequency	2
Number of excitatory inputs	100
Stagger input starts?	Yes
Firing Jitter (ms)	2
Dopamine pulse on?	No
Inhibition reversal potential (mV)	-58
Variable parameter	Inhibition start time
Parameter start value	-200ms
Parameter end value	140ms
Parameter step size	10ms
Number of runs per parameter step	1000

Table 5-2 Parameters for simulations of variation of IPSP timing

The timing of the inhibition start is shown relative to the timing of the start of excitation.

5.4.2.1 Single IPSP

Ini file: Single IPSP.ini

As shown above, a single IPSP can produce a negative voltage deflection of the order or

-1.4mV in the up state. The effect of one such IPSP, occurring at varying times in relation to the excitation, on the time of the first action potential is shown in Figure 5-13.

In this, and subsequent figures, the zero on the x-axis is the time at which excitation starts. At x = -100ms, the inhibition is starting 100ms before the excitation. The y-axis in these graphs shows how long after excitation started the first action potential occurred. The earliest start for the inhibition is x = -200. As the excitation starts 200ms into the simulation, this means that the inhibition then occurs at the start of the simulation. The latest start for the inhibition is at 150ms after excitation has started. This is 350ms into the simulation and just under half way through the period of excitation. It was not felt necessary to continue the simulation longer than this as, by this time, the first action potential was reliably occurring before the start of the inhibition.

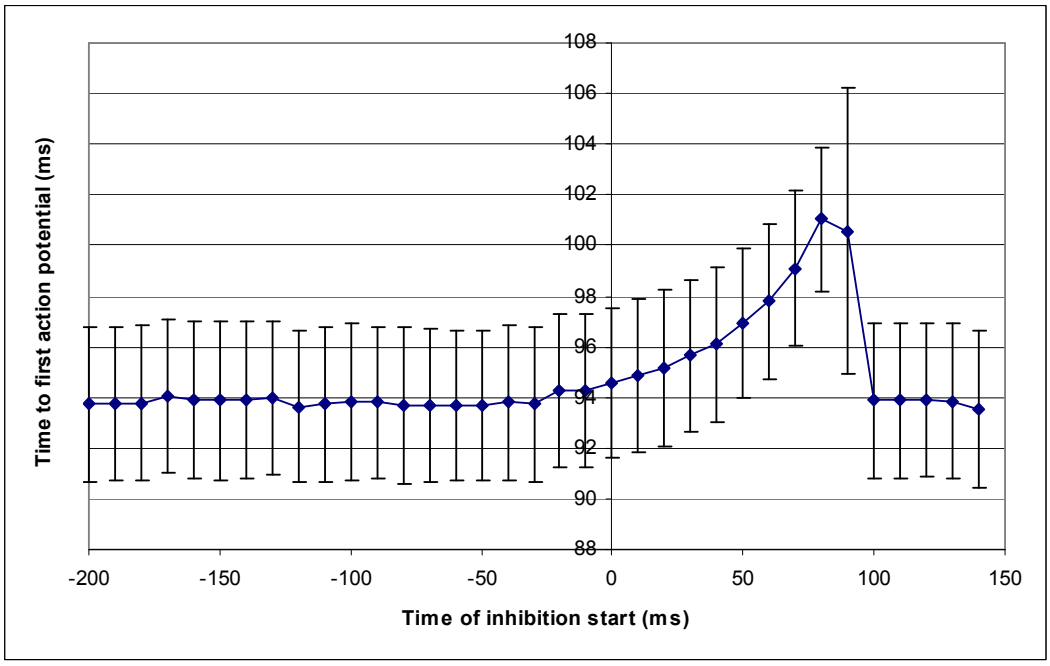

Figure 5-13 Effect of variation of timing of a single IPSP on first action potential timing. Average of 1000 runs for each parameter step. Error bars are ±1 standard deviation. The zero on the x-axis is the time at which high intensity excitation started. There is no demonstrated decrease in time to first action potential when the IPSP occurs just before the onset of excitation. The maximum delay of the first action potential produced by a single IPSP is 7.24ms. This occurs when the IPSP starts 80ms after the excitation starts, which is equivalent to the action potential in the FS interneuron occurring 14ms before the first action potential in the MS neuron would occur without the influence of inhibition.

The IPSP had no effect on the timing of the first action potential when it occurred more than 30ms before the start of excitation (between x = -200 and x = -30). The average time of the first action potential with no effect from the IPSP was 93.8ms after the start of excitation. The maximum delay to the first action potential was 7.24ms. This occurred when the IPSP occurred 80ms after the start of excitation. This would equate to the action potential in the FS interneuron occurring roughly 14ms before the first action potential in the MS neuron. The maximum delay of 7.24ms was very comparable with an experimental delay of 5.4±1.7ms seen in organotypic culture[184].

When the IPSP started more than 100ms after the start of excitation, the first action potential in the MS neuron occurred before the inhibition started producing little or no effect on the subsequent spiking activity.

This leaves a window of 130ms when the feedforward inhibition produces a steadily increasing delay in the first action potential from the MS neuron. The error bars in Figure 5-13 show the standard deviation of the time to first action potential.. This remains relatively constant at ±3ms across the simulation, which represents 40% of the maximum delay.

5.4.2.2 IPSP burst

Ini file: Ten IPSP timing.ini

A burst of ten IPSPs when the MS neuron is in the up state summate to produce a negative voltage deflection of greater than 5mV. The effect of this burst of IPSPs is shown in Figure 5-14.

When there was no influence from the IPSPs the first action potential occurred at 93.8ms after the start of excitation. The maximum delay caused by the burst of IPSPs was 100ms which again occurred at 80ms after the start of excitation. As shown by the red line in Figure 5-14, the rate of increase of delay produced by the IPSPs occurring in the range of 0 to 80ms after the start of excitation was linear.

During this period of linear increase of first action potential delay, the error bars were approximately ±3ms, as for the single IPSP. In the case of the burst of ten IPSPs however, this only represents 3% of the maximum delay.

There was no evidence that the occurrence of a burst of IPSPs before the transition to the up state could cause the first action potential to fire earlier than without the influence of inhibition.

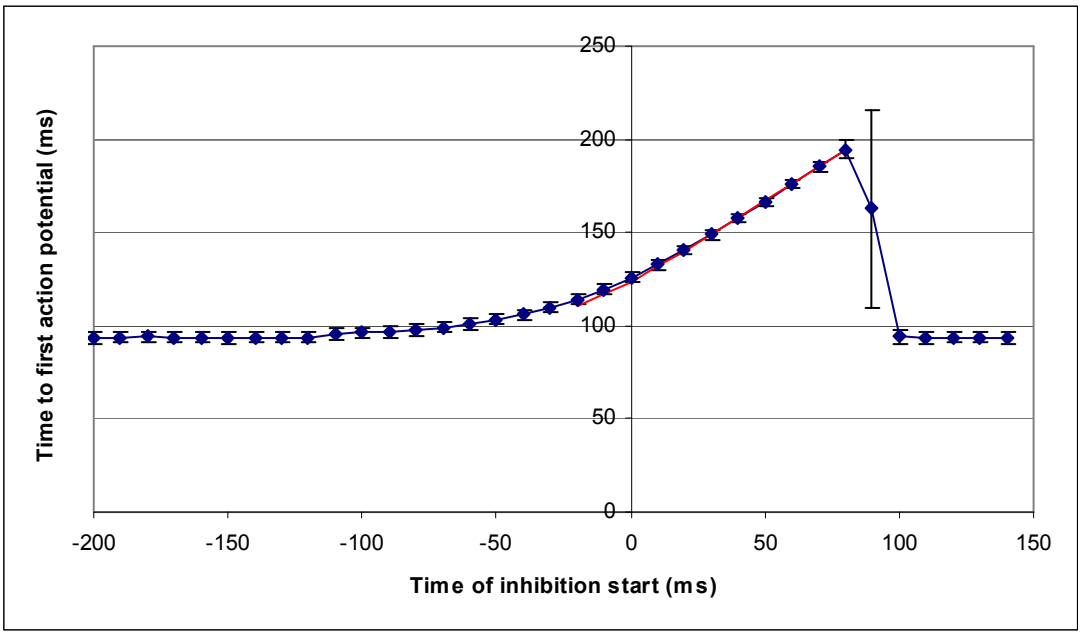

Figure 5-14 Effect of variation of timing of a burst of ten IPSPs on timing of first action potential. The red line is a straight line drawn through the topmost point to illustrate the linearity in the period when the inhibition starts after the start of excitation. Each point is the average of 1000 runs. There is again no evidence that the IPSPs starting when the MS neuron is in the down state leads to the first action potential in the MS neuron occurring earlier. The delay due to the inhibition is linearly related to the timing of the start of the IPSPs over the range where the IPSPs started 10ms before the excitation until the IPSPs started 80ms after the excitation. The maximum delay due to a train of 10 IPSPs was 100ms.

A burst of IPSPs starting more than 100ms after the start of excitation again failed to produce any effect on the timing of the first action potential. However a late occurring burst of ten IPSPs did have an effect on the subsequent firing as shown in Figure 5-15. The burst of IPSPs was able to suppress firing during the up state for 120ms.

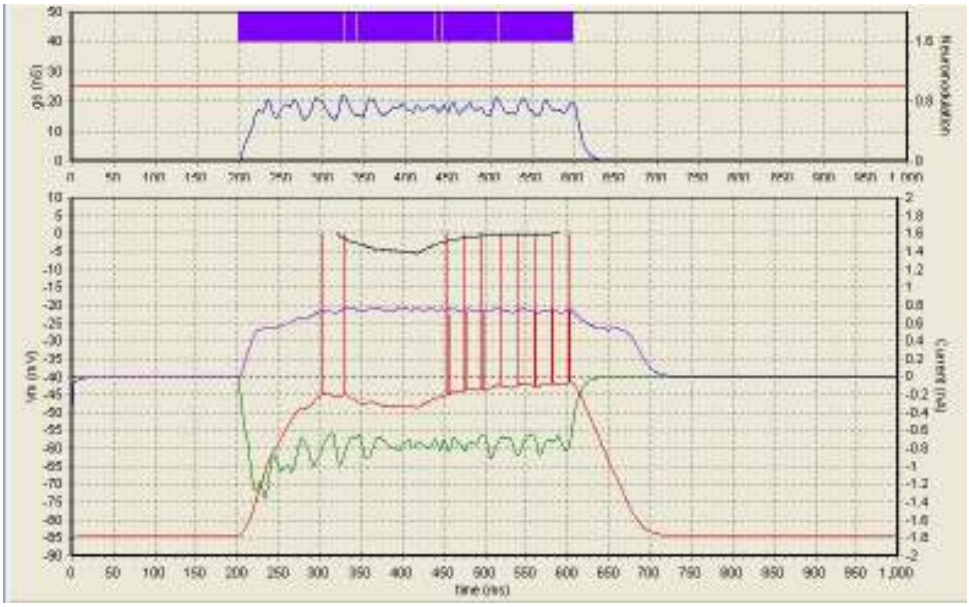

Figure 5-15 Effect of a burst of ten IPSPs occurring during firing of a MS neuron. The train of IPSPs shown here starts 100ms after the start of excitation, which is too late to influence the time of the first action potential in the MS neuron, but suppresses the firing of the neuron for a period of 120ms during the up state.

The spike timing histograms in Figure 5-16 show the consistency of first action potential firing when the inhibition is having no effect, in the periods from 0 to 80ms and 300 to 340ms. In these histograms the times are relative to the start of the simulation and so are 200ms greater than timings relative to the start of excitation.

The histograms also show the breakthrough of first action potential timing occurring at 290ms (90ms after start of excitation). In some runs the first action potential occurs after the inhibition, but in approximately one third of cases, the action potential occurs before onset of the inhibition. This accounts for the large error bar seen at this time step in Figure 5-14.

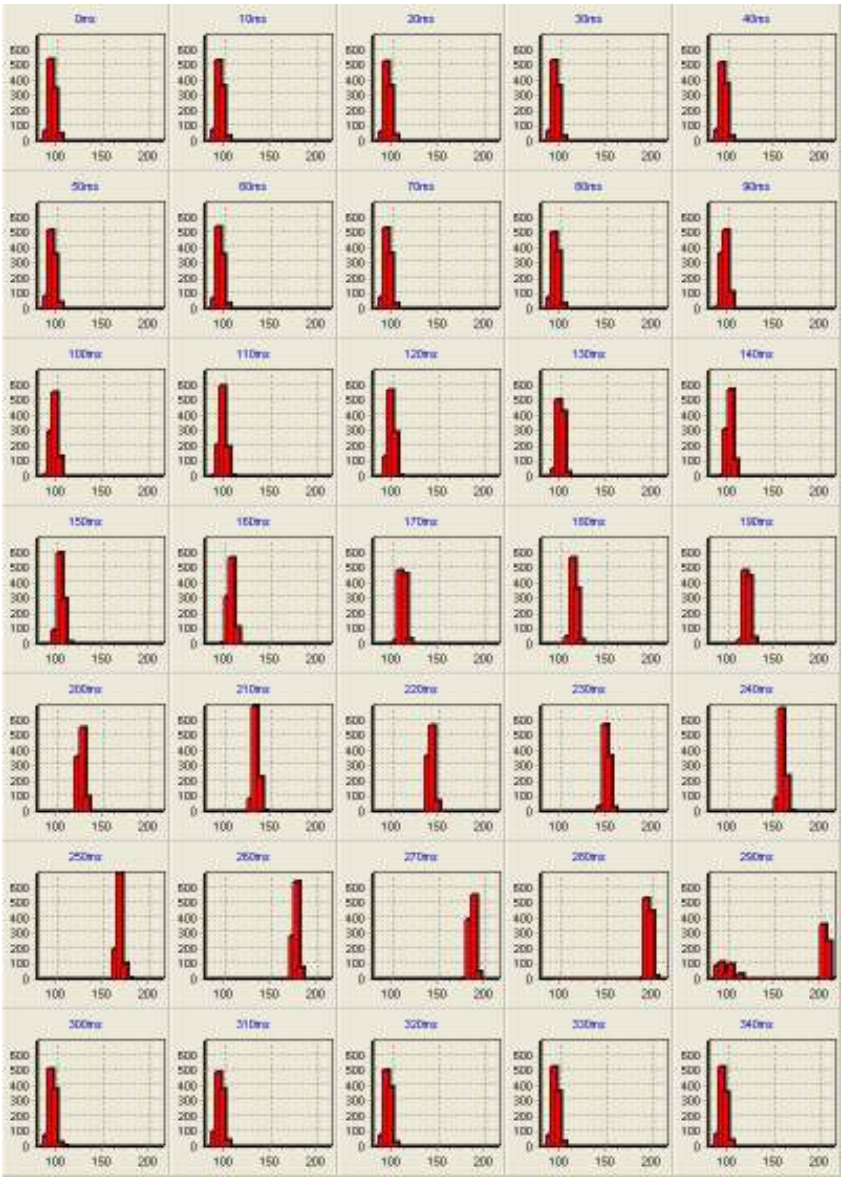

Figure 5-16 First action potential timing histograms for variation in timing of a burst of ten IPSPs. When the train of IPSPs start at a critical point in time, here 340ms (140ms after the start of excitation), the train of IPSPs sometimes suppress the first action potential, but sometimes do not. With the train of IPSPs starting later than this critical point, the first action potential occurs with the same delay after the start of excitation as in the situation when there was no inhibition.

5.4.3 Variation of IPSP count

Ini file: Inhibition count.ini

The previous simulations showed how the timing of inhibition affected the timing of the first action potential in the MS neuron. This set of simulations examines how the number of IPSPs in the burst affects the timing of the first action potential.

First the IPSP burst simulation was repeated with burst counts of 1,2,5,7 and 10 IPSPs. This showed that the most effective timing for the IPSPs to start, irrespective of length of the burst was 85ms after the start of excitation (Figure 5-17). The area from 80 to 90ms after the start of excitation was then simulated with a smaller time step to determine more closely the most effective timing of the start of inhibition. Figure 5-18 shows that the most effective time for the inhibition to start was between 86 and 86.5ms after the start of excitation for all counts of IPSPs in the inhibitory burst. The average time for the first action potential without any inhibition was 94.5ms after the start of excitation. Therefore the most effective time for the inhibition to start was between 8 and 8.5ms before the first MS neuron action potential.

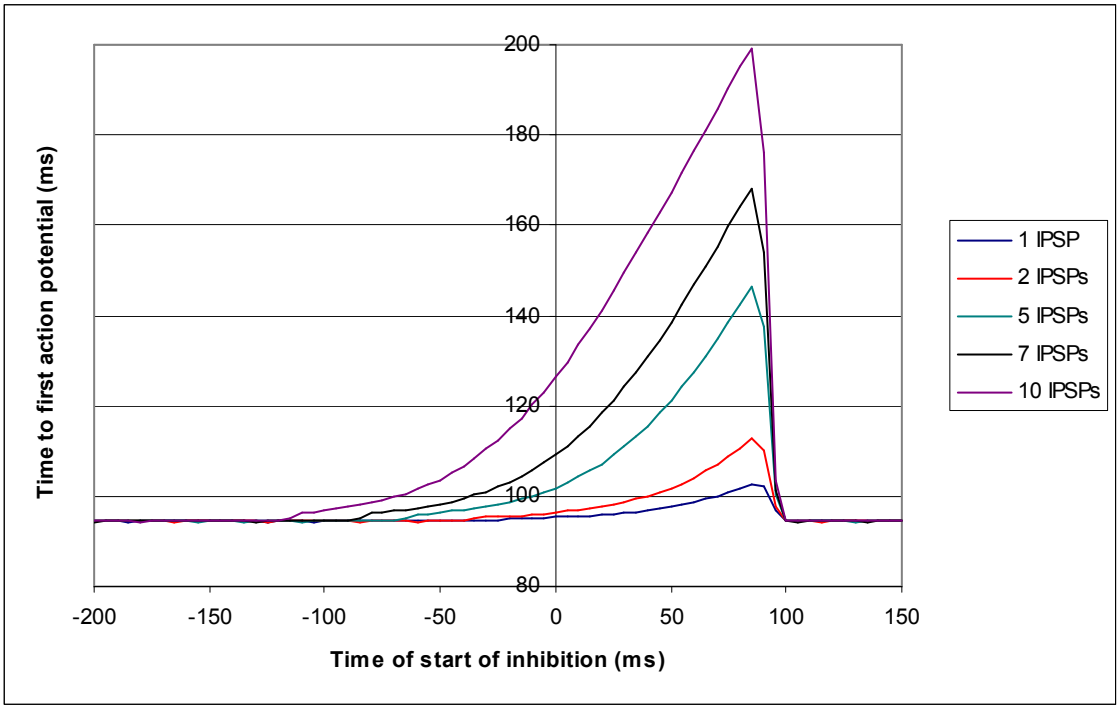

Figure 5-17 Effect of various lengths of IPSP bursts on timing of first action potential. For all lengths of burst, the most effective time of start of the burst is between 80ms and 90ms after the start of excitation.

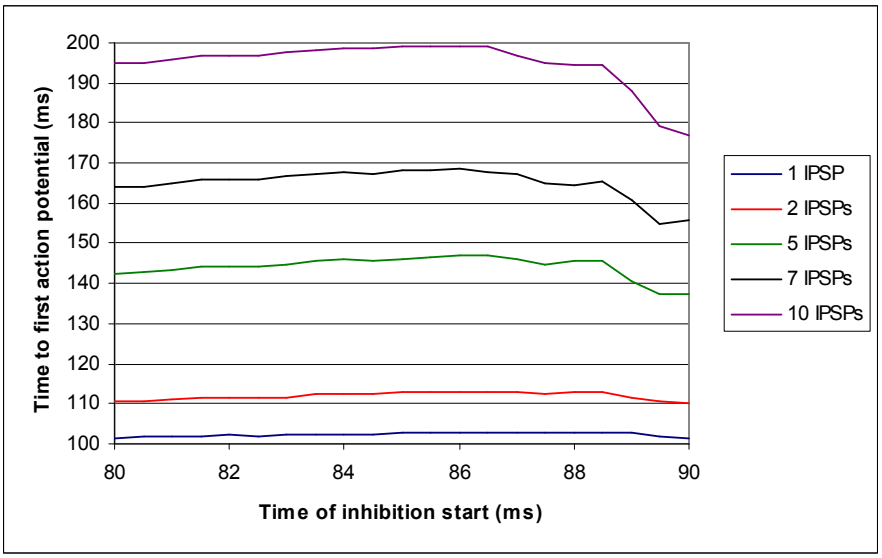

Figure 5-18 Effect of various lengths of IPSP bursts on timing of first action potential – Area of greatest effectiveness with inhibition starting between 80 and 90ms after excitation. This is an expansion part of Figure 5-17 and narrows down the most effective time for a train of IPSPs to start to 86ms to 86.5ms after the start of excitation.

The next simulation investigated delay to the first action potential with a variable number of IPSPs. The burst of IPSPs was started at 85ms after the start of excitation as the previous simulations had found that this was the timing that produced the largest delay in first action potential firing.

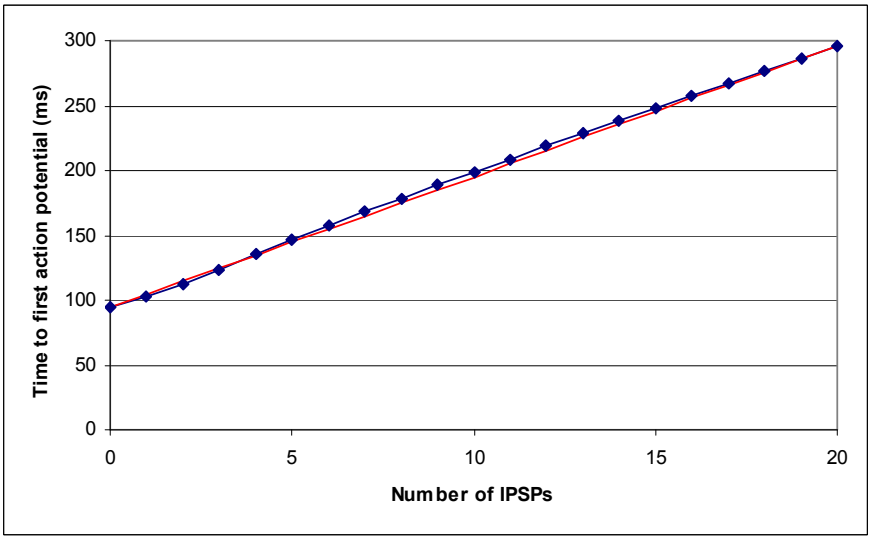

Figure 5-19 Variation of time of first action potential with number of IPSPs in burst. The red line is a straight line drawn through the first and last points in order to illustrate the linearity of the simulated points

In Figure 5-19 a straight line connecting the first and last points is shown in red. This simulation shows that the delay to the first action potential caused by the inhibition is very close to linearly related to the number of spikes in the inhibitory burst.

5.4.4 Multiple FS interneurons firing

Ini file: Multi spike.ini

It has been shown that each MS neuron is contacted by between four and twenty seven FS interneurons with electrical coupling between at least one third of FS interneurons[184]. This suggests the possibility that multiple FS interneurons may fire within a very short period of time, all of which have synapses with the same MS neuron. Koos and Tepper (1999) showed that doublet spikes in a single FS interneuron occurring 4ms apart produced increased delays in the firing of the MS neuron[184]. They also showed that triplets of spikes occurring in a period of approximately 4ms, from another class of inhibitory interneuron, the low-threshold spiking (LTS) interneurons (which are the NOS and somatostatin co-localizing interneurons mentioned earlier), were able to produce delays of up to 20ms in the firing of the MS neuron. As the characteristics of the IPSPs produced by the LTS interneurons were found to be indistinguishable from those produced by the FS interneurons, it would be reasonable to compare the delays produced by multiple spikes at high frequency in the simulator with the experimental results from both FS and LTS interneurons.

These simulations test the effect of multiple IPSPs within a short space of time. This would be equivalent to more than one FS interneuron, all of which have a synapse onto the same MS neuron, firing in a short time period. To replicate the experimental data, spike trains of 0 to 5 IPSPs at 1kHz are used. The delay of the first action potential compared to no inhibition is shown in Figure 5-20. As previously noted, this shows a delay of 7ms attributable to a single IPSP. A train of three IPSPs produced a delay of 20.9ms, very comparable to the experimental findings of the delay caused by spike triplets from the LTS interneuron.

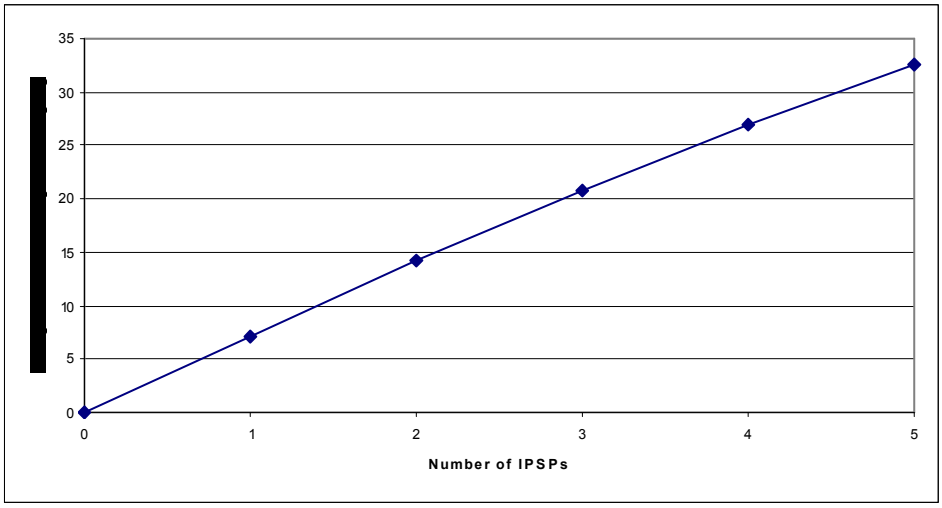

Figure 5-20 Delay to first action potential due to variable length trains of 1kHz IPSPs. The addition of spikes to the train at this frequency produced a linear increase in the delay to the first action potential. The delay produced by a set of three IPSPs is very comparable to that observed experimentally from a train of three action potentials from a LTS interneuron at a similar frequency.

5.4.5 Variation of tonic dopamine level

The tonic dopamine level affects the inwardly rectifying potassium current, I_{Kir}, and the L-type calcium current, $I_{Ca\text{-}L}$. These simulations investigate whether, by affecting the contribution of these currents to the state transition, the tonic dopamine level changes the amount of delay to the first action potential that inhibition causes.

In this simulation the tonic dopamine level was varied from 0.7 to 1.4. This was done both with a set of ten IPSPs, occurring at their point of maximum effectiveness, 85ms after the start of excitation and without any inhibition. Excitation was set at 26Hz.

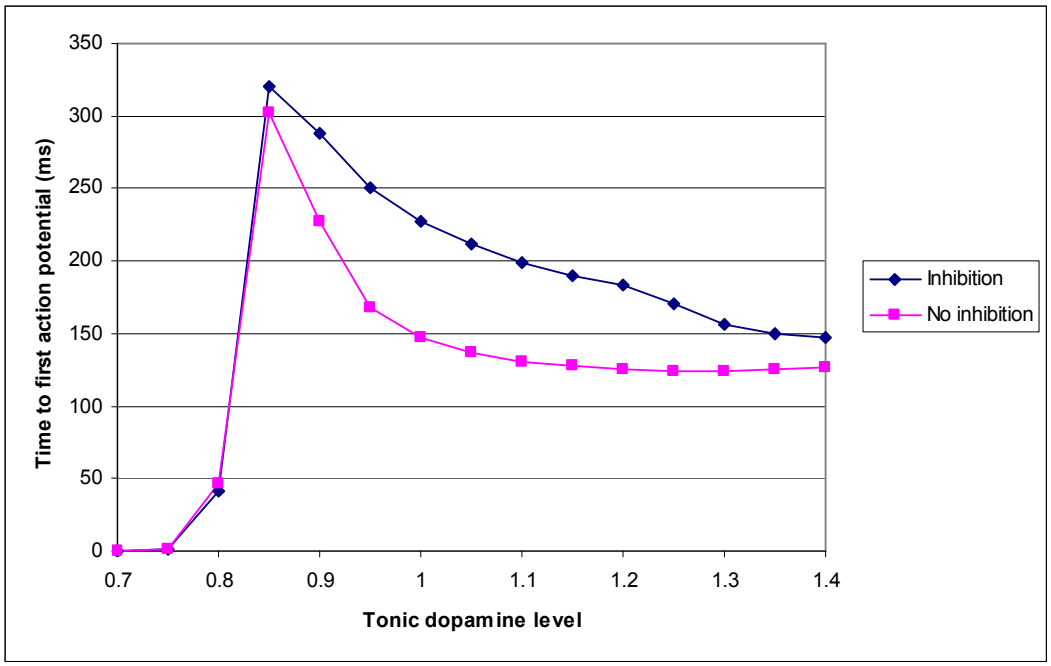

Figure 5-21 Variation of time to first action potential with varying tonic dopamine level, with (pink line) and without (blue line) inhibition. The inhibition produces delays, but the amount of delay is non-linearly related to the dopamine level.

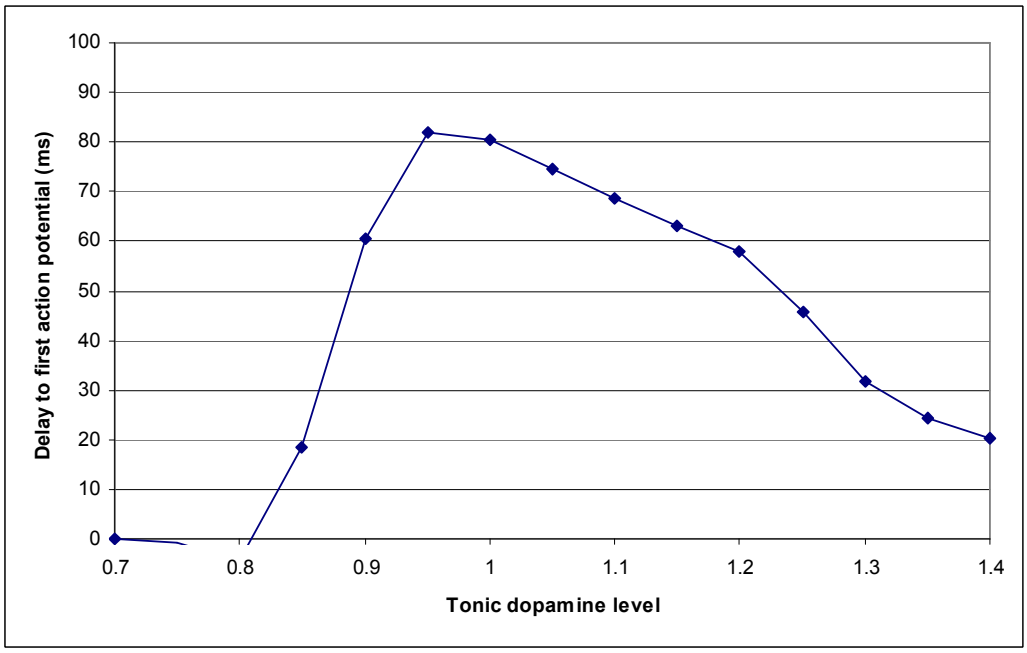

Figure 5-22 Increased delay in first action potential due to inhibition at various tonic dopamine levels. This is the difference between the simulations with and without inhibition in the previous figure. The maximum delay that the inhibition produces is at a dopamine level of 0.9.

Figure 5-21 shows that the time to the first action potential was increased by the introduction of the burst of IPSPs. This is emphasised in Figure 5-22 by showing the extra delay in the first action potential due to the inhibition. This was calculated as the difference between the pink and blue lines in Figure 5-21. Whilst the extra delay induced by the inhibition is very non-linear, the effect of this added to the effect caused by the variation of the tonic dopamine level in the absence of inhibition is to produce a much more linear relationship between tonic dopamine level and the time to the first action potential.

5.5 Discussion

5.5.1 Does the model fit with reality?

The firing of single IPSPs, trains of IPSPs and short, high frequency bursts of IPSPs all produced delays in firing of the MS neuron that were comparable with those found experimentally. This would seem to indicate that the currents used in the model of the MS neuron are adequate for the behaviour investigated and that the parameters chosen are suitable and also that the method of implementing the simulation of feedforward inhibition adequately captures the biophysical effect of feedforward inhibition on the MS neuron.

5.5.2 Could feedforward inhibition control spike timing?

These simulations investigated how the timing of the first action potential could be affected by several different ways of varying inhibition. Some ways of controlling inhibition produced more linear control of the timing of the first spike, with less variation than others.

5.5.2.1 Timing by a single IPSP

Varying the timing of a single IPSP produced maximum delays that were similar to those produced by experimental data. However, the standard deviations of approximately 3ms are 40% of size of the delays produced. This suggests that the control of the timing by a single IPSP is not sufficiently tight to release behaviours with more than 50ms accuracy. Whether this is sufficient for controlling the release of behaviours is not clear.

5.5.2.2 Timing by a burst of IPSPs

Using bursts of ten IPSPs at 100Hz produced much larger maximum delays in the firing of the MS neuron. The maximum delay produced was approximately 100ms. This occurred at the same time as the maximum delay caused by a single IPSP. In both cases the most effective time for inhibition to start was 8-8.5ms before the time a first action potential would occur without inhibition. The burst of ten IPSPs led to the same 3ms standard deviation in spike delay as the single IPSP. As each 10ms change in the timing of the inhibition during its linear phase produced a 9ms change in timing of the first action potential, the variation of delays was far less relevant. This suggests that controlling the timing of a burst of ten IPSPs could control the timing of the release of a behaviour to an accuracy of greater than 10ms.

5.5.2.3 IPSP count

Varying the number of IPSPs within a burst also produced a linear control of the timing of the first action potential in the MS neuron. This simulation was conducted with the inhibition starting at the most effective time point, as revealed by the two previous simulations. The simulation showed that each additional spike added to the burst increased the delay to the firing of the first action potential by 10ms.

As with varying the number of spikes in a burst simulating on FS interneuron firing, simulating the variation of the number of spikes produced by multiple FS interneurons firing in a short space of time also produced a linear control of the timing of the first action potential in the MS neuron. In this case the additional delay produced by each additional spike was 7ms. This fits well with experimental evidence for the delay produced by one spike and a triplet of spikes.

5.5.2.4 Tonic dopamine level

Varying the tonic dopamine level simulates not only what may to a small extent occur naturally over time in behaving individuals, but also to a greater extent in untreated and medicated Parkinson's disease. The minimum level used in these simulations, 0.7 of normal tonic dopamine level may not be as profound a drop as is seen in untreated Parkinson's disease, but as no action potentials were produced at this level of dopamine with the level of excitation used in this simulation, there was no point in testing lower

levels. The upper limit of dopamine used in this simulation, 1.4 times normal tonic dopamine level, was chosen as this is the maximum that the dopamine sensitive currents can be increased by[160].

These simulations showed that increasing the tonic level of dopamine had little effect on the timing of the first action potential when no inhibition was present. Decreasing the tonic level of dopamine when no inhibition was present first produced an increase in the delay to the first action potential, but a further small change in the tonic dopamine level caused this increase to rapidly disappear and finally for no action potentials to occur at all with a tonic dopamine level below 0.75. The increase in time to first action potential as the tonic level is dropped slightly is attributable to swinging the balance in favour of the inwardly rectifying potassium current, thus slowing the rise from the down to the up state. As this effect continues with lower levels of tonic dopamine, the membrane potential finally does not make it to the firing threshold within the time window of the high excitation, and no action potentials are produced.

In the simulation which varied tonic dopamine level the picture changes. When inhibition is introduced at low dopamine levels a similar effect is seen, with no action potentials. At higher dopamine levels the inhibition introduces an increased delay to the first action potential. This delay is maximal at about the standard tonic dopamine level, but is still about 20ms at the maximum dopamine level. This suggests that varying dopamine levels in medicated Parkinson's disease would create a situation where accurately timed release of behaviours becomes difficult due to unpredictable variations in the effect of feedforward inhibition.

5.5.2.5 Mechanisms

From these simulations there would seem to be three main mechanisms which can give a linear control of the timing of the first action potential from a MS neuron, at least over part of their ranges; the timing of the start of inhibition, the number of spikes in a burst from an FS interneuron and the number of FS interneurons firing within a time window where the influence of each action potential has not decayed more than one time constant before the occurrence of the next action potential.

Consideration of all three mechanisms then begs the question of how to control the

timing and burst length of firing of the FS interneuron. It is not necessary to control the absolute timing of firing of the FS interneuron, only the timing relative to the time that the first action potential would be fired by the MS neuron if there were no inhibition.

There are some potential mechanisms for controlling the firing of MS and FS neurons that would keep them in step.

FS interneurons have been shown to be excited by dopamine via D1 receptors[194]. In chapter 4 it was shown that as the tonic dopamine level decreased, the excitation frequency needed to drive the MS neuron to the up state and generate an action potential decreased (Section 4.2.5, page 58). This effect would be offset by the effect of the changing dopamine level on the FS interneuron. As the tonic dopamine level increased, the MS neuron would be more likely to fire under control of a given level of cortical excitation. At the same time the FS interneuron would also be more likely to fire, thus suppressing the firing of the MS neuron. As dopamine causes a depolarization of the FS interneurons, the time to firing of the FS interneuron would be shortened in higher dopamine states, as would the time to firing of the MS neuron in the absence of inhibition. This could combine to keep the timing of the first action potential from the MS neuron, and thus the release of the relevant behaviour, relatively constant.

FS interneurons are also affected by acetylcholine levels[195]. The effects of ACh on FS interneurons have been found to be more complex than that of dopamine, producing excitation via somatic nicotinic receptors but also attenuating the effects of the FS interneurons on the MS neurons by pre-synaptically decreasing the IPSCs induced by the FS interneurons in the MS neurons via muscarinic receptors. FS interneurons also inhibit the cholinergic interneurons forming a feedback pathway. As tonic levels of ACh do not seem to inhibit release of GABA from FS interneurons[196], decreased levels of ACh, as seen when tonic levels of dopamine decrease in Parkinson's disease, could lead to decreased firing of FS interneurons and therefore facilitate the firing of MS neurons. This could be a partial explanation for why such profound loss of mid-brain dopamine neurons occurs in Parkinson's disease before symptoms manifest. Conversely, as suggested by Koos and Tepper[184], increased levels of ACh could also lead to a decrease

in inhibition of MS neurons by reducing the release of GABA each time the FS interneuron fires. This is proposed by Koos and Tepper to offer a mechanism whereby the increased cortical activity during arousal leads to increased striatal activity.

Clearly these complex interactions between neuromodulators, feedforward and feedback inhibition in the striatum could provide ample scope for further modelling studies. However these simulations have shown that there is a possible mechanism within the striatum which would allow learning of timed release of behaviours based on the firing time and pattern of FS interneurons.

5.5.2.6 Phase locking

It has been argued that oscillations in cortico-basal ganglia circuits play an important part in normal and abnormal function [197]. Cells in the dorsal striatum of rats have been found to be entrained to high-voltage spindle (HVS) oscillations, occurring at a frequency of approximately 8Hz[198]. These HVSs also recruit large areas of frontal and somatosensory cortex [199] Berke et al (2004) [198] found that FS interneurons consistently fired at an earlier phase of the spindle than the MS neurons, on average by about 23ms.

Whilst this is less than the optimum time of 85ms calculated from simulations (section 5.4.3, p98), it is still within the time window where significant delays can be caused by a burst of IPSPs.

Therefore the phase locking of firing of FS interneurons and MS neurons may demonstrate that the FS interneurons are controlling the time of firing of the MS neurons.

6 Reward location learning

6.1 Introduction

Chapter 5 explored one putative striatal function, timed control of release of behaviours. This chapter considers a complementary function, learning to select between behaviours. One of the main proposed functions of the basal ganglia as a whole is that they act to release behaviours that would lead to desired actions. The output nuclei do this by releasing the tonic inhibition supplied by the basal ganglia output nuclei[200] [201] [202] [203] [204] [205]. Such a function would require adaptive behaviour, using the environmental context to assess desirability of actions[206].

The aim of the simulations in this chapter is to show that this action selection could be occurring at the level of the input nucleus of the basal ganglia, the striatum. This will be done by using a small network of the model striatal MS neurons developed in the previous chapters and showing that this network of neurons is able to learn the location of a reward and the sequential action selections required to learn a path to efficiently reach the reward.

6.1.1 The teaching signal

An adaptive network, able to learn from experience, needs to have both the ability to recognise that the environmental context is similar to a rewarding situation which was previously encountered and a teaching signal which updates the network based on the outcome of the actions taken in a given environmental context.

The striatum receives input from many other brain areas, including virtually all cortical regions, as documented in chapter 1 of this thesis. It therefore has available a large amount of information about the current environmental context.

The discovery that dopaminergic (DA) neurons of the substantia nigra pars compacta (SNc) and ventral tegmental area (VTA) fire in a phasic fashion in response to rewarding situations[207] [208] provided support for the concept that the basal ganglia are involved in motivation of action[209] by learning from reward[210]. This has come together with ideas from machine learning over the last ten years to establish the idea that dopamine acts as a scalar teaching signal and leads to long term ultrastructural changes

in the striatum.

In a series of experiments (reviewed in Schultz et al (1998)[211]) learning of prediction of reward by DA neurons in monkeys in vivo during acquisition and performance of behavioural tasks was demonstrated. The DA neurons always respond to unexpected reward with a phasic increase in firing. If the occurrence of the reward is reliably predicted by an earlier stimulus, the response of the DA neurons transfers to the time of the earlier stimulus. Once the relationship between the stimulus and the reward has been learned, the DA neurons no longer respond at the time of reward. If, however, the expected reward is omitted the DA neurons respond at the expected time of reward by a phasic dip in firing rate.

Reinforcement learning models have developed from Pavlov's original conditioning experiments[212] via the Rescorla-Wagner model[213], where Pavlovian learning was shown to be dependant on the degree of unpredictability of the reward, and animal learning theory[214]. The temporal difference (TD) model of reinforcement learning uses a reinforcement prediction error signal to learn a reinforcement prediction signal[215]. The learning of the reinforcement prediction signal in a TD model was seen to be very similar to the learned response of the DA neurons[216].

The TD learning algorithms have been adapted for basal ganglia models, mostly in the form of actor-critic models[217 218]. In this class of model the actor learns to perform the action which maximises the weighted sum of future rewards. The rewards are weighted by how far in the future they are predicted to occur, with more temporally distant rewards given a lower weighting than rewards predicted to occur sooner. The critic learns to predict the weighted sum of future rewards based on the current environmental context and the actions the actor takes. The critic learns using the TD learning rule by measuring the scalar error between estimates of reward at two time steps and using this to update its weights[215].

Most actor-critic models of the basal ganglia have concentrated on the learning of the temporal dynamics of the DA cell firing. The actor in these models has generally not been biophysically based and the detail of modelling of the striatum has especially been low. The simulations in this chapter attempt to show how the striatum could work as the

actor. The teaching signal will occur at the time of reward and will not evolve adaptively as the model learns.

Many of the examples in Sutton and Barto's original book on Reinforcement Learning[219] use a gridworld to demonstrate learning of the reinforcement signal. These simulations therefore use a similar approach and demonstrate the learning of spatial navigation by a network of the biophysically inspired model MS neurons developed in the earlier chapters of this thesis.

It has been shown that long term potentiation (LTP) in MS neurons requires a pulsatile dopamine signal[220]. As stated above, the firing rate signals of the dopamine neurons look very similar to the reward prediction error signals of the TD model, but LTP in the striatal neurons is caused by actual dopamine levels, and these may not be the same as the firing rate signals.

There are two main threads of evidence that the dopamine concentration signal may differ from the dopamine firing signal.

The first of these is that the dopamine is probably acting volumetrically in the striatum. The first ideas that dopamine may be involved in learning in the striatum came from anatomical studies showing that excitatory synapses on the spines of MS neurons were commonly co-localised with synaptic terminals of dopaminergic neurons on the neck of the spine. This gave a clear site of action for the learning. However two lines of evidence lead to the conclusion that this is not the major path for the action of dopamine in the striatum. Firstly, whilst all MS neuron spines have an excitatory synapse located at the head of the spine, only 17% of spines also have a dopamine synapse co-located on the neck of the spine. Secondly, most dopamine release sites in the striatum have been shown to be located on extra-synaptic vesicles which release dopamine into the extra-synaptic space[221 222] from where it diffuses to receptors primarily located on the shaft of the MS neuron dendrites. This leads to the current idea that dopamine is more likely to be acting volumetrically[223]. It does leave a conceptual problem with the role of the co-localised dopamine and excitatory synapses in the spine, but at present there seems to be little speculation, let alone evidence, about this.

This form of volumetric action is more difficult to reconcile with current theories of the

mechanism of LTP in synapses located on spines. It pre-supposes that a learning signal becomes global to the neuron due to activation of many dopamine receptors at different points on the dendritic tree. This global learning signal can then be combined with another global signal with information about when the neuron last fired (see section 6.1.8 on credit assignment) to give a signal which conveyed information about what told the neuron had played in releasing an action which led to reward. This signal would then need to be conveyed to individual spines where it would be used to calculate the amount of LTP based on a trace signal in the excitatory synapse detailing when it last received excitation. This is the basis of the three factor learning rule developed in section 6.1.7.

If dopamine is acting volumetrically, concentration time courses at the synapses are then dependent on amount released from terminals, distance from multiple release sites, diffusion dynamics of the dopamine through the extracellular space and uptake rates of the dopamine along the route that it has to diffuse along[224 225]. At points distant to the release terminals this would lead to a temporal spread of the dopamine concentration signal which would be exacerbated by dopamine release from multiple sites at different distances from the receptor.

The second piece of evidence that the dopamine concentration signal may differ from the dopamine firing signal is that release of dopamine from terminals has been shown to be dependent not only on firing rate but also on acetylcholine (ACh) levels[226]. This work showed that if the tonic background level of ACh were maintained, the dopamine output in response to phasic firing was quite low, but that if a drop in ACh occurred at the same time as the phasic dopamine firing, the dopamine output was much increased.

This may not be so important in terms of the signalling as another line of recent work has shown that, at the time of dopamine phasic firing, in both reward and cue situations, there is a closely time-correlated decrease in ACh output[227].

As neither the dynamics of the dopamine concentration change nor the concentration dependent effects of dopamine on signalling pathways are well understood, dopamine signals will be modelled as the simple scalar level changes used in reinforcement learning models.

6.1.2 Construction of simulation

The simulator used in the previous chapters was not suitable for these simulations due to the requirememt for a network of model MS neurons to learn over repeated firings. For the investigations here a new simulator with a more complex interface between the model MS neurons and the excitatory input was developed. To demonstrate the learning of reward location also required the development of learning rules to fit in with the known learning signals in the striatum. This allowed the tracking of learning across multiple trials and repetition of runs of multiple trials to provide averages of behavioural learning.

6.1.3 Simulation environment

The simulations aim to show reward location learning in a gridworld environment. The environment used is shown in Figure 6-1. The current position in the network is represented by an animat. This animat is introduced to the grid at one grid position and must migrate to another grid position to obtain reward.

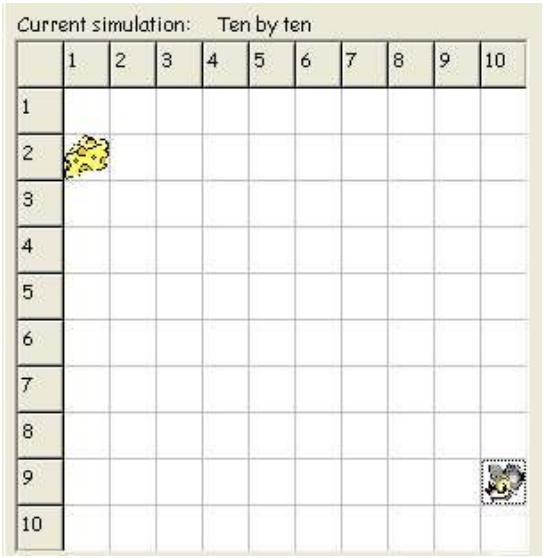

Figure 6-1 Gridworld simulation environment. The animat is shown in the starting position at (10,9). The reward is shown at (1,2). The animat moves one square at a time, left, right, up or down depending on which of four MS neurons fires first.

6.1.4 Spiny neurons

The network consists of four model MS neurons, each of which is associated with movement in a different direction. Firing of a neuron leads to movement in the assigned

direction. This is equivalent to the striatal network deciding amongst four proposed motor programs. The decision over which motor program to execute is taken by the first spiny neuron to fire. This then leads to disinhibition of that motor program. This works in an equivalent way to a winner takes all network, but without competitive lateral inhibition.

6.1.5 Excitatory inputs

The number of excitatory inputs can be specified by the user. In the above example of a ten by ten grid, 12,000 inputs have been used. The excitation is random as detailed in section 2.3.10 (page 25). The amplitude of the EPSPs at the start of the simulation is set to 0.4ns. This is slightly lower than in the previous simulations but allows room for the boosting of amplitude given by LTP without producing unfeasibly large synapses.

6.1.5.1 Connection to spiny neurons

Individual cortical locations give rise to multiple separate foci of innervation in the striatum[228]. Also corticostriatal axons from functionally related cortical regions innervate common foci[229]. These foci are roughly the same size as the dendritic arborisation of a MS neuron. An assumption in these simulations is that the four spiny neurons forming the network are from one focus, innervated by cortical and thalamic neurons conveying information required to make a decision amongst a mutually exclusive set of related behaviours.

It has been estimated that two spiny neurons occupying areas with their dendritic trees totally overlapping would be independently connected to on average 5360 corticostriatal neurons and would only have approximately 75 corticostriatal inputs in common[125]. To simplify slightly for the purposes of these simulations, there will be no overlap of connection from corticostriatal neurons to the four MS neurons of the network. Each excitatory corticostriatal input will be connected to only one spiny neuron.

In the simulations it is possible to connect the inputs to the spiny neurons entirely randomly or to specify that each MS neuron has the same number of excitatory inputs.

6.1.5.2 Connections to grid

Corticostriatal inputs are highly processed, multimodal representations of the

environmental context. The relationship of the firing of a large number of these inputs to features in the environment would be very difficult to obtain and is beyond the scope of these investigations. It is necessary, however, to make a decision as to which corticostriatal inputs will fire in which environmental contexts.

In each simulation each corticostriatal input is connected to a pre-determined, randomly chosen set of grid positions and therefore fires when the animat is any of these grid positions. There is no assumption of any spatial relationship between the grid positions that an input is connected to. In the example 10 by 10 grid shown in Figure 6-1, each input is connected to an average of 5 grid positions, with a standard deviation of 2. An example distribution of the number of grid positions that each input connects to is shown in Figure 6-2. In order to create a level playing field at the start of the simulation, the inputs are connected in such a way that each grid position has the same number of excitatory inputs and each spiny neuron has the same number of excitatory inputs in each grid position. In the example simulation, each MS neuron has approximately 150 inputs in each grid position. This number fits very well with estimates of the number of excitatory inputs firing within a time window of approximately 40ms required to take an MS neuron from the down state to the up state[128].

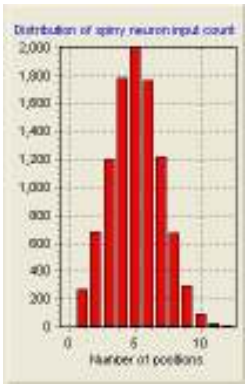

Figure 6-2 Distribution of spiny neuron input count. Inputs are assigned to a mean of five grid positions with a standard deviation of two grid positions.

A summary of the connection scheme for the excitatory inputs is shown in Figure 6-3. Excitatory input 1 will fire when the animat is in any of the positions to which it is connected in the environment and will excite the MS neuron which, when it fires, will cause movement in the up direction.

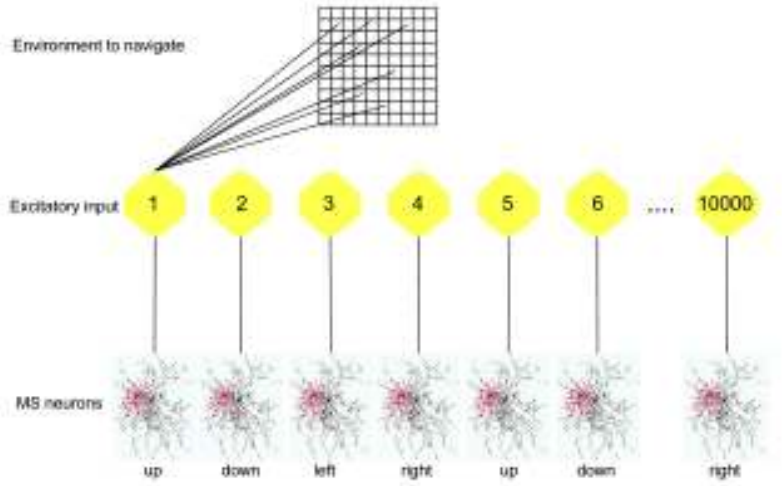

Figure 6-3 Connections of excitatory inputs to grid and MS neurons. In this example, 10,000 excitatory inputs are represented by the yellow circles; the environment is shown as the grid at the top with the positions that the first excitatory input fires in shown by black lines. The MS neurons are shown at the bottom connected to the excitatory inputs on a basis of each input only connecting to one neuron. The MS neurons are therefore represented multiple times.

6.1.6 Movement

The general scheme for movement is as follows. On arriving at a new grid position all the excitatory inputs associated with that grid position start to fire. As with excitatory inputs in previous simulations, some degree of randomness is introduced to the firing of the inputs.

The first spiny neuron to fire causes the plan associated with that MS neuron to be executed. Movement to the new grid position takes 100ms and once the new grid position is reached, the new set of excitatory inputs associated with that grid position start to fire. If no reward is gained in the new grid position, long–term depression (LTD) occurs, and the synaptic weights are updated. The rules used to calculate the synaptic weight changes due to LTD and long-term potentiation (LTP) are laid out in the following sub-section (7.1.7).

Movement is continued until the reward position is reached or the animat stops due to accumulation of LTD. When the reward position is reached, LTP occurs and the synaptic weights associated with each excitatory input are updated. A new trial of that

run of the simulation is then started, unless the previous trial had been the last of that run. In that case, the results for that run are recorded and the first trial of the next run started. The number of trials in a run and runs in a simulation is set by the user. For each new run the excitatory inputs are reconnected, giving the same numbers of connections on each run but a different random pattern of connection to the environment.

For each trial the following data are recorded:

- Total number of MS neuron firing events
- Number of legal MS neuron firing events. This is the number of firing events that actually led to movements and therefore the number of moves taken to reach the reward point.
- Number of illegal MS neuron firing events. These are neurons that fired in positions where their action decision could not be implemented. These are treated as aversive events on the assumption that in real life an animal would find implementing a motor program that involved walking into a wall aversive.
- Number of contended MS neuron firing events. This shows how often two (or more) neurons fired in the same time step. Even when two neurons fire in the same time step, one of the neurons always fires first and this is the neuron used to determine the direction of movement.
- Which spiny neuron fired to cause the final step to obtaining the reward. This is useful for assessment of runs in which contention occurred at the time of this final step to obtain reward. In such cases the neuron that fired later will also receive a significant amount of LTP. The problems which this can lead to are discussed in section 6.2.10 (page 156).

6.1.7 Learning

At the start of the simulation, each excitatory input has a synaptic weight of one. As the simulation progresses, learning occurs by modification of this synaptic weight. The synaptic weight provides a multiplication factor for the conductance. So changing the synaptic weight is equivalent to changing the maximum excitatory conductance. The

synaptic weight is used for display purposes as it makes comparison of learning across simulations clearer when the starting maximum excitatory conductance is varied.

The synaptic weight is updated in three circumstances.

- The weight is decreased each time the neuron fires.
- The weight is increased when reward is obtained.
- The weight is decreased when an aversive event occurs.

This is equivalent to long term depression (LTD) occurring each time a neuron fires[230] or an aversive event occurs and long term potentiation (LTP) when reward is obtained[220]. The learning in both cases is based on spike timing dependent plasticity (STDP) rules[231] [232], with a modification such that strong synapses undergo relatively less potentiation than weak synapses[233]. Under these rules synapses are potentiated or depressed based on the relative timing of an input synaptic event with an output postsynaptic potential. In a standard implementation of these rules in hippocampal neurons, a synaptic event occurring before a postsynaptic potential will lead to LTP and a synaptic event occurring after a postsynaptic potential will lead to LTD[234]. In this model it is not the timing of the synaptic input in relation to the postsynaptic potential which is important, but the coincident occurrence of a dopamine pulse and the rules for when LTD and LTP occur have been modified accordingly.

For LTD the update rule is as used in van Rossum et al (2000)[233] and is shown in (6.1).

$$W \to W - C_d.W\left(e^{\delta t_{input}/T_{STDP}}\right) \qquad (6.1)$$

Where W is the current synaptic weight, C_d is the average amount of depression from one pairing, δt_{Input} is how long before firing an excitatory input occurred at this synapse and T_{STDP} is the decay time constant for the synaptic input. Note that, from this rule, the weight change is proportional to the current weight. Therefore the smaller the synaptic weight the less LTD will occur from one input spike-output spike pairing.

For LTP the update rule is more complex. This expresses the proposed three factor rule for striatal learning[203], which involves the conjunction of pre- and post-synaptic activity

with a dopamine reward signal. Previously, this rule has only been expressed qualitatively. The reasons for using these particular formulations for the pulsatile dopamine and the post-synaptic activity are discussed below.

$$W \to W + \Delta D\left(e^{-\delta t_{fire}/T_{DDP}}\right)\left(e^{-\delta t_{input}/T_{STDP}}\right) \tag{6.2}$$

where ΔD is the proportional dopamine change, δt_{fire} is the time since the MS neuron fired, T_{STDP} is the decay time constant for the synaptic input trace and T_{DDP} is the decay time constant for the neuron firing. T_{STDP} is the trace for synaptic input in both the LTP and LTD rules. This represents a process such as influx of calcium into the dendritic spine occurring after the depolarization of the dendritic spine compartment caused by an excitatory input[235]. In theory this constant should be the same in both LTP and LTD.

In the LTP rule the weight change is independent of the current weight. Therefore a synapse with a small weight will receive the same amount of potentiation as a stronger synapse which had a coincident input. But this amount of potentiation will be a greater proportion of the original synaptic weight for the smaller synapse. This potentiation could continue with each reinforcing event as there is no upper bound on the synaptic strength introduced by (6.2). As there is a limit to how much a synapse can grow, a constant upper bound is introduced into the simulations. Generally in these simulations that limit has been set to 3, although the effect of varying this limit is investigated. This produces a maximum EPSP amplitude of 1.2nS.

The three factors in the LTP learning rule used here are the change in dopamine level, the time since the neuron last fired and the time since the synapse last received input. The timings for the update are measured from the time that the reward is received. This treats the dopamine signal as if it were a delta pulse. In reality the dopamine release has a rise and fall time lasting over a couple of hundred milliseconds and the amount of LTP occurring will be related to the dynamics of the rise and fall of dopamine concentration in convolution with the falling calcium concentrations in the dendrite and synapse. As the dynamics of these interactions have not been modelled, it is reasonable to treat the timing of the reward as taking a snapshot of the dendritic and spine calcium and basing the LTP on the picture at that moment in time.

The change in dopamine level is not here constrained to the 1.4 times baseline level that was used in the previous chapters as we are not here considering the effects of dopamine on the I_{Kir} potassium and L-type calcium currents, but rather the effects of calcium influx through NMDA channels[236] and calcium release from internal stores[237] leading to LTP and LTD. Although the influx of calcium may be limited by the characteristics of the channel or the buffering of the internal stores, there is no evidence as to whether the effects of calcium on LTP or LTD induction are linearly related to the amount of calcium influx. So, although this variable has the same name as that used in the earlier simulations, it models a different process and is not constrained in the same manner. A default value of 1.6 for the rise of dopamine is used as this produces an approximate doubling of synaptic weight in a synapse that was activated less than 5ms before firing leading to reward occurred.

There is no account taken in this model of the learning of the dopamine signal that would occur in an actor-critic model architecture. This model is examining only the actor and whether it has the capability of learning the navigation task based on receiving reward at the termination of the task. There is also no account taken of habituation to the reward. It is possible that using reward habituation would allow higher learning rates at the start of the model without producing unfeasibly high average synaptic weights by the end of the simulation. As there is no evidence for this effect, the worst case scenario of stable reward values across the simulation is used.

6.1.8 Credit assignment

In reinforcement learning models the difficulty of correctly attributing credit for a rewarding outcome, which may happen at many time steps removed from the event which led to the outcome, is known as the credit assignment problem.

Some reinforcement learning models of basal ganglia function have tried to solve this by the use of mechanisms such as temporal stimulus representation[238] [239] [240]. However, no model with a reasonable biophysical mechanism for credit assignment has yet been produced.

Recent studies of calcium imaging in MS neurons by Kerr and Plenz (2004) have shown that an action potential produces a back-propagating calcium concentration spike[186].

These calcium transients penetrate to the tertiary dendrites, the site of many spines and, therefore, excitatory input. The peak of the calcium transient was shown to be inversely related to the time of the first action potential after the MS neuron transferred to the up state. Figure 6-4 below (part of Figure 4B of the Kerr and Plenz paper[186]) shows the time course of several calcium transients occurring at different delays after transit to up state. From the calcium transient that occurred due to an action potential 10ms after the start of the up state, it can be seen that the calcium transient in the tertiary dendrite did not return to baseline for approximately 2s after the action potential occurred. This duration of signal may well be long enough to provide credit assignment in MS neurons.

Kerr and Plenz interpreted their findings as showing that the later the action potential the smaller the magnitude of the calcium transient. To this end in their Figure 4B they superimpose the rise of each of the dendritic calcium transients. If, instead, each transient is right shifted so that the decays are superimposed this could be looked at in a slightly different way. If, say, the action potential occurs 10ms or 100ms after up state is reached then at, say, 200ms the dendrite sees the same calcium level due to either timing. That is to say that the calcium level seen is not related to the time of firing, but to the time that the neuron entered the up state.

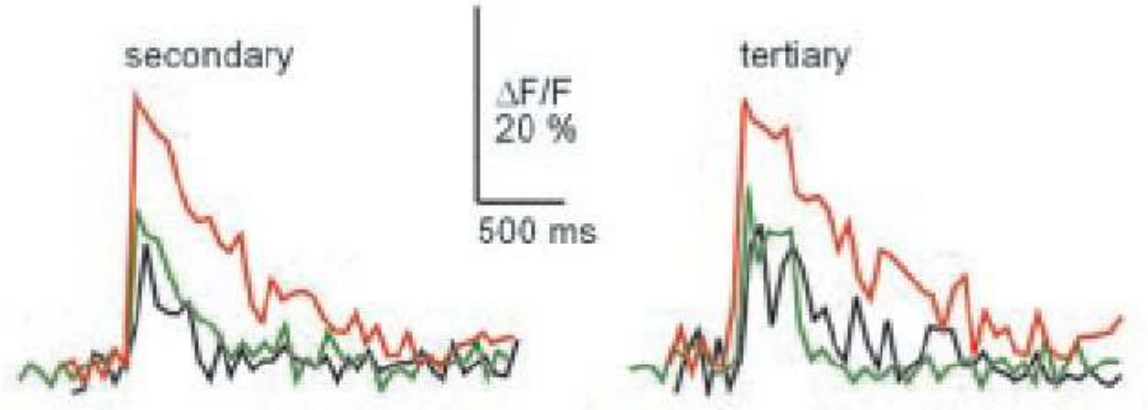

Figure 6-4 Calcium transients evoked by action potentials (acknowledged to Kerr and Plenz[186]). The three transients shown are evoked by action potentials occurring 10ms (red), 78ms (green) and 100ms (black) after the start of the up state.

One way to model this would be to start the decay of a calcium transient with maximal amplitude when the up state is entered. This could be considered to be when the

membrane potential rises above -55mV. The amplitude that the calcium transient reaches when the MS neuron fires can be found by the exponential decay from the potential maximum amplitude at the time the neuron transited to the up state.

Assuming an exponential decay of the calcium signal, the figure of 2 seconds to return to baseline levels would give a time constant of approximately 400ms for T_{DDP} in the LTP weight update equation (6.2). This figure may be rather longer than the physiological figure as the method of calcium measurement involves use of an agent, FURA, which acts as a buffer of the calcium, binding it very rapidly but releasing it more slowly. A conservative figure to use for T_{DDP} in the simulations, 200ms, has therefore been adopted.

This gives a method for determining the credit when a reward is obtained. However the calculation of the LTP is based on more than just this credit assignment. LTP is also dependent on the change in dopamine level and the synaptic trace. The credit assignment variable and the dopamine level are the same for all synapses in the neuron, but the synaptic trace depends on when each synapse received excitatory input. Although this means that only synapses that had input in the grid positions within a few steps of the reward will be potentiated, it should be noted that, because each excitatory input fires in multiple grid positions, synapses which are active in all grid positions are strengthened by the reward.

6.1.9 Disappointment

Since all four MS neurons are activated in all grid positions, it is possible to select a plan which is impossible, such as going left when the animat is already against the left wall. Based on the idea that an animal would find banging its head against a wall aversive, a disappointment factor is applied in these situations.

To model disappointment, the dopamine level is dropped and the trough level used to calculate amount of LTD. The update rule is a cross between the LTP and LTD rules. The weight decrease is proportional to the current weight as for the LTD rule. And, as for the LTP rule, this is three factor learning using the proportional drop in dopamine level, a synaptic trace showing how long before the neuron fired that particular synapse had an excitatory input and a back propagation trace showing how long before the

dopamine pulse the neuron fired.

$$W \to W - W.\Delta D\left(e^{-\delta t_{fire}/T_{DDP}}\right)\left(e^{-\delta t_{input}/T_{STDP}}\right) \quad (6.3)$$

Again, T_{STDP} would seem to be implementing the same synaptic trace mechanism as in the earlier LTP and LTD rules, so should in theory be assigned the same value.

Evidence for dopaminergic neuron firing decreasing in aversive situations is controversial[241], and the earlier cited work showing that ACh levels control dopamine release in response to DA cell firing adds another variable to this equation. Even if the mechanism modelled for disappointment here is incorrect, it is probable that there is some similar striatal mechanism for learning of aversive events. How this disappointment factor affects learning will be examined in the simulations.The default values for learning parameters are shown in Table 6-1.

Symbol	*Description*	*Value*
W	Initial synaptic weight	1
C_d	Average amount of depression after one pairing	0.01
ΔD	Reward proportional dopamine level change	1.6
ΔD	Disappointment proportional dopamine level change	0.6
T_{STDP}	Time constant for synaptic input trace	150ms
T_{DDP}	Time constant for credit assignment	200ms
W_{max}	Maximum synaptic weight	3

Table 6-1 Default values for reward location learning simulations

6.1.10 Simulator interpretation

As explained above, the simulation environment used here is different to that in the previous chapters and therefore has a different user interface. A typical state of the simulation environment at the end of a run of 100 trials is shown in Figure 6-5. In this simulation the reward was in position (1,2) [All positions used here are represented (column,row)]. As it is very difficult to interpret the raw, changing synaptic weights during simulations, there are two graphical representations of the synaptic weights in the simulator.

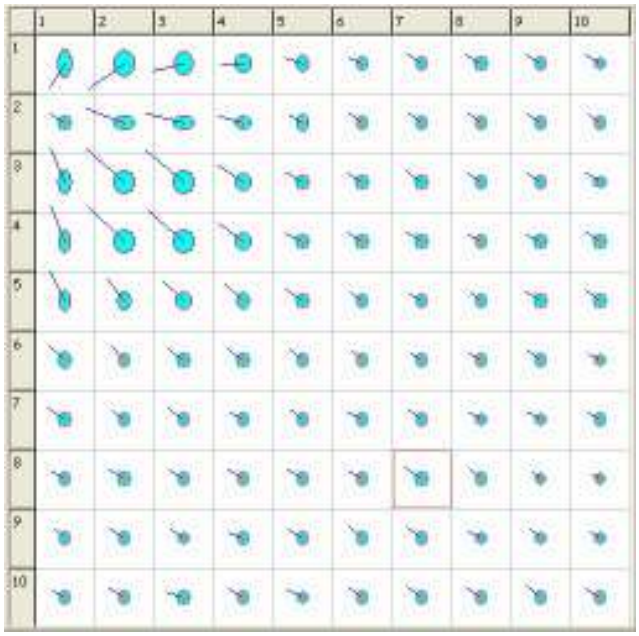

Figure 6-5 Simulator status at the end of a run of 1000 trials. The reward was located at (1,2) and the animat started each trial from (10,9). The vectors from all positions are tending to move the animat towards the reward position. The vectors nearer the reward position show a larger absolute magnitude as the ellipses are larger, but the differentiation between directions over the whole grid is good.

The blue lines show the magnitude and direction of the resultant synaptic weights. The horizontal component of the vector is calculated as (synaptic weight [left] – synaptic weight [right]). Synaptic weight [x] is the average of all the synaptic weights for the neuron specifying direction x in that particular grid position. A similar calculation gives the vertical component of the vector. This line gives a visual indication of the probability that a move will be made in a given direction when the animat reaches this square. Due to the noise in the excitation and effects of activation and inactivation of the slowly inactivating potassium current[135] this value can never definitely specify which direction the animat will take. However, the longer the line and the more it is oriented towards one square, the more likely that direction is to be taken.

The aqua ellipses show the total horizontal and vertical strength of synapses in a grid position. The horizontal component of the ellipse is calculated as (synaptic weight [left] + synaptic weight [right]). This combination of lines and ellipses gives

$$V_H = L - R \tag{6.4}$$

$$V_V = U - D \tag{6.5}$$

$$E_H = L + R \tag{6.6}$$

$$E_V = U + D \tag{6.7}$$

where V_H is the horizontal component of the line vector, V_V is the vertical component of the line vector, E_H is the horizontal component of the ellipse, E_V is the vertical component of the ellipse, L is the total synaptic weight in the current grid position of the MS neuron which specifies left movement and R, U and D are the same for the MS neurons specifying respectively right, up and down movements.

From these equations the synaptic weights in each direction can be specified as a combination of the line and ellipse components.

$$L = \frac{1}{2}\left(E_H + V_H\right) \tag{6.8}$$

$$R = \frac{1}{2}\left(E_H - V_H\right) \tag{6.9}$$

$$U = \frac{1}{2}\left(E_V + V_V\right) \tag{6.10}$$

$$D = \frac{1}{2}\left(E_V - V_V\right) \tag{6.11}$$

From these equations it can be seen that if the ellipse has a large horizontal component but the line has a small horizontal component then the impulse to both the left and right will be very similar.

Figure 6-6 shows the output of the simulator at the early stages of a simulation to illustrate graphically the different informational content of the line vector and the ellipse. In position (1,1) the line vector shows the predominant synaptic weight as directing movement to the right. However, the ellipse shows that there are also similarly strong synaptic weights leading up and down. The up and down synaptic weights produce no resultant tendency in the vertical plane, but are as likely to be the direction decided upon as going rightwards would be when the animat reaches position (1,1). Only direction left is unlikely to occur in this position. Position (1,3) is similar. Here the vector indicates a strong disposition to go to the left, but the ellipse shows that the most

likely directions to be taken are either up or down. The vector shows that up is slightly more likely than down.

When one direction becomes much stronger than all others, a representation such as that seen at (2,2) occurs. The line vector is strongly in one direction and the width of the ellipse in the orthogonal direction is low.

As the simulation progresses, the line and circle tend to show information that is more in step, but having both sets of information aids detecting reasons for failure of simulations as will be shown later.

If the average synaptic weight of all four neurons at a certain grid position falls below 0.75, the ellipse turns completely red as shown in Figure 6-7.

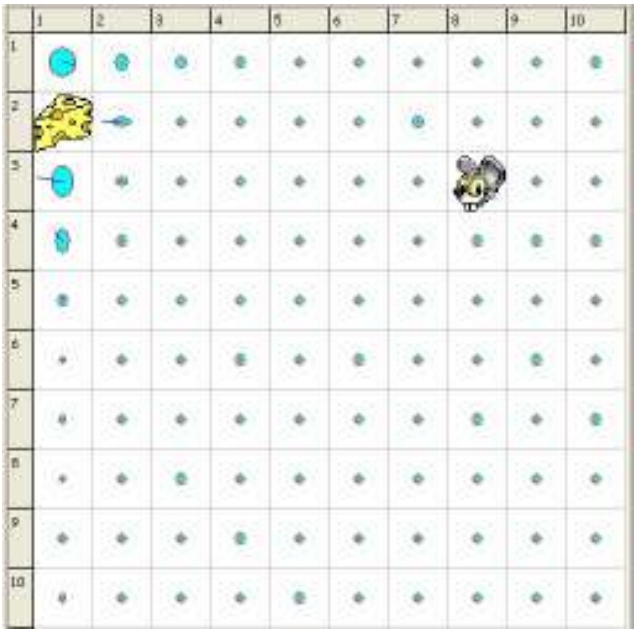

Figure 6-6 Simulator output from early in a run showing ellipses with different interpretations. The ellipse at (1,1) shows that both up and down have strong vectors as well as right. The ellipse at (1,3) shows that up and down have strong vectors and that there is a strong left vector, though not as strong as the up and down. The ellipse at (2,2) shows a strong single vector in the left direction.

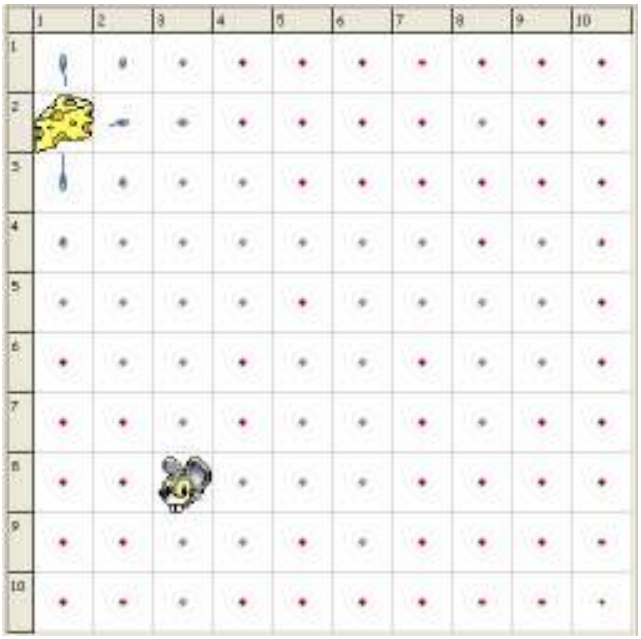

Figure 6-7 Low weight synaptic vectors are shown in red to indicate areas where the simulation might fail. The colour change occurs for positions with an average synaptic strength over all four directions of less than 0.75.

6.1.11 LTP and LTD from single events

The amount of potentiation and depression seen by a single synapse is dependent on several factors. For potentiation these are the time since input to the synapse, the time since the neuron fired and the proportional change in dopamine levels. For depression the main factors are how long before firing an input occurred and the proportional depression from one event.

It is thus difficult to visualise how much potentiation or depression will occur from one pairing. This section presents some graphical illustrations of potentiation and depression.

The depression from one pairing is described by the single exponential in equation (6.1) (page 118). The value used in these simulations for the depression from one pairing, C_d, is 0.01, with a time constant of 150ms. This produces the exponential decay of synaptic depression shown in Figure 6-8. Even if firing occurs immediately after the synaptic event, the amount of depression is only 1% of the synaptic weight. If the synaptic event occurs 100ms before firing, the depression amounts to only 0.5%.

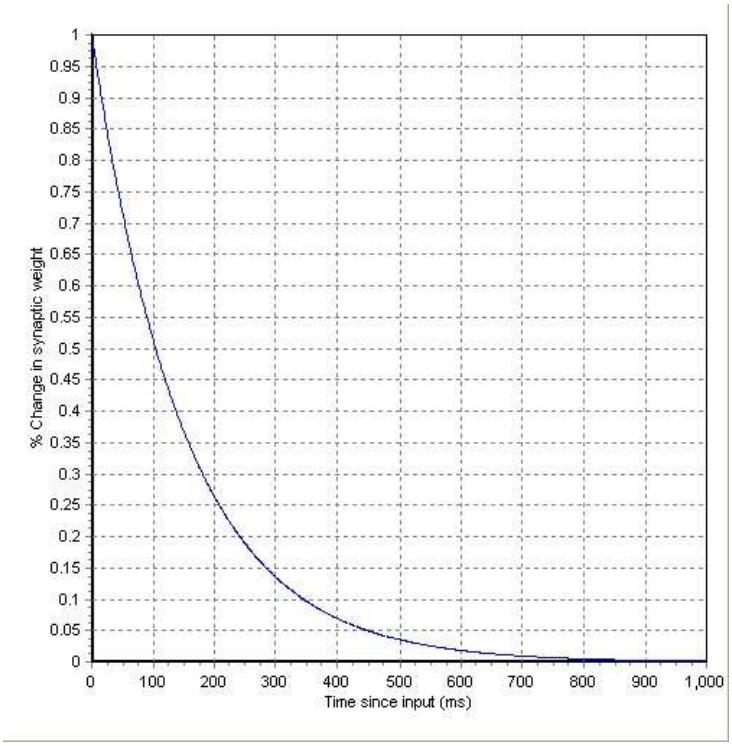

Figure 6-8 Percentage synaptic depression from one pairing. The amount of depression decreases exponentially as time that the synaptic input occurs before firing increases..

Potentiation is more complex as it is the product of two exponentials (equation (6.2), page 119). The value used for the back propagation time constant in these simulations is 200ms.

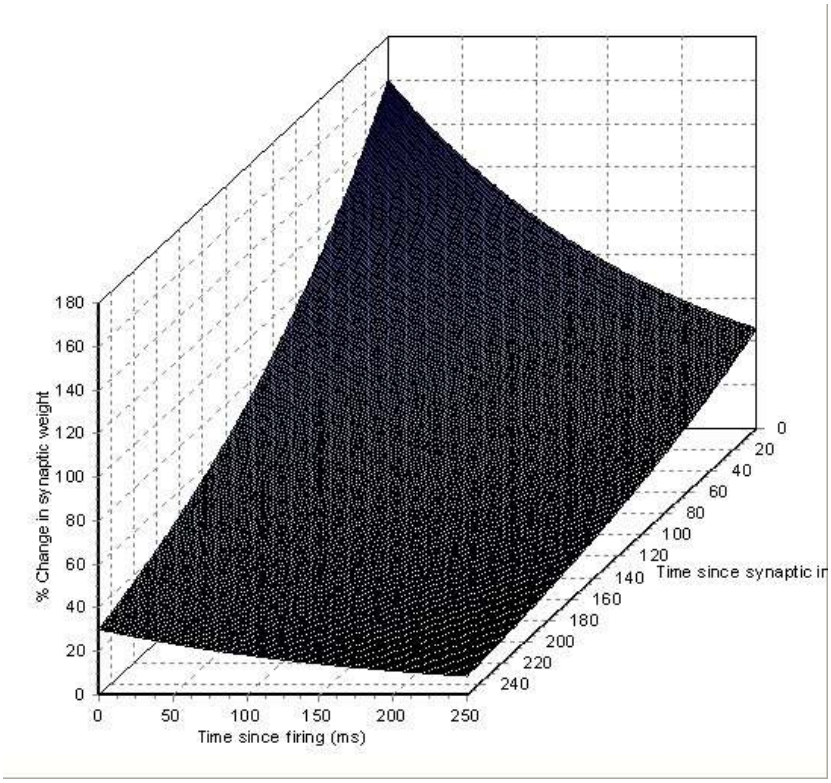

Figure 6-9 Variation of percentage potentiation with time since synaptic input and time since firing. The Z-axis is inverted to show the coincidence of synaptic input, firing and reward in the top left hand corner. If the synaptic input and firing occur at the same moment as the reward, the increase in synaptic strength is 160%. If the synaptic input and firing occur 250ms before reward, the increase in synaptic strength is 8.66%.

Using a dopamine pulse level of 1.6 times base level, this gives a maximum synaptic potentiation of 160% when the input and firing occur at the same moment as reward. This decreases to 8.66% potentiation when both the input and the firing occurred 250ms before the reward. The general shape of the surface these two exponentials produce can be seen in Figure 6-9, although individual figures are still hard to discern.

Studies using intracranial self stimulation (ICSS) in rats have shown that a single pairing of post-synaptic potential with ICSS reward can lead to increases in PSP amplitude of up to 97%[242].Figure 6-10 shows the relationship between values of time since synaptic input and time since firing which can produce a 100% potentiation of synaptic strength. It can be seen from this graph that, for instance, if synaptic input occurs 50ms before a reward, then if firing occurs 27.3ms before reward then the synaptic size will double with a phasic dopamine level of 1.6 times.. From this graph it can also be seen that if the synaptic input occurs less than 40ms before reward, then the

firing would have to occur before the synaptic input to only produce a doubling of the synaptic size. If the firing occurs after the synaptic input in this case, the increase in synaptic weight would be greater than 100%. This implies that in the normal situation where firing occurs after synaptic input, when a reward is obtained, all synapses which had input less than 40ms before the reward was obtained will have their synaptic weights at least doubled.

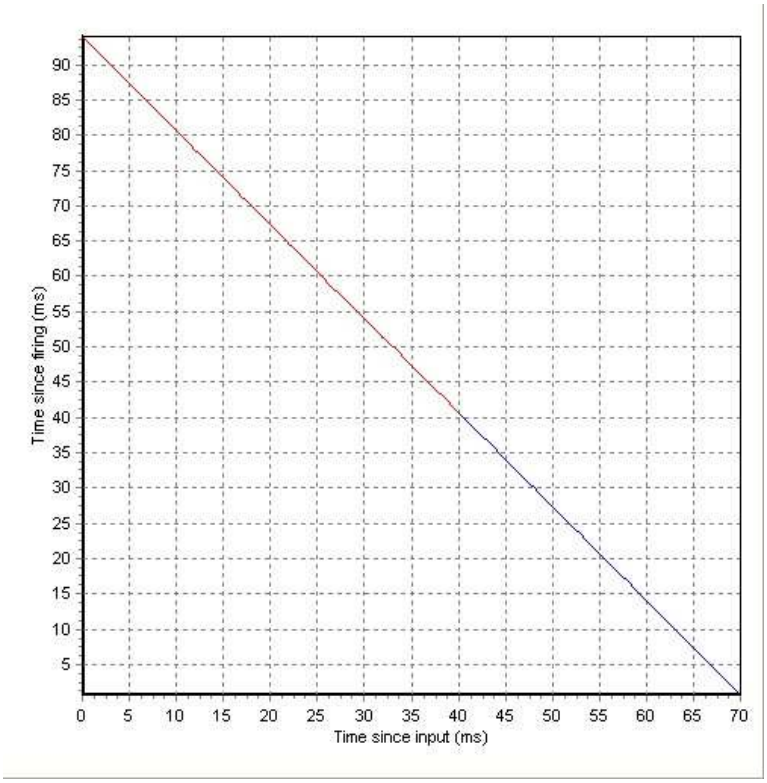

Figure 6-10 Possible values of time since firing and time since input to produce a doubling of synaptic weight. Times where synaptic input occurs before firing are shown in blue; times where synaptic input occurs after firing are shown in red.

A 10% increase can be produced by synaptic inputs and firing occurring far earlier in relation to reward. For instance a synaptic input 250ms before reward paired with firing 221ms before reward would produce a 10% potentiation. This would allow for significant potentiation of not only the neuron that led directly to the reward, but also the neuron that caused the penultimate move leading to reward. The crossover point between input and firing coming first shows that any synapse receiving input less than 240ms before reward will gain at least 10% in synaptic weight.

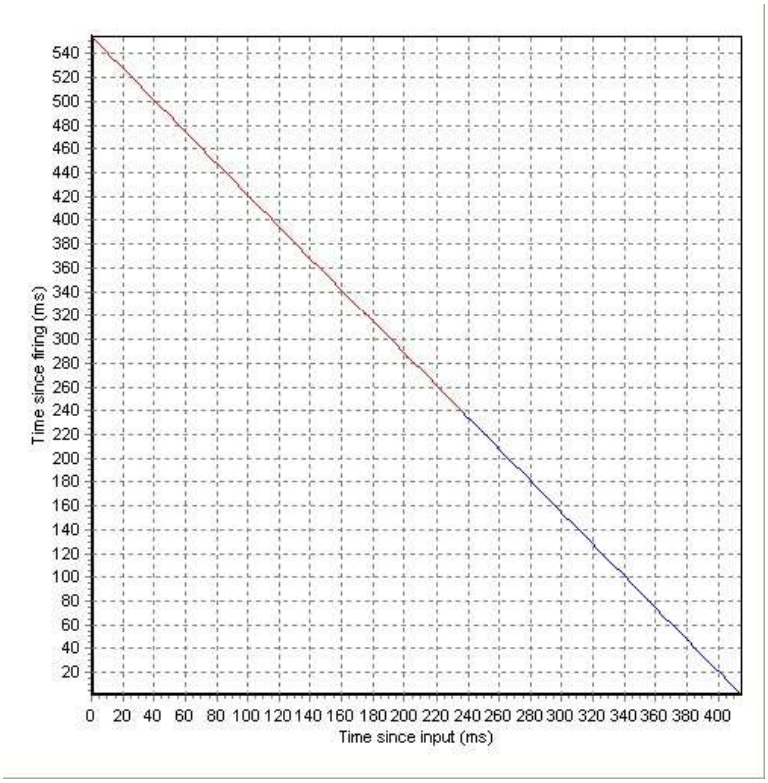

Figure 6-11 Possible values of time since firing and time since input to produce a 10% potentiation in synaptic weight. Times where synaptic input occurs after firing are shown in red.

6.2 Simulations

6.2.1 Assessment of simulations

The aim of these simulations is to show learning of the spatial navigation task and analyze some of the factors affecting that learning.

Assessment of whether learning has occurred can be made by considering path lengths. In the illustrated simulations above, using a ten by ten grid, the shortest path is 16 moves. For these simulations learning of the path will be taken to be when the animat completes three consecutive runs taking no more than 20 steps. This allows for two errors to be made and retraced during the run.

A secondary requirement is that the synaptic weights stabilise over the course of a simulation. If the synaptic weights keep decreasing the simulation will eventually stop as the excitation is insufficient to cause firing. If the synaptic weights keep increasing there are two consequences. Firstly, the effects of learning will be lost as all synaptic weights become close to the maximum allowed weight. Secondly, if average synaptic

weights increase they will fall outside the size that could be realistically expected biologically.

The rate of failures in simulations is also important. If the animat stays in a grid position for more than five seconds of simulation time, that run is said to have failed and the simulation is resumed at the next run with a new set of input connections and synaptic weights reset to one. It is known that in vivo not all animals will always successfully find the reward in an environment. If they do not find the reward after a delay of a few minutes, they will stop searching and possibly settle down to sleep, so instances of this sort of failure are not entirely unexpected. In these simulations a failure rate of greater than 10% of runs is considered to show that learning and/or exploration are inadequate. Some pointers as to why failures may occur are given in later simulations.

6.2.2 Optimum parameters

This first set of simulations uses a set of parameters which have a very high completion rate, with rapid learning. As will be seen in later simulations there are many parameter sets which are equally successful, but the parameters used here have the most conservative values whilst maintaining an almost perfect learning record.

Parameter	Value
Trials per run	1000
Runs per simulation	50
Number of excitatory inputs	12000
Tonic dopamine level	1
Dopamine pulse level	1.6
Dopamine trough level	0.6
Backpropagation time constant (ms)	200
Synaptic time constant (ms)	150
Maximum synaptic weight	3
Proportional depression from one pairing	0.01
LTD selection method	Proportional to time of last input
Contention selection method	Do move for spiny which fired first
Use disappointment	Yes
Disappointment method	Neuron causing illegal move

Table 6-2 Standard learning parameters for reward location

Excel spreadsheets of the results from these simulations are included on the CD, in the Reward Learning Results directory. The results files used are detailed at the start of

each simulation sub-section.

Results file: 1000 trials - standard.xls

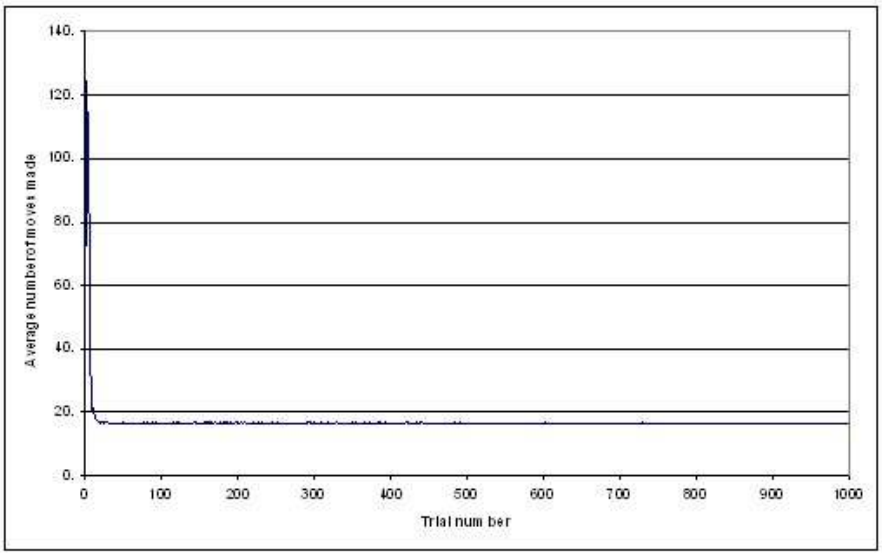

Figure 6-12 Average number of moves made on each trial of a run. This has been averaged over 50 runs, each consisting of 1000 trials The minimum number of moves to reach the reward in this 10x10 grid is 16.. The number of moves is high for the first few trials, then settles to a value close to the optimum with little variation over the remainder of the trials.

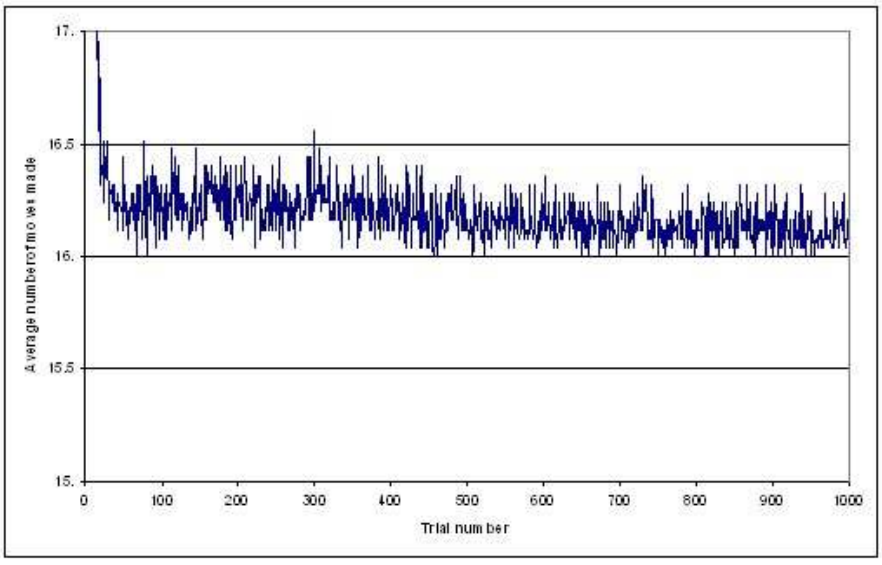

Figure 6-13 Close up of average number of moves made over 1000 trials. The optimum number of moves is 16. This is rarely achieved. This shows the trial-to-trial variation is maximally 0.6.

In this set of simulations, each run consisted of one thousand trials, with LTP occurring at the end of each trial. 50 runs were averaged to produce the simulation results. Of the

50 runs only one failed to complete.

Figure 6-12 shows the average number of moves taken for each trial of the run. The shortest path in this 10 by 10 grid requires 16 moves. The average number of moves taken over the last 500 trials was 16.13. The small amount of trial to trial variation once the path has been learnt is shown in Figure 6-13.

Figure 6-14 shows a histogram of the number of trials until the learning criterion of three consecutive trials taking less than 20 moves was met for each run. The data for this histogram was taken from a separate set of 250 runs of 100 trials to get a larger sample for the histogram (file: 12000 inputs Learning rate.xls). The average number of trials until learning was achieved over the 250 runs measured was 10.0 with a standard deviation of 3.4.

A second criterion of successful learning is the establishment of stable synaptic weights. Figure 6-15 shows the development of the average synaptic weight over the course of the simulation. The final weight is 1.18. The weight had been stable since trial 130 of the run. This gives an effective average EPSP amplitude, once learning is completed, of 0.472nS.

The parameters used in this simulation fulfilled the criteria for successful learning of this spatial navigation task. The next sets of simulations will investigate how changing some of the learning parameters varies the rate and success of learning.

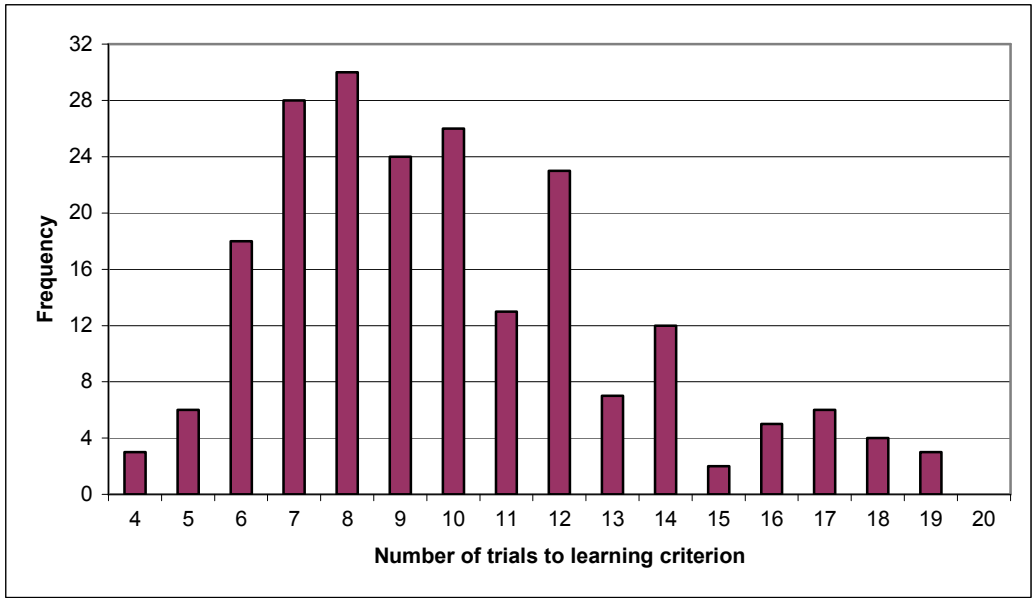

Figure 6-14 Histogram of number of moves taken on each of 250 runs to reach learning criterion. The mean number of trials taken was 10.0.

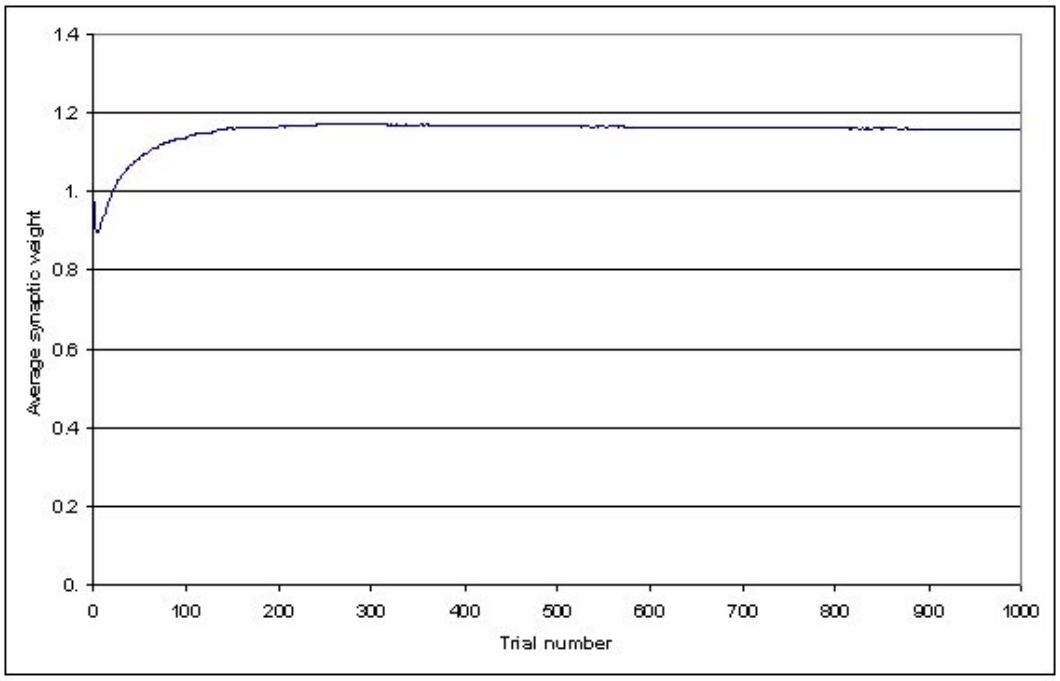

Figure 6-15 Average synaptic weight over the 1000 runs of a trial. This is the average for all four neurons. The synaptic weight decreases initially on the trials where a large number of moves are taken on average to find the reward. Once the path length taken stabilises, the synaptic weight also stabilises at approximately 1.18.

6.2.3 Variation of dopamine pulse amplitude

Results files: Delta_d.xls
Standard 1200 inputs a.xls
Delta_d 1.2.xls
Delta_d 1.4.xls
Delta_d 1.8.xls
Delta_d 2.0.xls

The proportional rise of dopamine acts as a multiplier on the two exponentials in the LTP learning equation and thus controls the rate of learning. These simulations investigate the effect of varying the magnitude of the dopamine pulse with a constant tonic dopamine level.

As the proportional rise of dopamine is increased, the rate of synaptic weight potentiation also increases (Figure 6-16). At first sight it would seem most advantageous to have the highest learning rate possible. However Figure 6-17 shows that for the highest proportional dopamine rise, a factor of 2, the number of moves made in the early exploration phase is drastically increased. This leads to learning problems which are demonstrated by the metrics shown in Table 6-3. From these it can be seen that the highest level of pulsatile dopamine had the longest average path length, the highest number of failed runs and the greatest number of contended runs (the problem with contended runs is discussed in sub-section 6.2.9).

The lowest rise of dopamine also started to show an increase in path length, failure rate and contention.

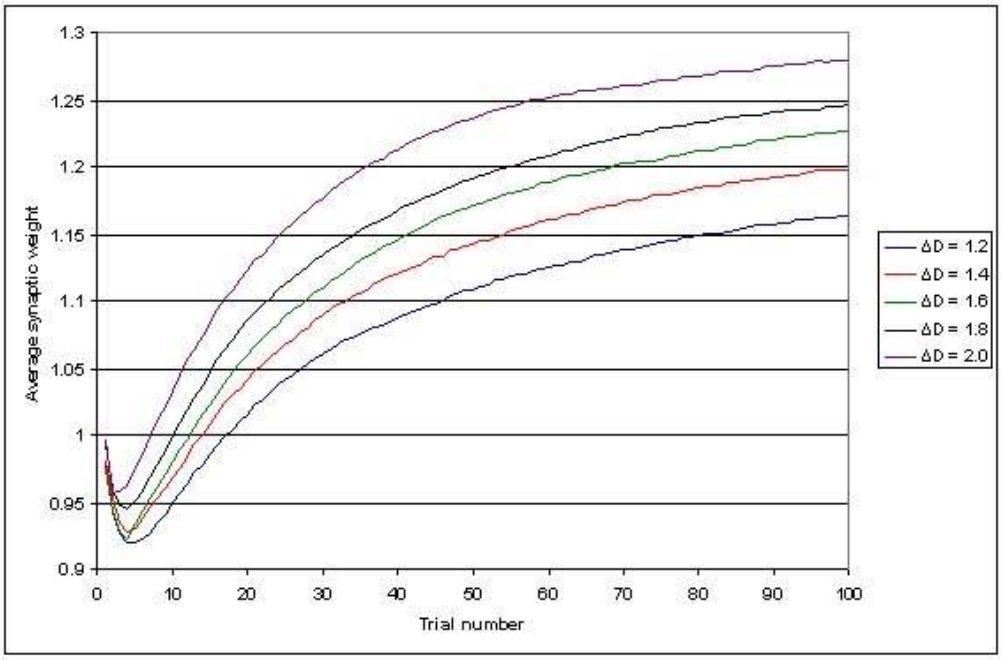

Figure 6-16 Evolution of average synaptic weight at various levels of pulsatile dopamine. As the proportional rise in dopamine level at time of reward is increased, the average synaptic weight also increases. With higher pulsatile dopamine levels, the drop in synaptic weight at the start of runs is smaller.

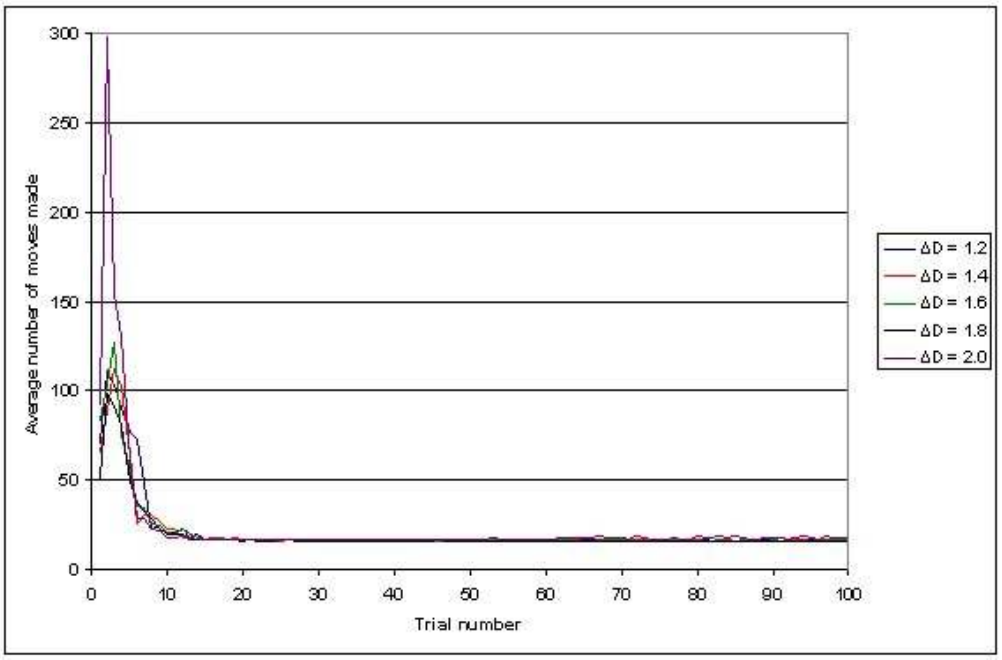

Figure 6-17 Average number of moves made to reach reward at various levels of pulsatile dopamine. The highest level of dopamine produces higher average numbers of moves in the exploratory phase, but all levels of dopamine settle to the same final average path length.

From this it can be seen that pulsatile levels of dopamine from 1.2 to 1.8 all produce very similar learning metrics, with a very high run success rate, rapid learning and little contention. A proportional rise of 1.6, which falls in the middle of the range, will therefore be used in the following simulations.

Proportional dopamine increase	1.2	1.4	1.6	1.8	2.0
Average move path learnt	11.06	10.84	10.90	11.04	11.24
Number of failures	2	0	1	0	4
Number of contended runs	8	4	3	4	10
Final synaptic weight	1.16	1.20	1.23	1.25	1.28

Table 6-3 Effects of different levels of pulsatile dopamine on learning. The highest level of pulsatile dopamine produced an increased number of failed runs and contended runs with a slightly higher number of moves to learning on average. The lowest level of pulsatile dopamine also showed and increase in contended runs and a small increase in failed runs.

6.2.4 Variation of tonic dopamine levels

As shown in chapter 4, decreasing the tonic dopamine level decreases the plateau membrane potential (sub-section 4.2.5, page 58). This effect is shown again in Figure 6-18 and Figure 6-19. In these figures, non-random excitation has been used to give a clear picture of the plateau membrane potential. Decreasing the tonic dopamine level from 1.0 to 0.9 pushes back the time of the first action potential from 108ms to 140ms after excitation starts.

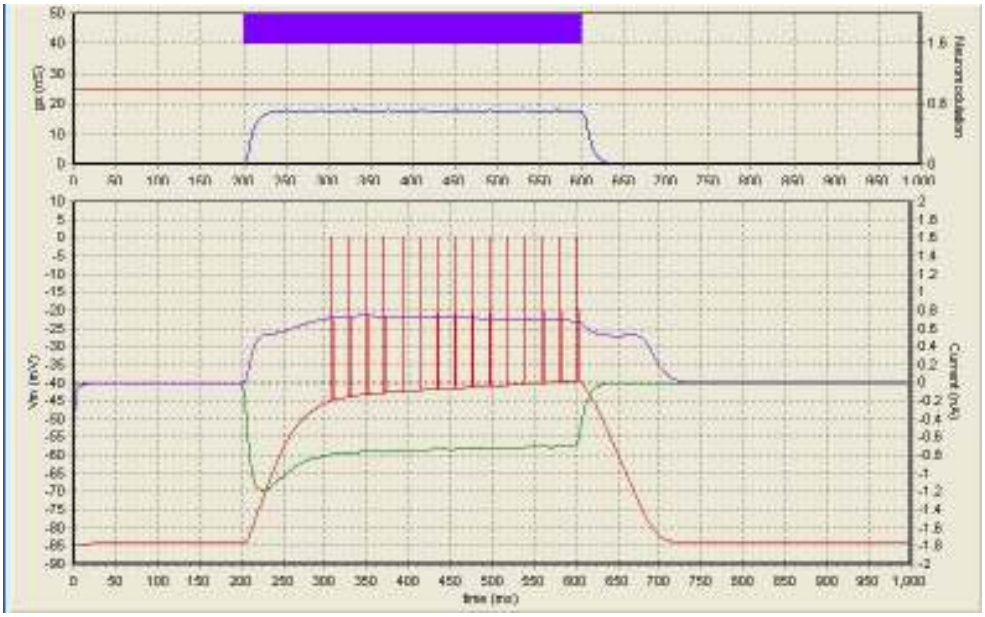

Figure 6-18 Plateau membrane potential with tonic dopamine = 1. The first action potential (red line) occurs 108ms after the start of excitation.

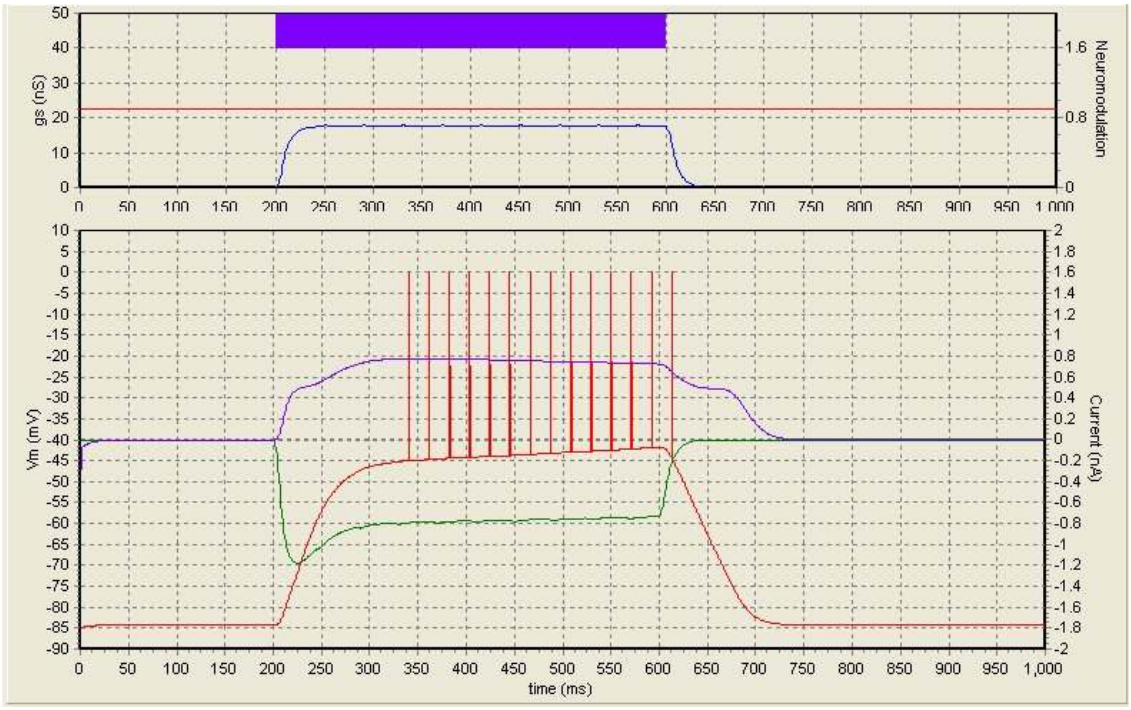

Figure 6-19 Plateau membrane potential with dopamine = 0.9. The first action potential occurs 140ms after the start of excitation, 32ms later than with a tonic dopamine level of 1.

These simulations examine whether this decrease in dopamine levels has an effect on the path learning to gain reward. There are two possibilities to be considered when changing the tonic dopamine level with regard to the pulsatile dopamine. One possibility is that the proportional increase in dopamine in the pulses stays the same at 1.6 times the tonic level. The other is that the absolute level of pulsatile dopamine remains the same at 1.6, therefore giving a higher proportional increase for lower tonic levels. These possibilities are illustrated in Figure 6-20, using a pulsatile dopamine level of 2 for simplicity.

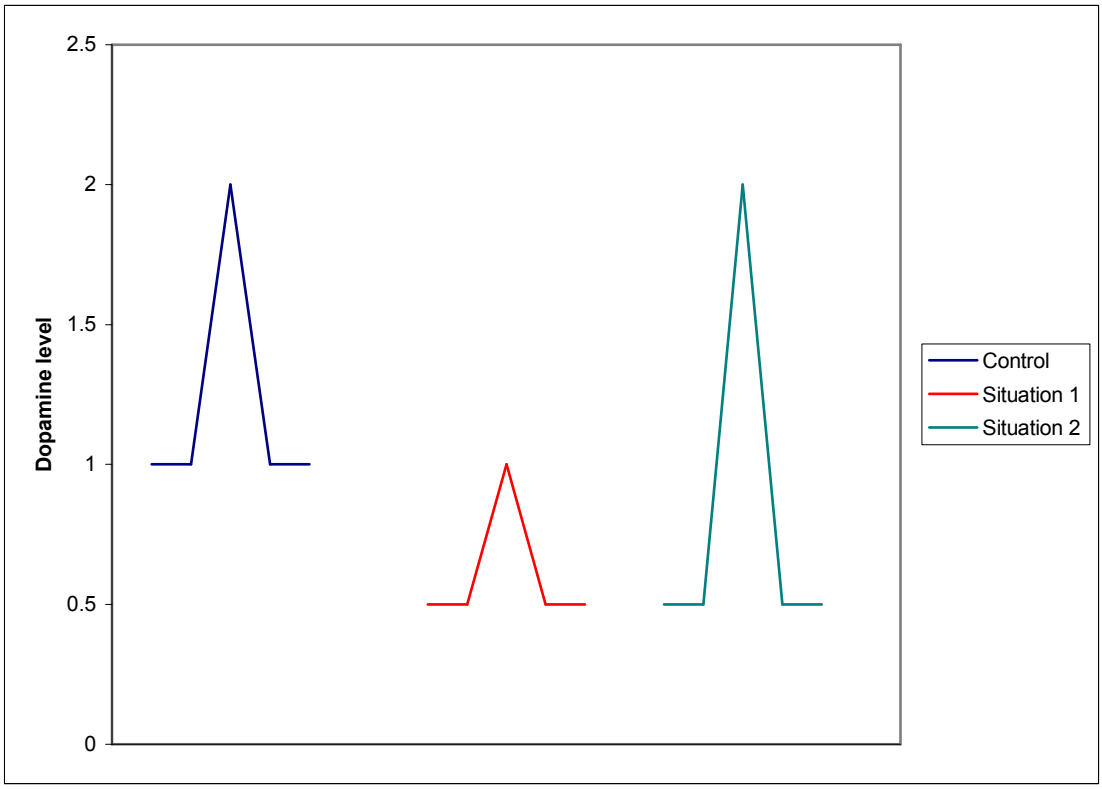

Figure 6-20 Two possible dopamine pulse profiles with reduced tonic dopamine levels. The normal pulse is shown in blue, with a tonic level of 1 rising to a pulse level of 2. Situation one shows the tonic dopamine level reduced to 0.5 and the pulsatile dopamine level reduced in proportion to the reduction in tonic dopamine level. Situation two shows the pulsatile level of dopamine maintained despite the reduction in tonic dopamine level.

6.2.4.1 Constant proportional rise

Results files: Dopamine – tonic 2.xls

Dopamine – tonic 0.8.xls

Dopamine – tonic 0.9.xls

Standard – 12000 inputs a.xls

Decreasing the tonic dopamine level increased the proportion of runs that failed (Table 6-4). This effect was quite sudden, appearing as the tonic dopamine level decreased from 0.9 to 0.8 and producing a rise in the number of runs failing from 2 to 12 out of the 50 in the simulation. Despite the increased number of failures at the lower dopamine level, the average number of trials taken to learn the path stayed constant. The number of contended moves per trial decreased as tonic dopamine levels were decreased. This is a reflection of the lower plateau potential with lower tonic dopamine levels.

Tonic dopamine level	1.00	0.90	0.80
Pulsatile dopamine level	1.60	1.44	1.28
Average trials to learning criterion	10.90	10.71	10.76
Average contended moves per trial	2.23	1.79	1.58
Failed runs	1	2	12
Final synaptic weight	1.23	1.24	1.26

Table 6-4 Effect of tonic dopamine level on learning when maintaining a constant proportional dopamine rise for reward. Decreasing the tonic dopamine level to 0.8 increases the number of failed runs to 24%, but produces fewer contended moves per trial.

The characteristics of the runs which failed with a tonic dopamine level of 0.8 are shown in Table 6-5. All the runs failed early, on average during the fourth trial. The average synaptic weight at which the runs failed was quite high at 0.89 and the number of moves made before failing was quite low at an average of 773.7. This is to be expected due to the effects of dopamine on the plateau membrane potential shown above.

Run number	Trial number	Average synaptic weight	Total moves made	Position stopped
2	5	0.86	1011	7,9
3	4	0.92	710	10,9
11	3	0.93	373	9,1
16	3	0.90	529	9,1
19	5	0.88	774	1,8
2	1	0.83	757	7,7
21	3	0.86	978	5,10
25	4	0.88	627	1,9
31	5	0.88	851	7,1
32	6	0.88	1223	9,5
48	3	0.90	648	9,2
49	6	0.92	803	2,10
Average	4.0	0.89	773.7	

Table 6-5 Characteristic of runs where failure occurred with tonic dopamine = 0.8. The average synaptic weight was more than 10% below the start value and an average of over 750 moves were made before the run failed.

Comparison of the average synaptic weight at these three dopamine levels shows a slight increase with decreasing tonic dopamine levels (Figure 6-21). The final synaptic weight increased from 1.23 to 1.26 as tonic dopamine was decreased from 1.0 to 0.8. Decreasing the level of tonic dopamine had no observable effect on the average numbers of moves made in each run (Figure 6-22), nor did it affect the path lengths

during the exploration phase.

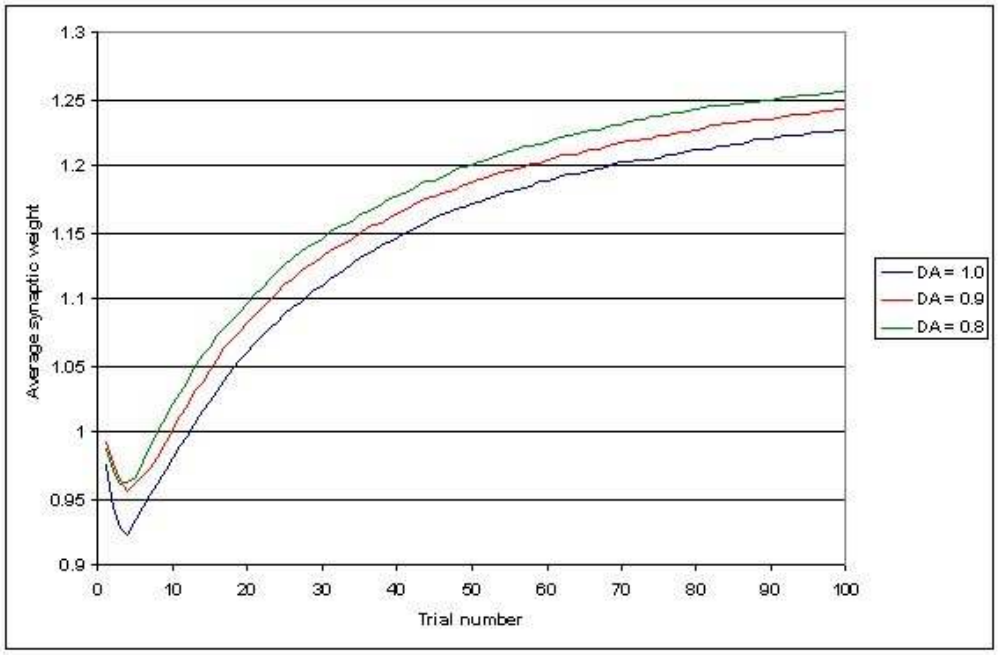

Figure 6-21 Average synaptic weight at three levels of tonic dopamine with a constant proportional dopamine rise. As the tonic dopamine level is reduced below normal, the average synaptic weight attained at the end of the run increases.

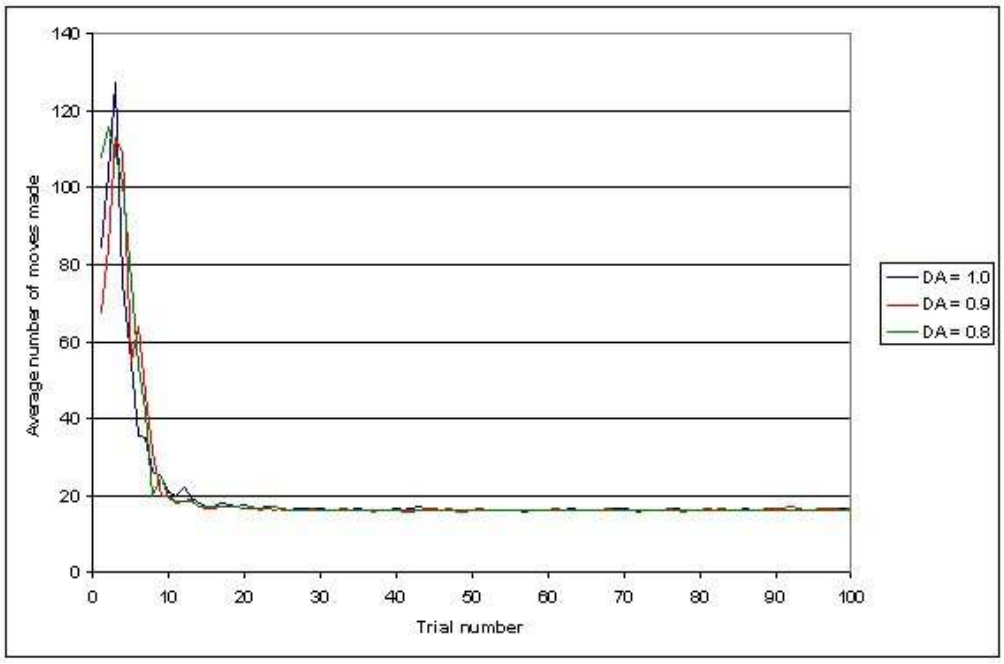

Figure 6-22 Average number of moves made at three levels of tonic dopamine with a constant proportional dopamine rise. Decreasing the tonic dopamine level below normal had no effect on the path length either in the exploration or the exploitation phases of runs.

6.2.4.2 Constant pulsatile dopamine level

Results files: Dopamine – tonic 3.xls
Dopamine – tonic 0.8 delta_d 1.6.xls
Dopamine – tonic 0.9 delta_d 1.6.xls
Standard – 12000 inputs a.xls

In this simulation the pulsatile dopamine level was always 1.6, giving an increasing proportional rise as the tonic dopamine level was lowered. As with the results for the simulations where the proportional dopamine rise was kept constant, the number of failed runs increased as the tonic dopamine level was lowered. There was also a rise in final synaptic weights, which this time was more expected as the proportional dopamine rise was providing more potentiation per trial with lower tonic dopamine levels. Again the rate of learning was not much affected by tonic dopamine level changes.

Tonic dopamine level	**1.00**	**0.90**	**0.80**
Proportional dopamine rise	1.60	1.76	1.92
Average trials to learning criterion	10.90	9.45	10.56
Average contended moves per trial	2.23	1.81	1.76
Failed runs	1	3	14
Final synaptic weight	1.23	1.24	1.29

Table 6-6 Effect of tonic dopamine level on learning when maintaining a constant pulsatile dopamine level for reward. Decreasing the tonic dopamine level to 0.8 increased the failed runs to 28% but decreased the number of contended trials per run and increased the final average synaptic weight.

The evolution of the synaptic weights over the trials showed that the lowest level of tonic dopamine produced a curve which grew proportionally more rapidly than that of the step from 1 to 0.9 (Figure 6-23). The number of moves made in the exploitation phase was not affected, but the tonic dopamine level of 0.9 had a longer path length during the early exploratory phase, despite having the lowest average number of moves to path learning.

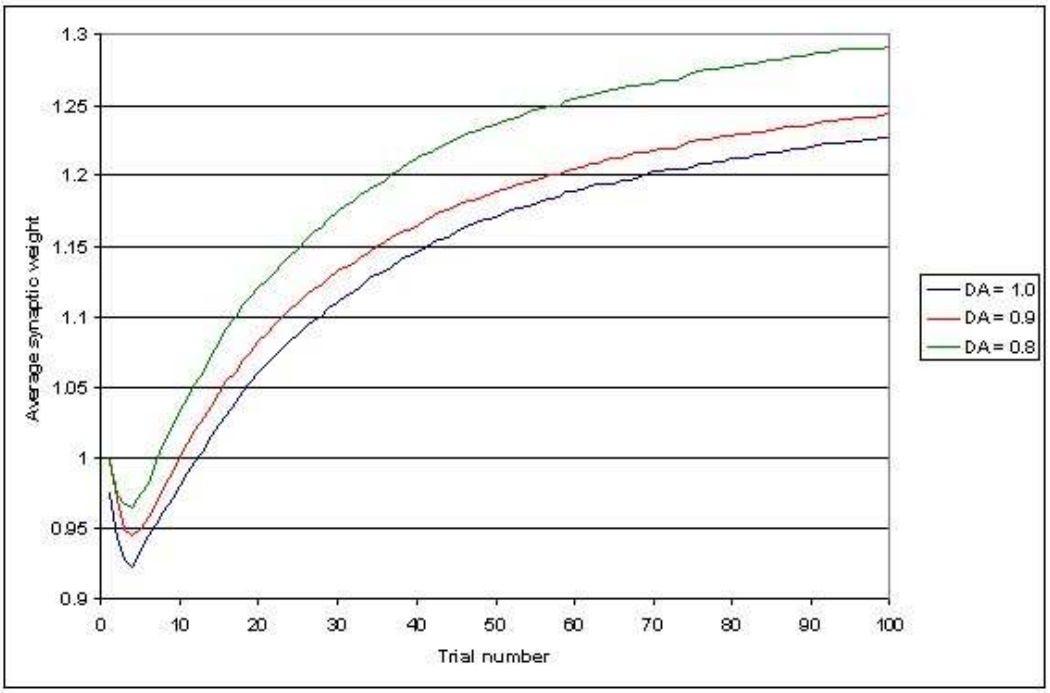

Figure 6-23 Average synaptic weight at three levels of tonic dopamine with a constant pulsatile dopamine level. Decreasing the tonic dopamine level led to a rise in the average synaptic weight at the termination of the run.

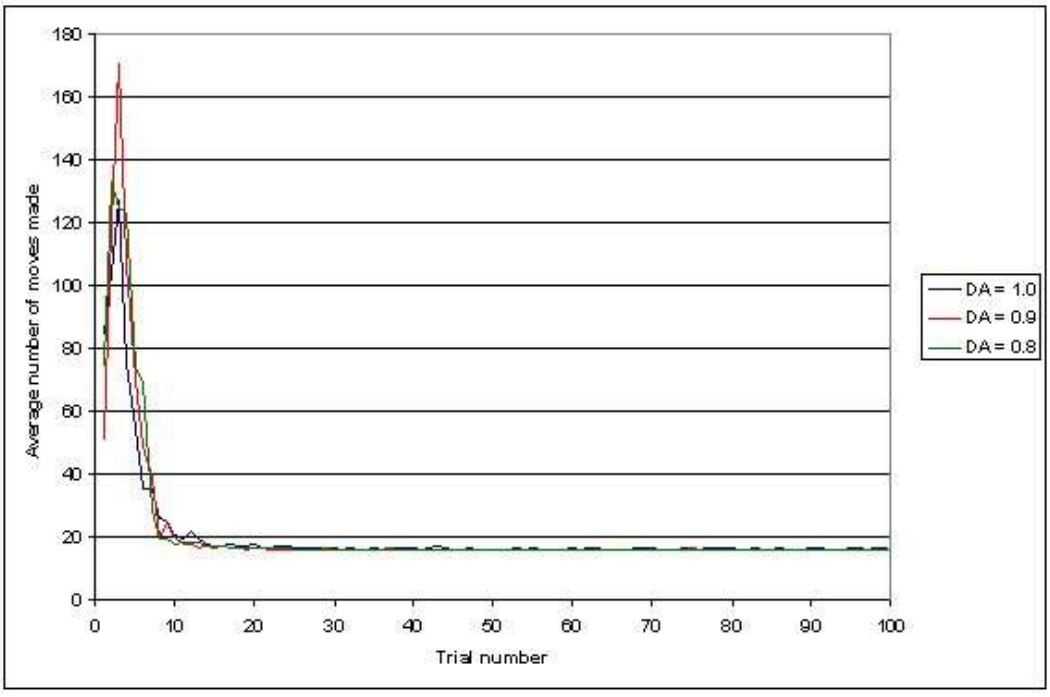

Figure 6-24 Average number of moves made at three levels of tonic dopamine with a constant pulsatile dopamine level. Decreasing the tonic level of dopamine had no effect on the path length.

6.2.5 Variation of synaptic trace time constant

Results files: Synaptic time constant.xls
Synaptic time constant 200a
Synaptic time constant 100a.xls
Synaptic time constant 50a.xls
Standard – 12000 inputs a.xls

The synaptic trace time constant is used in the learning rules to determine how long before the neuron fired each synapse had received an excitatory input. In the previous simulations, the synaptic trace constants were set to 150ms. These simulations consider how varying this constant, T_{STDP} in equations (6.1) to (6.3), affected learning.

In, Figure 6-25 the evolution of the average synaptic weight for three time constants is shown. Reducing this time constant reduces the rise in average synaptic weight over the course of a run. At a time constant of 150ms an almost ideal situation is reached where there is, on average about 25% potentiation, giving a final synapse size of about 5nS. Increasing the synaptic trace time constant to 200ms produced an 8.9% rise in final synaptic weight (Table 6-7), although the synaptic weight at the longer time constant had clearly not stabilised after 100 trials. Increasing the synaptic trace time constant also shortened the average number of trials taken until the learning criterion was reached, whilst having no effect on the, already very low, failure rate.

Reducing the synaptic trace time constant to 100ms produced a 13% drop in final synaptic weight, back to a level which was barely higher than the starting level. Despite this lack of change in average synaptic weights, there were only two failures in the course of 50 runs and the contention rate was lowest for any value of this time constant.

A further reduction of the synaptic trace time constant to 50ms produced a failure of learning. The synaptic weight continued to fall over the course of 100 trials and over half of the runs failed, on average after 75.2 runs. Only three of the runs failed to reach the criterion for learning, but the average number of trials until learning was achieved was greatly increased at 25.5.

Only the lowest value for the time constant had any effect on the number of moves in each trial during the exploitation phase, but the highest level was the most effective at

producing short path lengths in the exploration phase (Figure 6-26).

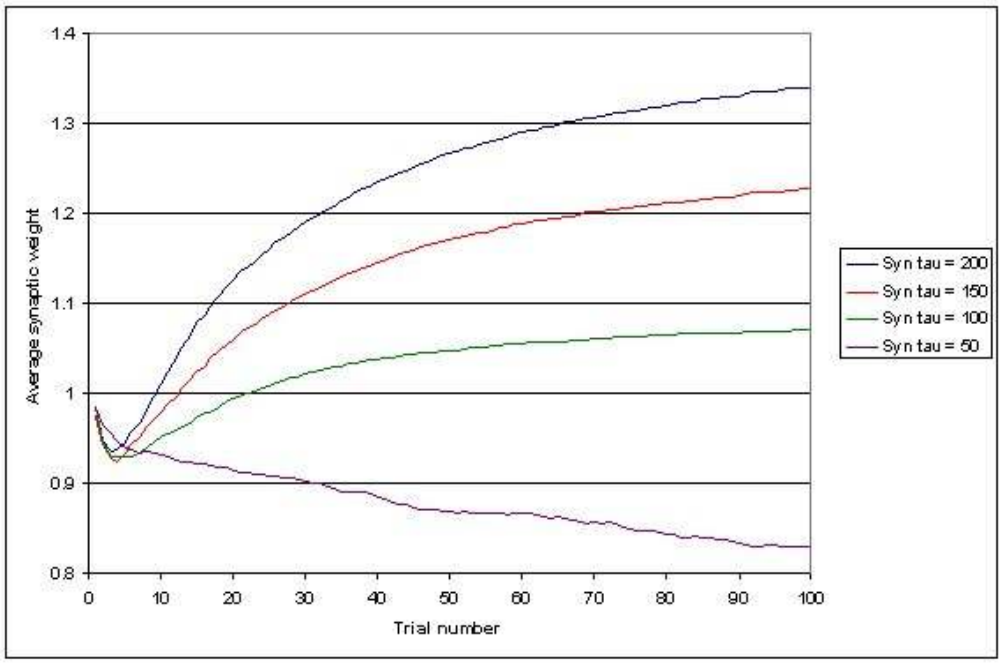

Figure 6-25 Effect of synaptic trace time constant change on average synaptic weight over one hundred trials. Decreasing the synaptic trace time constant decreased the final synaptic weight. In the case of a synaptic trace time constant of 50ms, the average synaptic weight continued to fall across the run.

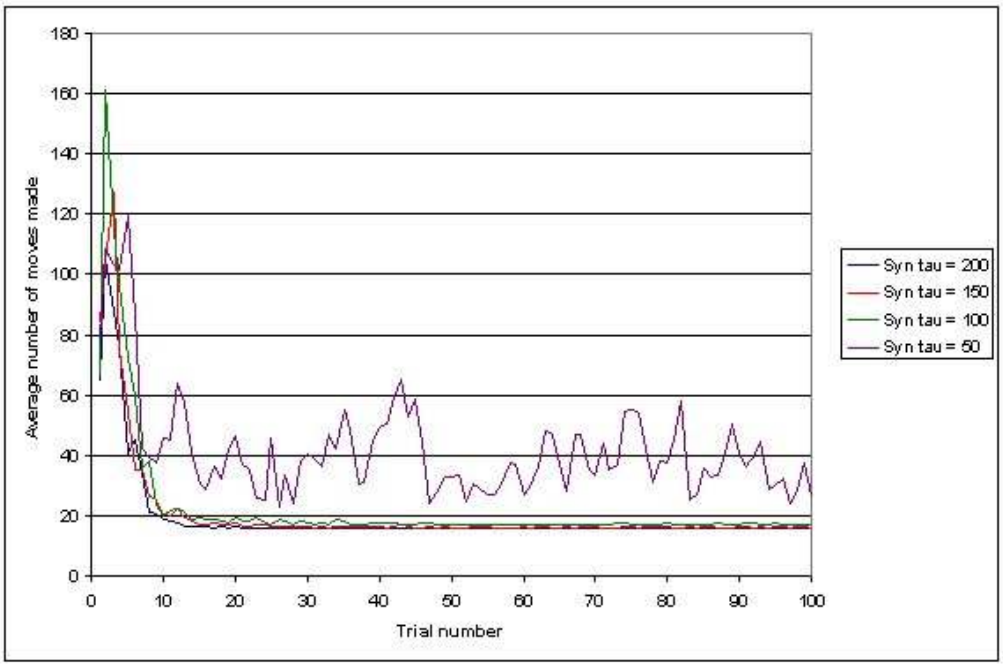

Figure 6-26 Effect of synaptic trace time constant change on average number of moves made over one hundred trials. Reducing the synaptic trace time constant to 50ms led to an increased path length across the run.

Synaptic time constant (ms)	50	100	150	200
Average trials to learning criterion	25.5	12.2	10.9	9.6
Average contended moves per trial	2.41	1.44	2.23	2.49
Failed runs	27	2	1	1
Final synaptic weight	0.83	1.07	1.23	1.34

Table 6-7 Effect of varying synaptic trace time constant on learning. A synaptic time constant of 100ms has the lowest contention rate and a final average synaptic weight only 7% above the starting value. Reducing the time constant further to 50ms increased the failure rate to 27 out of 50 runs. The longest time constant had the lowest number of trials to learning criterion.

6.2.6 Variation of backpropagation time constant

Results files: Backpropagation tau.xls
Backpropagation tau 75.xls
Backpropagation tau 100.xls
Backpropagation tau 200.xls
Backpropagation tau 400.xls

The backpropagation time constant, T_{DDP}, represents how long the credit assignment signal remains effective. In these simulations this constant is varied between 75ms and 400ms.

With the standard level used across the simulations of a 200ms time constant and higher values, learning was effective with good evolution of the average synaptic weights (Figure 6-27) and stable path lengths once learning was completed (Figure 6-28).

Reducing the time constant to 100ms caused the average synaptic weight to remain below 1 throughout the run, stabilising at a value of 0.91 from trial 64 onwards. The average path length over the last 50 trials was also increased at 19.3 moves and four runs failed.

Reducing the time constant one step further to 75ms caused an even greater change in learning. Not only did the average synaptic weight remain below 1, after trial 40 it started to gradually decrease. There was a large increase in failed runs to 36 out of 50 (72%), with all the failures occurring after trial 20. Also the path length became longer and more erratic as the trials progressed.

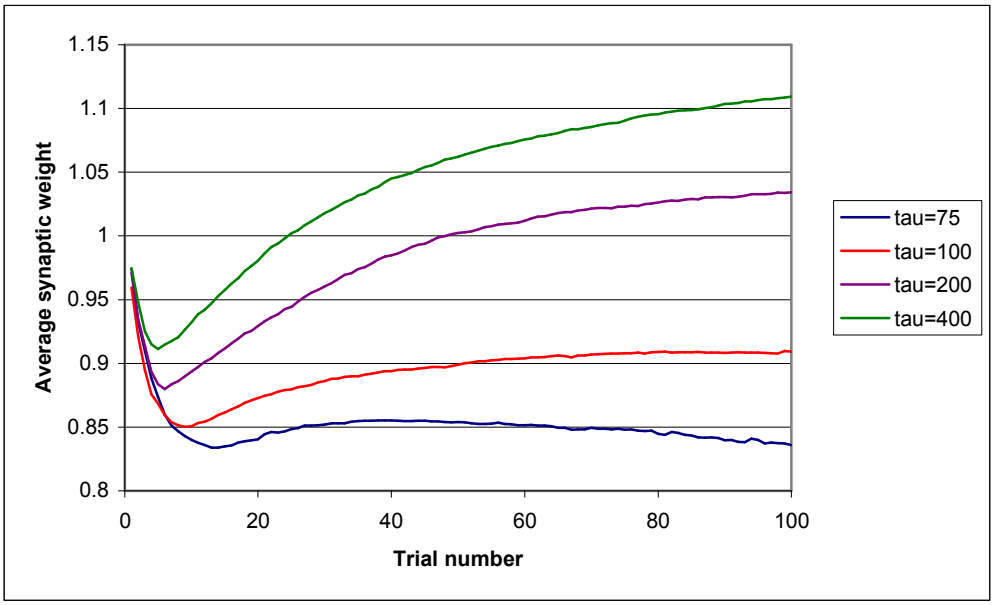

Figure 6-27 Variation of average synaptic weight at various levels of back propagation time constant. Reducing the backpropagation time constant to 100ms (red line) decreased the average synaptic weight at the end of runs to 0.91 Decreasing the time constant to 50ms (blue line) resulted in an average synaptic weight that was continuing to fall at the end of runs.

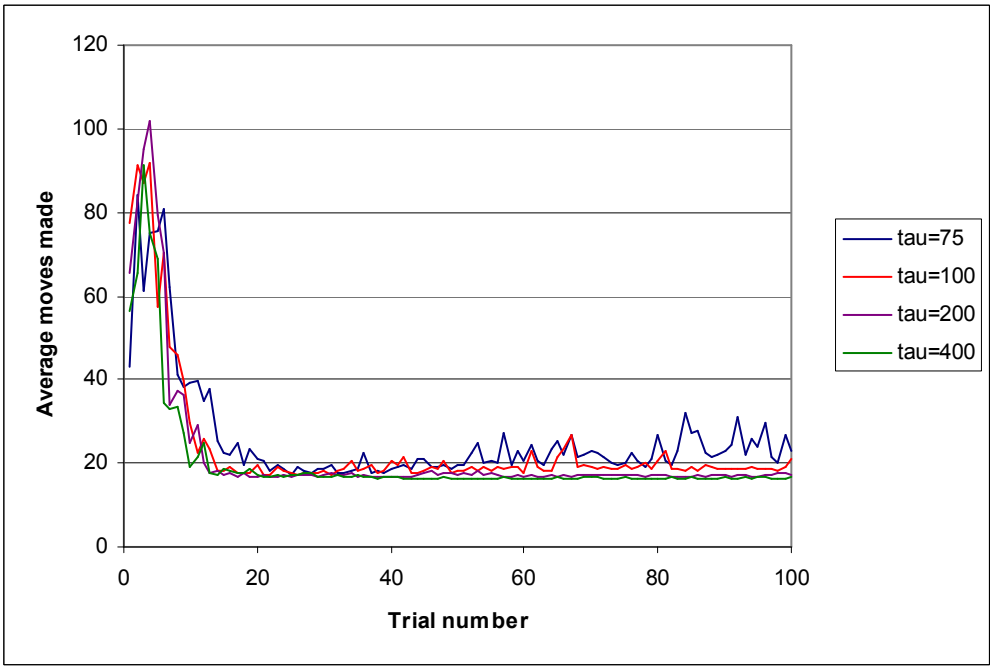

Figure 6-28 Variation in average number of moves made per trial with various levels of back propagation time constant. Decreasing the back propagation time constant to 100ms (red line) resulted in a slightly higher average path length in the exploitation phase. Decreasing the time constant to 75ms led to longer path lengths in the exploitation phase although there seems to be no effect on the path lengths in the exploration phase.

Back propagation time constant (ms)	75	100	200	400
Average trials to learning criterion	14.6	11.8	11	11
Average contended moves per trial	1.44	1.31	1.24	1.44
Failed runs	36	4	1	0
Final synaptic weight	0.84	0.91	1.03	1.11

Table 6-8 Effect of varying back propagation time constant on learning. Increasing the back propagation time constant to 400ms did not result in lower number of trials to learning criterion but did raise the number of contended trials per run. Decreasing the time constant also raised the average contended moves per trial. With a time constant of 75ms almost three quarters of all runs failed.

6.2.7 Variation of excitatory input count

Results files: Input count.xls
5000 inputs.xls
10000 inputs.xls
Standard – 12000 inputs a.xls
20000 inputs.xls

The previous simulations were carried out using 12000 excitatory inputs, each having a conductance amplitude of 0.4nS. This equates to an average of 152.5 inputs exciting each MS neuron in each grid position so giving a total excitation for each MS neuron in each position of 61nS.

In the following simulations the number of excitatory inputs is varied between 5000 and 20000 without varying the average number of inputs to each spiny neuron in each grid position. This is achieved by varying the proportion of positions each excitatory input is active in step with the variation of the number of inputs.

The average synaptic weights over the course of the trials with each excitatory input count is shown in Figure 6-29. This shows that the greater the number of excitatory inputs used, the smaller the drop in average synaptic weight during the exploratory phase, but conversely the lower the final synaptic weight.

Number of inputs	5000	10000	12000	20000
Proportion of positions per input	0.12	0.06	0.05	0.024
Inputs per position	151	151	152	151
Average move path learnt	12.9	10.6	10.9	11.2
Number of failures	7	1	1	0
Average contentions per trial	2.42	1.99	2.23	1.67
Final synaptic weight	1.45	1.26	1.23	1.14

Table 6-9 Effect of varying excitatory input count on learning. As the number of inputs is raised, the

proportion of positions per input decreases to maintain the same number of excitatory inputs per neuron per grid position. The lowest number of inputs leads to an increase in the number of failed runs to 14%.

Figure 6-30 shows that the number of moves taken during both exploration and exploitation did not seem to be dependent on the excitatory input count.

Table 6-9 shows that the lowest excitatory input count had a far greater proportion of failed runs, the highest number of trials to path learning and the greatest number of contentions per trial.

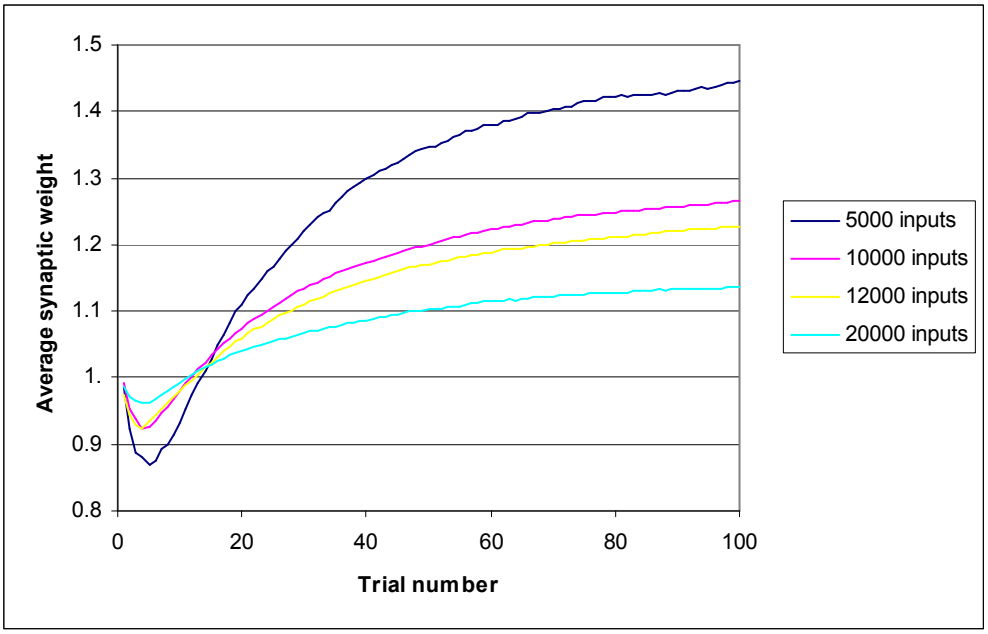

Figure 6-29 Development of average synaptic weight with various excitatory input counts. Increasing the number of inputs increased the final synaptic weight but also led to a greater decrease in synaptic weight during the exploratory period.

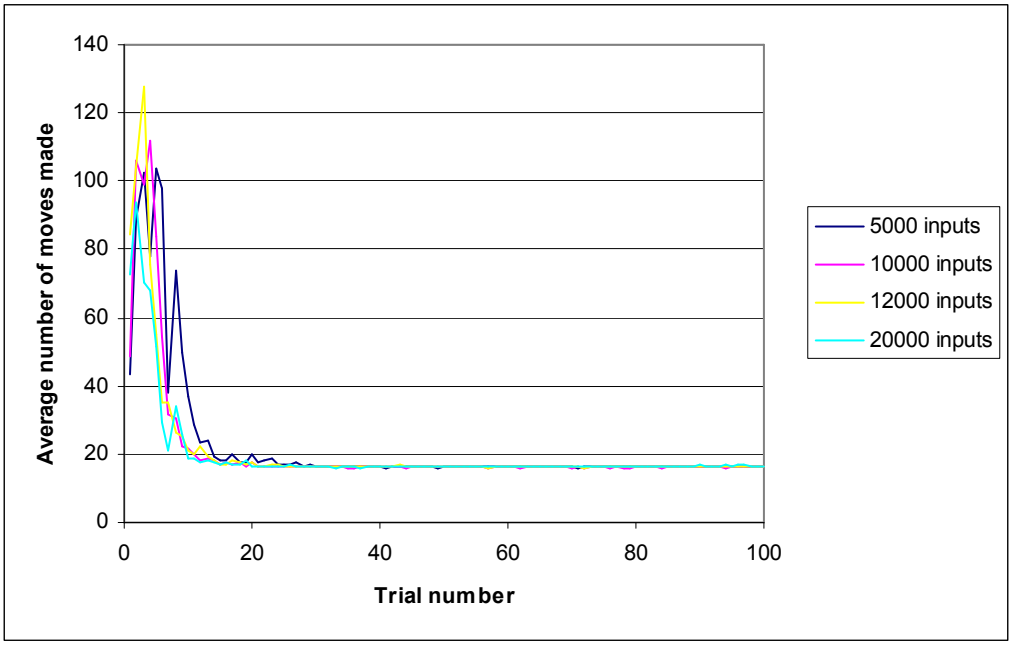

Figure 6-30 Average number of moves taken on each trial with various excitatory input counts. The lowest number of inputs has a second spike in path length at around trial 10, but all input counts led to a close to optimal path length by the end of the run.

6.2.8 Variation of maximum synaptic weight

Results files: Max synaptic weight.xls
Max synaptic weight 4.xls
Standard – 12000 inputs a.xls
Max synaptic weight 2.xls
Max synaptic weight 1.5.xls

The maximum synaptic weight used in the simulations thus far was selected on the basis that a synaptic size of 1.2nS would not be unrealistic, although there soes not seem to be any published evidence for the maximum corticostriatal synaptic size. These simulations therefore investigate learning with different maximum synaptic sizes.

Lowering the maximum synaptic weight had little effect on the efficacy of learning. Even at the lowest level of maximum synaptic weight used, 1.5 times starting value, there were no failures over 50 runs of 100 trials each (Table 6-10). It is probable that some of these runs would have failed with more trials per run as the synaptic weight was already falling by the end of 100 trials (Figure 6-31) and the number of moves per trial was starting to increase (Figure 6-32). This demonstrates that at the lowest

maximum synaptic weight, the difference between the strength of synapses in different directions was eroding. Otherwise there was surprisingly little to differentiate the performance of the simulations with maximum synaptic weights from two to four.

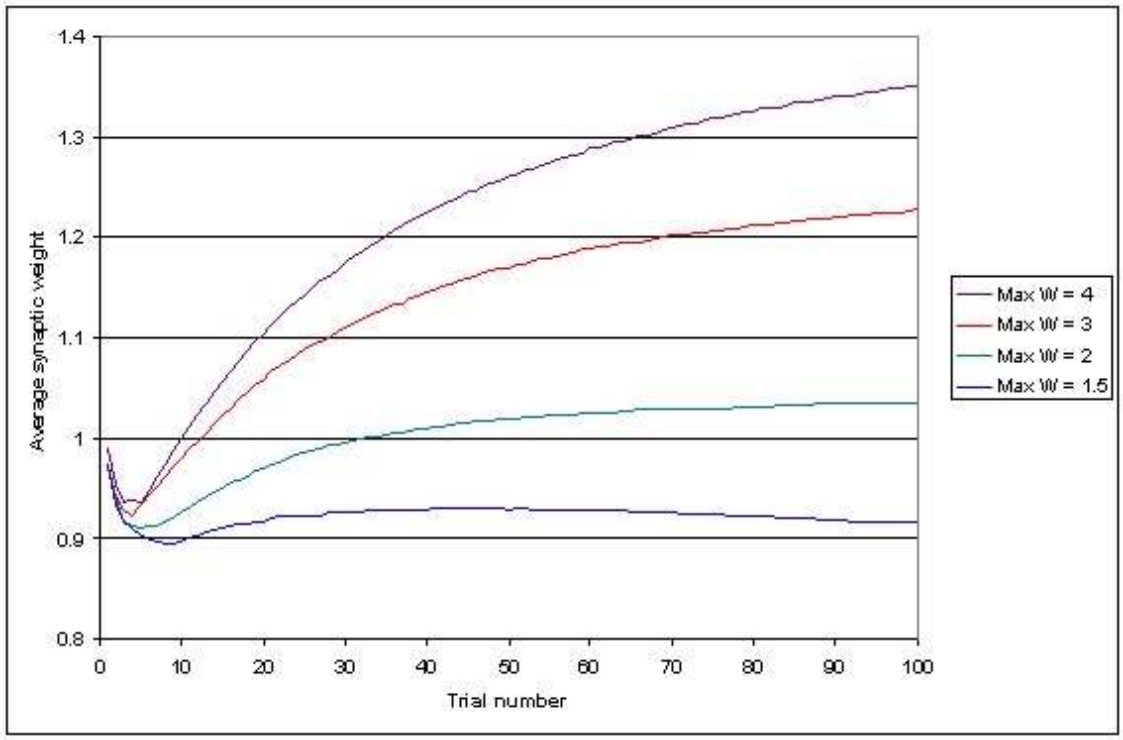

Figure 6-31 Average synaptic weight for various values of maximum synaptic weight. Increasing the maximum allowed synaptic weight increased the average synaptic weight at the end of runs. With a maximum weight of 1.5, the average synaptic weight at the end of 100 trials was decreasing.

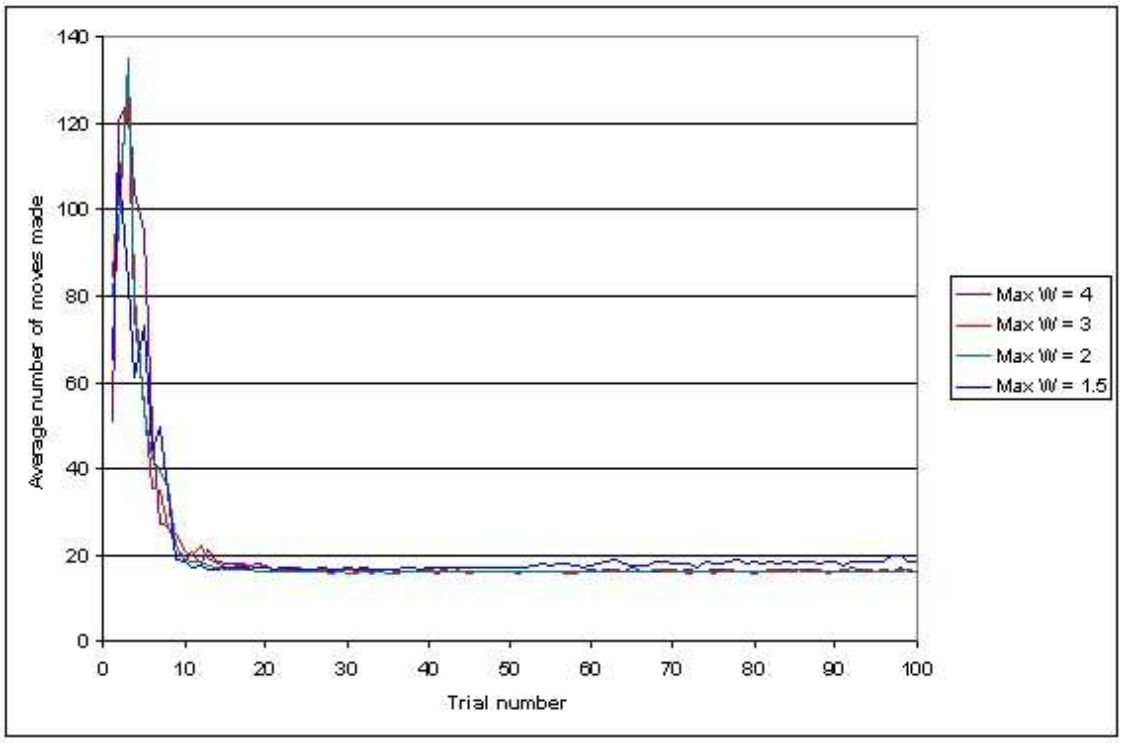

Figure 6-32 Average number of moves made to reach reward for various maximum synaptic weights. The synaptic weight had little influence on the path length either in the exploratory or the exploitatory phases.

Maximum synaptic weight	4	3	2	1.5
Average trials to learning criterion	10.5	10.9	9.7	10.2
Average contended moves per trial	2.21	2.23	1.44	1.72
Failed runs	0	1	1	0
Final synaptic weight	1.35	1.23	1.04	0.92

Table 6-10 Results of learning with various levels of maximum synaptic weight. The maximum synaptic weight only changed the average trials to learning criterion by a small amount, with a synaptic weight of 2 providing the fastest learning as well as the lowest number of contentions per trial.

6.2.9 No disappointment

Results file: No disappointment.xls

When the animat attempts to perform an action which is not allowed in the environment, such as moving upwards when already at the top of the grid the disappointment learning rule is applied. This treats such attempts as leading to an aversive outcome where the dopamine level drops for a short period, leading to LTD.

This simulation investigates the effect of turning off this learning rule. The average synaptic weight with the disappointment learning was slightly higher (1.23 vs. 1.22) (Figure 6-33). The rate of climb after the initial drop was very similar, but the amount

of LTD in the earlier runs was greater. This was due to far more moves taking place during the early exploration phase (Figure 6-34), the average on trial 2 of a run increasing from 104 moves to 438.6 without disappointment. When the runs which failed within the first few trials were removed from consideration, the average number of moves taken on trial 2 of runs with no disappointment learning was still 318.1.

The main difference observed in a simulation where disappointment learning was not used was in the number of runs that failed. With a pulsatile dopamine level of 1.6 times only one run out of 50 failed to complete, but using the same settings except for the lack of disappointment learning led to 9 runs (18%) failing. All these runs failed on early trials, between trial 2 and trial 6 (average trial 3.8). In 3 out of the 9 contention occurred on a reward gaining move in a trial before failure.

The number of trials taken to learn the path was very similar with and without disappointment, (10.9 trials with vs. 10.4 without), as was the average number of moves over the last 50 trials and the average number of neurons firing over the last 50 trials.

Criterion	With	Without
Peak number of moves made in a trial	127.5	438.6
Trial number no which peak moves made	3	2
Average synaptic weight	1.14	1.13
Final synaptic weight	1.23	1.22
Average number of trials to learning criterion	10.9	10.4
Average number of moves over last 50 trials	16.3	16.2
Average number of neurons fired over last 50 trials	18.5	18.5
Average number of contended moves per trial	2.2	13.5

Table 6-11 Comparison of learning with and without use of the disappointment learning rule. Not using disappointment led to some very long path lengths on the exploration phase and far more contended moves per trial.

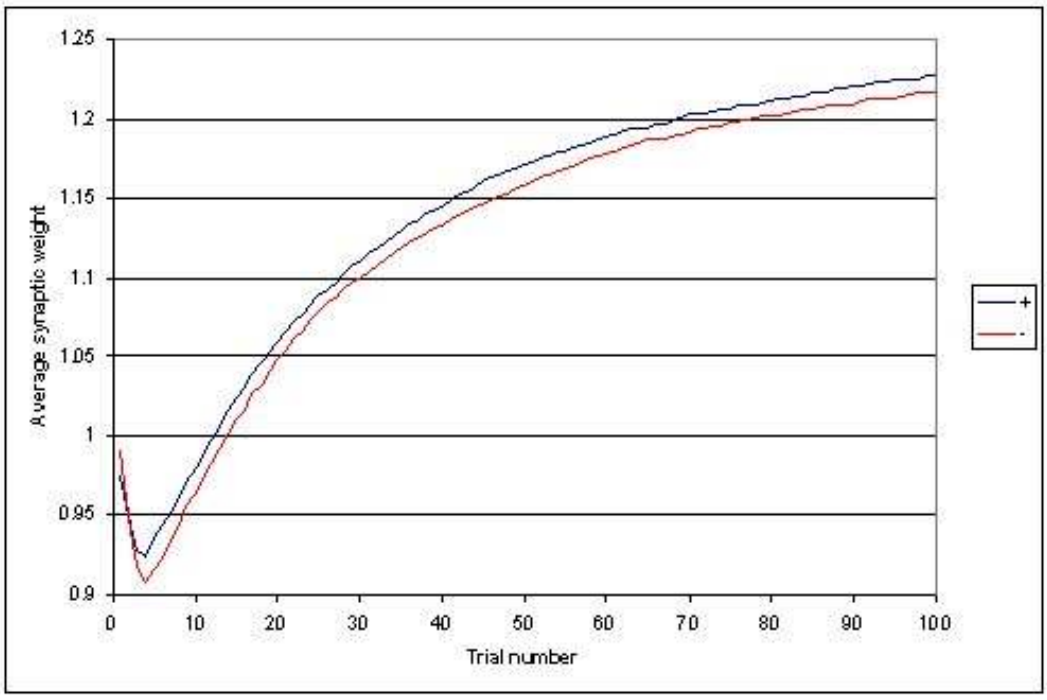

Figure 6-33 Evolution of average synaptic weights with (+) and without (-) use of the disappointment learning rule

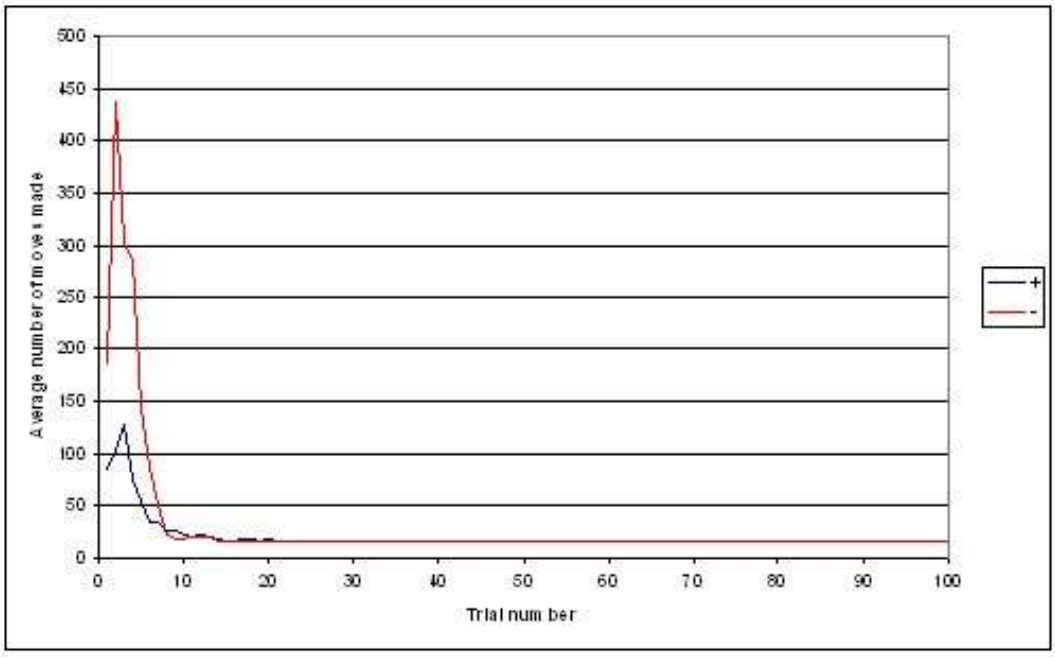

Figure 6-34 Average number of moves taken during each trial with and without use of the disappointment learning rule. Use of the disappointment learning led to far shorter path lengths during the exploration phase.

6.2.10 Reasons for failed runs

Results file: 12000 inputs Learning rate.xls

Using the optimum parameters, approximately 2% of runs fail. In order to investigate reasons for runs failing, the parameters were changed so that approximately 5% of runs failed to complete. The dopamine pulse level was lowered slightly to 1.4 times the tonic level and the dopamine trough level was increased to 0.7. 200 short runs of 20 trials each were performed in order to produce more data for analysis. A total of 12 runs failed, without seeming to change the nature of the failures. There seem to be two main causes for runs failing.

Firstly and most simply, the animat fails to learn the location of the reward during the exploration of the grid. Eventually the synaptic weights decline to a point where the level of excitation is insufficient to push any of the neurons to the threshold level in the current position the animat occupies. This requires a decrease of average synaptic weight for each neuron firing at the occupied position to below 0.7 when the starting EPSP amplitude is 0.4nS.

To estimate how long this would take, a simulation of 10 runs with no reward was performed. This showed that, on average, the animat would make 1536 moves over a period of 494 seconds before stalling, with a final average synaptic weight of 0.69.

In the 200 runs of the simulation used to determine the rate of path learning, 8 runs failed due to not finding the reward path. All eight failures occurred on the third or fourth trial of the run. The average number of moves before failure was 1361 and the average synaptic weight when the run was aborted was 0.78 (Table 6-12).

Run No.	Trial No.	Position	Total moves	Average synaptic weight
31	3	3,10	1254	0.79
52	3	2,10	1389	0.75
62	4	1,9	1253	0.79
92	3	1,10	1336	0.78
119	4	2,10	1537	0.78
162	4	9,9	1689	0.80
186	3	8,1	1304	0.75
196	3	9,10	1126	0.78
Averages	3.375		1361	0.78

Table 6-12 Characteristics of runs failing with no contention. The average synaptic weight of failed runs was 20% below the starting value and the number of moves taken over the trials before failure was over 1000.

							1		
R									
1								1	S
1	2	1						1	

Figure 6-35 Position in which run failed. The number indicates how many runs failed in a particular position. 'R' represents the reward position amd 'S' the start position. Runs tended to fail with the animat at or near one corner of the grid.

The positions where the runs failed are shown in Figure 6-35. This shows that the runs tended to fail at the edge of the grid near the corners.

The second cause of failed runs is contention at the time of obtaining reward. In approximately 5% of cases when a neuron fires to cause the animat to move to the reward position, another neuron fires within 2ms. In this case, the credit assignment fails and both neurons are potentiated to an almost equal degree. This only tends to happen the first or second time that the animat approaches the reward from a given direction. If it occurs once in a run it tends to recur nearly every time that the reward is

approached from the same direction.

In the simulation showing learning with a potentiation constant of 1.2 the incidences and outcomes of this contention were recorded. Out of the 50 runs, contention occurred in the first three trials on 19 occasions. Of these 3 runs failed to complete. The average synaptic weight at failure was 0.98, far higher than the weight of 0.69 for runs which failed without contention.

Run No	Trial No	Position	Weight	Contention	First contended run
20	780	1,8	0.97	U,R	1
27	108	10,9	0.99	U,D	1
49	143	10,9	0.97	L,R	3

Table 6-13 Runs with contention which failed to complete. The contention column shows which neurons fired. L = left, R = right, U = up, D = down. Position is the grid position where the simulation stalled on the specified trial number. Weight is the average synaptic weight of all neurons in the grid at the time the run failed,

A further 5 runs showed contention throughout the run, but still completed the run. These runs had an average synaptic weight at completion of 1.06.

Run No	Weight	Contention	First contended run
9	1.03	U,L	3
18	1.05	D,L	4
36	1.05	U,L	2
37	1.06	U,L	1
46	1.09	U,D,L	4

Table 6-14 Runs with contention which completed. These had nearly sub-normal final average synaptic weights, near to the starting value.

Eleven runs showed contention in the early trials, but recovered. These runs had an average synaptic weight of 1.16. No run had more than three incidences of contention and the last incidence of contention was seen on trial 12 in a run in which the only other incidence was on trial 5.

Run No	Weight	Contention	First contended run	Last contended run
1	1.13	U,L	3	3
2	1.16	U,D	1	1
8	1.17	D,R	5	12
14	1.17	U,L	1	4
15	1.17	U,L	2	2
19	1.18	L,R	2	2
22	1.17	U,L	1	1
30	1.17	U,R,L	1	9
38	1.12	D,L	2	2
40	1.18	U,L	3	3
44	1.17	D,R	5	5

Table 6-15 Runs with contention which recovered. These runs had nearly normal average synaptic weights.

A simulator screen shot of a typical run in which contention occurred, but the run completed is shown in Figure 6-36. In this run there had been contention occurring when the animat moved to the left to the reward square. It can be seen that in positions (2,2), (3,2), (4,2), (2,3), (3,3) the up and down synaptic weights are close to equal as the vector line is nearly horizontal. The up and down synaptic weights are also large as can be seen by the vertical length of the ellipse axis. This caused some indecision in the final moves before reward was obtained on each trial, increasing the path length. The major effect however was on the path following near the start. Figure 6-37 shows a comparison of the trial-by-trial path lengths for a contended run and the subsequent non-contended run. It can be seen that the contended run produced much longer and more variable path lengths. The average path length for the contended runs was 36.2 moves and for the non-contended 17.1 moves.

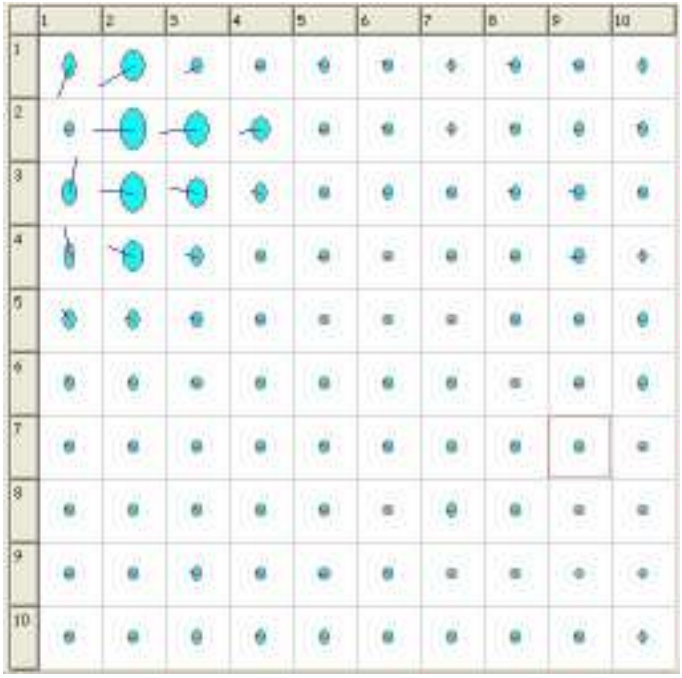

Figure 6-36 Distribution of synaptic weights at the end of a typical contended run. The grid positions to the right of the reward show that contention has occurred. The tendency in the up and down directions is very similar to that in the left direction. At the corners of the grid, there is no very definite tendency in any direction and average synaptic weights are low.

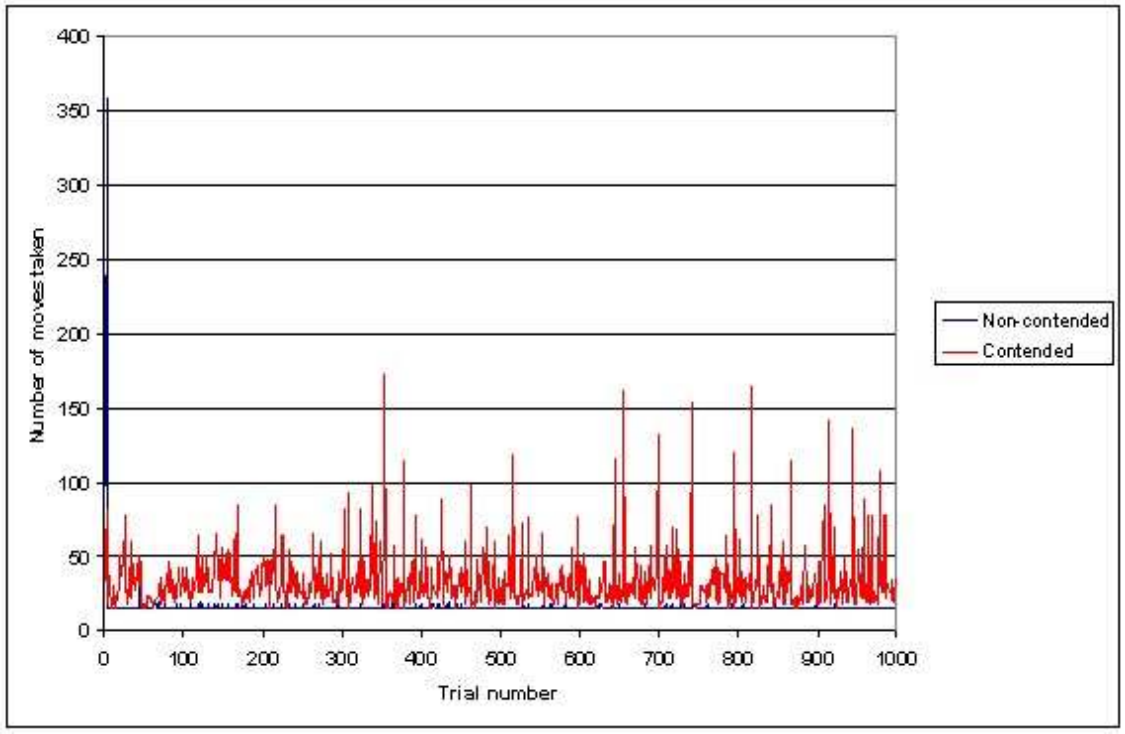

Figure 6-37 Comparison of moves made between a contended (red) and a non-contended (blue) run. The contended run had the up, down and left neurons firing when the animat moved upwards to gain reward.

This variation in path length was not caused by a difference in average synaptic weights occurring due to the contention. Table 6-16 and Table 6-17 show a comparison of the average synaptic weights between the contended and non-contended runs on a quadrant by quadrant basis. The average synaptic weights in the quadrant closest to the reward are very similar, as are the average synaptic weights in the quadrant furthest from the reward.

	Left	Right
Upper	1.47245	0.96512
Lower	1.02287	0.96531

Table 6-16 Average synaptic weight by quadrant - contended run

	Left	Right
Upper	1.44787	1.06701
Lower	1.07377	0.99168

Table 6-17 Average synaptic weight by quadrant - non-contended run

Comparing Figure 6-5 and Figure 6-36 shows that the main difference between the synaptic weights in a contended and a non-contended run is the development of direction specificity at a distance from the reward when the run is not contended.

6.2.11 Random start position

In all the previous simulations the animat has been started diagonally opposite the reward as this represented the longest path to learn within a given grid size. Simulations with the reward horizontally opposite the start position (results not shown) were found to be trivial. As soon as the animat had reached the reward from the left once, the path was learnt.

This simulation assessed whether the path could only be learnt from a repeated start position and whether, once learnt from one start position, the there was an optimum learnt path from any start position. The start position was varied for each trial within a run and 50 runs of 100 trials each were made. To make the simulation a little more realistic, it was decided to only allow starting positions to be along the edges of the grid and not to allow the reward position to also be a start position.

As the start position was varied, it was not possible to say what the optimum path length was from trial to trial. This made it difficult to assess when learning occurred, but the

graph of the average number of moves on each trial clearly shows learning does occur sometime shortly after the tenth trial on average. The average number of moves over the last fifty trials was 9.8

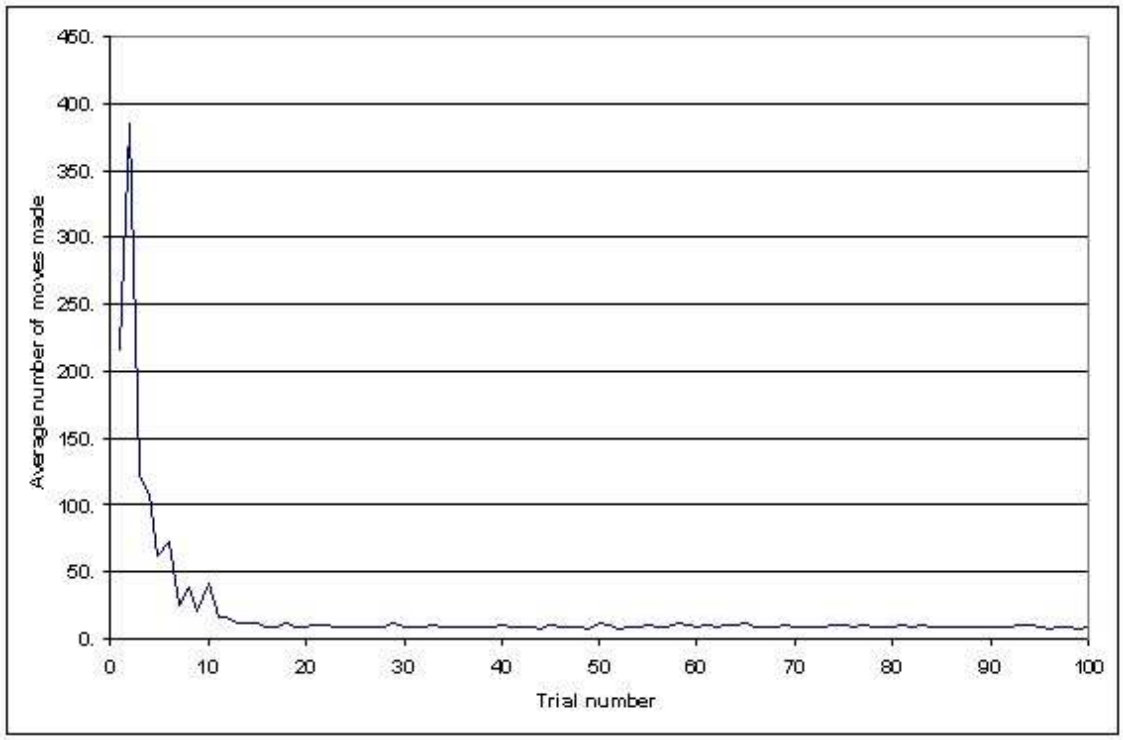

Figure 6-38 Average number of moves made in a simulation where the start position was varied from trial to trial

6.2.12 Different environments

So far, all the simulations have been conducted in a simple grid environment. The reward has been placed to make the path learning within that environment relatively difficult but there are still multiple optimum paths. Many animal experiments are carried out in more complex environments such as mazes. The simulations in this section investigate whether this network of MS neurons would be able to learn the location of the reward in a more challenging environment

6.2.12.1 T-maze

Results file: T Maze 3.xls

The first environment investigated is the T-maze. This is probably the simplest type of maze to learn to navigate. At first sight it would seem to be too similar to the standard

grid to pose a problem. The T-maze is formed by blocking off two of the corners of the square grid. To make this significantly different from a standard square the leg of the T must be sufficiently long that it blocks direct access to the arms by moving diagonally ie. One left, one up, one left, one up etc. This requires a slightly larger grid than the ten by ten size used in the previous simulations. For these simulations a twelve by twelve grid is used as shown in.

Preliminary simulations showed that the environmental exploration phase was longer in the T-maze than the standard square. This led to failure of virtually all runs before exploration was complete. To allow for a longer exploration period, the amplitude of EPSPs was increased to 0.5nS and the amount of potentiation from a single pairing was increased to 1.8. The start position was (7,12).

In a simulation of 50 runs, each consisting of 100 trials, the failure rate remained high at 17 failures from the fifty runs (34%). The environmental state from a successfully completed run is shown in Figure 6-39. Even though this run was successful, the synaptic weights along the wall to the left of the start position remained low. Each time that the animat gained the reward by moving leftward these weights would be potentiated. In the next trial the animat would then try to move left through the wall and application of the disappointment learning rule would knock the synaptic weights back down to a level where stalling of the run became likely.

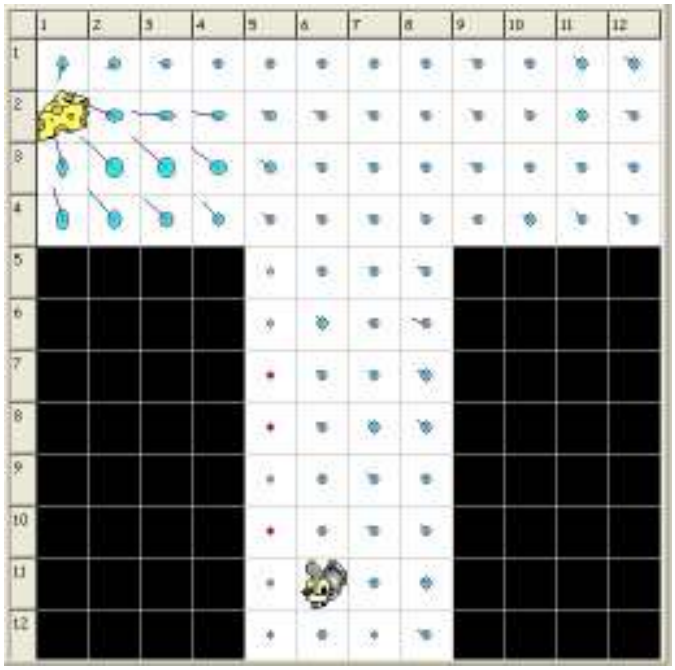

Figure 6-39 Environmental state during the last trial of a successful run in the T-maze simulation. The synaptic weights in the grid positions adjacent to the left wall of the stem of the T are very low. The synaptic weights in the left arm of the T have a good directionality. The synaptic weights in the right arm of the T tend to move the animat away from the stem with a general up and left directionality.

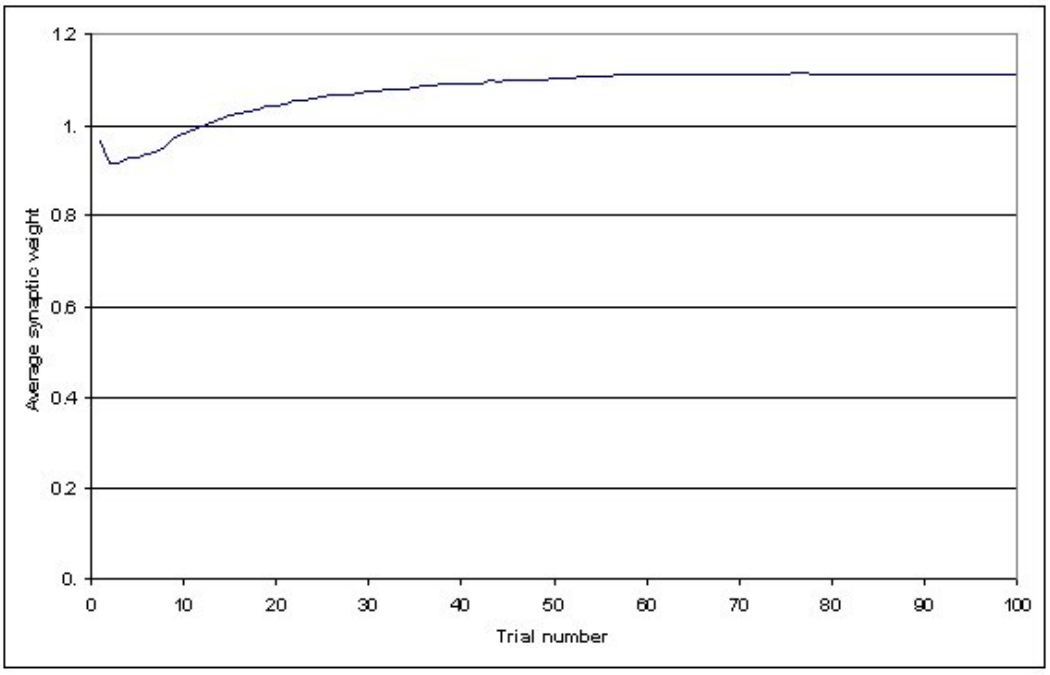

Figure 6-40 Average synaptic weights during learning of the T-maze task. Although the average synaptic weight at the end of runs is stable it is only a little above the starting synaptic weight.

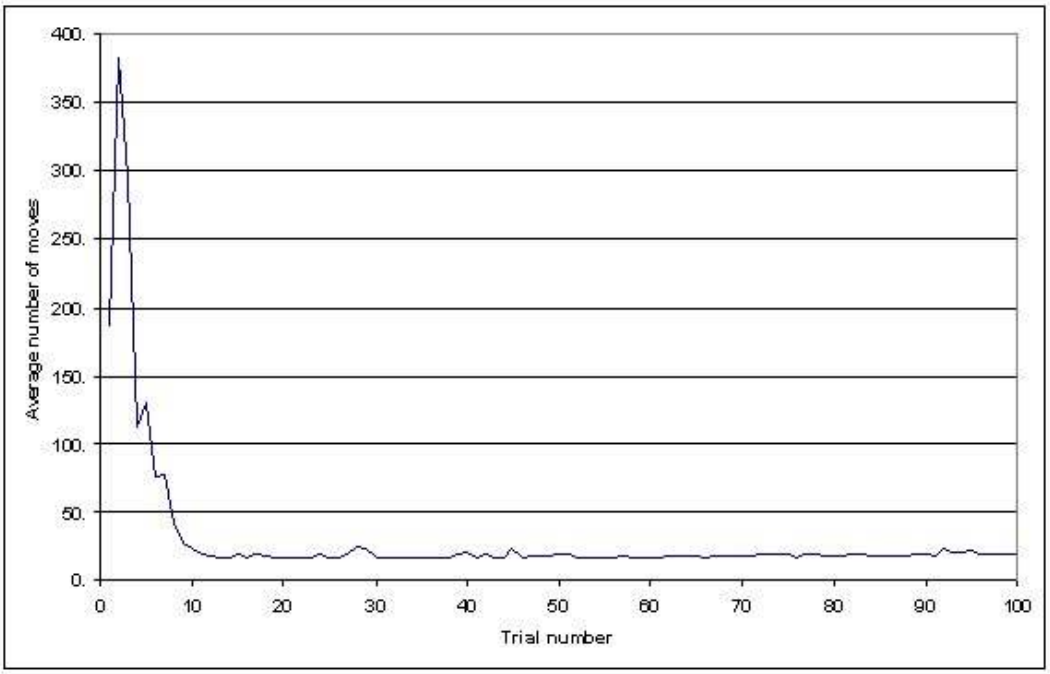

Figure 6-41 Average number of moves made during the learning of the T-maze task. The average path length over the last 50 trials was 20.7, more than 25% above optimum.

The average synaptic weight over the course of this task stabilised at 1.07, producing an average EPSP size of 5.35nS. The shortest path in the T-maze was sixteen steps. The average number of steps taken over the last 50 trials was 20.7. Discounting runs where learning of the path never occurred, the average number of trials until path learning was achieved was 9.0.

6.2.12.2 Wall

Results file: Wall.xls

In this simulation a wall is placed across the centre of the grid. The reward is set in position (1,5) and the animat is started from (10,5), directly opposite and behind the wall. The difficulty with this is that if the animat gains reward by moving to the left, on the next run it will tend to crash straight into the wall with a large amount of resultant LTD. If the animat gains the reward by moving up or down, it will then have a tendency to track up and down on the non-reward side of the wall. Both of these scenarios make this a more difficult task to learn the path to the reward than the T maze.

A ten by ten grid has been used for this simulation, with two squares gap at the top and bottom of the centrally placed vertical wall. Again preliminary investigations showed

that the exploration phase could be very extended. The amplitude of EPSP used was therefore again 0.5nS and the proportional potentiation from one pairing was set to 2.0.

In a simulation of 50 runs of 100 trials each, 15 runs (30%) failed. The environment state at the end of a successful run is shown Figure 6-42. It can be seen from this that, even in a successful run, the synaptic weights to the right hand side of the wall are low and that no up-down directional vector has developed in these positions. The average synaptic weight stabilised at 1.11 (Figure 6-43), giving an effective synapse size of 5.55nS. The average number of moves made over the last 50 trials of the runs was 18.4 (Figure 6-44) with an optimal path length of 15 moves.

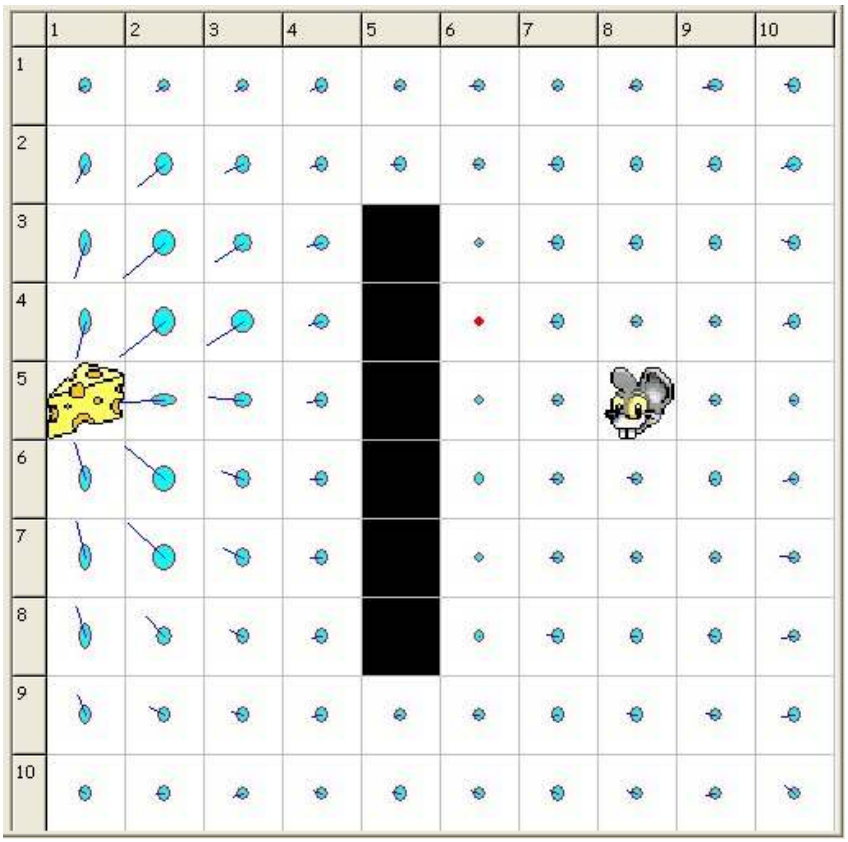

Figure 6-42 Environment state at the end of a successful run in the wall simulation. The synaptic weights in grid positions to the right of the wall are low with no up-down directionality developed to show that the animat has learnt to navigate parallel to the wall. However, directionality approaching the reward from both ends of the wall is good.

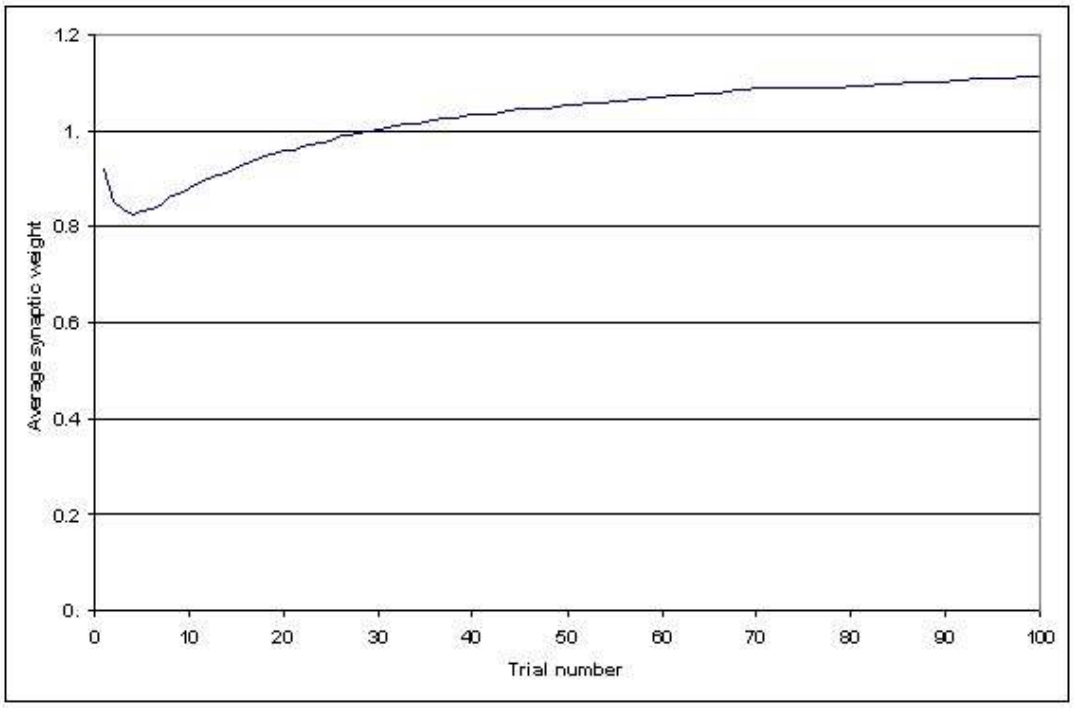

Figure 6-43 Average synaptic weights over 50 runs using the wall maze. The average synaptic weight is still rising after 100 trials.

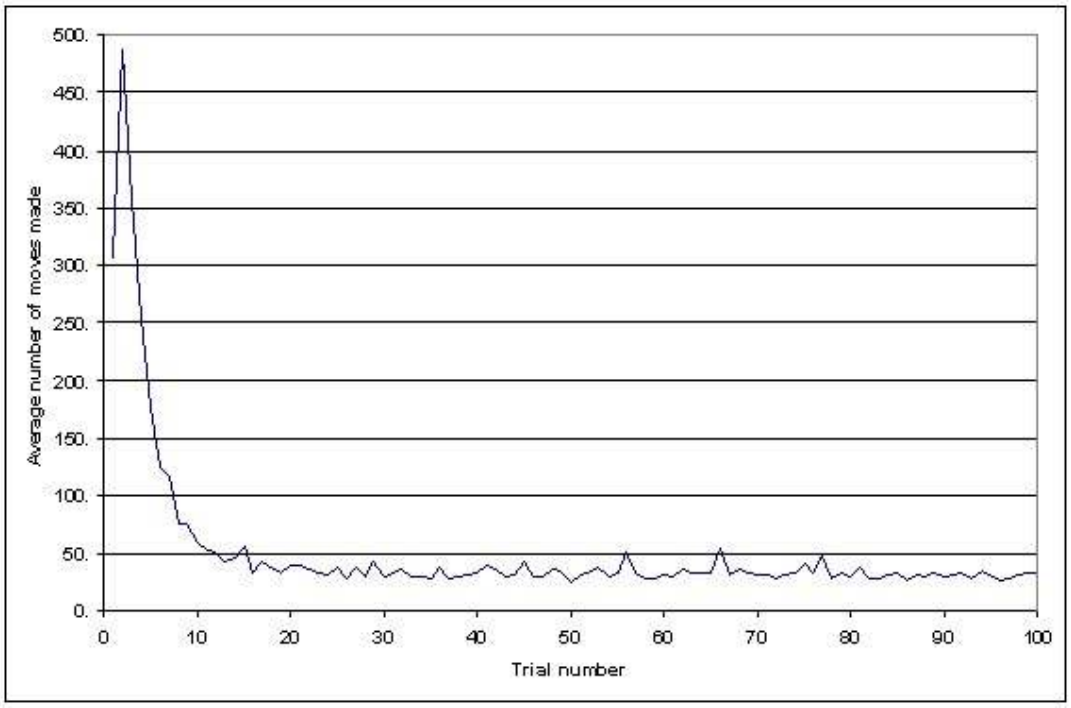

Figure 6-44 Average number of moves made over 50 runs using the wall maze. The average number of moves taken over the last 50 trials was 18.4 with an optimum path length of 15 moves.

6.2.12.3 *Plus maze*

Results file: Four arm maze.xls

This simulation explores learning in another commonly used experimental maze, shown in Figure 6-45. In this simulation the animat is started from (7,12).

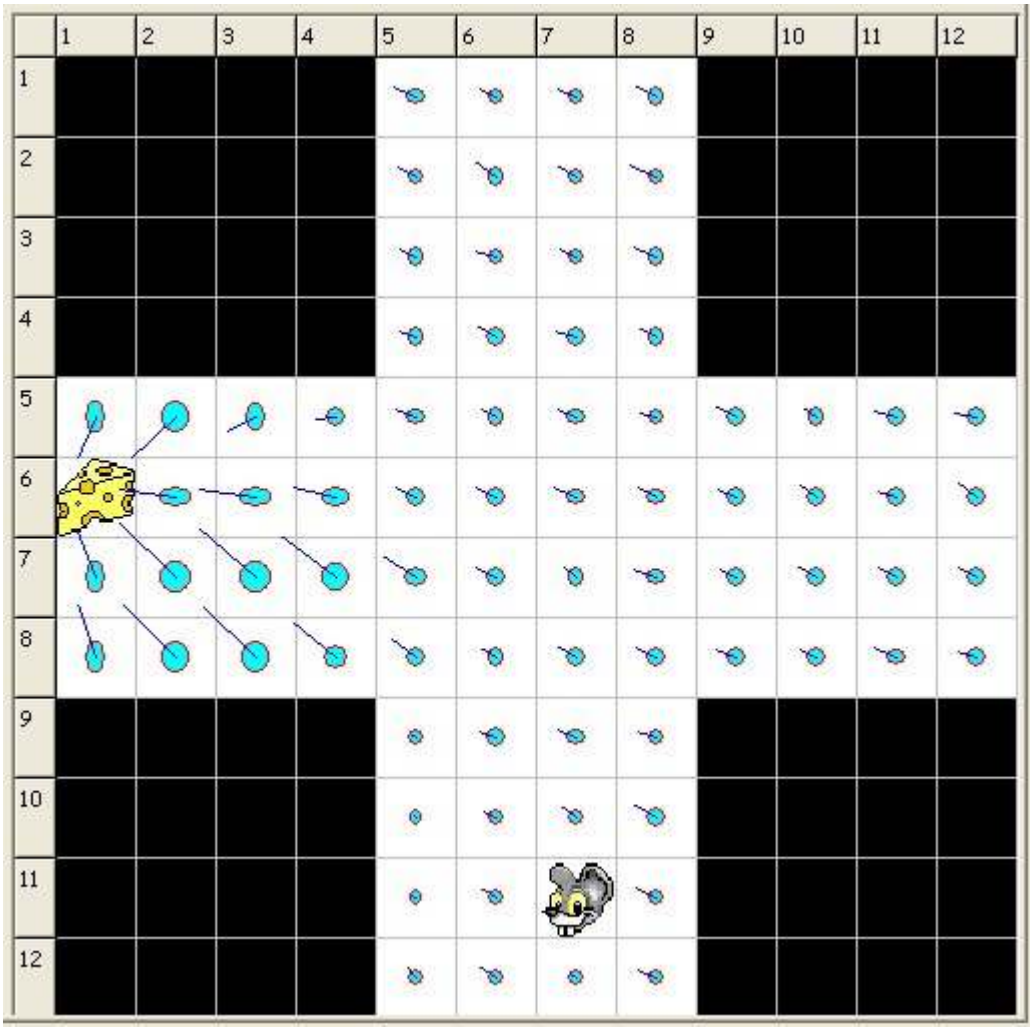

Figure 6-45 Environmental state at the end of a successful run in the four arm maze. Good directionality has developed in the right arm of the maze. Weights are low on the left side of the lower arm. The directionality in the upper arm would tend to keep the animat in that quadrant, but the directionality in the central area does not allow the animat to traverse the maze from bottom to top.

The difficulty in solving this maze lay in the strength of the upward tendency. If the animat entered the reward position by going upward, on the subsequent trial the animat had a tendency to enter the top arm of the maze. Once in this section, with the strongest synaptic weights all tending to send the animat upwards, the animat had a tendency to become stuck in this arm. This can be seen in the successful run in Figure 6-45. Here

the vectors in the upper arm would tend to keep the animat there. The animat no longer explores this section as the strongest vectors in the centre of the maze push the animat to the left.

In this environment 11 runs out of 50 (22%) failed. The average number of trials to learning in the successful runs was 8.1.

The average synaptic weight at the end of runs in this simulation was 1.16, giving an effective synaptic size of 5.8nS. The average number of moves over the last 50 trials was 14.4 with an optimum path length of 12 moves.

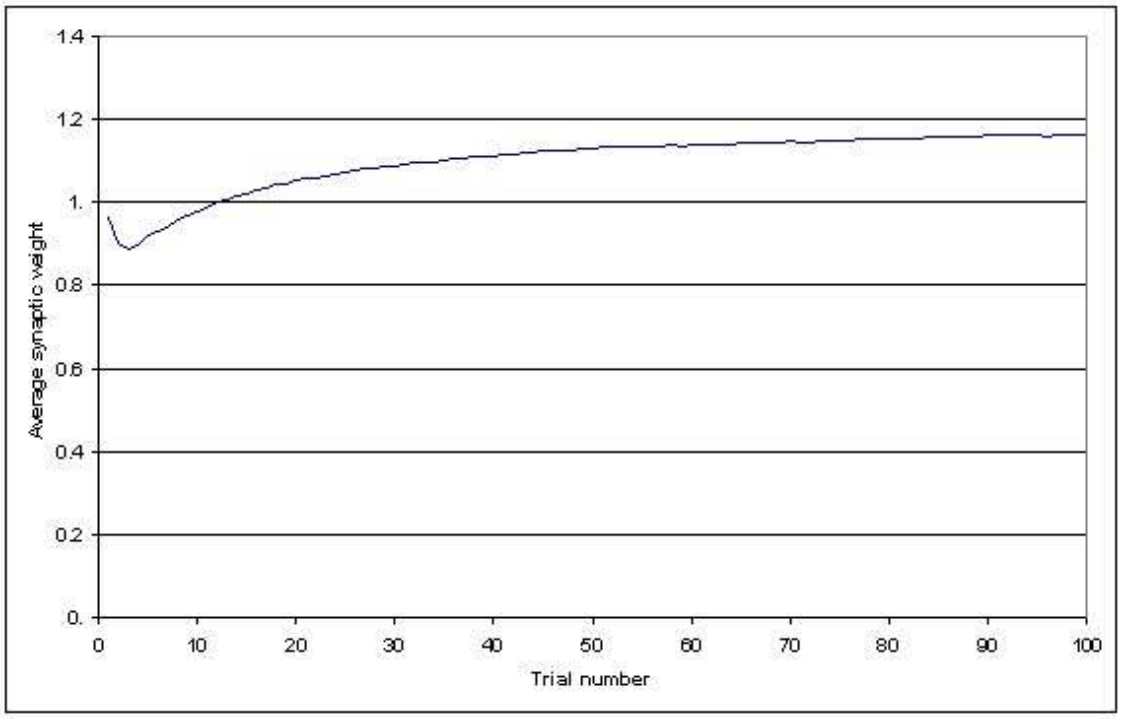

Figure 6-46 Average synaptic weights in four arm maze simulation. The average synaptic weight is still rising after100 trials. The final average synaptic size was 5.8nS.

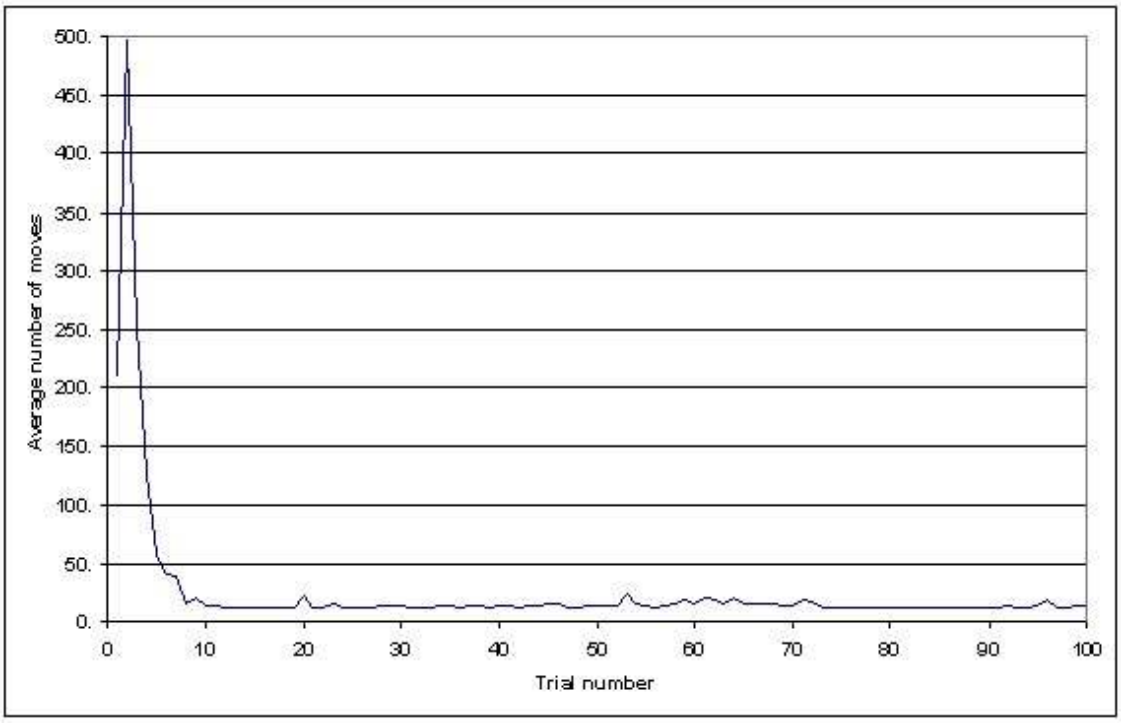

Figure 6-47 Average number of moves taken in four arm maze simulation. The average number of moves over the last 50 trials was 14.4 with an optimum path length of 12 moves.

6.3 Discussion

This simple network comprising just one class of striatal neuron was able to learn to locate a reward in a simple gridworld environment using a scalar learning signal. Despite using only four basic one-step motor programs and thus having no learning of longer sequences of moves, and having no mechanism of transfer of reward to earlier cues, the animat was able to learn a good route to the reward in about ten trials.

Although the animat did not tend to repeat the route taken to reach the reward on each trial, the path length used was generally close to the optimum once learning had been completed. Over long sequences of trials the learning was stable, with path length taken and average synaptic weight remaining relatively constant.

This provides a simple mechanism for using a reward teaching signal to learn the location of reward within an environment. There are however several aspects of the simulation which are required for this learning.

6.3.1 Grid environment

The environment is represented as a grid, with discrete steps from one position to another. As each step is taken, the environmental context changes, also in a discrete manner, with one set of excitatory inputs switched off and another (not totally exclusive) set of inputs switched on, after a delay to allow the movement to occur.

In a real environment it could be argued that the change in context is more continuous, with inputs gradually changing firing rates as movement occurs and different inputs having non-overlapping environmental areas of activity. If, however, the grid squares were considered not as point positions, all of equal size, but as areas of an environment which an organism enters, decides on a plan to cross and then leaves at the point that the plan leads to, the grid environment would map more convincingly to a real environment.

In most of the simulations used here, the environment was represented as a ten by ten grid. One implicit input from the environment would ultimately derive from hippocampal place cells. Experiments mapping the positions in which place cells fire, in environments not dissimilar to that used in these gridworld simulations, show that the place cells fire mainly in discrete regions[243]. The proportion of the environment in which the place cell fires would appear to be 5-20% of the total area. This could lead to the concept that the animal breaks down the environment into a quite small number of areas, probably roughly the same number as has been done in this gridworld.

6.3.2 Random connection of inputs

In the simulation the positions that an excitatory input fired in were allocated randomly, spread over the whole grid. Again considering place cell firing, maps of the region which a single place cell fires in would seem to be relatively well circumscribed in many tasks. There are two considerations as to why this may not be relevant to the connection strategy used in these simulations. Firstly the hippocampus does not have a direct connection to the dorsal striatum. The representation of place seen by the dorsal striatum when making decisions on motor actions has been filtered by cortex and may be re-represented from that seen in hippocampus. Secondly, the hippocampal place cells are not the only origin of environmental inputs. All sensory modalities are likely to

provide different environmental representations, often in a multi-modal format. It is not possible to make assumptions how these other inputs would be represented in the environment and the policy of distributing the representation randomly provides a worst case scenario in learning the reward location.

6.3.3 Resolution of contention

In previous striatal models, when lateral inhibition between MS neurons was thought to play a major role in deciding on plan execution, contention between competing motor programs at striatal level was not a problem. The competitive inhibition of the successful neuron in the winner takes all network would suppress the firing of all the other MS neurons and therefore would only allow disinhibition of one motor program.

Since it is not credible to use this mechanism in a biologically based network simulation, another mechanism for the suppression of competing MS neurons has to be considered. In these simulations the competition is mediated by the non-linear dynamics of the MS neuron membrane potential. As long as the firing threshold is maintained at a level close to the plateau potential, only a small difference in synaptic strengths between two MS neurons could be sufficient to create an adequate temporal separation of firing.

These simulations showed that such a mechanism could work, although not completely reliably. In the simulations shown, when more than one MS neuron fired during a single time step, the first neuron to fire was taken as the one to cause the release of a behaviour. This was in fact not necessary for learning. It was only necessary to make a random choice between the two actions and learning occurred. The only option that could be ruled out was selecting multiple actions if multiple neurons fired. In these simulations that would not create a conflict. If both the leftwards and upwards MS neurons fired, it would generally be possible to move one step left and one up. This strategy would not, however, generalise to other forms of behaviour which could conceivably be mutually exclusive, so was not implemented here.

The selection of one action, even with more than one MS neuron firing could be said to imply another level of selection at a later stage of processing in the basal ganglia. This would effectively reintroduce a winner takes all network, but with no clear mechanism. It is possible that the output nuclei of the basal ganglia could supply such a mechanism.

There is a degree of convergence from the striatum to the GPi. It has been shown that multiple striatal foci are excited by a single cortical region and that these foci reconverge at the level of the GPi[244]. It is possible that, if multiple striatal MS neurons fire in related foci, the GPi effectively takes a poll and releases the behaviour represented by the largest number of foci.

These simulations show that a mechanism for a strict winner takes all network is not required for a low failure of learning in the striatum, but that it could be useful to further increase the success rate of learning. One possible way to implement this would be to reintroduce lateral inhibition, but with a different role.

Although some degree of lateral inhibition has now been found between MS neurons, it has never yet been found to be reciprocal[245]. Given this lack of reciprocity and a low connectivity between MS neurons, it would be necessary to model a much larger network to detect any effect from lateral inhibition. If, though, in a large network lateral inhibition were used to control the rate of learning in single dendrites of MS neurons it may be possible to show that the degree of learning in contention situations could be reduced, thus mitigating the effects of contention.

6.3.4 Learning rules

There is evidence that LTP in MS neurons requires three factors[203]. Both pre-synaptic activity and a generated action potential are required, as in other brain areas[234]. Also phasic dopamine is required[220], without which LTD occurs[246]. This is the justification for the use of learning rules whereby each time an action is selected LTD occurs, but LTP only occurs when the phasic reward signal is received.

The form of the learning rules is based on that developed for STDP[233], although with some modifications. In the standard STDP learning rules, if a synaptic event occurs before a postsynaptic spike, the synapse is potentiated. This clearly runs counter to the expressed requirement for pulsatile dopamine in the striatum. So, in these simulations depression occurs when pre- and post-synaptic events are juxtaposed, no matter the temporal order.

Standard STDP learning also does not incorporate the third factor. The use of an

exponential decay relating back propagating calcium spikes and dopamine transients has been developed purely on a theoretical basis, although the success of the learning using time constants taken from experimental work on the calcium transients suggests this is a viable instantiation of the learning rule.

6.3.4.1 Pulsatile dopamine

Learning was shown to occur effectively across a wide range of pulsatile dopamine levels. This is not surprising since experiments in behaving animals have shown that motivationally different rewards produce different firing rates in dopaminergic neurons[247] as do different probabilities of reward[248]. A range of reward levels should therefore be effective at producing learning in the striatum.

It would also be considered likely that having a high reward level early in learning would make learning quicker. In these simulations that was not the case. The highest pulsatile level of dopamine had the longest path lengths in early learning. All lower levels seemed equally effective. This may be relevant if it can be shown that the concentration of dopamine subsequent to phasic release is not homogenous over volumes of the order of the size of striatal foci.

6.3.4.2 Disappointment learning

Use of the disappointment learning rule was entirely speculative, although based on experimental evidence of ACh release in motivating, non-reward situations which are likely to lead to a phasic dip in dopamine concentrations. That this improved learning rates highlights the observation that animals do not learn from reward alone. The reason why this seems to aid learning is that it effectively reduces the number of choices in the grid. In a 10 by 10 grid with four direction choices, there are 400 choices in total. By using disappointment learning, forty of these choices are effectively removed the first time they are tried. This decreases the choice space by 10% which produces a far larger effect on shortening the exploration phase and therefore reduces the failure rate.

6.3.4.3 Synaptic sizes

Figures for maximum synaptic sizes observed in experiments do not seem to be available. Experimental measurements show that the synapse can approximately double in size as the result of one train of high frequency stimulation[242]. In these simulations,

trials which started off with a synaptic size of 0.4nS and a maximum synaptic weight of 3 were very successful. This maximum synaptic size of 1.2nS does not seem excessive.

Average synaptic weights at the end of successful runs were in the range 1.15 to 1.25. This may be too small a difference to detect experimentally, unless it was possible to measure the sizes of many synapses after a period of learning in which a MS neuron was known to be involved.

If it were shown experimentally that the maximum final synaptic sizes or average final synaptic sizes were much larger than those observed here this would imply that the parameters for the learning rules in the striatum were set to allow greater amounts of LTP. These simulations showed that increasing the amount of LTP can cause credit assignment problems.

6.3.5 Simulation parameters

In the course of these simulations various values were used for parameters such as number of excitatory inputs, potentiation from one pairing, starting size of synapses, synaptic time constant and dopamine trough level. All of these parameters could be varied over ranges of plus or minus 20% with little effect on learning. This demonstrates that the learning by the network is relatively robust.

6.3.6 Dopamine levels

The tonic dopamine level affects two currents in this model, the inwardly rectifying potassium current Kir and the L-type calcium current Ca-L. Simulations in chapter 4 on varying parameters showed that, for any given level of excitation, increasing the tonic dopamine level caused the first action potential to fire earlier and that decreasing the tonic level below a certain point would cause the neuron to stop firing altogether.

The effect of these findings on learning is shown in the simulations where the tonic dopamine level is varied. The main finding is that, as tonic dopamine is decreased, a point is reached where the LTD during the exploration phase becomes a key factor in failure to learn the reward location. During the exploration phase the total excitation in each position is gradually decreased as movement occurs. When it has decreased past a

certain point, which is dependent on the tonic dopamine level, the first action potential caused by that level of excitation rapidly becomes later after the start of excitation. If reward is then obtained, the amount of potentiation is reduced because the up state started a long time before the move to the reward position, so limiting the amount of exploration possible on the next trial. Also, once the action potential has started to be delayed by the decreasing excitation, it only requires a small further decrease in excitation to stop action potentials altogether.

In Parkinson's disease the loss of nigrostriatal dopamine cells causes a decrease in tonic levels of dopamine. This raises two possibilities for the effect of the loss of cells on pulsatile dopamine levels. In the first instance the loss of cells leading to a decrease in tonic dopamine levels may be responsible for a similar decrease in the pulsatile levels of dopamine that can be produced. In the second case, the remaining dopamine cells may not be able to maintain the tonic level of dopamine, but may be able to respond to reward with a pulse of dopamine similar to that seen in the non-disease condition. The effect of these two different possibilities were examined in these simulations. With the peak dopamine pulse maintained the average synaptic weight at the end of the run was slightly higher (1.29 vs. 1.26), but conversely the number of runs that failed increased slightly from 12 to 14. Thus these simulations were not able to distinguish between the two possible cases.

An interesting effect was shown with increased pulsatile dopamine levels whereby the exploratory phase was prolonged. Too much strengthening of the synapses specifying one particular direction at an early stage of the run led to an inability to explore other possible directions until repeated LTD had caused the successful direction from the previous run to become weakened. This would seem to suggest that moderate learning rates are required to maintain flexibility during the learning process.

6.3.7 Synaptic trace time constant

As stated in the learning section (6.1.7), the synaptic trace time constant is modelling a process such as the influx of calcium into the dendritic spine which occurs at the time of an excitatory input. It is likely that this would occur in the dendritic spine and not the main dendrite as the change in membrane potential produced in the confines of the

dendritic spine compartment by a single excitatory input is much larger than in the main dendrite, sufficient to allow the opening of voltage dependant calcium channels. There is no experimental data for the decay of this signal nor for how multiple inputs may interact. It has therefore been modelled as a simple exponential decay and the simulations used to investigate suitable values for the decay time constant.

Learning in the simulations works well over a wide range of values for this constant. Having said that, the values that do work well are quite high, of the order of 100ms plus, implying a signal which is present for at least half a second.

Lower levels of this time constant lead to a failure of learning as the amount of LTD exceeds the amount of LTP. Once this starts happening, it becomes a downward spiral as subsequent trials take more steps, consequently acquiring more LTD for the same amount of LTP when the reward is obtained. The lower limit for this constant could be adjusted by decreasing the amount of LTD per move, but this is already set at a low figure, 1% depression maximum per firing event.

6.3.8 Backpropagation time constant

The backpropagation signal is the credit assignment signal discussed in section 6.1.8. As was explained there, the signal was considered as a simple exponential decay with a time constant of 200ms based on calcium imaging studies. The main aim of these simulations was to see whether learning required such a long time constant, producing a signal lasting approximately one second, or if robust learning could occur with a shorter time constant.

The simulations showed that good learning was possible with the backpropagation time constant decreased to 100ms, which would seem an entirely credible value from the calcium imaging experiments used to derive the starting value for this time constant.

6.3.9 Maximum synaptic weight

The maximum synaptic weight used as standard in these simulations was 3, which gave an effective maximum synaptic size of 1.2nS. This was considered to be not unrealistically large. These simulations investigated whether learning would still work when the maximum synaptic size was smaller. The possibility was that, with a smaller

maximum synaptic size, as learning progressed the differentiation between directions in certain positions may be lost, leading to increasing path lengths in the latter stages of runs.

This turned out not to be the case. Even with a maximum synaptic weight of 1.5 enough differentiation between directions was possible to enable rapid learning with a low failure rate. Using higher synaptic weights did not improve learning suggesting that, at most, a doubling of synapse size is necessary for efficient reward based learning.

6.3.10 Alternate environments

A few more complicated environments than the simple gridworld were used to assess learning. In all these environments it was found that, once learning had occurred, the path was followed well. Failure in these environments was due to failure of learning in the exploratory phase. This may not be surprising as the animat lacked the real world experience of an organism which has learned strategies for environment exploration. The ability of the animat to learn to navigate around a block or pick the correct arm of a maze in the majority of trials was an unexpected result using such a simple network with none of the other learning systems found in behaving animals.

It is probable that varying the learning constants to produce more LTP would improve the failure rate seen in these simulations. Whether this can be justified in a model trying to stay within biologically realistic parameters is debatable.

It is also entirely possible that introducing learning of the dopamine signal in a full actor-critic architecture would improve the learning in these more complicated environment. If that were so it could provide a good rationale for having learning of the teaching signal.

6.3.11 Exploration phase

When averaged over many runs, all simulations showed that during the exploratory phase there was an initial increase in the number of moves made after the reward had been located for the first time.

Observation showed that when the animat approached the reward for the first time from any direction, that side of the environment would then be explored in subsequent trials.

This would continue until the reward had been found once from each possible direction. At this point the animat would generally terminate the exploration phase and shift to exploitation. It would generally take one or two further trials for the path to be completely learnt and each subsequent trial would be completed in close to the optimum number of moves.

Although this differs from the ideal of one shot learning proposed for many types of learning, it does fit in with dissociation experiments of hippocampal and basal ganglia learning which show that the basal ganglia learning is slower and incremental compared to the rapid hippocampal learning[249].

6.3.12 Specification of direction

One assumption of these simulations is that each MS neuron specified a certain direction when firing. This would seem to imply that there is a hard wired loop from each striatal neuron back to the cortical neurons specifying the motor program (or other action). This is not in fact necessary. All that is required is that the same motor program be enacted each time that the same MS neuron fires over the course of learning.

As long as there is some degree of separation of basal ganglia loops and one MS neuron to fire for each of the possible proposed actions in a given environmental context, this random connection method would work. This also provides the possibility of relearning responses should cortical remodelling occur for any reason.

7 Conclusions

The discussion section at the end of each experimental chapter considers the implications of the results from that chapter. This chapter aims to draw together some of the ideas from the previous chapters to give more of an overview of the applicability of the results demonstrated in the previous chapters as well as considering some of the limitations of the work in this thesis.

The aims of this study were to produce a current level, biophysically based model of the striatal medium spiny neuron that was sufficiently computationally tractable to be used in simulations running over considerable lengths of time with small time steps, and with simulations repeated many times to provide averaged results of the behaviour of the simulated neurons.

Many simplifications were made in producing the model. Currents were omitted, the neuron was treated as a single, isopotential compartment and firing was modelled as simplistically as possible. Nevertheless, key aspects of the behaviour of MS neurons were replicated. This meant that, within the limits of the behaviours the model was compared against, results obtained using this model could be seen as meaningfully representing results obtained from real MS neurons, were similar experiments possible.

In the simulations using the model neuron, the main underlying assumption was that the behaviour of neurons at the input layer would affect how the basal ganglia as a whole control the release of behaviours. Previous models have tended to spread this decision making process over several nuclei of the basal ganglia. It was felt that showing simulations of the striatum to be capable of making behavioural decisions in isolation would provide impetus for producing updated models of a basal ganglia actor. This would then allow the assignment of different functions to other nuclei of the basal ganglia once one level of action selection has been performed by the striatum.

The two sets of simulations have shown that two key aspects of behaviour selection could be mediated by the striatum, the selection between competing behaviours and timing of the release of behaviours.

Clearly these two aspects are related as either alone would not provide adequate control

for a behaving organism. That the simulations here show both are mediated by the large rise from the down state to the up state and the non-linear characteristics of the MS neuron gives some credibility to the idea that both aspects are controlled by the striatum.

Due to the somatotopic organisation of the striatal inputs, the selection between competing behaviours is likely to work only in selecting between broadly similar classes of behaviour at a single temporal range of planning. In practise this would be advantageous as it would allow implementation of non-exclusive behaviours simultaneously.

The simulations showing the effects in the model of varying the level of dopamine provide an interesting insight into how different mechanisms may bring about different symptoms in Parkinson's disease. The reduced tonic level of dopamine decreases the likelihood of reaching the firing threshold for a given level of excitation. This could lead to a difficulty in initiating movement, especially when feedforward inhibition is increasingly effective at lower dopamine levels. A reduced pulse of dopamine decreases the learning from one rewarding episode and produces a slower rise in average synaptic weight during the course of learning. In the current simulations this did not reflect in an increase in number of trials taken to learn the path.

Parkinson's disease patients have been shown to be slow in stimulus-response based habit learning[249]. It may be that the gridworld learning task was too simplistic for the reduced rate of learning, as evidenced by the slower synaptic weight increase, to be reflected in the performance of the task.

One important aspect of this model is that it is not particularly susceptible to changes in many of the parameters controlling the behaviour of the model. This would seem to indicate that the variations seen amongst neurons in vivo would not affect the ability of MS neurons to perform action selection in the manner demonstrated in these simulations.

7.1 Limitations

Although this model is based more closely on the known biology of the MS neuron,

there are many assumptions and simplifications made in the design, mostly for reasons of computational tractability. Some of these are described in Chapter 2, the construction of the model neuron. There are other assumptions and simplifications that also deserve comment.

7.1.1 Experimental basis of the model

The biology of the model is based mainly on work conducted in vitro on striatal slice preparations. Other preparations include anaesthetised animals in vivo, behaving animals and organotypic cultures.

7.1.2 Currents

The voltage gated currents in this study were chosen because their time course of activation and inactivation fell within the remit of a model looking for effects which occur over tens to hundreds of milliseconds and their voltage activation range was relevant to the transition between the down and up states, the main focus of this study.

There are several other currents known to be present in MS neurons. Sodium currents were excluded because this study was not concerned with neuronal firing patterns, only the timing of the first action potential. This exclusion has had the effect that the transition from the up to the down state is not as rapid as it would be if sodium currents had been included. This may affect the timing of the first action potential in subsequent up states if the duration of the down state is short. This was accounted for by making the down state duration at least 150ms, but this may not be realistic. Exclusion of the sodium currents also made it impossible to realistically consider firing patterns in the up state. This was felt to be acceptable because the modelling was assuming that the most important factor to consider was the timing of the first action potential. It is possible that trains of action potentials may have a separate function. This model would not, as it stands, be suitable to investigate those functions.

7.1.3 Other striatal neurons

Whilst the MS neurons are the principal neurons of the striatum and the only neurons which project out of the striatum, there are several classes of interneuron. One class, the fast spiking (FS) interneurons were considered in chapter 5 on how feedforward

inhibition controls the timing of the firing of the first spike. There are other types of inhibitory interneuron which also produce feedforward inhibition and have different firing patterns. Their action may or may not be the same as that of the FS interneurons, but as they are even less numerous and less well characterised they have been ignored in these studies.

Another class of interneuron in the striatum is the cholinergic interneuron, also called the tonically active neuron (TAN). There has been brief mention of them in this work, mainly to dismiss their further study in this thesis as their connections with other classes of neuron are complicated and insufficient evidence of their purpose is available at present. It has long been clear that their influence is important, as witnessed by the successful use of anticholinergic mediations in Parkinson's disease. But the complications they introduce put them beyond the scope of a modelling project of the duration of this thesis. They may be especially important in the control of learning and, if further evidence in this direction is found, the learning rules used in this study will have to be updated to take that into account.

7.1.4 Lack of other basal ganglia structures

The striatum has been included in isolation. Although Chapter 1 did consider the other nuclei of the basal ganglia and the pathways between them, one of the main hypotheses of this work is that the striatum is capable of performing action selection and that the other basal ganglia structures are not required in making this selection. There is evidence from deep brain stimulation studies in animals and humans that changing the oscillations in the STN-GPe axis improves action selection in Parkinson's disease and similar animal disease models. The exact mechanism of this is not known, but it does point to a role of the other nuclei in action selection. That role may be assumed to be modulatory or focussing in nature, but it does not invalidate the main hypothesis here, that action selection can be performed by the striatum, at least to a first approximation.

7.1.5 Environmental connections in reward based learning

In Chapter 6 where reward location learning was considered, an assumption was made about the pattern of connections between the excitatory inputs to the MS neurons and the environment. It was assumed that neurons do not fire when the animal is in a locally

circumscribed location, but fire in multiple different locations in the environment, locations that are not related by any obvious spatial pattern, but may be related by unifying sensory inputs in those position, such as being able to see a certain landmark or smell a certain odour. There is no evidence for such a pattern of connections, as there is also no evidence for a pattern of connections similar to that seen in hippocampal place cells, where individual neurons fire in a circumscribed ellipsoid of positions around a central point.

If more evidence of the relationship of environmental stimuli to MS neuron connections were available, this connection pattern would have to be reconsidered.

8 Further work

There are three ways to carry on extending this model, all of which have their merits.

8.1 Up

By this I mean extending the modelling at a higher level of abstraction. For the striatal model itself this may be useful in that it would allow construction of larger scale network models of striatal function. This may, in the process, lose some of the discrimination between differing effects of tonic and pulsatile dopamine which would decrease the usefulness of the model for investigating Parkinson's disease. However, it may then become useful for investigating Huntington's chorea where the symptoms appear as striatal MS neurons are lost.

Although this model has shown the ability of the striatum alone to function as an actor, the striatum is embedded within a system of nuclei with complex interconnections. Only by understanding the function of the network as a whole will it be possible to get a full picture of reward based learning in the brain. This would require integrating not only models of the other basal ganglia nuclei, but also some thalamic nuclei and various areas of cortex. With current computational technology it would be difficult to accomplish this with all sub-units modelled at the same level as the MS neurons have been in these simulations. There would be a necessity to abstract to a higher level. There is an obvious first step to take in this process, which is to implement a full actor-critic model using the MS model produced here for the main aspects of the actor and instantiating a critic using Reinforcement Learning (RL) equations. This would allow for the modelling of more complex animal and human behavioural tasks

Once such a model was available, it should be possible to gradually extend it by introducing more physiologically based inputs to both the actor and critic. In the case of the actor this could involve modelling cortical and thalamic neurons in large numbers as simple integrate and fire neurons with learning based on standard STDP rules in the main, although incorporating the effects of dopamine on learning in a model prefrontal cortex (PFC).

One area that is lacking that could also be introduced into the model at this point would be a more physiologically based model of how the dopamine signal is produced This

would involve modelling input from the pedunculopontine tegmental nucleus to midbrain dopamine neurons to show how DA neurons respond to unexpected reward and modelling learning in the PFC and ventral striatum to show how inhibition can learn to counterbalance the response of DA neurons to expected reward and how prefrontal activation can stimulate the DA neurons at the time of reward indicative cues.

8.2 Down

This model has been produced using a minimal set of currents within a constrained physical geometry. It has been able to demonstrate some aspects of striatal behaviour but can have little to say about others. Specifically, this model cannot assess the activity of various inputs to MS neurons on firing rates and burst length. This would require the incorporation of a new set of currents, including sodium, potassium and calcium currents which would take the model to a higher level of complexity and probably render it unsuitable for use within a larger network model.

A second aspect of striatal function which would need a lower level model to investigate is the interaction of dopamine and calcium in the protein kinase pathways which leads to LTP and LTD. A better understanding of this process could probably then be abstracted back to this model, producing a more accurate method of modelling the time convolution of calcium and dopamine signals.

8.3 Sideways

The MS neuron, although comprising the vast majority of the cells, is not alone in the striatum. And the importance of the activities of the various classes of interneuron is gradually becoming clearer. These simulations have shown how the feedforward inhibition of FS interneurons can control the timing of firing in MS neurons, but the FS neurons are themselves also controlled by DA and ACh as well as excitatory cortical inputs. It would be very useful to have models of the FS interneuron and cholinergic interneuron at a similar level to the MS neuron used here to investigate the role of feedforward inhibition and the interaction of ACh with all other neuronal classes in the development of symptoms in Parkinson's disease. Without such models it will prove very difficult to untangle the complex interactions of these cell classes in response to various neuromodulatory conditions. Understanding of how the influence of these cell

classes is produced under various levels of neuromodulation could provide possibilities for new treatments for Parkinson's disease, perhaps to increase the efficacy of remaining dopamine in learning or reducing overactive inhibition.

Another aspect of MS neuron behaviour that has received increasing attention has been the small amounts of lateral inhibition between MS neurons that have been demonstrated within the last few years. The function of this lateral inhibition remains obscure as it is evidently insufficiently powerful to reinstate its former function in a winner takes all network. It would be possible to investigate proposals that this inhibition plays a role in learning by implementing a sparse lateral inhibition onto terminal dendrites within a large network of model MS neurons. It may be that it would be possible to show that this inhibition would limit the learning in situations where contention in the firing of MS neurons has occurred, as described in earlier simulations. One possible method of controlling the learning by the collateral inhibition would be to control the backpropagating calcium transient by locally varying the membrane potential in a dendrite and thus inhibiting learning at points distal to the inhibitory synapse.

The availability of multiple dimensions through which to extend the model here produced is an indication of the strength of the approach that has been used to modelling in these simulations.

8.4 Which direction is most warranted?

The previous sections showed that it may be possible to extend the model in a variety of directions. The most suitable directions to be taken depend on the strengths and weaknesses of the model. The clearest strengths are:

1. Computational tractability. It has proven possible to use the model neuron in a small network. These simulations have shown that the model is capable of being extended to larger networks to produce simulations that can be run in a reasonable time.
2. Separation of tonic and phasic dopamine effects. One major advantage of this

model over other biophysically based network models and reinforcement learning models is that tonic dopamine modulates the ionic currents in the neuron and phasic dopamine modulates the learning. This provides the ability to manipulate the levels of tonic dopamine separately from the phasic reward signal.

3. Extensibility. Other currents can be added in to the model to simulate firing. This would allow investigation of phenomena that are dependant on firing rates rather than the timing of the first spike.

The model also has some weaknesses that make it less suitable for some types of investigation.

1. Non-compartmental nature of the model. Some important aspects of the computations performed by MSNs may occur in the dendritic tree. This is particularly relevant to lateral inhibition which, whilst not playing the competitive inhibition role originally proposed, clearly has computational functions within the neuron that are ideal for modelling.
2. Lack of biophysical basis for the learning rules. The learning rules developed in this thesis are attempting to model the 3-factor learning known to occur in MSNs. Although the pathways where calcium and dopamine interact are known, the exact convolution of the two time varying signals is not known; neither is the relationship between this convolution and the amount of LTP produced.

This leads to the conclusion that the natural extension of the current model would be to model higher order processes, such as network learning in the basal ganglia. Reinforcement models of the basal ganglia are currently very influential. These models generally adopt the actor-critic architecture (see section 6.1.1, p.109.). As stated there, the instantiation of the actor in such models is generally not biophysically realistic. The reward based learning section of this thesis attempted to show how a more biophysical actor could learn action selection based on a reward signal. This model of action selection contained no learning of the dopamine signal itself, no critic in RL terms.

An interesting and viable next step for the modelling would be to develop a

biophysically based critic module to connect to the current actor module. This would enable more complex tasks to be modelled than those undertaken in this thesis.

This would also require the production of a network theory of how the dopamine signal is learned. Such a biophysical actor-critic network would then be suitable for use in investigating disorders of learning in the basal ganglia. The most obvious example of this would be Parkinson's disease.

In Parkinson's disease, the loss of cells in the SNc leads to a decrease of the tonic level of dopamine in the dorsal striatum[250]. As the VTA is less affected, especially in mild to moderate Parkinson's disease, the tonic levels of dopamine in the ventral striatum are substantially normal. However, learning in the striatum has been shown to be dependent not on the tonic levels of dopamine, but on phasic changes overlying the tonic dopamine level[220]. These phasic changes occur in response to unexpected rewards and unexpected cues which have been learned to reliably predict the upcoming occurrence of a reward[251]. The effect of the loss of the DA cells on the phasic changes, and therefore directly on learning, has proven difficult to investigate in both animal and human experiments. Given the ability of this model to dissociate the effects of tonic and phasic dopamine on the MSNs, the model is in an ideal position to be used to determine the likely changes to the phasic dopamine signal that occur in Parkinson's disease.

9 Bibliography

1 Alexander GE, DeLong MR, Strick PL. Parallel organization of functionally segregated circuits linking basal ganglia and cortex. *Annual Review of Neuroscience* **9** (1986), 357–38.

2 Penney JB, Young AB. Speculation on the functional anatomy of basal ganglia disorders. .*Annual Review of Neuroscience* **94** (1983), 73-94.

3 Albin RL, Young AB, Penney JB. The functional anatomy of basal ganglia disorders. *Trends in Neuroscience* **12** (1989), 366-375.

4 DeLong MR. Primate model of movement disorders of basal ganglia origin. *Trends in Neuroscience* **13** (1990), 281-859.

5 Middleton,FA, Strick, PL. Anatomical evidence for cerebellar and basal ganglia involvement in higher cognitive function. .*Science* **266** (1994), 458-461.

6 Brown LL, Schneider JS, Lidsky TI**.** Sensory and cognitive functions of the basal ganglia. *Current Opinion In Neurobiol*ogy **7** (1997), 157–163.

7 Wilson SAK. Progressive lenticular degeneration: A familial nervous system disease associated with cirrhosis of the liver. *Brain* **34** (1912), 295–507.

8 Nauta WJH and Mehler WH. Projections of the lentiform nucleus in the monkey. *Brain Research* **1** (1966), 3–42.

9 Parent A and De Bellefeuille L. Organization of efferent projections from the internal segment of globus pallidus in primate as revealed bye fluorescence retrograde labeling method. *Brain Research* **245** (1982), 201–213.

10 Crossman AR. Functional anatomy of movement disorders. *Journal of Anatomy* **196** (2000), 519-526.

11 Parent A, Hazrati L-N. Functional anatomy of the basal ganglia. I. The cortico-basal ganglia-thalamo-cortical loop. *Brain Research Reviews* **20** (1995), 91–127.

12 Parent A, Levesque M., Parent M. A re-evaluation of the current model of the basal ganglia. Parkinsonism & Related Disorders 7 (2001), 193-198.

13 Gurney K, Prescott TJ, Wickens JR, Redgrave P. Computational models of the basal ganglia: from robots to membranes. *Trends in Neuroscience* **27** (2004), 453-459.

14 Medina L., Reiner A. Structural and functional evolution of the basal ganglia in vertebrates. *Brain Research Reviews* **28** (1998), 235-285.

15 Gonzalez A., Marin O., Smeets W. Basal ganglia organization in amphibians: efferent connections of the striatum and the nucleus accumbens. *The Journal of Comparative Neurology* **380** (1997), 23-50.

16 Russchen FT, Smeets WJAJ, Hoogland PV. Histochemical identification of pallidal and striatal structures in the lizard Gekko gecko: evidence for compartmentalization. *Journal of Comparative Neurology* **256** (1987a), 329-341.

17 Reiner A, Anderson KD. The patterns of neurotransmitter and neuropeptide co-occurrence among striatal projection neurons: conclusions based on recent findings. *Brain Research Reviews* **15** (1990),

251-265.

18 Smeets WJAJ, Marin O, Gonzalez A. Evolution of the basal ganglia: new perspectives through a comparative approach. *Journal of Anatomy* **196** (2000), 501-517.

19 Vincent SR, Reiner PB. The immunohistochemical localization of choline acetyltransferase in the cat brain. *Brain Research* **18** (1987), 371-415.

20 Hoogland PV,Vermeulen-Vanderzee. Distribution of choline acetyltransferase immunoreactivity in the telencephalon of the lizard Gekko gecko. *Brain, Behavior and Evolution* **36** (1990), 378-390.

21 Marin O, Smeets WJAJ, Gonzalez A. Basal ganglia organization in amphibians: chemoarchitecture. Journal of Comparative Neurology **392** (1998), 285-312.

22 Kawaguchi Y, Wilson CJ, Augood SJ, Emson PC. Striatal interneurons: chemical, physiological and morphological characterization. *Trends in Neurosciences* **18** (1995), 527-535.

23 Albin RL, Young AB, Penney JB. The functional anatomy of basal ganglia disorders. *Trends in Neuroscience* **12** (1989), 366-375.

24 Alexander AGE, Crutcher MD, De Long MR. Basal ganglia-thalamocortical circuits: parallel substrates for motor, oculomotor, "prefrontal" and "limbic" functions. *Progress In Brain Research* **85** (1990), 119-146.

25 Penny GR, Afsharpour S, Kitai ST. The glutamate decarboxylase-, leucine enkephalin-, methionine enkephalin- and substance P-immunoreactive neurons in the neostriatum of the rat and cat: evidence for partial population overlap. *Neuroscience* **17** (1986), 1011–1045.

26 Graybiel AM. Neurotransmitters and neuromodulators in the basal ganglia. *Trends in Neurosciences* **13** (1990), 244–254.

27 Gerfen CR, Engber TM, Mahan LC, Susel Z, Chase TN, Monsma FJ, Sibley DR. D1 and D2 dopamine receptor-regulated gene expression of striatonigral and striatopallidal neurons. *Science* **250** (1990), 1429–1432

28 Moriizumi T, Nakamura Y, Okoyama S, Kitao Y. Synaptic organization of the cat entopeduncular nucleus with special reference to the relationship between the afferents to entopedunculothalamic projection neurons: an electron microscope study by a combined degeneration and horseradish peroxidase tracing technique. *Neuroscience* **20** (1987), 797-816.

29 Bolam JP, Smith Y. The striatum and the globus pallidus send convergent synaptic inputs onto single cells in the entopeduncular nucleus of the rat : a double anterograde labeling study combined with post-embedding immunocytochemistry for GABA. *Journal of Comparative Neurology* **321** (1992), 456-476.

30 Somogyi P, Hodgson AJ, Smith AD. An approach to tracing neuron networks in the cerebral cortex and basal ganglia. Combination of Golgi staining, rerograde transport of horseradish peroxidase and anterograde degeneration of synaptic boutons in the same material. *Neuroscience* **4** (1979), 1805-1852.

31 Smith Y, Bevan MD, Shink E, Bolam JP. Microcircuitry of the direct and indirect pathways of the basal ganglia. *Neuroscienc* **86** (1998), 353-387.

32 Aronin N, DiFiglia M, Graveland GA, Schwartz WJ, Wu JY. Localization of immunoreactive

enkephalins in GABA synthesizing neurons of the rat neostriatum. *Brain Research* **300** (1984), 376–380.

33 Chang HT, Wilson CJ, Kitai ST. Single neostriatal efferent axons in the globus pallidus : a light and electron microscopic study. *Science* **213** (1981), 915-918.

34 Smith Y, Bolam JP, Von Krosigk M. Topographical and synaptic organization of the GABA-containing pallidosubthalamic projection in the rat. *European Journal of Neuroscience* **2** (1990), 500-511.

35 Bevan MD, Crossman AR, Bolam JP. Neurons projecting from the entopeduncular nucleus to the thalamus receive convergent synaptic inputs from the subthalamic nucleus and the neostriatum. *Brain Research* **659** (1994), 99-109.

36 Feger J, Crossman AR. Identification of different subpopulations of neostriatal neurones projecting to globus pallidus or substantia nigra in the monkey: A retrograde fluorescence double-labeling study. *Neuroscience Letters* **49** (1984), 7–12.

37 Gerfen CR, Young III WS. Distribution of striatonigral and striatopallidal peptidergic neurons in both patch and matrix compartments: an in situ hybridization histochemistry and fluorescent retrograde tracing study. *Brain Research* **460** (1988), 161–167.

38 DiChiara G, Porceddu ML, Morelli M, Mulas ML, Gessa GL. Evidence for a GABAergic projection from the substantia nigra to the ventromedial thalamus and to the superior colliculus of the rat. *Brain Research* **176** (1979), 273–284.

39 Grofova I, Rinvik E. Cortical and pallidal projections to the nucleus ventralis lateralis thalami. Electron microscopical studies in the cat. *Anatomical Embryology* **146** (1974), 113–132.

40 Kultas-Ilinsky K, Ilinsky IA. Fine structure of the magnocellular subdivision of the ventral anterior thalamic nucleus (VAmc) of Macaca mulatta. II. Organization of nigrothalamic afferents as revealed with EM autoradiography. J*ournal of Comparative Neurology* **294** (1990), 479–489.

41 Bentivoglio M, Van der Kooy D, Kuypers HGM. The organization of the efferent projections of the substantia nigra in the rat. A retrograde fluorescent double labeling study. *Brain Research* **174** (1979), 110–117.

42 Beckstead RM, Frankfurter A. The distribution and some morphological features of substantia nigra neurons that project to the thalamus, superior colliculus and pedunculopontine nucleus in the monkey. *Neuroscience* **7** (1982), 2377–2388.

43 Parent A, Mackey A, Smith Y, Boucher R. The output organization of the substantia nigra in primate as revealed by a retrograde double labeling method. *Brain Research Bulletin* **10** (1983), 529–538.

44 Mink JW. The basal ganglia: focused selection and inhibition of competing motor programs. *Progress in Neurobiology* **50** (1996), 381-425.

45 Parent A, Hazrati LN. Anatomical aspects of information processing in primate basal ganglia. T*rends in Neurosciences* **16** (1993), 111–116.

46 Bergman H, Wichmann T, DeLong MR. Reversal of experimental Parkinsonism by lesions of the subthalamic nucleus. *Science* **249** (1990), 1436-1438.

47 Laitinen LV, Bergenheim AT, Hariz MI. Leksell's posteroventral pallidotomy in the treatment of

Parkinson's disease. *Journal of Neurosurgery* **76** (1992), 53-61.

48 Marsden CD, Obeso JA. The functions of the basal ganglia and the paradox of stereotaxic surgery in Parkinson's disease *Brain* **117** (1994), 877–97

49 Obeso JA, Guridi J, DeLong MR. Surgery for Parkinson's disease. *Journal of Neurological and Neurosurgical Psychiatry* **62** (1997), 2–8.

50 Albin RL, Young AB, Penney JB. The functional anatomy of disorders of the basal ganglia. *Trends in Neuroscience* **18** (1995), 63-64.

51 Shink E, Bevan MD, Bolam JP, Smith Y. The subthalamic nucleus and the external pallidum: two tightly interconnected structures that control the output of the basal ganglia in the monkey. *Neuroscience* **73** (1996), 335-357.

52 Bolam JP, Hanley JJ, Booth PAC, Bevan MD. Synaptic organisation of the basal ganglia. *Journal of Anatomy* **196** (2000), 527-542.

53 Obeso A, Rodríguez-Oroz MC, Rodríguez M, Lanciego JL, Artieda J, Gonzalo N,Olanow CW. Pathophysiology of the basal ganglia in Parkinson's disease. *Trends in Neurosciences* **23** (2000), S8–S19.

54 Smith Y, Bolam JP. Neurons of the substantia nigra reticulata receive a dense GABA-containing input from the globus pallidus in the rat. *Brain Research* **493** (1989), 160-167.

55 Kincaid AE, Penney JB, Young AB, Newman SW. Evidence for a projection from the globus pallidus to the entopeduncular nucleus in the rat. *Neuroscience Letters* **128** (1991), 121-125.

56 Kita H, Kitai ST. The morphology of globus pallidus projection neurons in the rat : an intracellular staining study. *Brain Research* **636** (1994), 308-319.

57 Bevan MD, Booth PAC, Eaton SA, Bolam JP. Selective innervation of neostriatal interneurons by a subclass of neuron in the globus pallidus of the rat. *Journal of Neuroscience* **18** (1998), 9438-9452.

58 Hazrati L-N, Parent A. Projection from the external pallidum to the reticular thalamic nucleus in the squirrel monkey. *Brain Research* **550** (1991), 142–146.

59 Levesque M, Bedard A,Cossette M, Parent A. Novel aspects of the chemical anatomy of the striatum and its efferents projections. *Journal of Chemical Neuroanatomy* **26** (2003), 271-281.

60 Aizman O, Brismar H, Uhlen P, Zettergren E, Levey AI, Forssberg H, Greengard P, Aperia A. Anatomical and physiological evidence for D_1 and D_2 dopamine receptor colocalization in neostriatal neurons. *Nature Neuroscience* **3** (2000), 226-230.

61 Graybiel AM, Ragsdale CW Jr. Histochemically distinct compartments in the striatum of human, monkey and cat demonstrated by acetylcholinesterase staining. *Proceedings of the National Academy of Science USA* **75** (1978), 5723–5726.

62 Gerfen CR. The Neostriatal Mosaic: Striatal Patch-Matrix Organization is Related to Cortical Lamination. *Science* **246** (1989), 385-388.

63 Gerfen CR. The neostriatal mosaic: multiple levels of compartmental organization. *Trends in Neurosciences* **15** (1992), 133-139.

64 Hedreen JC, De Long MR. Organization of striatopallidal, striatonigral, and nigrostriatal projections in the macaque. *Journal of Comparative Neurology* **304** *(1991), 569-595.*

65 Haber SN, Fudge JL, McFarland NR. Striatonigrostriatal Pathways in Primates Form an Ascending Spiral from the Shell to the Dorsolateral Striatum. *Journal of Neuroscience* **20** (2000), 2369-2382.

66 Schultz W, Dayan P, Montague PR. A Neural Substrate of Prediction and Reward. *Science* **275** (1997), 1593-1599.

67 Wichmann T, De Long MR. Oscillations in the basal ganglia. *Nature* **400** (1999), 621-622.

68 Bevan MD, Magill PJ, Terman D, Bolam JP, Wilson CJ. Move to the rhythm: Oscillations in the subthalamic nucleus – external globus pallidus network. *Trends in Neurosciences* **25**, 525-531.

69 Wickens J. Basal ganglia: structure and computations. *Network Computation in Neural Systems* **8** (1977), R77-R109.

70 Arbuthnott GW, MacLeod N, Rutherford A. The rat cortico-striatal pathway in vitro. *Journal of Physiology London* **367** (1985), 102P.

71 Kemp JM, Powell TPS. The corticostriate projection in the monkey. *Brain* **93** (1970), 525-546**.**

72 McGeer PL, McGeer EG, Scherer U, Singh K. A glutamatergic corticostriatal pathway?.*Brain Research* **128** (1977), 369-373.

73 Cherubini E, Herrling PL, Lanfrrmey L, Stanzione P. Excitatory amino acids in synaptic excitation of rat striatal neurones in vitro. *Journal of Physiology* **400** (1988), 677-690.

74 Lapper SR, Bolam JP. Input from the frontal cortex and the parafascicular nucleus to cholinergic interneurons in the dorsal striatum of the rat. *Neuroscience* **51** (1992), 533–545.

75 Sadikot AF, Parent A, Francois C. Efferent connections of the centromedian and parafascicular thalamic nuclei in the squirrel monkey: A PHA-L study of subcortical projections. *Journal of Comparative Neurology* **315** (1992), 137-159.

76 Fallon JH, Moore RY. Catecholamine innervation of the basal forebrain. IV. Topography of the dopamine projection to the basal forebrain and neostriatum. *Journal of Comparative Neurology* **180** (1978), 545–580.

77 Smith AD, Bolam JP. The neural network of the basal ganglia as revealed by the study of synaptic connections of identified neurones. *Trends in Neuroscience* **13** (1990), 259-265.

78 Chang HT, Wilson CJ, Kitai ST. A Golgi study of rat neostriatal neurons: light microscopic analysis. *Journal of Comparative Neurolog.y* **208** (1982), 107– 26

79 Graveland GA, DiFiglia M. The frequency and distribution of medium-sized neurons with indented nuclei in the primate and rodent neostriatum. *Brain Research* **327** (1985), 307-311.

80 Cicchetti F, Prensa L, Wu Y, Parent A. Chemical anatomy of striatal interneurons in normal individuals and in patients with Huntington's disease. *Brain Research Reviews* **34** (2000), 80-101.

81 Morris G, Arkadir D, Nevet A, Vaadia E, Bergman H. Coincident but Distinct Messages of Midbrain Dopamine and Striatal Tonically Active Neurons. *Neuron* **43** (2004), 133-143.

82 Smith AD, Bolam JP. The neural network of the basal ganglia as revealed by the study of synaptic connections of identified neurons. *Trends in Neurosciences* **13** (1990), 259-265.

83 Kawaguchi Y. Physiological, morphological, and histochemical characterization of three classes of interneurons in rat neostriatum, immunohistochemical study of enkephalins and other neuropeptides *Journal of Neuroscience* **13** (1993), 4908–4923.

84 Kubota Y, Mikawa S, Kawaguchi Y. Neostriatal GABAergic interneurones contain NOS, calretinin or parvalbumin *NeuroReport* **5** (1993), 205-208.

85 Gerfen CR, Baimbridge GK, Miller JJ. The neostriatal mosaic: Compartmental distribution of calcium-binding protein and parvalbumin in the basal ganglia of the rat and monkey . *Proceedings of the National Academy of Sciences of the United States of America* **82** (1985), 8780-8784.

86 Cowan RL, Wilson CJ, Emson PC, Heizman CW. Parvalbumin-containing gabaergic interneurons in the rat neostriatum. *The Journal of Comparative Neurology* **302** (1990), 197-205.

87 Bennett BD, Bolam JP. Characterization of calretinin-immunoreactive structures in the striatum of the rat. *Brain Research* **609** (1993), 137-148.

88 Figueredo-Cardenas G, Morello M, Sancesario G, Bernardi G, Reiner A. Colocalization of somatostatin, neuropeptide Y, neuronal nitric oxide synthase and NADPH-diaphorase in striatal interneurons in rats. *Brain Research* **735** (1996), 317–324.

89 Kita H. GABAergic circuits of the striatum. *Progress in Brain Research* **99** (1993), 51-72.

90 Gillies A, Arbuthnott G. Computational models of the basal ganglia. *Movement Disorders* **15** (2000), 762-770.

91 Houk JC, Adams JL, Barto AG. A model of how the basal ganglia generate and use reward signals that predict reinforcement. In: J.C. Houk, J.L. Davis and D.G. Beiser, Editors, Models of information processing in the basal ganglia, MIT Press, Cambridge (1995), 249–270.

92 Suri RE, Schultz W. Learning of sequential movements by neural network model with dopamine-like reinforcement signal. *Experimental Brain Research* **121** (1998), 350–354.

93 Barto AG. Adaptive critic and the basal ganglia. In: J.C. Houk, J.L. Davis and D.G. Beiser, Editors, Models of information processing in the basal ganglia, MIT Press, Cambridge (1995), 215–232.

94 Gurney K, Prescott TJ, Redgrave P. A computational model of action selection in the basal ganglia. I. A new functional anatomy. *Biological Cybernetics* **84** (2001), 401–410.

95 Berns GS, Sejnowski TJ. A computational model of how the basal ganglia produce sequences. *Journal of Cognitive Neuroscience* **10** (1998), 108–121.

96 Schultz W, Tremblay L, Hollerman JR. Changes in behavior-related neuronal activity in the striatum during learning. *Trends in Neuroscience* **26** (2003), 321-328 .

97 Groves PM. A theory of the functional organization of the neostriatum and the neostriatal control of voluntary movement. *Brain Research* **286** (1983), 109–132.

98 Wickens JR, Alexander M. Analysis of Striatal Dynamics: The Existence of Two Modes of Behaviour. *Journal of Theoretical Biology* **163** (1993), 413-438.

99 Kotter R, Wickens JR. Striatal mechanisms in Parkinson's disease: new insights from computer modeling. *Artificial Intelligence in Medicine* **13** (1998), 37-55.

100 Suri RE, Schultz W. A neural network model with dopamine-like reinforcement signal that learns a spatial delayed response task. *Neuroscience* **91** (1999), 871-890.

101 Woodward DJ, Kirilov AB, Myre CD, Sawyer SF. Neostriatal circuitry as a scalar model: modelling and ensemble neuron recording. In: J.C. Houk, J.L. Davis and D.G. Beiser, Editors, Models of information processing in the basal ganglia, MIT Press, Cambridge (1995), 315-336.

102 Bar-Gad I, Bergman H. Stepping out of the box: information processing in the neural networks of the basal ganglia. *Current Opinion in Neurobiology* **11** (2001), 689-695.

103 Bishop GA, Chang HT, Kitai ST. Morphological and physiological properties of neostriatal neurones: an intracellular horseradish peroxidase study in the rat. *Neuroscience* **7** (1982), 179–91.

104 Somogyi P, Bolam JP, Smith AD. Monosynaptic cortical input and local axon collaterals of identified striatonigral neurons. A light and electron microscopic study using the Golgi-peroxidase transport-degeneration procedure. *Journal of Comparative Neurology* **195** (1981), 567-584.

105 Wilson CJ, Groves PM. Fine structure and synaptic connection of the common spiny neuron of the rat neostriatum: a study employing intracellular injection of horseradish peroxidase. *Journal of Comparative Neurology* **194** (1980), 599-615.

106 Oorschot DE. Total number of neurons in the neostriatal, pallidal, subthalamic and substantia nigral nuclei of the rat basal ganglia: a stereological study using the Cavalieri and optical dissector methods. *Journal of Comparative Neurology* **366** (1996), 580-599.

107 Park MR, Lighthall JW, Kitai ST. Recurrent inhibition in the rat neostriatum. *Brain Research* **194** (1980), 359–69.

108 Pasik P, Pasik T, Holstein G, Hamori J. GABAergic elements in the neuronal circuits of the monkey neostriatum: a light and electron microscopic immunocytochemical study. *Journal of Comparative Neurology* **270** (1988), 157–70.

109 Aronin N, Chase K, DiFiglia M. Glutamic acid decarboxylase and enkephalin immunoreactive axon terminals in the rat neostriatum synapse with striatonigral neurones. *Brain Research* **365** (1986), 151–158.

110 Jaeger D, Kita H, Wilson CJ. Surround inhibition among projection neurons is weak or nonexistent in the rat neostriatum. *Jouornal of Neurophysiology* **72** (1994), 2555-2558.

111 Fujiyama F, Fritschy JM, Stephenson FA, Bolam JP. Synaptic localization of GABA(A) receptor subunits in the striatum of the rat. *Journal of Comparative Neurology* **416** (2000), 158-172.

112 Wilson CJ, Kita H, Kawaguchi Y. GABAergic interneurons, rather than spiny cell axon collaterals, are responsible for the IPSP responses to afferent stimulation in neostriatal spiny neurons. *Society of Neuroscience Abstracts,* **15** (1989), 907.

113 Koos T, Tepper JM. Inhibitory control of neostriatal projection neurons by GABAergic interneurons. *Nature Neurosci.ence* **2** (1999), 467–472.

114 DeLong MR. Putamen: Activity of single units during slow and rapid arm movements. *Science* **179** (1973), 1240–1242

115 Crutcher MD, DeLong MR. Single cell studies of the primate putamen I. Functional organization. *Experimental Brain Research* **53** (1984), 233–243

116 Tepper JM, Koos T, Wilson CJ. Feedforward and Feedback Inhibition in the Neostriatum. In The Basal Ganglia VIII edited by Bolam JP, Ingham A, Magill PJ. (2005), 457-466.

117 Tunstall MJ, Oorshot DE, Kean A, Wickens JR. Inhibitory Interactions Between Spiny Projection Neurons in the Rat Striatum. *Journal of Neurophysiology* **88** (2002), 1263-1269.

118 Guzman JN, Hernandez A, Galarraga E, Tapia D, Laville A, Vergara R, Aceves J, Bargas J. Dopaminergic modulation of axon collaterals interconnecting spiny neurons of the rat striatum. *Journal of Neuroscience* **23** (2003), 8931-8940.

119 Czunbyako U, Plenz D. Fast synaptic transmission between striatal spiny projection neurons. *Neuroscience* **99** (2002), 15764-15769.

120 Taverna S, van Dongen YC, Groenewegen HJ, Pennartz CMA. Direct Physiological Evidence for Synaptic Connectivity Between Medium-Sized Spiny Neurons in Rat Nucleus Accumbens In Situ. *Journal of Neurophysiology* **91** (2004), 1111-1121.

121 Koos T, Tepper JM, Wilson CJ. Comparison of IPSCs Evoked by Spiny and Fast-Spiking Neurons in the Neostriatum . *Journal of Neuroscience* **24** (2004), 7916-7922.

122 Gustafson N, Ghireesh-Darmaraj N, Czubyako U, Blackwell KT, Plenz D. A Comparative Voltage and Current-Clamp Analysis of Feedback and Feedforward Synaptic Transmission in the Striatal Microcircuit in vitro. *Journal of Neurophysiology* **95** (2006), 737-752.

123 Plenz D. When inhibition goes incognito: feedback interaction between spiny projection neurons in striatal function. *Trends in Neurosciences* **26** (2003), 436-443.

124 Bishop GA, Chang HT, Kitai ST. Morphological and physiological properties of neostriatal neurones: an intracellular horseradish peroxidase study in the rat. *Neuroscience* **7** (1982), 179–91

125 Kincaid AE, Zheng T, Wilson CJ. Connectivity and Convergence of Single Corticostriatal Axons. *The Journal of Neuroscience* **18** (1998), 4722-4731.

126 Oorschot DE. Total number of neurons in the neostriatal, pallidal, subthalamic and substantia nigral nuclei of the rat basal ganglia: a stereological study using the Cavalieri and optical dissector methods. *Journal of Comparative Neurology*, **366** (1996), 580-599.

127 Zheng T, Wilson CJ. Corticostriatal Combinatorics: The Implications of Corticostriatal Axonal Arborizations. *Journal of Neurophysiology*, **87** (2002), 1007-1017.

128 Wilson CJ, The generation of natural firing patterns in neostriatal neurons. In: *Progress in Brain Research. Chemical Signaling in the Basal Ganglia*, edited by G. W. Arbuthnott, and P. C. Emson . Amsterdam: Elsevier, **99** (1993), 277-297

129 Crutcher MD, DeLong MR. Single cell studies of the primate putamen. I. Functional organization. *Experimental Brain Research,* **53** (1984), 233-43.

130 Jiang Z-G, North RA. Membrane properties and synaptic responses of rat striatal neurones *in vitro*. *Journal Of Physiology* **443** (1991), 533–553.

131 Stern EA, Kincaid AE, Wilson CJ. Spontaneous Subthreshold Membrane Potential Fluctuations and

Action Potential Variability of Rat Corticostriatal and Striatal Neurons In Vivo. *The Journal of Neurophysiology* **77** (1997), 1697-1715.

132 Wilson CJ, Groves PM. Spontaneous firing patterns of identified spiny neurons in the rat neostriatum. *Brain Research* **220** (1981), 67–80.

133 Wilson CJ, Kawaguchi Y. The origins of two-state spontaneous membrane potential fluctuations of neostriatal spiny neurones. *Journal of Neuroscience* **16** (1996), 2397-2410.

134 Gruber AJ, Solla SA, Surmeier DJ, Houk JC. Modulation of Striatal Single Units by Expected Reward: A Spiny Neuron Model Displaying Dopamine-Induced Bistability. *Journal of Neurophysiology*, **90** (2003), 1095-1114.

135 Mahon S, Deniau JM, Charpier S, Delord B. Role of a Striatal Slowly Inactivating Potassium Current in Short-Term Facilitation of Corticostriatal Inputs: A Computer Simulation Study. *Learning and Memory*, **7** (2000), 357-362.

136 Kawaguchi Y, Wilson CJ, Emson PC. Intracellular recording of identified neostriatal patch and matrix spiny cells in a slice preparation preserving cortical inputs. *Journal of Neurophysiology,* **62** (1989), 1052–1068.

137 Kita T, Kita H, Kitai ST. Passive electrical membrane properties of rat neostriatal neurons in an in vitro slice preparation. *Brain Research* **300** (1984), 129-139.

138 Nisenbaum ES, Wilson CJ,. Potassium currents responsible for inward and outward rectification in rat neostriatal spiny projection neurons. *Journal of Neuroscience* **15** (1995), 4449-4463.

139 Mermelstein PG, Song W-J, Tkatch T, Yan Z, Surmeier DJ. Inwardly rectifying potassium currents are correlated with irk subunit expression in rat nucleus accumbens medium spiny neurons. *Journal of Neuroscience* **18** (1998), 6650–6661.

140 Uchimura N. Cherubini E. North RA. Inward rectification in rat nucleus accumbens neurons. *Journal of Neurophysiology* **62** (1989), 1280-l286.

141 Hagiwara S, Miyazaki S, Rosenthal NP. Potassium current and the effect of cesium on this current during anomalous rectification of the egg cell membrane of a starfish. *Journal of General Physiology* **67** (1976), 621-638.

142 Nisenbaum ES, Xu ZC, Wilson CJ. Contribution of a slowly-inactivating potassium current to the transition to firing of neostriatal spiny projection neurons. *Journal of Neurophysiology* **71** (1994), 1174-l189.

143 Surmeier DJ, Foehring R, Stefani A, Kitai ST. Developmental expression of a slowly-inactivating voltage dependent potassium current in rat neostriatal neurons. *Neuroscience Letters* **122** (1991), 4l-46.

144 Surmeier DJ, Xu ZC, Wilson CJ, Stefani A, Kitai ST. Grafted neostriatal neurons express a late-developing transient potassium current. *Neuroscience* **48** (1992), 849-856.

145 Nisenbaum ES, Wilson CJ, Surmeier DJ. Depolarization evokes a slowly-activating K+ current in rat striatal neurons. *Society of Neuroscience Abstracts* **20** (1994), 564.

146 Surmeier DJ, Wilson CJ, Eberwine J. Patch-clamp techniques for studying potassium currents in mammalian brain neurons. In: *Methods in neurosciences: methods for the study of ion channels*

(1994), 39-67. San Diego: Academic.

147 Wilson CJ. The generation of natural firing patterns in neostriatal neurons. In: Progress in Brain Research. *Chemical Signaling in the Basal Ganglia*, edited by G. W. Arbuthnott and P. C. Emson. Amsterdam: Elsevier, **99** (1993), 277–297.

148 Wilson CJ, Chang HT, Kitai ST.Disfacilitation and long-lasting inhibition of neostriatal neurons in the rat. *Experimental Brain Research* **51** (1983), 227-235.

149 Calabresi P, Mercuri NB, Stefani A, Bernardi G. Synaptic and intrinsic control of membrane excitability of neostriatal neurons. I. An in viva analysis. *Journal of Neurophysiology* **63** (1990), 651-662.

150 Calabresi P, Mercuri NB, Bernardi G. Synaptic and intrinsic control of membrane excitability of neostriatal neurons. II. An in vitro analysis. J*ournal of Neurophysiology* **63** (1990), 663-675.

151 Bargas J, Gallarraga E, Aceves J. An early outward conductance modulates the firing latency and frequency of neostriatal neurons of the rat brain. *Experimental Brain Research,* **75** (1989), 146–156.

152 Bargas J, Howe A, Eberwine J, Surmeier JD. Cellular and molecular characterization of Ca2+ currents in acutely isolated, adult rat neostriatal neurons. *Journal of Neuroscience* **14** (1994), 6667–6686.

153 Song WJ, Surmeier DJ. Voltage-dependent facilitation of calcium channels in rat neostriatal neurons. J*ournal of Neurophysiology* **76** (1996), 2290–2306.

154 Perrier JF, Hounsgaard J. Development and regulation of response properties in spinal cord motoneurons. *Brain Research Bullutin,* **53** (2000), 529-535.

155 Carlin KP, Jones KE, Jiang Z, Jordan LM, Brownstone RM. Dendritic L-type calcium currents in mouse spinal motoneurons: implications for bistability. *European Journal of Neuroscience,* **12** (2000), 1635-1646.

156 Seamans JK, Gorelova NA, Yang CR. Contributions of voltage-gated Ca^{2+} channels in the proximal *versus* distal dendrites to synaptic integration in prefrontal cortical neurons. *Journal of Neuroscience*, **17** (1997), 5936-5948.

157 Wilson CJ. Passive cable properties of dendritic spines and spiny neurons. *Journal of Neuroscience* **4** (1984),281-297.

158 Pacheco-Cano MT, Bargas J, Hernandez-Lopez S. Inhibitory action of dopamine involves a subthreshold cs+-sensitive conductance in neostriatal neurons *Experimental Brain Research* **110** (1996), 205–211.

159 Surmeier DJ, Kitai ST. D1 and D2 dopamine receptor modulaiton of sodium and potassium currents in rat neostriatal neurons. In: *Progress in Brain Research* edited by Arbuthnott GW and Emson PC. Amsterdam: Elsevier, **99** (1993), 309–324.

160 Surmeier DJ, Bargas J, Hemmings HC, Jr, Nairn AC, Greengard P. Modulation of calcium currents by a D1 dopaminergic protein kinase phosphatase cascade in rat neostriatal neurons. *Neuron* **14** (1995), 385–397.

161 Surmeier DJ, Song W-J, Yan Z. Coordinated expression of dopamine receptors in neostriatal medium spiny neurons. *Journal of Neuroscience* **16** (1996), 6579–6591.

162 Hernández-López S, Bargas J, Surmeier DJ, Reyes A, Galarraga E. D1 Receptor Activation Enhances Evoked Discharge in Neostriatal Medium Spiny Neurons by Modulating an L-Type Ca2+ Conductance. *Journal of Neuroscience.* **17** (1997), 3334 - 3342.

163 Press WH, Teukolsky SA, Vetterling WT, Flannery BP. Numerical recipes: The art of scientific computing, 2nd ed. (1992), Cambridge University Press, Cambridge, UK.

164 Nisenbaum ES, Wilson CJ, Foehring RC, Surmeier DJ. Isolation and characterization of a persistent potassium current in neostriatal neurons. *Journal of Neurophysiology*, **76** (1996), 1180-1194.

165 Gabel LA.,Nisenbaum ES. Biophysical characterization and functional consequences of a slowly inactivating potassium current in neostriatal neurons. *Journal of Neurophysiology*. **79** (1998), 1989-2002

166 Hille B. *Ionic Channels of Excitable Membranes* .Chapter 13. Sunderland, MA: Sinauer,(1992).

167 Wickens JR, Wilson CJ. Regulation of Action-Potential Firing in Spiny Neurons of the Rat Neostriatum In Vivo. *The Journal of Neurophysiology* **79** (1998), 2358-2364.

168 Rinzel J, Ermentrout GB. Analysis of neural excitability and oscillations. In: Methods in Neuronal Modeling, edited by Koch C and Segev I. Cambridge, MA: MIT Press, (1989), 135–169.

169 Venton BJ, Zhang H, Garriss PA, Phillips PEM, Sulzer D.Real-time decoding of dopamine concentration changes in the caudate-putamen during tonic and phasic firing. *Journal of Neurochemistry* **87** (2003), 1284-1295.

170 Nicola SM, Woodward Hopf F, Hjelmstad GO. Contrast enhancement: a physiological effect of striatal dopamine? *Cell and Tissue Research* **318** (2004), 93-106.

171 Wickens JR, Wilson CJ. Regulation of Action-Potential Firing in Spiny Neurons of the Rat Neostriatum In Vivo. *Journal of Neurophysiology*, **79** (1998), 2358 -2364.

172 Petersen RS, Panzeri S, Diamond ME. The role of individual spikes and spike patterns in population coding of stimulus location in rat somatosensory cortex. *Biosystems* **67** (2002), 187–193.

173 Petersen RS, Panzeri S, Diamond ME. Population coding in somatosensory cortex. *Current Opinion in Neurobiology* **12** (2002), 441–447.

174 Diamond ME, Petersen RS, Harris JA, Panzeri S. Investigations into the organization of information in sensory cortex. *Journal of Physiology – Paris*. **97** (2004), 529-536.

175 Oorschot DE. Total number of neurons in the neostriatal, pallidal, subthalamic and substantia nigral nuclei of the rat basal ganglia: a stereological study using the Cavalieri and optical dissector methods. *Journal of Comparative Neurology*, **366** (1996), 580-599.

176 Blackwell KT, Czubayko U, Plenz D. Quantitative Estimate of Synaptic Inputs to Striatal Neurons during Up and Down States In Vitro . *Journal of Neuroscience* , **23** (2003), 9123-9132.

177 Jones RS, Buhl EH. Basket-like interneurones in layer II of the entorhinal cortex exhibit a powerful NMDA-mediated synaptic excitation, *Neuroscience Letters* **149** (1993), 35–39.

178 Kawaguchi Y, Katsumaru1 H, Kosaka1 T, Heizmann CW, Hama K. Fast spiking cells in rat hippocampus (CA1 region) contain the calcium-binding protein parvalbumin, *Brain Research* **416** (1987), 369–374.

179 Kawaguchi Y, Wilson CJ, Augood SJ, Emson PC. Striatal interneurons: chemical, physiological and morphological characterization. *Trends in Neurosciences* **18** (1995), 527-535.

180 Luk KC, Sadikot AF. GABA promotes survival but not proliferation of parvalbumin-immunoreactive interneurons in rodent neostriatum: an in vivo study with stereology. *Neuroscience* **104** (2001), 93-103.

181 Bennett BD, Bolam JP. Synaptic input and output of parvalbumin-immunoreactive neurons in the neostriatum of the rat. *Neuroscience* **62** (1994), 707-719.

182 Koós T, Tepper JM, Wilson CJ. Comparison of IPSCs Evoked by Spiny and Fast-Spiking Neurons in the Neostriatum. *Journal of Neuroscience* **24** (2004), 7916-7922.

183 Rudkin TM, Sadikot TF. Thalamic input to parvalbumin-immunoreactive GABAergic interneurons: organization in normal striatum and effect of neonatal decortication. *Neuroscience* **88** (1999), 1165-1175.

184 Koós T, Tepper JM. Inhibitory control of neostriatal projection neurons by GABAergic interneurons. *Nature Neuroscience*, **2** (1999), 467-472.

185 Plenz D, Kitai ST. Up and Down States in Striatal Medium Spiny Neurons Simultaneously Recorded with Spontaneous Activity in Fast-Spiking Interneurons Studied in Cortex-Striatum-Substantia Nigra Organotypic Cultures. *The Journal of Neuroscience*, **18** (1998), 266-283.

186 Kerr JND, Plenz D. Action Potential Timing Determines Dendritic Calcium during Striatal Up-States. *The Journal of Neuroscience*, **24** (2004), 877-885.

187 Suri RE. TD models of reward predictive responses in dopamine neurons. *Neural Networks* **15** (2002), 523-533.

188 Bar-Gad I, Bergman H. Stepping out of the box: information processing in the neural networks of the basal ganglia, *Current Opinion in Neurobiology.* **11**, (2001), 689-695.

189 Kerr JND, Plenz D. Dendritic Calcium Encodes Striatal Neuron Output during Up-States. *The Journal of Neuroscience*, **22** (2002), 1499-1512.

190 Calabresi P, Pisani A, Mercuri NB, Bernardi G. Post-receptor mechanisms underlying striatal long-term depression. *Journal of Neuroscience,* **14** (1994)**,** 4871-4881.

191 Brown JW, Bullock D, Grossberg S. How laminar frontal cortex and basal ganglia circuits interact to control planned and reactive saccades. *Neural Networks* **17** (2004), 471-510.

192 Gustafson N, Gireesh-Dharmaraj E, Czubayko U, Blackwell KT, Plenz D. A Comparative Voltage and Current-Clamp Analysis of Feedback and Feedforward Synaptic Transmission in the Striatal Microcircuit in vitro. *The Journal of Neurophysiology* **95** (2006), 737-752.

193 Wickens JR, Wilson CJ. Regulation of Action-Potential Firing in Spiny Neurons of the Rat Neostriatum In Vivo. *The Journal of Neurophysiology* **79** (1998), 2358-2364.

194 Bracci E, Centonze D, Bernardi G, Calabresi P. Dopamine Excites Fast-Spiking Interneurons in the Striatum. *The Journal of Neurophysiology* **87** (2002), 2190-2194

195 Koós T, Tepper JM. Dual Cholinergic Control of Fast-Spiking Interneurons in the Neostriatum. *The Journal of Neuroscience*, **22** (2002), 529-535.

196 Smolders I, De Klippel N, Sarre S, Ebinger G, Michote Y Tonic GABAergic modulation of striatal dopamine release studied by in vivo microdialysis in the freely moving rat. *European Journal of Pharmacology* **284** (1995), 83-91

197 Brown P, Marsden CD. What do the basal ganglia do?. Lancet 351, (1998), 1801–1804.

198 Berke JD, Okatan M, Skurski J, Eichenbaum HB. Oscillatory Entrainment of Striatal Neurons in Freely Moving Rats. *Neuron* **43**, (2004), 883-896.

199 Shaw FZ. Is spontaneous high-voltage rhythmic spike discharge in Long Evans rats an absence-like seizure activity?. *J. Neurophysiol*. **91**(2004), 63–77.

200 Cools AR. Role of the neostriatal dopaminergic activity in sequencing and selecting behavioural strategies: facilitation of processes involved in selecting the best strategy in a stressful situation, *Behavioural Brain Research* **1** (1980), 361–378.

201 Robbins TW, Brown VJ, The role of the striatum in the mental chronometry of action: a theoretical review, *Reviews in the Neurosciences* **2** (1990), 181–213.

202 Mink JW. The basal ganglia: Focused selection and inhibition of competing motor programs, *Progress In Neurobiology* **50** (1996), 381–425.

203 Wickens JR. Basal ganglia: structure and computations, *Network-Computation in Neural Systems* **8** (1997) R77–R109.

204 Redgrave P, Prescott TJ, Gurney KN. The basal ganglia: a vertebrate solution to the selection problem?, *Neuroscience* **89** (1999), 1009–1023.

205 Prescott TJ, Montes Gonzalez FM, Gurney KN, Humphries MD, Redgrave P. A robot model of the basal ganglia: Behavior and intrinsic processing. *NeuralNetworks* **19** (2006), 31-61.

206 Robbins TW, Everitt BJ. Neurobehavioural mechanisms of reward and motivation. *Curent Opiniion in Neurobiology*. **6** (1996), 228–236.

207 Schultz W. Responses of midbrain dopamine neurons to behavioral trigger stimuli in the monkey. *The Journal of Neurophysiology* **56** (1986), 1439-1461.

208 Romo R, Schultz W. Dopamine neurons of the monkey midbrain: contingencies of responses to active touch during self-initiated arm movements. *The Journal of Neurophysiology* **63** (1990), 592-606.

209 Herrick CJ. The Brain of the Tiger Salamander. Chicago: University of Chicago Press (1948).

210 Crow TJ, Arbuthnott GW. Function of catecholamine-containing neurones in mammalian central nervous system. *Nature New Biology* **238** (1972), 245-246.

211 Schultz W, Tremblay L, Hollerman JR. Reward prediction in primate basal ganglia and frontal cortex. *Neuropharmacology* **37** (1998), 421–429.

212 Pavlov IP. Conditioned reflexes. Oxford: Oxford University (1927).

213 Rescorla RA, Wagner AR. A Theory of Pavlovian conditioning: variations in the effectiveness of reinforcement and nonreinforcement. In A. H. Black, & W. F. Prokasy (Eds.), Classical conditioning II: current research and theory. New York: Appleton- Century-Crofts (1972).

214 Dickinson A. Instrumental conditioning. Animal learning and cognition, San Diego: Academic Press (1994), 45–78.

215 Sutton R. Learning to predict by methods of temporal difference. *Machine Learning*, **3** (1988), 9-44.

216 Montague PR, Dayan P, Sejnowski TJ. A framework for mesencephalic dopamine systems based on predictive hebbian learning. *Journal of Neuroscience*, **16** (1996), 1936–1947.

217 Barto AG. Adaptive critic and the basal ganglia. In J. C. Houk, J. L. Davis, & D. G. Beiser (Eds.), Models of information processing in the basal ganglia. (1995), 215–232. Cambridge: MIT Press.

218 Houk JC, Adams JL, Barto AG. A model of how the basal ganglia generate and use reward signals that predict reinforcement. In J. C. Houk, J. L. Davis, & D. G. Beiser (Eds.), Models of information processing in the basal ganglia. (1995), 249–270. Cambridge: MIT Press.

219 Sutton RS, Barto AG. Reinforcement Learning: An Introduction. MIT Press., 2000.

220 Wickens JR, Begg AJ, Arbuthnott GW. Dopamine reverses the depression of rat corticostriatal synapses which normally follows high-frequency stimulation of cortex *In vitro*. *Neuroscience* **70** (1996), 1-5.

221 Yung KKL, Bolam JP, Smith AD, Hersch SM, Ciliax BJ, Levey AI. Immunocytochemical localization of D1 and D2 dopamine receptors in the basal ganglia of the rat: light and electron microscopy. *Neuroscience* **65**, (1995), 709–730.

222 Hersch SM, Ciliax BJ, Gutekunst CA, Rees HD, Heilman CJ, Yung KK, Bolam JP, Ince E, Yi H, Levey AI. Electron microscopic analysis of D1 and D2 receptor proteins in the dorsal striatum and their synaptic relationships with motor corticostriatal afferents. *Journal of Neuroscience*. **15**, (1995), 5222–5237.

223 Rice ME Distinct regional differences in dopamine-mediated volume transmission. In Volume Transmission Revisited (Agnati, L.F. et al., eds), . (2000), 275–288, Elsevier.

224 Nicholson C. Interaction between diffusion and Michaekis-Menten uptake of dopamine after iontophoresis in striatum. *Biophysics* **68** (1995), 1699-1715.

225 Cragg SJ, Rice ME. DAncing past the DAT at a DA synapse. *Trends in Neurosciences* **27** (2004), 270-277.

226 Cragg SJ. Meaningful silences: how dopamine listens to the ACh pause. *Trends in Neurosciences* **29** (2006), 125-131

227 Morris G, Arkadir D, Nevet A, Vaadia E, Bergman H. Coincident but Distinct Messages of Midbrain Dopamine and Striatal Tonically Active Neurons. *Neuron* **43** (2004), 133-143.

228 Parthasarathy HB, Schall JD, Graybiel AM. Distributed but convergent ordering of corticostriatal projections: analysis of the frontal eye field and the supplementary eye field in the macaque monkey. *Journal of Neuroscience* **12** (1992), 4468–4488.

229 Flaherty AW, Graybiel AM. Corticostriatal transformations in the primate somatosensory system. Projections from physiologically mapped body-part representations. *Journal of Neurophysiology* **66** (1991), 1249 –1263.

230 Calabresi P, Maj R, Pisani A, Mercuri NB, Bernardi G Long-term synaptic depression in the

striatum—physiological and pharmacological characterization. Journal of Neuroscience **12** (1992), 4224–4233.

231 Bell CC, Han VZ, Sugawara Y, Grant K. Synaptic plasticity in cerebellum-like structure depends on temporal order. *Nature* **387** (1997),278-281.

232 Markram H, Lübke J, Frotscher M, Sakmann B. Regulation of synaptic efficacy by coincidence of postsynaptic APs and EPSPs. *Science* **275** (1997),213-215.

233 Van Rossum MCW,Bi GQ,Turrigiano GG. Stable Hebbian Learning from Spike Timing-Dependent Plasticity. *Journal of Neuroscience,* **20** (2000),8812-8821

234 Bi G-Q, Poo M-M. Synaptic modifications in cultured hippocampal neurons: dependence on spike timing, synaptic strength, and postsynaptic cell type. *Journal of Neuroscience* **18** (1998), 10464-10472.

235 Bonsi P, Pisani A, Bernardi G, Calabresi P. Stimulus frequency, calcium levels and striatal synaptic plasticity. *Neuroreport* **14** (2003), 419–422.

236 Schramm NL, Egli RE, Winder DG. LTP in the mouse nucleus accumbens is developmentally regulated. *Synapse* **45** (2002), 213–219.

237 Robbe D, Kopf M, Remaury A, Bockaert J, Manzoni OJ. Endogenous cannabinoids mediate long-term synaptic depression in the nucleus accumbens. *Proceedings of the National Academy of Science USA* **99** (2002), 8384–8388.

238 Suri RE, Schultz W. A neural network model with dopamine-like reinforcement signal that learns a spatial delayed response task. *Neuroscience* **91** (1999), 871-890.

239 Suri RE, Bargas J, Arbib MA. Modeling functions of striatal dopamine modulation in learning and planning. *Neuroscience* **103** (2001), 65-85.

240 Brown J, Bullock D, Grossberg S. How the basal ganglia use parallel excitatory and inhibitory learning pathways to selectively respond to unexpected rewarding cues. *Journal of Neuroscience* **19** (1999), 10502-10511.

241 Horvitz JC. Mesolimbocortical and nigrostriatal dopamine responses to salient non-reward events. *Neuroscience* **4** (2000), 651-656.

242 Reynolds JNJ, Hyland BI, Wickens JR. A cellular mechanism of reward-related learning. *Experimental Neurology* **413** (2001), 67-70.

243 Lenck-Santini PP, Muller RU, Save E, Poucet B. Relationships between place cell firing fields and navigational decisions by rats. *The Journal of Neuroscience* **22** (2002), 9035-9047.

244 Flaherty AW, Graybiel AM. Input-output organization of the sensorimotor striatum in the squirrel monkey *The Journal of Neuroscience* **14** (1994), 599–610.

245 Tunstall MJ, Oorschott DE, Kean A, Wickens JR. Inhibitory Interactions Between Spiny Projection Neurons in the Rat Striatum. *Journal of Neurophysiology* **88** (2002), 1263-1269.

246 Calabresi P, Maj R, Mercuri NB, Bernardi G. Coactivation of D1 and D2 dopamine receptors is required for long-term synaptic depression in the striatum. *Neuroscience Letters* **142** (1992), 95–99.

247 Tobler PN, Fiorillo CD, Schultz W. Adaptive Coding of Reward Value by Dopamine Neurons. *Science* **307** (2005), 1642-1645.

248 Fiorillo CD, Tobler PN, Schultz W. Discrete Coding of Reward Probability and Uncertainty by Dopamine Neurons. *Science* **299** (2003), 1898-1902.

249 Myers CE, Shohamy D, Gluck MA, Grossman S, Kluger A, Ferris S, Golomb J, Schnirman G, Schwartz R. Dissociating hippocampal versus basal ganglia contributions to learning and transfer. *Journal of Cognitive Neuroscience* **15** (2003), 185-193.

250 Ehringer H, Hornykiewicz O. Verteilung von noradrenalin und dopamin (3-hydroxytyramin) im gehirn des menschen und ihr verhalten bei erkrankungen des extrapyramidalen systems. Klin Wschr **38**, (1960), 1236–1239.

251 Schultz W. Getting Formal with Dopamine and Reward. *Neuron* **36**, (2002), 241-263.